Geometric Tomography With Topological Guarantees

Pooran Memari

Université de Nice Sophia Antipolis
école Doctorale STIC

N° attribué par la bibliothèque

THÈSE

pour obtenir le grade de

Docteur de Sciences

Spécialité : **Informatique**

préparée au laboratoire **INRIA Sophia Antipolis**

dans le cadre de l'École Doctorale **STIC**

présentée et soutenue publiquement
par

Pooran MEMARI

le 26 mars 2010

Titre:
Geometric Tomography With Topological Guarantees

Directeur de thèse: **Jean-Daniel Boissonnat**

Jury

Mme. Dominique Attali,	Examinateur
M. Gill Barequet,	Rapporteur
M. Michel Barlaud,	Examinateur
M. Jean-Daniel Boissonnat,	Directeur de thèse
M. Bernhard Geiger,	Examinateur
M. André Lieutier,	Examinateur
M. Jonathan Richard Shewchuk,	Rapporteur
M. Gert Vegter,	Rapporteur

A Omid

A mes parents

A ma famille

Acknowledgment

My thanks go first to my adviser *Jean-Daniel Boissonnat* for all his help, support and contribution of time and insights. His knowledge, patience and good humor helped me bring this thesis to completion.

I gratefully acknowledge *Gill Barequet, Jonathan Richard Shewchuk and Gert Vegter* for accepting to review this manuscript, and for their valuable time and very constructive advices that helped me to improve the presentation. And I thank *Dominique Attali, Michel Barlaud, Bernhard Geiger,* and *André Lieutier* for their time, helpful comments and suggestions. I was honored by their presence in my Ph.D committee.

I am also thankful to *Olivier Devillers* for introducing me to the computational geometry with his fantastic classes at Ecole Polytechnique. I appreciate the research suggestions and encouraging comments from *Mariette Yvinec.* I'm especially grateful to *David Cohen-Steiner* and *Pierre Alliez* for valuable discussions and guidance. Thanks to *Monique Teillaud*, *Frédéric Cazals* and *Raphaëlle Chaine* for their guidance and cooperation. I'm especially grateful to my friends *Christophe Delage*, *Sebastien Loriot* and *Laurent Saboret.* Their help was instrumental in the implementation of my algorithm.

I convey special acknowledgment to all my friends, especially *Alexandre, Florian, Pierre, Guillaume, Alexis, Jane, Quentin, Marie, Camille, Christophe, Steve, Pedro, Manuel, Lionel, Maria, Sapna, Emilie, Florence, Héloise, Dobrina and Céline* for these fantastic years at Côte d'Azur. Thanks are also extended to all other members of Geometrica for all their help and sympathy.

I would like to express my heart-felt gratitude to my family, to whom this dissertation is dedicated. *My parents* deserve special mention for their love, inseparable support and encouragement; thank you. Words fail me to express my appreciation to *Omid* for his dedication, love and persistent confidence in me. I have benefited greatly from his valuable advice and encouragement and to him I am extremely grateful.

Finally, I would like to thank everybody who was important to the successful realization of this thesis, as well as expressing my apology that I could not mention personally one by one.

Preface

Reconstructing an object from its sections with a set of planes has intrigued computer science researchers for the last decades. The need for such reconstructions is a result of the advances in medical imaging technology. From data obtained by CT, MRI, or other systematic scanning devices, contours representing the boundaries of the organs may be extracted on slices, and then interpolated in order to reconstruct and visualize human organs. 3D reconstructions of organs are widely considered to be an important diagnostic aid in the medical world. However, the actual simulation results, namely in 3D ultrasonic simulation, are not reliable to be used in diagnosis. In fact, there is a lack of research examining the quality of the simulation with respect to the original shape (organ).

The purpose of my doctoral thesis was to provide a method to reconstruct three dimensional shapes from cross-sections, and to analyze the theoretical guarantees related to such a reconstruction. A geometric reconstruction method with theoretical guarantees was performed during this thesis. This work is the first geometric analysis of the reliability and validity of reconstruction methods from cross-sectional data.

The theoretical studies of this thesis have consistently shown that if the sample of cutting planes is sufficiently dense, an accurate approximation of the unknown object can be provided. These studies provide the way to guide the sampling process to achieve the purposed *density* of cutting planes, or more formally, to verify the provided sampling conditions on the sections. The hope is that this thesis will be a first step to provide solid foundations and theoretical guarantees for medical diagnostic software. Of course, further research and investment is needed to apply these theoretical guidelines in developments of medical imaging softwares.

Organization of the Thesis

We start with a general introduction of the reconstruction problem and its applications. A section is devoted to cite briefly the existing methods for some restricted cases of the problem, where the planes that cut the shape have a fixed orientation and are all parallel to each other. Then, the few existing methods for the general case of arbitrarily oriented planes are presented. Then we provide an overview of the content and the contributions of the thesis. We start with a formal description of the problem, and introduce the partition (*arrangement*) of the space by the cutting planes. Using this partition, the reconstruction problem is replaced by some subproblems (corresponding to the reconstruction in each cell of the partition). Also a general reconstruction methodology in each cell is presented which is based on a distance function from the boundary of the cell. The method corresponding to the Euclidean distance coincides with the method presented by Liu et al. in [LBD+08]. Chapter 1 of this manuscript is devoted to analyzing this method. We prove that under appropriate sampling conditions this reconstruction method preserves the homotopy type of the original shape. Using the homotopy equivalence, we also show that the reconstructed object is homeomorphic (and isotopic) to the original object. This is the first time that 3D shape reconstruction from cross-sections comes with such theoretical guarantees. These theoretical guarantees have been also presented in [ABM09].

In the second chapter of this thesis, we present a different reconstruction method which performs more connections between the sections compared to the first method and is motivated by applications in reconstruction of tree-like structures from sparse data. This method is based on the Voronoi diagram of the sections. A detailed description of the reconstruction procedure in each cell of the partition, as well as theoretical guarantees are given in Sections 2 and 3. Then, in Section 4, we introduce the dual structure which has a better geometrical shape and has the same topological guarantees. We will see that in the discrete case of the problem, the dual structure is a subcomplex of the Delaunay complex of the sample points of the sections.

Indeed, the Delaunay-Voronoi duality leads us to a third method, presented in Chapter 3, which is the generalization of Boissonnat and Geiger's method [BG93] that was restricted to the case of parallel sections. In that method, in order to improve the branching procedure between the sections, the authors consider some additional points on the orthogonal projection of the medial axis of the sections of one cutting plane onto the adjacent plane. This strategy of approximating the branching locus have been followed since then in several methods. We justify this strategy by characterizing the branching locus of the Delaunay structure in the general case of arbitrarily oriented cutting planes. This work has been published in the proceedings of the Symposium on Geometry Processing 2007, [BM07]. Experimental results for each proposed algorithm are provided at the end of the corresponding sections. (Note that an efficient adaptation of this algorithm for the 2D variant of the problem with theoretical guarantees has been published in 2008 in Computer Graphics Forum, see [MB08].) The last section contains a conclusion and directions for future work.

Related Publications

[BM07] J.-D. Boissonnat, P. Memari. *Shape Reconstruction From Unorganized Cross Sections*, Symposium on Geometry Processing (SGP), 89-98, **(2007)**.

[MB08] P. Memari, J.-D. Boissonnat. *Provably Good 2D Shape Reconstruction from Unorganized Cross Sections*, Computer Graphics Forum, Vol.27, No. 5, 1403-1410, **(2008)**.

[ABM09] O. Amini, J.-D. Boissonnat, P. Memari. *Geometric Tomography With Topological Guarantees*, INRIA Research Report 7147, **(2009)**. Proceedings of the 26th Symposium on Computational Geometry 2010.

Contents

Introduction

One of the main problems in computational geometry is to reconstruct a shape $\mathcal{O}$ from a sparse sample of $\mathcal{O}$ (*partial* data). This problem is mainly motivated by the need for development of methods for 3D simulations in computer aided design, medical imaging and industrial modeling. Due to the finite amount of memory, only discretized versions of data can be represented by a computer. The choice of data representation depends highly on the application considered. The most classical data acquisition is done by scanners that provide a finite set of points sampled from the object. The problem of reconstructing an object from a set of sample points, known also as *reconstruction from point clouds*, has been widely considered and studied by different authors. We refer the reader to [Dey07] and [CGY04] for a comprehensive survey.

Another data representation is considered in *Geometric tomography* which consists of reconstructing a 3-dimensional object from 2-dimensional information such as *projections* or *sections*. In this thesis, we are interested in the reconstruction of a 3D object from its intersections with a set of planes, called *cross-sections*. Many solutions to the reconstruction problem from parallel cross-sections have been proposed, see Section 2 of this introduction. However, this thesis focuses on the harder and more general case of arbitrarily oriented (multi-axial) planes, which has received much less attention.

1 Applications

Let us first present some applications of reconstruction from cross-sections.

Biological Morphology

In many tasks, we have to extract object information from a sparse sample. Particularly, in medical applications, parts of human body are represented by an image sequence of parallel slices. These slices can be acquired by magnetic resonance imaging (MRI), computer tomography (CT), or by mechanical slicing and digitization. Reconstructions from slices obtained by CT and MRI are exploited for surgery and radiation therapy planning [Gei93]. They have also already been used for volumetry in ultrasound [HDM+96] and in the microscopy of cells [MLP88], [MLB05]. Figure 1 show a reconstruction example from [MLB05].

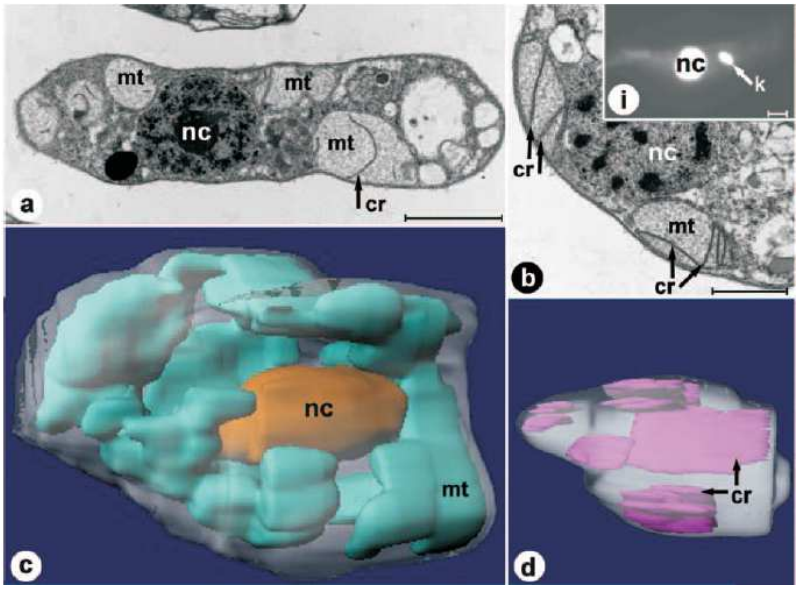

Figure 1: Figure from [MLB05] (with permission): Images from an Electron microscopy (a and b), and 3D reconstruction (c and d) based on 48 consecutive sections.

One of the limitations of classical microscopic technologies is related to the fact that to provide the sectional data we should cut the specimen we are studying. In particular, as the cuts are destructive, living specimens cannot be studied. Moreover, one can only provide non intersecting slices. In other words the reconstruction problem corresponds to the case of serial sequence of planes. A very novel microscopic technology called *Single Plane Illumination Microscope* provides *slices* by illuminating the specimen along a plane (a light sheet). This allows us to study living specimens and having non parallel slices of the specimen.[1]

SPIM Microscopy

The SPIM (Single Plane Illumination Microscope) is an original microscope which was developed by the European Molecular Biology Laboratory in Germany around 2004 [HSD+04]. It allows us to study functional aspects of living specimens and raises several challenges in different fields such as optics, image processing, mathematical modelling and scientific computing. Contrarily to more mature imaging technologies like confocal or multi-photon microscopes, SPIM does not rely on scanning a single focal point throughout the sample: a light sheet is produced and is used to illuminate a slice of the whole sample. This light sheet is positioned in the focal plane of a microscope objective. The (cutting) plane can be translated and rotated. This furnishes a stack of images as shown in Figure 2.

SPIM seems to be the current state-of-the-art for studies of cancer development. How-

[1]Special thanks to Pierre Weiss (Institut de Mathématiques de Toulouse) for providing information about the SPIM technology.

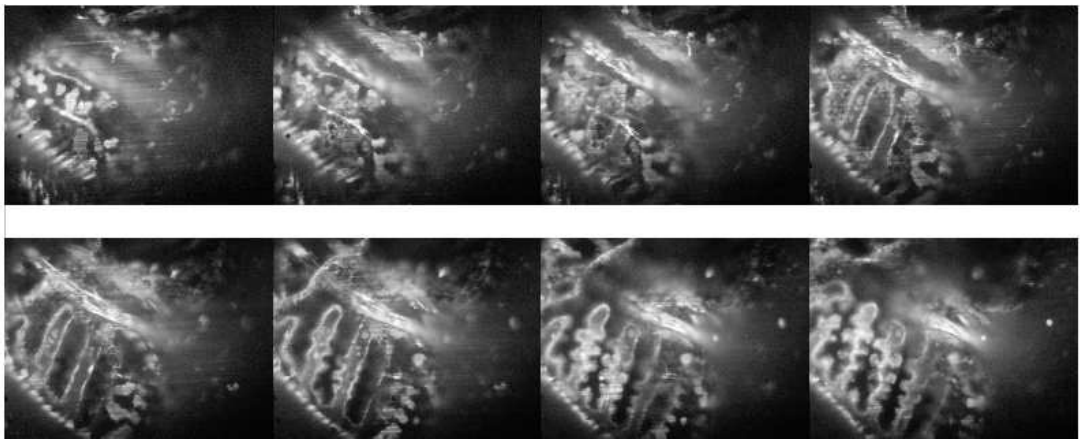

Figure 2: An example of cross-sections (of gills of a fish embryo), generated by the SPIM developed in the LBCMCP laboratory in Toulouse (UMR5088).

ever, it still requires heavy developments in order to be used at its fullest. Since the slices provided by SPIM have different orientations and positions, the reconstruction of 3D structures using these data is a difficult inverse problem that is still open. In order to apply reconstruction methods from cross-sections, a first step would be to develop techniques that detect efficiently the contours of the biological structures in each slice.

We caution that this image **segmentation** step, a requirement of the methods we consider in this thesis, is a major issue. Typical image-segmentation approaches used for medical images are thresholding, manual editing, and region growing. Figure 3 shows an example. The difficulty of the segmentation procedure is directly related to how noisy the images are. This is a major issue specially for ultrasound images, in which the noise level is extremely high. However, in spite of noisy data, we believe that the theoretical guarantees provided in this thesis may help to provide solid foundations in order to improve simulations by freehand 3D ultrasound.

Freehand 3D-Ultrasound

For more than 40 years, ultrasound has been extensively used in medical imaging, which has proved helpful for the diagnosis and staging of disease. Although three-dimensional ultrasound (3DUS) is available for more than 10 years, it was only through the development of the most recent computer technologies and its adjustment to ultrasound systems that 3DUS attained the high level of sensitivity and performance required to be seriously considered in clinical practice. This ability of providing data in any plane and in any direction has enormous potential for medical ultrasound diagnosis.

Conventional freehand 3D ultrasound is performed with a hand-held probe which transmites ultrasound pulses into the body and receives the echos. The magnitude and timing of the echos are used to create a 2D gray scale image of a cross-section of the body in the scan plane. A position sensor is attached to the probe that is used to determine the

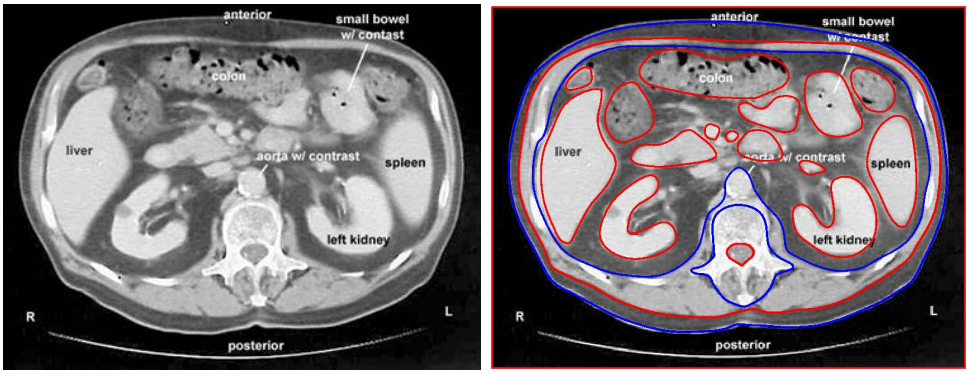

Figure 3: In order to apply the reconstruction methods provided in this thesis, a segmentation step is required to extract the contours of each slice.

positions and the orientation of the cross-sections (cutting planes). Since the motion of the probe is unconstrained, the cutting planes are arbitrarily oriented. The goal of freehand 3D ultrasound techniques is to construct a 3D approximation of the organ from a series of 2D ultrasonic images.

3D ultrasound has the potential to be a revolutionary powerful tool of perinatal medical sonography, see Figure 4. This is a very active research area, and a comprehensive survey of the actual techniques can be found in [KMA+07]. Figure 5 (extracted from this survey) shows some examples of 3D reconstruction of fetal facial expression.

Figure 4: A figure from Web: an example of 3D reconstruction of a fetal using the newest technologies.

Due to the lack of resarch examinning the quality of the simulations, 3D ultrasound is not yet widely used in prenatal diagnosis. Additional research is needed to provide diagnostic tools to determine the clinical role of 3D ultrasound for the diagnosis of disease, anomalies and detection of abnormal behavior in high-risk fetuses. The hope is that the theoretical guarantees we present in this thesis help to provide solid foundations for

ultrasound diagnostic software.

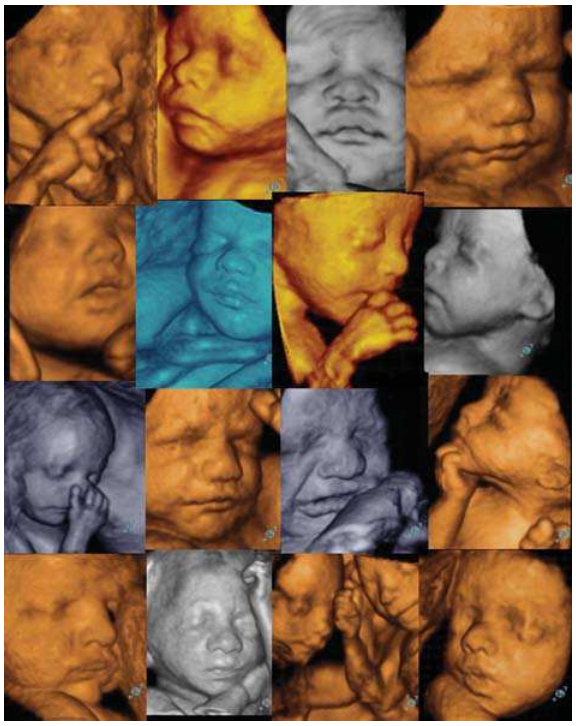

Figure 5: A figure from [KMA+07] (with permission): 3D reconstruction of fetal facial expression.

Particle Image Velocimetry

Another potential application is particle image velocimetry (PIV) which is an optical method of fluid visualization. It is used to obtain instantaneous velocity measurements and related properties in fluids. The fluid is seeded with tracer particles which follow the flow dynamics. It is the motion of these seeding particles that is used to calculate velocity information of the flow being studied. In general, the particles are illuminated by pulsed sheets of light at precise time intervals to produce images that are recorded on photographic film or on a video camera array (see for example [Pra00] for more details). Other techniques used to measure flows are Laser Doppler velocimetry and Hot-wire anemometry. The main difference between PIV and those techniques is that PIV produces two dimensional vector fields, while the other techniques measure the velocity at a point.

In general, PIV system requires four basic components:

1. An optically transparent test-section containing the flow seeded with tracer particles;
2. A light source (laser) to illuminate the region of interest (plane or volume);

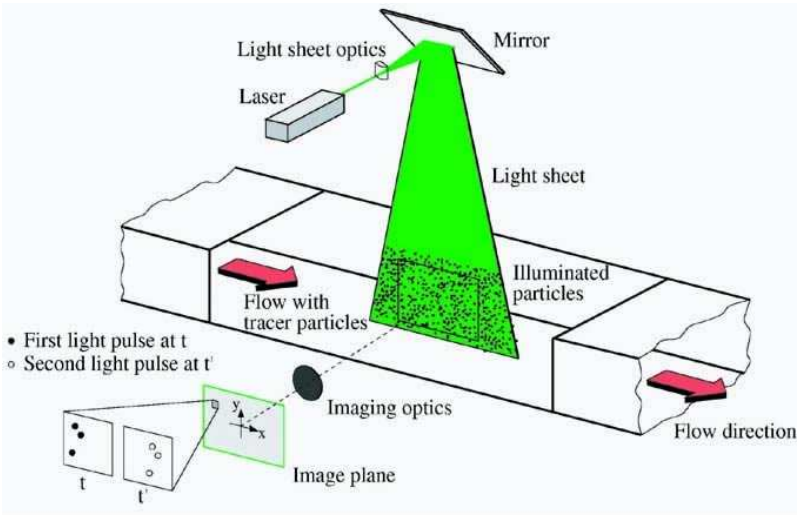

Figure 6: Particle Image Velocimetry System.

3. Recording hardware consisting of either a CCD camera, or film, or holographic plates;

4. A computer with a *reconstruction software* to process the recorded images and extract the 3D velocity information from the tracer particle positions.

The reconstruction procedure consists of approximating the 3-dimensional velocity information from a set of 2-dimensional sections. Many types of algorithms for PIV reconstruction have been developed from simple cross-correlation method to binary image cross-correlation method, Delaunay tessellation method [SYIM99], velocity gradient tensor method, variational approach [RGPS05] and recursive cross-correlation method [IM06], etc.

Geology/Geography

Applications have been made in the reconstruction of terrain from topographic elevation data [HSS03], [SJ05] (Figure 7), and of invertebrate fossils from serial grinding data [HJT95], [Nul98]. Such reconstruction methods are also useful in sedimentology and seismology. Figure 7 shows an example of terrain reconstruction from topographic contours proposed in [HSS03]. This corresponds to a particular case of the general reconstruction problem we are considering, since the orthogonal projection of elevation contours are supposed to be nested (and never intersect eachother).

Reconstruction of Coronary Arterial Tree

Let us distinguish some particular anatomical entities such as coronary arterial tree, which consist of thin branching structures distributed over a large volume. The reconstruction

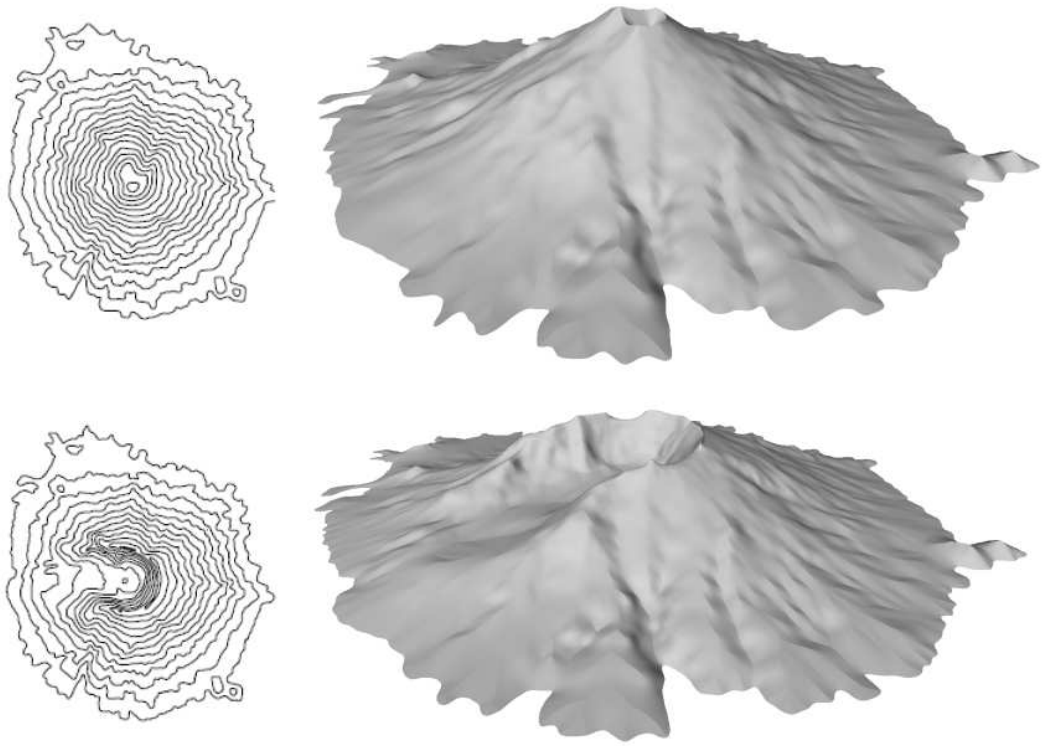

Figure 7: Figure from [HSS03] (with permission), an example of terrain reconstruction from topographic contours.

of such a structure from a sparse sample is a very challenging problem. Most of existing reconstruction methods fail in such complex cross-sectional branching situations. Coronary artery disease is a major cause of death and disability in the world. Investigation of three-dimensional simulation tools in human arteries is an important issue in vascular disease characterization and assessment.

Angiography is the common medical imaging technique used to visualize the arteries, veins and the heart chambers. This is done by injecting a radio-opaque contrast agent into the blood vessel and imaging using X-ray based techniques such as fluoroscopy. The result is a 3D view (image) of vascular structures. The common use of 3D angiography images for the diagnosis of vascular abnormalities provides a natural motivation for three dimensional reconstruction from slices. Indeed, a potential strategy to extract the biological structures from a 3D image is the following:

1. Consider some 2-dimensional cuts (slices) of the 3D-image.

2. Perform a segmentation process on each slice.

3. Reconstruct the 3D structure from the two dimensional extracted contours.

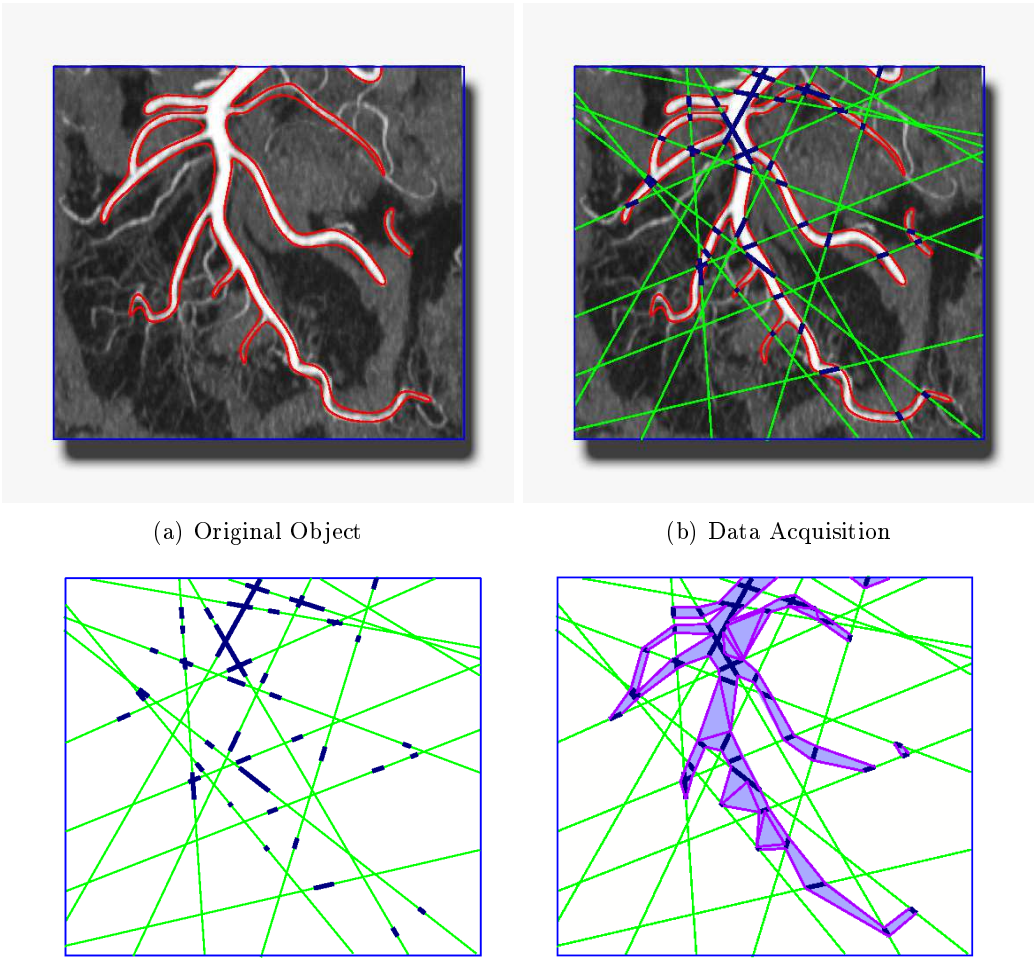

(a) Original Object (b) Data Acquisition

(c) Input of the Algorithm (d) Output of the Algorithm

Figure 8: Reconstruction example of our method presented in [MB08].

The reconstruction step is usually based on some interpolation methods, some classical references can be found in [HMR93]. Considerable improvements have been achieved by more recent works, such as [CM03] by Chen and Molloi which performs complex sequential procedures of 3D image formation, preprocessing, segmentation, thinning, skeleton pruning and tree construction. Note that there exist other techniques that make use of the 3D image directly, and extract the biological structure by variants of classical methods such as Marching-cube or Level-sets, see [AEIR03] for an example. However, to the best of our knowledge, no formal analysis and guarantees have been obtained for existing methods until now. The hope is that the reconstruction algorithm for tree-like structures, that we present in Section 2 of Chapter 3, and its theoretical guarantees help to develop reconstruction software that work satisfactorily in such complex branching situations. The reconstruction example from a set of 14 sections, illustrated in Figure 8, shows how the 2-dimensional variant of our algorithm performs well in such cases.

Geometrical Point of View

Another motivation for the reconstruction from cross-sections is from a proper geometrical point of view. The d-dimensional framework of the problem consists of reconstructing a d-dimensional shape from its intersections with hyperplanes, of dimension $(d-1)$. Finding efficient methods for this reconstruction problem may be used in *topological coding of objects* or in *dimension reduction strategies*. Adding *time* as the fourth dimension to three-dimensional space, the fourth dimensional variant of the reconstruction problem can be applied to *moving objects* (for example the beating heart). In the sense that the movement of the object can be reconstructed knowing the position of the object at some constant values of time.

While the reconstruction from cross-sections is of utmost importance in many fields, no reconstruction method from cross-sections came with theoretical guarantees before this thesis. Even in the case of parallel cross-sections, no formal analysis and guarantees have been obtained. This contrasts with the problem of reconstructing a shape from unorganized point sets, which is now well understood both theoretically and practically. To give more intuition, let us analyze the topological guarantees that have been developed for the reconstruction problem from point sets. The proofs of correctness of these methods rely on sampling conditions that control the local density of the sample points (the input).

Closed Ball Property The first sampling condition for reconstruction from point sets was introduced by Edelsbrunner and Shah [ES97] and is called the *Closed Ball Property*. Let $\mathcal{O}$ denote the original shape and S be a set of sample points. The closed ball property states that every d-face of the Voronoi diagram of the sample points S has an intersection with $\mathcal{O}$ that is either empty or topologically equivalent to a d-ball. Edelsbrunner and Shah proved that, under this condition, some subcomplex of the Delaunay triangulation of S, called $\mathrm{Del}_{|\mathcal{O}}(S)$, has the same homotopy type as $\mathcal{O}$.

ϵ-samples Amenta and Bern [AB99] proposed the ϵ-sampling condition for reconstructing smooth surfaces. A finite set S of sample points of $\mathcal{O}$ forms an ϵ-sample of $\mathcal{O}$ if every point p of $\mathcal{O}$ is closer to S than $\epsilon d(p, \mathrm{MA}(\mathcal{O}))$, where $\mathrm{MA}(\mathcal{O})$ is the medial axis of $\mathcal{O}$ (defined in Section 4 of this introduction). Amenta and Bern proved that, if S is a ϵ-sample of $\mathcal{O}$, for a sufficiently small ϵ, then the Closed Ball Property of Edelsbrunner and Shah is satisfied. Hence, $\mathrm{Del}_{|\mathcal{O}}(S)$ has the same homotopy type as $\mathcal{O}$. They also proved that $\mathrm{Del}_{|\mathcal{O}}(S)$ lies at Hausdorff distance $\epsilon^2 c(\mathcal{O})$ from $\mathcal{O}$, where the constant $c(\mathcal{O})$ depends only on $\mathcal{O}$.

Sectional Data Compared to Point Cloud Data

Suppose that we are given a set of cross-sections of an unknown shape $\mathcal{O}$. Consider a sample S of the given cross-sections or their boundaries (contours). A natural idea is to apply provably good reconstruction methods from point clouds to these sample points. For example, $\mathrm{Del}_{|\mathcal{O}}(S)$ that is homotopy equivalent to $\mathcal{O}$, if the closed ball property is verified.

Let us study the closed ball property in this case by considering the Voronoi diagram of the sample points. As the 2D example of Figure 9 shows, the Voronoi cell of a point b on a plane P forms a thin quadrilateral orthogonal to P. To ensure the closed ball property, the intersection of such a thin quadrilateral with $\mathcal{O}$ should be *contractible*. Clearly, even the *connectivity* of this intersection is a very strong condition and is unverifiable in practice. Therefore, the closed ball property is not an appropriate sampling condition for reconstruction from cross-sections. In this thesis, we present a similar Delaunay-based algorithm for the case of cross-sections, with appropriate sampling conditions. These conditions are better adapted to the problem of reconstruction from cross-sections, and make use of the additional given information (with respect to point clouds) which is the planes orientations.

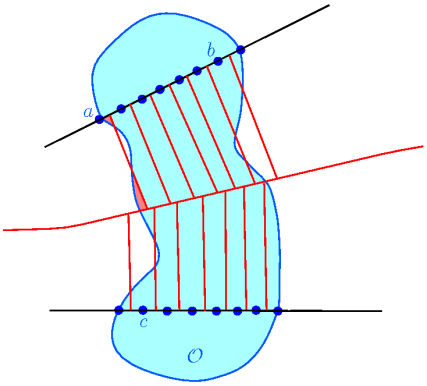

Figure 9: A 2D shape $\mathcal{O}$ (in blue) is cut by two lines (in black). Take a sample of the two sections of $\mathcal{O}$ and consider the Voronoi diagram of the sample points (restricted to the region between the two cutting lines). The Voronoi cells of points a, b and c intersect $\mathcal{O}$ in non-connected sets.

It is difficult to compare the conditions that we will propose with $\epsilon-$sample condition. Indeed, these conditions imply that the sample is a 2-sample, and the converse is not true.

2 Previous Work

The reconstruction problem from unorganized cross-sections has been considered in 2D and 3D. Few methods exist for reconstructing 2D shapes from line cross sections. The incremental algorithm proposed by Coll and Sellares in [CS01] processes the cutting lines sequentially. At each step, a new line is added and the reconstruction is updated. The time complexity of each step is logarithmic in the total number of cutting lines.

The work by Sidlesky, Barequet and Gotsman [SBG06] studies the topological properties of the possible solutions of the 2D reconstruction problem from cross-sections. The authors make use of the arrangement of the cutting lines and consider the portions of one-dimensional cross-sections lying on the boundary of each cell of the arrangement. Then,

using some inter-cell relations, they enumerate all possible classes of homotopy equivalent reconstructions that conform to the given cross-sections, see Fig 10 for an example. However, as it is mentioned in [SBG06], the related question of finding conditions for

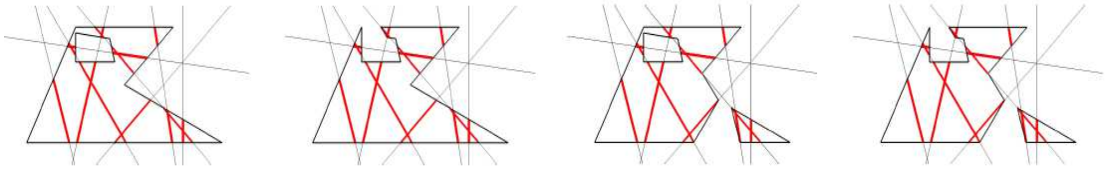

Figure 10: Four reconstructions from a same input, presented in [SBG06] (figure taken with permission).

uniqueness of the reconstructed object with consistent topology remained open. In Section 3 of Chapter 1, we also provide an answer to this question by giving appropriate sampling conditions for reconstruction from line cross-sections. To the best of our knowledge, this is the only work that guarantees a topologically correct solution for the 2D reconstruction problem from cross-sections.

Let us now study the 3-dimensional existing methods. In 3D, different configurations can be considered for the cutting planes, as it is illustrated in Figure 11. A so-called *serial sequence* of planes partitions the space into several *slices*, each bounded by a pair of cutting planes. The classical case, that has been considered widely in the previous work, is the case of parallel cutting planes. The reconstruction of a shape cut by a serial sequence of planes can be done in the slices bounded by two consecutive planes, independently. This technique has been employed in most of reconstruction methods from parallel (or serial) cross-sections, that we will survey in the next section.

In the general case, the cutting planes may be arbitrarily oriented. The purpose of this thesis is reconstructing a 3D shape from its sections with arbitrarily oriented cutting planes. In the literature, this problem is also known as reconstruction from *unorganized or multiaxial or non-parallel* cross-sections. The few existing methods on this area will be studied in Section 2.2 of this introduction.

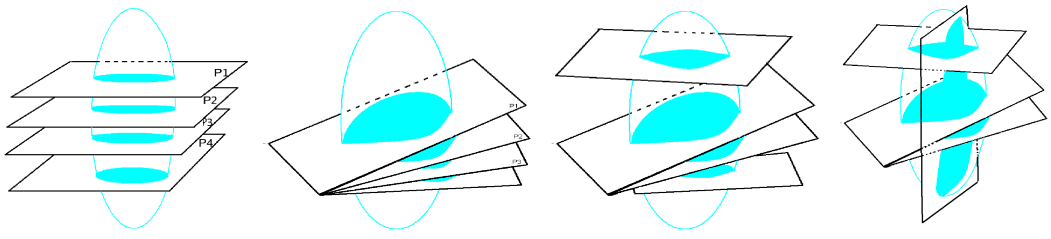

(a) Parallel serial sequence of planes

(b) Non-parallel serial sequence

(c) Unorganized cutting planes

Figure 11: Different cross-sections configurations in 3D case of the problem.

2.1 Parallel Sections

The existing techniques for reconstruction from parallel sections may be roughly classified into two main groups: the *surface extraction* and the *tiling* approaches.

Functional Approach

In a functional approach, the surface is *indirectly* extracted from a volume generated by the sections. The surface can be obtained as the zero-set of a scalar function with 3D argument (implicit surfaces) or as mappings from a pair of parameters to 3D space (parametric surfaces).

Implicit Surfaces : In surface reconstruction from cross-sections, the surface may be the zero-set of a generalized distance function to the given section-contours. For example, we refer the reader to [COL96], [Da02], [Bra05] and [MBMB06].

Parametric Surfaces : B-splines are the most widely used parametric surfaces. B-splines have been used for reconstruction from parallel cross-sections by [PK96] and [PT96], as well as the hybrid approach proposed in [Par05] which uses B-spline surface approximation. We can also cite the recent work [GGK06] of Gabrielides et al. that can create smooth branching between the contours.

The *voxel-reconstruction* techniques can also be classified as isosurfacing methods. These techniques are currently used in most of existing 3D medical imaging softwares. We can cite Marching Cubes (introduced in [LC87], and (corrected and) completed in [NH91]), that is widely used in softwares, but no theoretical guarantees are available to make the resulting reconstruction appropriate for diagnosis.

Tiling Approach (Correspondence, Interpolation and Branching)

In a tiling approach, the surface is *directly* constructed by interpolating the section-contours. Most of tiling methods assume that the contours are *sampled* and are given as polygons. The surface itself is made up of triangle-strips to be constructed between the points that belong to each couple of consecutive contours.

In Meyers' Ph.D-thesis [Mey94], on reconstruction from parallel sections, the problems related to tiling approaches are divided into three main groups: *correspondence* problem, *interpolation* problem and *branching* problem.

Correspondence Problem The correspondence problem consists of defining the topological adjacency relationships between the contours and the holes of consecutive sections. A commun technique to solve this problem, used in most of previous work as [EPO91] and [CP94], is to superpose the contours of two adjacent cross-sections, and to consider them as connected if they overlap.

In Chapter 1 of this thesis, a generalization of this *overlapping criterion* for the case of unorganized cross-sections, proposed by Liu et al. in [LBD+08], is analyzed. Moreover, we show that under appropriate sampling conditions, the resulting adjacency relationships between the contours preserves the topology of the original object.

Interpolation Problem Having defined the connectivity between the contours, the central problem consists in finding the best interpolating surface between two adjacent contours. Since Keppel's work [Kep75] on interpolation between parallel polygonal contours, numerous algorithms were introduced for parallel inter-slice interpolation. The problem is considered to be quite difficult because the topology of the contours may change between slices. Most of former methods can not handle branching between the contours and assume that there is a one-to-one correspondence between the contours. Using this correspondence, the interpolating surface (triangulation) is determined by constrained optimization of various costs. The earliest solution [Kep75] by Keppel maximized the volume of the reconstruction for convex contour segments and minimized it for concave segments. This was soon followed by Fuchs et al. in [FKU77], with a minimal surface area solution. Other criteria have included minimal length of the next edge in [CS78], optimal verticality of the edges in [GD82], minimal radii of circumscribed circles of triangles (a variant of Delaunay triangulation of the contours) in Meyers' Ph.D thesis [Mey94], and minimal sum of absolute value of angle between the contour edge parts of successive triangles [WW94]. More criteria are provided in [DP97] and [Zse05].

Most of these interpolation techniques will fail when confronted with contours which cannot be interpolated without the addition of extra vertices. In such *branching* cases, these methods may lead to self-intersecting surfaces.

Branching Problem In the earliest branching method [CS78], Christiansen and Sederberg proposed to concatenate all contours in one cutting plane into a single contour using new edges called bridges. In [EPO91], in order to simplify the branching, each contour is decomposed into elementary convex subcontours. [CP94] reduces branching problems to a series of one-to-one cases by generating new slices between the input slices.

Some significant progress was made with the introduction of the Delaunay-based technique of Boissonnat [Boi88], and the method of Bajaj et al. [BCL96]. Both approaches attempt to handle the most general case, in which the geometries and topologies of the contours in every slice are totally unrestricted. Subsequently, Barequet and Sharir [BS96] suggested an interpolation method based on geometric hashing.

The necessary addition of extra vertices within a contour to provide suitable splitting points for branching was addressed for the first time by Shantz in [Sha81]. In this method the additional points are obtained by projection of the medial axis of the sections of one cutting plane onto the adjacent plane. This method of approximating the branching locus have been followed since then in several methods as [CP94], [BG93]. (In Section 4.1 of Chapter 2 of this thesis, we will generalize and justify this branching locus.) Later, Barequet et al. [BGLSS04] suggested another interpolation algorithm that uses the medial axis of the superposition of the two slices.

A commun interpolation technique that can handle the branching between neighboring sections consists of defining a parametric domain using the superposition of the contours of the two adjacent sections. The mapping is implicitly defined through some form of interpolation of the Z coordinates of the neighboring sections. In many approaches, the parametric domain is triangulated and then the resulting triangulation is mapped to three dimension. As examples of methods based on parametric domain triangulation we can cite [OPC96], [CP01], [WHMW06].

Delaunay-Based Approach

The 3D reconstruction method that we will present in this thesis is based on Delaunay triangulation. Delaunay-based reconstruction from parallel cross-sections has been investigated by Boissonnat in [Boi88]. This approach simultaneously handles the correspondence, interpolation and branching problems. Using the properties of Delaunay triangulations, this method produces the largest volume of the triangulation consistent with the contours. An improvement on the branching between dissimilar sections was performed by Boissonnat and Geiger in [BG93], by adding vertices inside the contours. These *additional points* lie on the projection of the medial axis of the adjacent contour, as had been proposed in [Sha81]. However, Boissonnat and Geiger indicated how these points could be efficiently obtained from the Delaunay triangulations of the sections. Figure 12 illustrates a reconstruction result of this method. Some variants of this method for the case of serial cross-sections have been studied and implemented, for example [TCC94] and [CD99]. Some implementations, as [DVA+96], are currently used in some medical imaging labs.

In [BCDT96], the authors provide an efficient output sensitive algorithm to compute the Delaunay triangulation of a set of n points that lie on two planes, in $O(n\log(n) + t)$ time, where t is the size of the output (number of tetrahedra in the triangulation). This result allows an efficient computation of the Delaunay triangulation for Delaunay-based reconstruction methods from serial cross-sections.

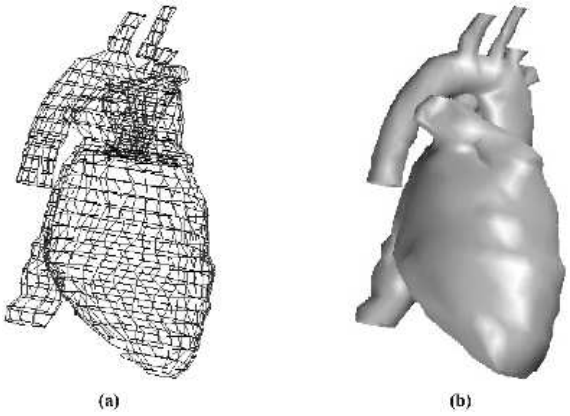

Figure 12: A reconstruction example of [BG93] Delaunay-based method.

In 1997 in a technical report [DP97], Dance and Prager have presented a generalization

of Boissonnat and Geiger's method for the case of unorganized cross-sections. In [BM07], we presented a more complete generalization of [BG93] method for the case of unorganized cross-sections. This work is presented in Section 2 of Chapter 3 of this thesis.

2.2 Unorganized Sections

We now consider the more difficult problem of 3D reconstruction from arbitrarily oriented (unorganized) cross-sections (see Figure 11-c). The need for such reconstructions is a result of the advances in medical imaging technology, as we mentioned in the previous section.

While the reconstruction from unorganized cross-sections is of utmost importance in many fields, it is only very recently that this reconstruction problem has been considered: A very first work [PT94] by Payne and Toga was restricted to easy cases of reconstruction that do not require branching between the sections. In [BG93], Boissonnat and Geiger proposed a Delaunay-based algorithm for the case of serial planes, that has been generalized to arbitrarily oriented planes in [DP97] and [BM07]. Some more recent work [LBD+08] and [BV09] can handle the case of multilabel sections (multiple materials). Barequet and Vaxman's work [BV09] extends the work of [LBD+08] and can handle the case where the sections are only partially known. This method makes use of straight skeletons of polyhedra, can be cited as the most recent work that appeared in this area. Most of

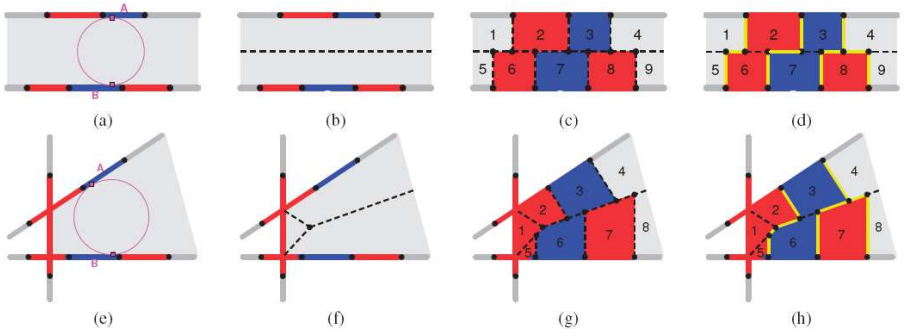

Figure 13: A projection-based method proposed in [LBD+08]: In each cell of the arrangement of the cutting lines, the medial axis of the cell is computed. The sections are lifted orthogonally onto this medial axis. Two sections are connected in the reconstruction if their lifts on the medial axis of the cell intersect.

existing methods for the case of parallel cross-sections are based on the simple idea of connecting two sections if their orthogonal projections overlap. In a recent paper, Liu et al. [LBD+08] proposed a generalization of this *overlapping criterion* to the case of unorganized cross-sections. (Indeed, this method is based on an approach for the case of parallel cross-sections proposed in [JWC+05].) Following the divide-and-conquer step we proposed in [BM07], the arrangement of the cutting planes is first constructed, then the reconstruction problem is solved in each cell independently. To reconstruct the portion of the object that lies in a given cell of the arrangement, this method makes use of the medial axis of the cell (also called the Voronoi Skeleton of the cell). Two sections are connected in

the reconstruction if their *lifts* on the medial axis of the cell intersect. Figure 13 describes this criterion that is a generalization of the overlapping criterion for the case of parallel sections. (In the first chapter of this thesis, we analyze this method and prove that under some appropriate provided sampling conditions, the reconstructed object is homeomorphic to the original shape.)

3 Overview of the Thesis

Let us summarize the content and the contributions of this thesis. Here is the problem we consider.

3.1 Statement of the problem

Let $\mathcal{O} \subset \mathbb{R}^3$ be a compact 3-manifold with boundary (denoted by $\partial\mathcal{O}$) of class C^2. The manifold $\mathcal{O}$ is cut by a set $\mathcal{P}$ of so-called cutting planes that are supposed to be in general position in the sense that none of these cutting planes are tangent to $\partial\mathcal{O}$. For any cutting plane $P \in \mathcal{P}$, we are given the intersection $\mathcal{O} \cap P$. There is no assumption on the geometry or the topology of these intersections. The goal is to reconstruct $\mathcal{O}$ from the given intersections. The problem being ill-posed, we are interested in finding an approximation $\mathcal{R}$ of $\mathcal{O}$ such that $\mathcal{R}$ is homotopy equivalent to $\mathcal{O}$ and the intersections of $\mathcal{R}$ with all the cutting planes in $\mathcal{P}$ coincide with the given sections (this is called the *conformity* of the reconstructed object with the given sections).

3.2 Arrangement of the Cutting Planes

We can decompose the problem into several subproblems as follows. Consider the *arrangement of the cutting planes*, i.e., the subdivision of $\mathbb{R}^3$ into convex polyhedral cells induced by the cutting planes. Without loss of generality, we can restrict our attention to a cell of this arrangement and reduce the reconstruction of $\mathcal{O}$ to the reconstruction of $\mathcal{O}_\mathcal{C} := \mathcal{O} \cap \mathcal{C}$ for all cells $\mathcal{C}$ of the arrangement. Since the various reconstructed pieces will conform to the given sections, it will be easy to glue them together in the end to get the overall reconstructed object $\mathcal{R}$.

We note that the computation of the arrangement of k planes can be done in $O(k^3)$ time, according to [Ede87]. However, in Section 5 of Chapter 2, we will present an easy way to find the groups of sections that are on the same cell of the arrangement of the cutting planes. This allows us to avoid the computation of the entire arrangement of the cutting planes.

Sections: Input of the Reconstruction Algorithm. We now focus on a cell $\mathcal{C}$ of the arrangement and describe how the reconstructed object $\mathcal{R}_\mathcal{C}$ is defined in $\mathcal{C}$. On each face f of $\mathcal{C}$, the intersection of the object $\mathcal{O}$ with f is given and consists of a set of connected regions called *sections*, see Figure 14.

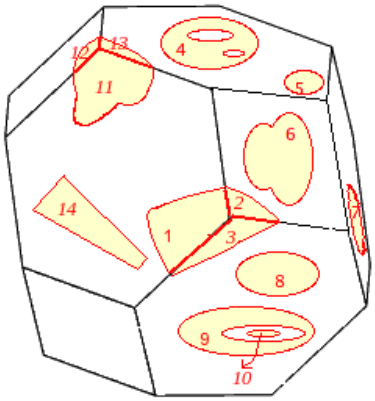

Figure 14: A section is a connected component of the intersection of $\mathcal{O}$ with a face of a cell of the arrangement. This cell has 14 sections.

By definition, the sections of a face of $\mathcal{C}$ are disjoint. However, two sections (on two neighbor faces of $\mathcal{C}$) may intersect along the intersection between their two corresponding faces. The boundary of a section S is denoted by ∂S and is a set of closed curves, called *section-contours*, that may be nested. In the sequel, $\mathcal{S}_\mathcal{C}$ denotes the union of sections of all the faces of $\mathcal{C}$, and a point of $\mathcal{S}_\mathcal{C}$ is called a *section-point*.

3.3 Methodology

We know that a point on the boundary of $\mathcal{C}$ is in $\mathcal{O}$ if it lies in $\mathcal{S}_\mathcal{C}$. The goal is now to determine whether a point x inside $\mathcal{C}$ belongs to $\mathcal{O}$ or not. The reconstruction method that we will present is based on the notion of *distance from* $\partial\mathcal{C}$ (the boundary of $\mathcal{C}$):

A point $x \in \mathcal{C}$ is in the reconstructed object if one of its **nearest points** in $\partial\mathcal{C}$ is in $\mathcal{S}_\mathcal{C}$.

Different distance functions (from the boundary of $\mathcal{C}$) may be used in order to satisfy properties of interest for different applications. For example, to impose a favorite direction to connect the sections, or to promote the connection between sections in the case of sparse data (as we will see in Chapter 2). A natural idea is to use the Euclidean distance as the distance function from $\partial\mathcal{C}$. In this case, the reconstructed object coincides with the method introduced by Liu et al. in [LBD+08].

Consider the medial axis of the cell (also called the Voronoi Skeleton of the cell). For each point a in a section A, the locus of all the points $x \in \mathcal{C}$ that have a as their nearest point in $\partial\mathcal{C}$ is the line segment joining a to its *lift* on the Voronoi Skeleton of the cell. Therefore, the reconstructed object $\mathcal{R}_\mathcal{C}$ is the union of all the line-segments $[a, \text{lift}(a)]$ for a point a in a section $A \in \mathcal{S}_\mathcal{C}$. By this definition, two sections are connected in the reconstructed object if their *lifts* on the medial axis of the cell intersect. See Figure 15-middle.

This method is *symmetric* with respect to the sections and their complementary in each cutting plane, in the sense that the points on the boundary of $\mathcal{C}$ that are *in* or *not in* $\mathcal{S}_\mathcal{C}$

play a symmetric role in the reconstruction procedure. This is due to the fact that the definition of the nearest point in $\partial\mathcal{C}$ to a point $x \in \mathcal{C}$, does not depend on the object and its sections.

In the first chapter of this thesis we will analyze this method and present appropriate sampling conditions providing topological guarantees for the resulting reconstructed object. This is the first time that reconstruction from cross-sections comes with theoretical guarantees.

In the second chapter, we propose a method with a different distance function from the boundary of $\mathcal{C}$ which depends on $\mathcal{O}$ and is based on the Voronoi diagram of the sections. Consider the 2-Skeleton of the Voronoi diagram of the sections, called the Voronoi Skeleton of the sections. For each point $x \in \mathcal{C}$ and in the Voronoi cell of a section A, the nearest point to x in the boundary of $\mathcal{C}$ is the projection of x onto the boundary of $\mathcal{C}$ in the direction orthogonal to A. A point $x \in \mathcal{C}$ is in the reconstructed object $\mathcal{R}'_{\mathcal{C}}$ if one of its **nearest points** in $\partial\mathcal{C}$ is in $\mathcal{S}_{\mathcal{C}}$. By this definition, two sections are connected in the reconstruction if their *lifts* on the Voronoi Skeleton of the sections intersect. See Figure 15-right.

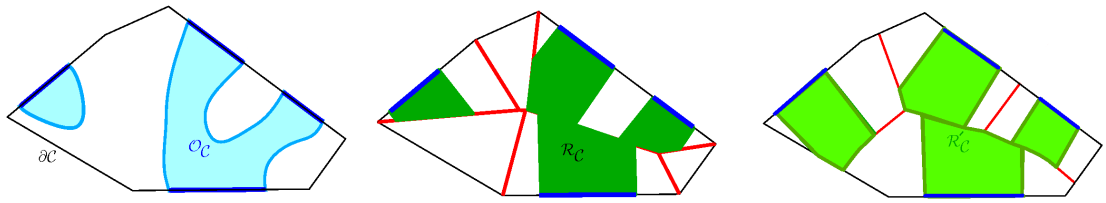

Figure 15: Reconstruction example in a cell of the arrangement: Left) Unknown Object in blue. Middle) First Reconstructed Object in green, Voronoi Skeleton of the cell in red. Right) Second Reconstructed Object in green, Voronoi Skeleton of the sections in red.

The main idea is that with this new distance function we increase *the influence zone* of each section compared to the first method. Such an *asymmetric* function allows us to perform more connections between the sections, and is motivated by reconstruction of tree-like structures which consist of thin branching structures distributed over a large volume.

Another motivation for presenting this Voronoi-based method is its dual *Delaunay-based* approach. Indeed, the Delaunay-Voronoi duality, leads us to a third method which is presented in Chapter 3. This method can be seen as the generalization of Boissonnat and Geiger's method [BG93] to the case of unorganized sections. Unlike the two first methods, this method cannot be presented with a distance function to $\partial\mathcal{C}$ and a lifting procedure. However, as we will see, we can compare the connectivity between the sections induced by these three methods as follows:

Let $\mathcal{G}$, $\mathcal{G}'$ and $\mathcal{G}''$ be the connectivity graph between the sections induced by Methods 1, 2 and 3 respectively. Then $\mathcal{G}$ is a subgraph of $\mathcal{G}'$, and $\mathcal{G}'$ itself is a subgraph of $\mathcal{G}''$, i.e., $\mathcal{G} \subseteq \mathcal{G}' \subseteq \mathcal{G}''$. Figure 16 compares the connectivities between a set of four sections performed by the three methods.

In other words, if two sections are connected by the two first methods, then they are connected in the resulting reconstruction of the third method as well, and moreover additional connection may be performed. Increasing the connectivity between the sections is motivated by reconstructing tree-like structures from sparse sectional data. The preliminary experimental results of the third method, presented in Chapter 3, are quite promising, regarding the practicality of the approach to reconstruct complex cross-sectional branching situations such as the coronary arterial tree. See Figure 8 for a 2D example.

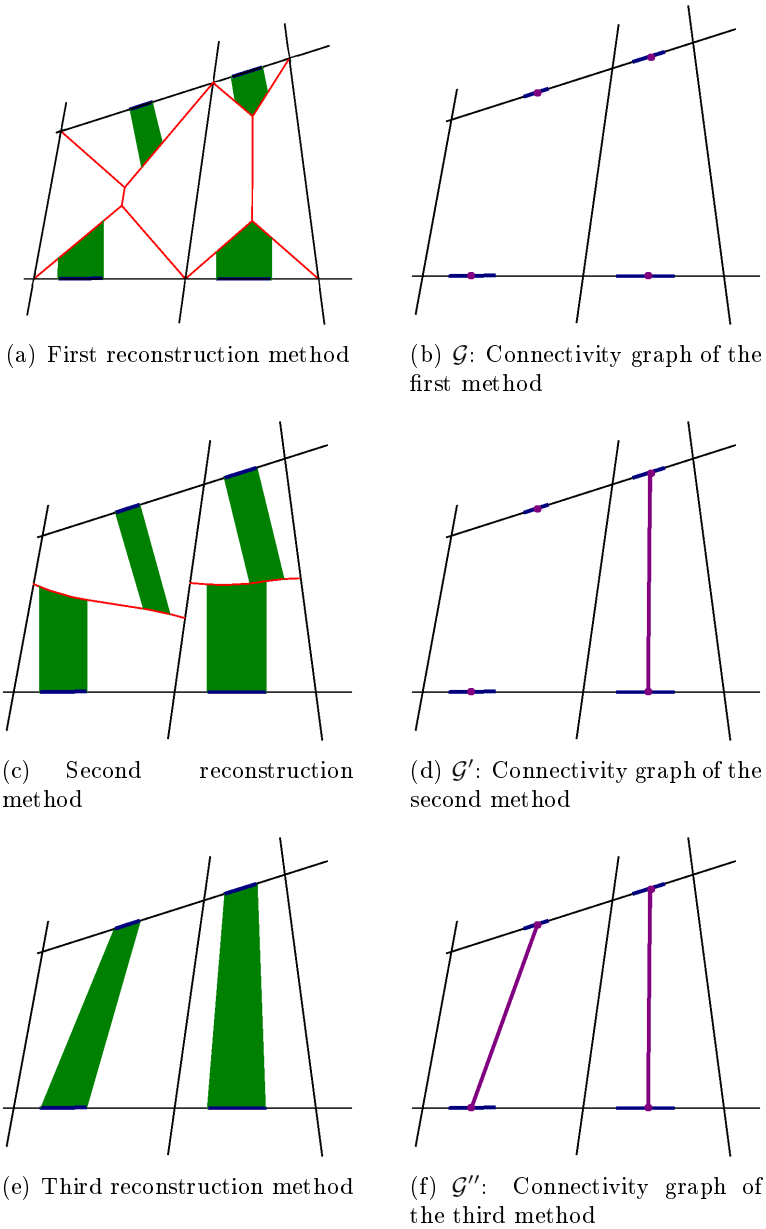

(a) First reconstruction method

(b) $\mathcal{G}$: Connectivity graph of the first method

(c) Second reconstruction method

(d) $\mathcal{G}'$: Connectivity graph of the second method

(e) Third reconstruction method

(f) $\mathcal{G}''$: Connectivity graph of the third method

Figure 16: The connectivity performed by the three methods presented in this thesis.

3.4 Contributions

We list the main contributions of this thesis below:

First Method

A theoretical analysis of the method proposed by Liu et al. in [LBD+08] is carried out. We prove that under appropriate sampling conditions, the connection between the sections provided by this method is coherent with the connectivity structure of the object, and the proposed reconstructed object is homotopy equivalent to the object. Moreover, under these conditions, we provide a homeomorphism between the reconstructed object $\mathcal{R}$ and the original shape $\mathcal{O}$, and prove that they are indeed isotopic. Here is a summery of the topological guarantees presented in the first chapter of this thesis:

Let $\mathcal{O}$ denote the original shape we want to reconstruct. Consider the boundary of $\mathcal{O}$, denoted by $\partial\mathcal{O}$, as a 2-manifold without boundary embedded in $\mathbb{R}^3$. Let $\mathrm{MA}(\partial\mathcal{O})$ be the medial axis of $\partial\mathcal{O}$. It contains two different parts (see Figure 17) : the so-called *internal* part, denoted by $\mathrm{MA}_i(\partial\mathcal{O})$, which lies in $\mathcal{O}$ and the so-called *external* part, denoted by $\mathrm{MA}_e(\partial\mathcal{O})$, which lies in $\mathbb{R}^3 \setminus \mathcal{O}$. In particular, if $\mathcal{O}$ is convex then $\mathrm{MA}_e(\partial\mathcal{O})$ is empty.

The key idea is to make use of $\mathrm{MA}_i(\partial\mathcal{O})$ which has the same homotopy type as $\mathcal{O}$, which is trivial due to the fact that the boundary of $\mathcal{O}$ is supposed to be of class C^2. [2]

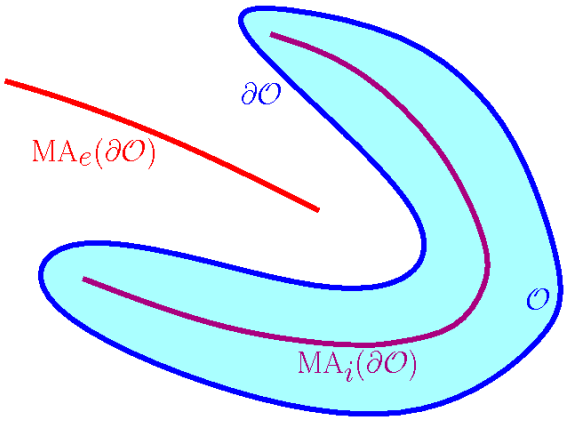

Figure 17: Internal and external parts of the medial axis of $\partial\mathcal{O}$.

Given a cell $\mathcal{C}$ of the arrangement, let us define $\mathrm{reach}_{\mathcal{C}}(\mathcal{O})$ as the distance of the boundary of $\mathcal{O}$ from (the union of the two parts of) its medial axis, in a neighborhood of $\mathcal{C}$ (see Section 2.3 of Chapter 1 for a formal definition). We also define the height of the cell $\mathcal{C}$,

[2] This *double-smoothness* assumption is to simplify a technical part of the homotopy equivalence proof. Indeed, the same topological guarantees hold for a more general case where $\partial\mathcal{O}$ is of class $C^{1,1}$ (i.e., it is continuously differentiable and its normal satisfies a Lipschitz condition). The proof is generally the same, except the retraction from $\mathcal{O}$ to $\mathrm{MA}_i(\partial\mathcal{O})$ which is more sophisticated and makes use of Lieutier's work [Lie04].

denoted by $h_{\mathcal{C}}$, as the maximum distance of a point $x \in \mathcal{C}$ to the boundary of $\mathcal{C}$ (which is less than half the diameter of $\mathcal{C}$).

We will propose two sampling conditions for the set of cutting planes, that will be called the *Separation Condition* and the *Intersection Condition*.

• **Separation Condition :** The first sampling condition we consider for the set of cutting planes is called the Separation Condition: This condition requires that the part of the medial axis of $\partial\mathcal{O}$ which lies inside $\mathcal{O}$ lies inside $\mathcal{R}$, and symmetrically, the part of the medial axis of $\partial\mathcal{O}$ which lies outside $\mathcal{O}$ lies entirely outside $\mathcal{R}$. In other words, $\partial\mathcal{R}$ *separates* the internal and the external parts of the medial axis of $\partial\mathcal{O}$. We will show that the Separation Condition is verified if the set of cutting planes is sufficiently dense so that we have:

($C1$) **Density Condition :** for any cell $\mathcal{C}$ of the arrangement, $h_{\mathcal{C}} < \text{reach}_{\mathcal{C}}(\mathcal{O})$.

Connectivity Guarantees : We show that under the Separation Condition, the connectivity between the sections in the reconstructed object $\mathcal{R}$ coincides with the connectivity in the original unknown shape $\mathcal{O}$.

This implies the homotopy equivalence between $\mathcal{R}$ and $\mathcal{O}$ for the two following particular cases:

Case I) Reconstructing Union of Convex Bodies with Topological Guarantees: An efficient adaptation of the algorithm to the case of reconstructing a union of convex bodies is proposed. In Section 3 of Chapter 1, we prove that under the Separation Condition, the resulting reconstructed object is homeomorphic to the original shape.

Case II) 2D Reconstruction from Line-Sections with Topological Guarantees : The Separation Condition offers the same topological guarantees for the 2D variant of the problem (see Section 3 of Chapter 1), and $\mathcal{R}$ is homeomorphic (and isotopic) to $\mathcal{O}$.

However, the Separation Condition does not ensure in general the homotopy equivalence between $\mathcal{R}$ and $\mathcal{O}$. We need to impose a second condition called *Intersection Condition*.

• **Intersection Condition :** For the sake of simplifying the presentation in this introduction, we only give a sufficient condition and refer to Section 4.4 of Chapter 1 for the formal definition of the Intersection Condition. We will show that the Intersection Condition is verified if the cutting planes are *sufficiently transversal* to the boundary of $\mathcal{O}$. More formally, if the following condition is verified:

($C2$) **Transversality Condition :** for any cell $\mathcal{C}$ of the arrangement,

$$h_{\mathcal{C}} < \frac{1}{2}\left(1 - \sin(\alpha)\right) \text{reach}_{\mathcal{C}}(\mathcal{O}),$$

where α is an upper bound on the angle between the cutting planes and the normals to the boundary of $\mathcal{O}$ along the sections.

Remark: As it can be seen, the Transversality Condition is stronger than the Density Condition. However, such a condition based on transversality seems to be reasonable in practice, especially for applications in 3D ultrasound. Since from a technical point of view, if a *cut* is not *sufficiently* transversal to the organ, the quality of the resulting 2D ultrasonic image is not acceptable for diagnosis (see [Rou03] for more technical details).

Main theorem of Chapter 1 : Under the Separation and the Intersection Conditions, the reconstructed object $\mathcal{R}$ is homeomorphic (and isotopic) to the unknown original shape $\mathcal{O}$.

This is the first time that 3D shape reconstruction from cross-sections comes with such theoretical guarantees. Even in the case of parallel cross-sections, no formal analysis and guarantees have been obtained before this thesis.

Second Method

Using the Voronoi diagram of the sections, we present a second method which performs more connections between the sections compared to the first method. In the sense that the new reconstructed object, denoted by $\mathcal{R}'$ contains the reconstructed object of the first method $\mathcal{R}$. Increasing the connectivity between the sections is motivated by constructing tree-like structures from sparse sectional data. Most of existing reconstruction methods fail in such complex cross-sectional branching situations. We prove that the resulting reconstructed object $\mathcal{R}'$ is homeomorphic to the original shape $\mathcal{O}$ under appropriate sampling conditions. The provided sampling conditions, leading to topological guarantees, are well-suited to tree-like structures. In this introduction, we briefly present these sampling conditions and refer to Section 3 of Chapter 2 for formal definitions.

In this context the height of a cell $\mathcal{C}$, denoted by $h'_{\mathcal{C}}$, is defined as the maximum distance of a point $x \in \mathcal{C}$ to the cutting plane of the section A whose Voronoi cell contains x. We define two new quantities that correspond to the distance of the boundary of the object from the internal and external parts of the medial axis:

$$\mathrm{reach}_i(\mathcal{O}) := \min_{m \in \mathrm{MA}_i(\partial\mathcal{O})} d(m, \partial\mathcal{O}) \quad \text{and} \quad \mathrm{reach}_e(\mathcal{O}) := \min_{m \in \mathrm{MA}_e(\partial\mathcal{O})} d(m, \partial\mathcal{O}).$$

The key idea is that usually in thin branching structures $\mathrm{reach}_i(\mathcal{O})$ is much smaller than $\mathrm{reach}_e(\mathcal{O})$. The Density Condition of the first method depends on both $\mathrm{reach}_i(\mathcal{O})$ and $\mathrm{reach}_e(\mathcal{O})$, and may be too restrictive for thin branching structures. Instead, we suggest a *Weak Density Condition* which bounds the height of the cells from above only by $\mathrm{reach}_e(\mathcal{O})$.

($C'1$) Weak Density Condition : For any cell $\mathcal{C}$ of the arrangement $h'_{\mathcal{C}} < \mathrm{reach}_e(\mathcal{O}_{\mathcal{C}})$.

Nevertheless, to ensure good connectivities between the sections, we would need an additional condition, called *Weak Transversality Condition* defined as follows:

($C'2$) Weak Transversality Condition : For any cell $\mathcal{C}$ of the arrangement and for any section A of $\mathcal{C}$, the orthogonal projection of $\partial\mathcal{O}_{\mathcal{C}} \cap \mathrm{V}(A)$ onto the plane of A is at

distance less than $\text{reach}_i(\mathcal{O}_\mathcal{C})$ from the boundary of A. More intuitively, the orthogonal projection of the boundary of the object restricted to the Voronoi cell of A, onto the plane of A, moves of at most $\text{reach}_i(\mathcal{O}_\mathcal{C})$. This is based on how the cutting planes are transversal to $\partial\mathcal{O}$. As we will see in Section 3.2 of Chapter 2, this condition seems reasonable for tree-like structures that are composed of *quasi-linear features* (branches). Indeed, for *piecewise linear shapes*, the Weak Transversality Condition implies $h'_\mathcal{C} < \cot(\alpha)\,\text{reach}_\mathcal{C}(\mathcal{O})$.

Connectivity Guarantees : If the sample of cutting planes verifies the two above sampling conditions, then $\mathcal{R}'_\mathcal{C}$ induces the same connectivity between the sections as $\mathcal{O}_\mathcal{C}$.

Approximation Guarantees : If the sample of cutting planes verifies the Weak Density Condition and the Weak Transversality Condition then we have $d_H(\mathcal{O}, \mathcal{R}') \leq \max_\mathcal{C} h'_\mathcal{C}$, where α is an upper bound on the angle between the cutting planes and the normals to the boundary of $\mathcal{O}$ along the sections.

However, these conditions do not ensure in general the homotopy equivalence between $\mathcal{R}'$ and $\mathcal{O}$. Similarly to the first method, we need to impose a stronger condition :

($C'3$) **Transversality Condition :** For any cell $\mathcal{C}$ of the arrangement :

$$h'_\mathcal{C} < \frac{1}{2}\left(1 - \sin(\alpha)\right)\text{reach}_\mathcal{C}(\mathcal{O})$$

where α is an upper bound on the angle between the cutting planes and the normals to the boundary of $\mathcal{O}$ along the sections. (Note that since $\cot(\alpha) \geq \frac{1}{2}\left(1 - \sin(\alpha)\right)$ for $\alpha \leq \frac{\pi}{2}$, the Transversality Condition is stronger than the Weak Transversality Condition.)

Topological Guarantees (Main theorem of Chapter 2): If the cutting planes verify the Weak Density Condition and the Transversality Condition, then the reconstructed object $\mathcal{R}'$ is homeomorphic (and isotopic) to the unknown original shape $\mathcal{O}$.

Therefore, we obtain the same topological guarantees as the ones we obtained for the first method, under sampling conditions that are better adapted to be satisfied for tree-like structures.

Voronoi-Delaunay Duality : The advantage of considering the Voronoi diagram of the sections, instead of the Voronoi diagram of the cell, is that a dual structure can be defined. The dual structure, that will be called *the spine*, is composed of *Delaunay simplices* between the points of the sections. We will show that the spine has the same homotopy type as $\mathcal{R}'$. As a consequence, the topological guarantees for $\mathcal{R}'$ are valid for the spine as well. We will see that considering the dual structure allows us to improve the appearance of the reconstructed object $\mathcal{R}'$ and leads to a discrete reconstruction algorithm which provides a triangulated surface.

We consider the discrete case of the problem where we are given a set of polygonal contours on the cutting planes. We present an easy way to find the groups of sections

that are on the same cell of the arrangement of the cutting planes. This allows us to avoid the computation of the entire arrangement of the cutting planes. (In particular, we do not need to compute empty cells in which no portion of $\mathcal{O}$ is reconstructed.) We then present a Delaunay-based reconstruction method which characterizes the singularities in the Delaunay structure in each cell of the arrangement, and provide an incremental algorithm to remove them. This algorithm can be seen as a generalization of Boissonnat and Geiger's method [BG93] that was restricted to the case of parallel sections. In that method, in order to improve the branching procedure between the sections, the authors consider some additional points on the orthogonal projection of the medial axis of the sections of one cutting plane onto the adjacent plane. This strategy of approximating the branching locus have been followed since then in several methods. We justify this strategy by characterizing the branching locus of the Delaunay structure in the general case of arbitrarily oriented cutting planes:

We show that in each cell $\mathcal{C}$ of the arrangement, the branching locus of a face f of $\mathcal{C}$ lies on a 2-dimensional *Moebius diagram* (a generalized Voronoi diagram) of the orthogonal projection of the points of the sections on the other faces of $\mathcal{C}$ onto f. (We will see that in the case of parallel planes, this diagram coincides with the projection of the medial axis of the sections of one cutting plane onto the adjacent plane.) Using these diagrams, we provide an efficient algorithm to find the connectivity between the sections induced by the Delaunay simplices, without computing the whole 3D Delaunay triangulation.

This efficient algorithm for the correspondence problem between the sections may be used independently of the Delaunay structure. As we mentioned before, there are methods which consider the correspondence and the interpolation problems independently. So one can use our algorithm to obtain the connectivity and then interpolate the corresponding sections with a different method, depending on the properties of interest for the reconstructed surface in each application.

Third Method

In Chapter 3 of this thesis, we present another Delaunay-based reconstruction. This method is a generalization of Boissonnat and Geiger's method [BG93] to the case of unorganized sections, and performs more connections between the sections compared to the two first methods. Increasing the connectivity between the sections is motivated by reconstructing tree-like structures from sparse sectional data. We have implemented this algorithm in C++, using the CGAL library [CGA]. The preliminary experimental results are promising, regarding the practicality of the approach to reconstruct complex cross-sectional branching situations. The hope is that this thesis will be a first step in providing solid foundations and theoretical guarantees for more sophisticated reconstruction software. A nice extension of our work would be to combine the theoretical guidelines of this thesis with existing image processing techniques for development of medical diagnostic software. We refer to the last section of this thesis which provides some future research directions in order to make a bridge from geometry to medical applications.

4 Preliminaries

4.1 Notations and Terminology

In this section, we state the notations and recall some basic concepts used in this thesis.

Notation Given a subset X of $\mathbb{R}^d$, $int(X)$, $\bar{X}$, and ∂X, stand respectively for the interior, closure, and boundary of X.

Definition 1 (Set Difference) For two sets A and B, the *set difference* $A \setminus B$ is defined as:

$$A \setminus B = \{ x : x \in A \text{ and } x \notin B \}.$$

Definition 2 (Distances between subsets of $\mathbb{R}^n$) Given a point p and a subset X of $\mathbb{R}^n$, the distance from p to X is denoted $d(p, X)$ and defined as follows:

$$d(p, X) = \inf\{d(p, q), q \in X\}$$

If $X = \emptyset$, then $d(p, X)$ is infinite. Otherwise, $d(p, X)$ is finite and non-negative. Moreover, $d(p, X) = 0$ iff (if and only if) p belongs to the closure $\bar{X}$ of X.

Given two subsets X and Y of $\mathbb{R}^n$, the Hausdorff distance between X and Y is

$$d_H(X, Y) = \max\{\sup_{p \in X} d(p, Y), \sup_{q \in Y} d(q, X)\}$$

Note that $d_H(X, Y) = 0$ iff $\bar{X} = \bar{Y}$.

We now present several objects that will be used throughout the thesis.

Definition 3 (Medial Axis, Medial Balls) Let S be a compact subset of $\mathbb{R}^n$. For all point $x \in \mathbb{R}^n$, $\delta(x)$ is defined as the set of the nearest points in S to x, i.e,

$$\delta(x) = \{y \in S, d(x, y) = d(x, S)\}$$

The *medial axis* of S, noted $\mathrm{MA}(S)$, is the topological closure of the set of points of $\mathbb{R}^n$ that have more than one nearest point in S, i.e.,

$$\mathrm{MA}(S) = \{x \in \mathbb{R}^n, |\delta(x)| \geq 2\}.$$

For a point $m \in \mathrm{MA}(S)$, the *medial ball* of m is the open ball centered at m passing through the point(s) of $\delta(m)$. Since $\delta(m)$ is defined as the set of the nearest points in S to m, the medial ball of m is empty of points of S.

We now consider a particular case, where S is the finite union of closed connected subsets of $\mathbb{R}^n$. In such a case, the medial axis of S coincides with a well-known geometrical diagram, called the *Voronoi diagram* of S, defined as follows.

Definition 4 (Voronoi diagrams and Delaunay triangulations) Let S be a collection of finite closed connected subsets of $\mathbb{R}^n$, i.e. $S = \{s_i\}_{i \in I}$, where I is finite and s_i is a closed connected subset of $\mathbb{R}^n$, for all $i \in I$.

The Voronoi cell of s_i is the set of all points of R^n that are closer to s_i than to any other s_j, $j \in I$. The Voronoi diagram of S is the partition of $\mathbb{R}^n$ formed by the Voronoi cells of s_i, $i \in I$.

Definition 5 (Reach) For a point $p \in \mathbb{R}^n$, we call distance to the medial axis at p, and write $d_{\mathrm{MA}(S)}(p)$, the Euclidean distance from p to the medial axis of S. The reach of S is the infimum over S of the distance to $\mathrm{MA}(S)$:

$$\mathrm{reach}(S) = \inf\{d_{\mathrm{MA}(S)}(p), p \in S\}$$

As proved in [Fed59a], $\mathrm{reach}(S)$ is positive when S is $C^{1,1}$-continuous, i.e. continuously differentiable and its normal satisfies a Lipschitz condition.

4.2 Topology Preliminaries

In this section, we briefly recall some definitions that are used in this thesis.

Definition 6 (Homotopy) A *homotopy* between two continuous functions f and g from a topological space X to a topological space Y is defined to be a continuous function $H : X \times [0,1] \to Y$ such that for all points $x \in X$, $H(x,0) = f(x)$ and $H(x,1) = g(x)$. f is said to be *homotopic* to g if there exists a homotopy between f and g.

Definition 7 (Homotopy Equivalence) Two topological spaces X and Y are *homotopy equivalent* or of the *same homotopy type* if there exist continuous maps $f : X \to Y$ and $g : Y \to X$ such that $g \circ f$ is homotopic to the identity map id_X and $f \circ g$ is homotopic to id_Y.

Definition 8 (Homotopy Groups, Fundamental Group) Let X be a space with a base point $x_0 \in X$. Let S^i denote the i-sphere for a given $i \geq 1$, in which we fixed a base point b. The i-dimensional homotopy group of X at the base point x_0, denoted by $\pi_i(X, x_0)$, is defined to be the set of homotopy classes of maps $f : S^i \to X$ that map the base point b to the base point x_0.

Thus if X is path-connected, the group $\pi_i(X, x_0)$ is, up to isomorphism, independent of the choice of base point x_0. In this case the notation $\pi_i(X, x_0)$ is often abbreviated to $\pi_i(X)$.

Let X be a path-connected space. The first homotopy group of X, $\pi_1(X)$, is called the *fundamental group* of X.

Definition 9 (Simply-Connected Spaces) The path-connected space X is called *simply-connected* if its fundamental group is trivial.

Definition 10 (Weak Homotopy Equivalence) A map $f : X \to Y$ is called a weak homotopy equivalence if the group homomorphisms induced by f on the corresponding homotopy groups, $f_* : \pi_i(X) \to \pi_i(Y)$, for $i \geq 0$, are all isomorphisms. It is easy to see that any homotopy equivalence is a weak homotopy equivalence, but the inverse is not necessarily true. However, Whitehead's Theorem states that the inverse is true for maps between CW-complexes.

Theorem 1 (Whitehead's Theorem) If a map $f : X \to Y$ between connected CW-complexes induces isomorphisms $f_* : \pi_i(X) \to \pi_i(Y)$ for all $i \geq 0$, then f is a homotopy equivalence.

Definition 11 ((Strong) Deformation Retract) Let X be a subspace of Y. A homotopy $H : Y \times [0,1] \to Y$ is said to be a (strong) deformation retract of Y to X if:

- For all $y \in Y$, $H(y,0) = y$ and $H(y,1) \in X$.
- For all $x \in X, H(x,1) = x$.
- (and for all $x \in X, H(x,t) = x$.)

Definition 12 (Homeomorphism) Two topological spaces X and Y are *homeomorphic* if there exists a continuous and bijective map $h : X \to Y$ such that h^{-1} is continuous. the map h is called a homeomorphism from X to Y.

Definition 13 (Isotopy) Two topological spaces X and Y embedded in $\mathbb{R}^d$ are *isotopic* if there exists a continuous map $i : [0,1] \times X \to \mathbb{R}^d$ such that $i(0,.)$ is the identity over X, $i(1,X) = Y$ and for any $t \in [0,1]$, $i(t,.)$ is a homeomorphism from X onto its image. The map i is called an isotopy from X to Y.

Let us recall the definition of the universal cover, and refer to classical books in topology for more details.

Definition 14 (Universal Cover) Let X be a topological space. A *covering space* of X is a space C together with a continuous surjective map $\phi : C \to X$ such that for every $x \in X$, there exists an open neighborhood U of x, such that $\phi^{-1}(U)$ is a disjoint union of open sets in C, each of which is mapped homeomorphically onto U by ϕ. A connected covering space is called a *universal cover* if it is simply connected.

The universal cover exists and is unique up to homeomorphism.

Lemma 1 (Lifting Property of the Universal Cover) Let X be a (path-) connected topological space and $\widetilde{X}$ be its universal cover, and $\phi : \widetilde{X} \to X$ be the map given by the covering. Let Y be any simply connected space, and $f : Y \to X$ be a continuous map. Given two points $\tilde{x} \in \widetilde{X}$ and $y \in Y$ with $\phi(\tilde{x}) = f(y)$, there exists a unique continuous map $g : Y \to \widetilde{X}$ so that $\phi \circ g = f$ and $\phi(y) = \tilde{x}$. This is called the *lifting property* of $\widetilde{X}$.

Since all the spheres S_i of dimensions $i \geq 2$ are simply connected, we may easily deduce.

Corollary 1 For any (path-) connected space X with universal cover $\tilde{X}$, we have $\pi_i(\tilde{X}) = \pi_i(X)$ for all $i \geq 2$.

We now recall the definition of the Hurewicz map $h_i : \pi_i(X) \to H_i(X)$. For an element $[\alpha] \in \pi_i(X)$ presented by $\alpha : S^i \to X$, $h_i([\alpha])$ is defined as the image of the fundamental class of S^i in $H_i(S^i)$ under the map $\alpha_* : H_i(S^i) \to H_i(X)$, i.e., $h_i([\alpha]) = \alpha_*(1)$.

Theorem 2 (Hurewicz Isomorphism Theorem) The first non-trivial homotopy and homology groups of a simply-connected space occur in the same dimension and are isomorphic. In other words, for X simply connected, the Hurewicz map $h_i : \pi_i(X) \to H_i(X)$ is an isomorphism for the first i with π_i (or equivalently H_i) non-trivial.

Chapter 1

First Method and Related Topological Guarantees

In this chapter of the thesis, we consider the problem of reconstructing a compact 3-manifold (with boundary) embedded in $\mathbb{R}^3$ from its cross-sections $\mathcal{S}$ with a given set of cutting planes $\mathcal{P}$ having arbitrary orientations. Using the fact that a point $x \in \mathcal{P}$ belongs to the original object if and only if it belongs to $\mathcal{S}$, we follow a very natural reconstruction strategy: we say that a point $x \in \mathbb{R}^3$ belongs to the reconstructed object if (at least one of) its nearest point(s) in $\mathcal{P}$ belongs to $\mathcal{S}$. This coincides with the algorithm presented by Liu et al. in [LBD+08]. We will characterize the resulting reconstructed object and present appropriate sampling conditions providing topological guarantees for the reconstructed object.

1 Reconstructed Object Definition

Let us first give a definition of the reconstructed object in a cell $\mathcal{C}$ of the arrangement of the cutting planes, which is related to the Voronoi diagram of $\mathcal{C}$ defined as follows.

Voronoi Diagram of a Cell. For a face f of $\mathcal{C}$, the Voronoi cell of f, denoted by $\mathrm{V}_{\mathcal{C}}(f)$, is defined as the set of all points in $\mathcal{C}$ that have f as the nearest face of $\mathcal{C}$, i.e.,

$$\mathrm{V}_{\mathcal{C}}(f) = \{\ x \in \mathcal{C} \mid d(x,f) \leq d(x,f'),\ \forall \text{ face } f' \text{ of } \mathcal{C}\ \}.$$

Where $d(.,.)$ is the Euclidean distance. The collection of all $\mathrm{V}_{\mathcal{C}}(f)$ of the faces of $\mathcal{C}$ forms a tiling of $\mathcal{C}$, called the *Voronoi diagram of* $\mathcal{C}$.

We write $\partial\mathrm{V}_{\mathcal{C}}(f)$ for the boundary of $\mathrm{V}_{\mathcal{C}}(f)$. The union of $\partial\mathrm{V}_{\mathcal{C}}(f)$ for all the faces f of $\mathcal{C}$ is called the *Voronoi Skeleton of* $\mathcal{C}$, and is denoted by $\mathrm{VorSkel}(\mathcal{C})$. $\mathrm{VorSkel}(\mathcal{C})$ is also called *the medial axis of the cell*, and is the locus of points in $\mathcal{C}$ that are at the same distance from at least two faces of $\mathcal{C}$. To simplify notation, when the cell $\mathcal{C}$ is understood from the context, we simply remove the index $\mathcal{C}$ and write $\mathrm{V}(f)$, $\partial\mathrm{V}(f)$, etc.

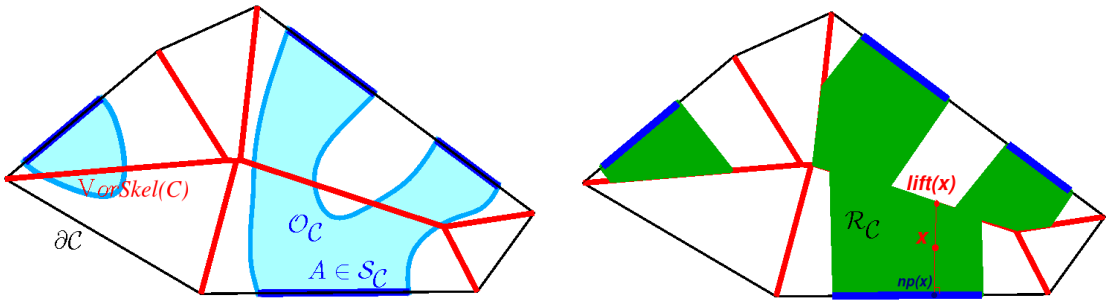

Figure 1.1: A 2D illustration of the partition of a cell $\mathcal{C}$ by the Voronoi Skeleton VorSkel($\mathcal{C}$). Left) The original shape $\mathcal{O}_\mathcal{C}$. Right) The reconstructed object $\mathcal{R}_\mathcal{C}$.

Definition 15 (Nearest Point) For any point x in $\mathcal{C}$, the *nearest point* in $\partial\mathcal{C}$ to x is the orthogonal projection of x onto the nearest face f of $\mathcal{C}$. This projection is denoted by $\mathrm{np}_f(x)$. The set of all nearest points to x in $\partial\mathcal{C}$ is denoted by $\mathrm{Np}_\mathcal{C}(x)$. Note that for any $x \notin \mathrm{VorSkel}(\mathcal{C})$, $\mathrm{Np}_\mathcal{C}(x)$ is reduced to a single point. Based on this, and to simplify the presentation, sometimes we drop the index f, and by $\mathrm{np}(x)$ we denote a point of $\mathrm{Np}_\mathcal{C}(x)$.

We can now define the reconstructed object in a given cell $\mathcal{C}$. We first give the formal definition, and then present a more detailed geometric characterization of the reconstructed object using the lifting procedure described below.

Definition 16 (Reconstructed Object $\mathcal{R}_\mathcal{C}$ in a cell $\mathcal{C}$) The *reconstructed object* $\mathcal{R}_\mathcal{C}$ is the set of all points x in $\mathcal{C}$ such that a nearest point $\mathrm{np}(x)$ lies in $\mathcal{S}_\mathcal{C}$, i.e., $\mathrm{Np}_\mathcal{C}(x) \cap \mathcal{S}_\mathcal{C} \neq \emptyset$. Note that in the case where $\mathcal{S}_\mathcal{C}$ is empty, $\mathcal{R}_\mathcal{C}$ will be the empty set as well.

Definition 17 (Lift Function) Let $x \in \mathcal{C}$ be a point in the Voronoi cell of a face f of $\mathcal{C}$. The *lift of x in $\mathcal{C}$*, denoted by $\mathrm{lift}_\mathcal{C}(x)$ (or simply $\mathrm{lift}(x)$ if $\mathcal{C}$ is trivially implied), is defined to be the unique point of $\partial\mathrm{V}_\mathcal{C}(f)$ such that the line defined by the segment $[x, \mathrm{lift}(x)]$ is orthogonal to f. In other words, $\mathrm{lift}(x)$ is the unique point in $\partial\mathrm{V}_\mathcal{C}(f)$ that orthogonally projects to $\mathrm{np}(x)$ on f.

The *lift of a set of points* $X \subseteq \mathcal{C}$, denoted by $\mathrm{lift}(X)$, is the set of all the points $\mathrm{lift}(x)$ for $x \in X$, i.e., $\mathrm{lift}(X) := \{\, \mathrm{lift}(x) \,|\, x \in X \,\}$.

The function $\mathcal{L} : \mathcal{C} \to \mathrm{VorSkel}(\mathcal{C})$ that maps each point $x \in \mathcal{C}$ to its lift in VorSkel($\mathcal{C}$) will be called the *lift function* in the sequel. For any $Y \subset \mathrm{VorSkel}(\mathcal{C})$, $\mathcal{L}^{-1}(Y)$ denotes the set of points $x \in \mathcal{C}$ such that $\mathrm{lift}(x) = y$ for some $y \in Y$.

Characterization of the Reconstructed Object $\mathcal{R}_\mathcal{C}$. If $\mathcal{S}_\mathcal{C} = \emptyset$, then as we said before, for any point $x \in \mathcal{C}$, $\mathrm{np}(x) \notin \mathcal{S}_\mathcal{C}$, and so $\mathcal{R}_\mathcal{C}$ is empty. Otherwise, let $A \in \mathcal{S}_\mathcal{C}$ be a section lying on a face of $\mathcal{C}$. For each point $a \in A$, the locus of all the points $x \in \mathcal{C}$ that have a as their nearest point in $\partial\mathcal{C}$ is the line segment $[a, \mathrm{lift}(a)]$ joining a to its lift. Therefore, the reconstructed object $\mathcal{R}_\mathcal{C}$ is the union of all the line-segments $[a, \mathrm{lift}(a)]$ for

a point a in a section $A \in \mathcal{S}_\mathcal{C}$, i.e.,

$$\mathcal{R}_\mathcal{C} = \bigcup_{A \in \mathcal{S}_\mathcal{C}} \bigcup_{a \in A} [a, \text{lift}(a)] = \mathcal{L}^{-1}(\text{lift}(\mathcal{S}_\mathcal{C})).$$

Note that according to this characterization, if the lifts of two sections intersect in $\text{VorSkel}(\mathcal{C})$, then these two sections are connected in $\mathcal{R}_\mathcal{C}$. This is the generalization of the classical overlapping criterion for the case of parallel cutting planes. The union of all the pieces $\mathcal{R}_\mathcal{C}$ over all cells $\mathcal{C}$ will be the overall reconstructed object $\mathcal{R}$.

Remark We note that the presented reconstruction method can handle the case of multilabel sections, i.e. multiple materials, see Figure 1.2. We also note that this method can be considered for higher dimensional variants of the problem. Where the goal is to reconstruct an n-dimensional shape from its $(n-1)$-dimensional intersections with hyperplanes. This method seems to be the most natural way to tackle high dimensional reconstruction problem from cross-sections.

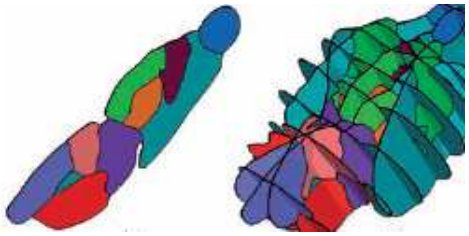

Figure 1.2: A figure from [LBD+08] showing multilabel sections example.

In the following sections, we will prove that the connectivity between the sections induced by this reconstructed object is topologically coherent, under appropriate sampling conditions. Moreover, it preserves the homotopy type of the original shape. However, due to the non-continuity of the interpolation between the sections, the reconstructed object may exhibit a jagged and unnatural appearance. The reconstructed object as it is cannot be directly used in applications where smooth surfaces are desired. A *smoothing step* should be performed to improve the visual appearance of $\mathcal{R}_\mathcal{C}$, as it is suggested and applied in [LBD+08]. The below figure from [LBD+08] shows an example of this improvement.

We also propose another strategy which consists of considering a continuous interpolation between the sections which induces the same connectivity as the proposed reconstructed object $\mathcal{R}$. Let us present very briefly an interpolation, defined in the following section, which is a new joint project in progress with Jean-Daniel Boissonnat and Helio Lopez.

1.1 Interpolation

Let $P_1, \ldots, P_k$ denote the cutting planes and let $S_1, \ldots, S_k$ be their intersections with $\mathcal{O}$. The goal is to define an implicit function $f(x)$ defined over $\mathbb{R}^3$ whose zero-set interpolates the sections S_i, $i = 1..k$.

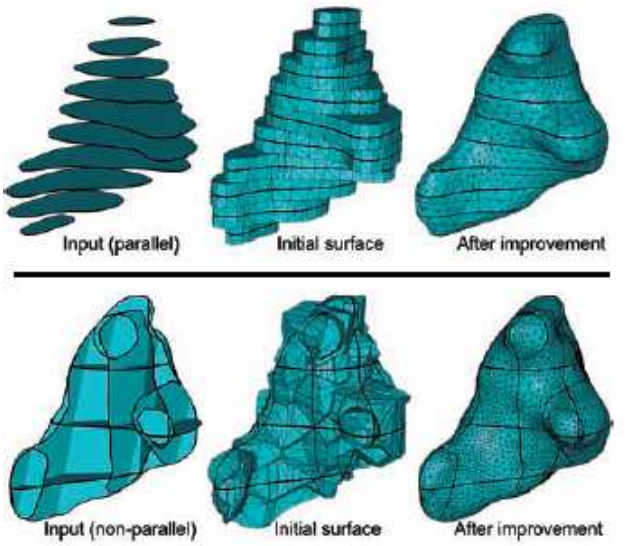

Figure 1.3: A figure from [LBD+08] showing the smoothing step for parallel and non-parallel sections.

The construction is as follows. We first define in each cutting plane P_i a continuous function f_i which vanishes on the boundaries of S_i, and is negative inside S_i and positive outside S_i.

We then define the restriction $f_{|\mathcal{C}}$ of f to a cell $\mathcal{C}$ of the arrangement of the cutting planes. For convenience, we relabel the sections so that the cutting planes bounding $\mathcal{C}$ are $P_1, \ldots, P_m$. We further write $F_i = \mathcal{C} \cap P_i$ for the facet of $\mathcal{C}$ supported by P_i, $i = 1, \ldots, m$. Let x be a point of $\mathcal{C}$. We associate to each P_i, $i = 1..m$, the projection x_i of x onto P_i and denote by $h_i(x) = g(\|x - x_i\|)$, where g is a non decreasing function. We further write $w_i(x) = 1/h_i(x)$ and $w(x) = \sum_{i=1}^{m} w_i(x)$. We can now define

$$f_{|\mathcal{C}}(x) = \sum_{i=1}^{m} \frac{w_i(x)}{w(x)} f_i(x_i)$$

This interpolant is known as Shepard's interpolant [She68] and has the following properties.

1. If all f_i, $i = 1..k$, are of class C^∞ then $f_{|\mathcal{C}}$ is of class C^∞.
2. Assuming that 0 is not a singular value of $f_{|\mathcal{C}}$, $f_{|\mathcal{C}}^{-1}(0)$ is of class C^∞.
3. $f_{|F_i} = f_i$ and $f_{|\mathcal{C}}^{-1}(0) \cap F_i = \partial O_i \cap F_i$.

From Property 3, we deduce that if x belongs to two cells $\mathcal{C}$ and $\mathcal{C}'$, $f_{|\mathcal{C}}(x) = f_{|\mathcal{C}'}(x)$. Hence, h is well defined and continuous over $\mathbb{R}^3$. According to the first property, f is of class C^∞ inside each cell. However, it is only continuous on the boundaries of the sections.

Similarly, assuming that 0 is not a singular value of f, $f^{-1}(0)$ is of class C^∞ inside each cell but only continuous on the boundaries of the sections.

In the case where we have two parallel cutting planes and $h_i(x) = \|x - x_i\|$ (i.e. g is the identity), we obtain the standard linear interpolation between the distance functions to the contours.

We have much latitude in defining f_i and h_i. A natural choice is to take the euclidean distance to ∂S_i for f_i and $h_i(x) = \|x - x_i\|$ (i.e. g is the identity). But other choices could be also appropriate, e.g. the square function for g. See Figure 1.4 and Figure 1.5 for some examples.

Approximation of $f^{-1}(0)$: We approximate $f^{-1}(0)$ using a surface mesh generator such as the marching cube or the CGAL Delaunay-based surface mesh generator. We describe below how to proceed with the CGAL surface mesh generator [BO05] and [RY09].

We first sample the contours ∂S_i. More precisely, we first compute the vertices of the arrangement of the cutting planes that belong to $\mathcal{O}$ and then sample ∂S_i, $i = 1..k$.[1] Let E be the resulting set of sample points and write $E_i = E \cap P_i$. We store, in each P_i the 2-dimensional Voronoi diagram of E_i, denoted $\mathrm{V}(E_i)$.

We initialize the surface mesher with E. We then simply need to be able to evaluate f at any given point $x \in \mathbb{R}^3$. To do so, we need two procedures. The first one computes the cutting planes that support a cell $C(x)$ that contains x. It will then be easy to compute the x_i and the $w_i(x)$. A simple $O(k^2)$-time algorithm constructs the projections of x onto the k cutting planes and, for each of them, say x_i, checks whether no other cutting plane P_j, $j \neq i$, cuts the line segment $[x, x_i]$.

The second procedure computes $f_i(x_i)$. Using $\mathrm{V}(E_i)$, it is easy to compute the point of E_i closest to x. The exact distance to the polygonal line joining the sample points can then easily be deduced if more precision is required.

Preliminary results for the analogous 2-dimensional problem are shown in Figures 1.4 and 1.5. The sections are the yellow segments on the edges of a cube $[-3, +3] \times [-3, +3]$. The yellow domain is the reconstructed shape $R_f = \{x \in \mathbb{R}^3, f(x) \leq 0\}$.

Case of $h_i = \|x - x_i\|^n$ for a sufficiently large n corresponds to the proposed reconstructed object $\mathcal{R}$: When $h_i = \|x - x_i\|^n$ for a sufficiently large n we have: $f_{|\mathcal{C}}(x) \simeq f_j(x_j)$ such that $w_j(x) = \max_i w_i(x)$. In this case, $\|x - x_j\| = \min_i(\|x - x_i\|)$, and x_j is the projection of x onto the closest plane. Therefore, the reconstructed object R_f is close to the reconstructed object $\mathcal{R}$ obtained by the algorithm of [LBD+08].

This provides a surface of class C^∞ that induces the same connectivity on the sections as the proposed reconstructed object $\mathcal{R}$. Therefore, the connectivity guarantees for $\mathcal{R}$ that will be presented in the next section, are valid for this new reconstruction as well.

[1] We refer to Section 5 of the second chapter for more details on this procedure.

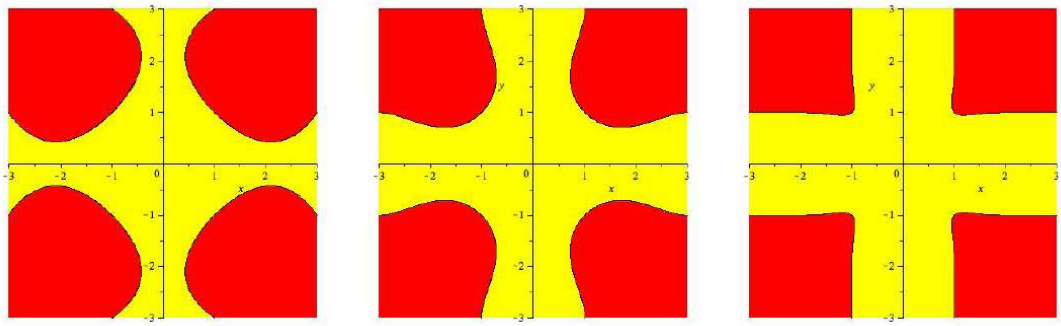

Figure 1.4: The sections are : $S_S = [-1,+1]\times -3$, $S_N = [-1,+1]\times +3$, $S_W = -3\times[-1,+1]$, $S_E = +3\times[-1,+1]$. In all cases, f_i is the signed euclidean distance to the closest boundary. Left : $h_i(x) = \|x - x_i\|$. Middle : $h_i = \|x - x_i\|^2$. Right : $h_i = \|x - x_i\|^{10}$.

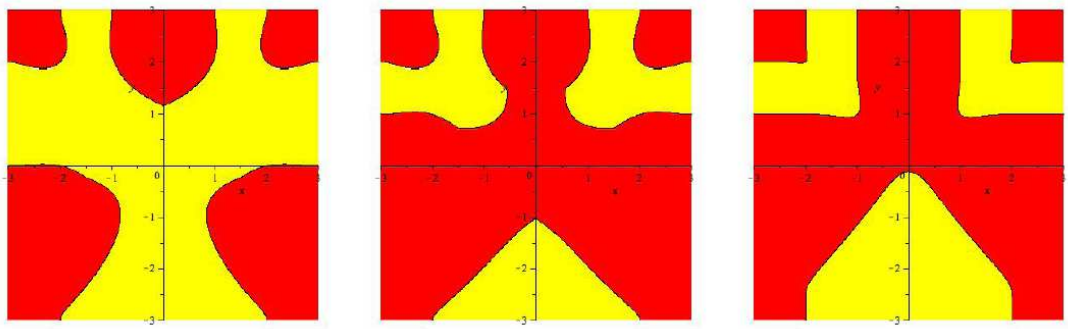

Figure 1.5: In all cases, f_i is the signed euclidean distance to the closest boundary. Left and middle: $h_i(x) = \|x - x_i\|^2$. Right : $h_i = \|x - x_i\|^{10}$. The sections in the middle and on the right are the same.

2 Guarantees on the Connectivity between the Sections

The rest of the chapter is devoted to prove that under two appropriate sampling conditions, $\mathcal{R}$ and $\mathcal{O}$ are homotopy equivalent, and are indeed homeomorphic (and isotopic). Let us first infer the following simple observation from the described characterization of $\mathcal{R}_\mathcal{C}$.

Proposition 1 *The lift function $\mathcal{L} : \mathcal{R}_\mathcal{C} \to \text{lift}(\mathcal{S}_\mathcal{C})$ is a homotopy equivalence.*

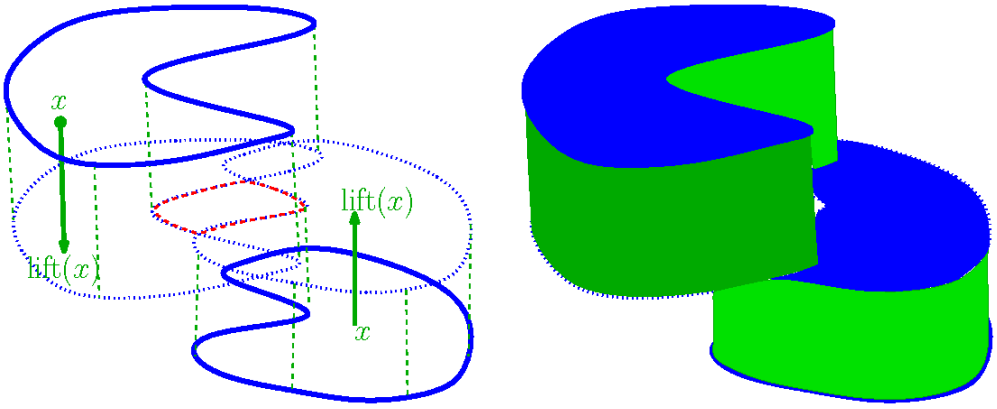

Figure 1.6: A 3D reconstruction example from a pair of parallel sections (in blue). The lift function retracts $\mathcal{R}_\mathcal{C}$ (in green) onto the lift of the sections.

This is inferred trivially from the fact that the lift function retracts each segment $[a, \text{lift}(a)]$ onto $\text{lift}(a)$ continuously. See Figure 1.6 for an example.

2.1 First Sampling Condition : Separation Condition

In this section, we provide the first sampling condition, under which the connection between the sections in the reconstructed object $\mathcal{R}$ are the same as in the original object $\mathcal{O}$. Our discussion will be essentially based on the study of the *medial axis*, that we define now.

Definition 18 (Medial Axis of $\partial\mathcal{O}$, Internal and External Retracts)

- Consider $\partial\mathcal{O}$ as a 2-manifold without boundary embedded in $\mathbb{R}^3$. The medial axis of $\partial\mathcal{O}$, denoted by $\text{MA}(\partial\mathcal{O})$, contains two different parts : the so-called *internal* part, denoted by $\text{MA}_i(\partial\mathcal{O})$, which lies in $\mathcal{O}$ and the so-called *external* part, denoted by $\text{MA}_e(\partial\mathcal{O})$, which lies in $\mathbb{R}^3 \setminus \mathcal{O}$.
- The *internal retract* $m_i : \partial\mathcal{O} \to \text{MA}_i(\partial\mathcal{O})$ is defined as follows : for a point $x \in \partial\mathcal{O}$, $m_i(x)$ is the center of the maximum ball entirely included in $\mathcal{O}$ which passes through x. For any $x \in \partial\mathcal{O}$, $m_i(x)$ is unique. Symmetrically, we define *the external retract* $m_e : \partial\mathcal{O} \to \text{MA}_e(\partial\mathcal{O})$: for a point $x \in \partial\mathcal{O}$, $m_e(x)$ is the center of the maximum ball entirely included in $\mathbb{R}^3 \setminus \mathcal{O}$ which passes through x. For any $x \in \partial\mathcal{O}$, $m_e(x)$

is unique but may be at infinity. In the sequel, we may write $m(a)$ for a point in $\{m_i(a), m_e(a)\}$.

The interesting point is that as discussed below if the sample of cutting planes is sufficiently dense, then the internal part of $\mathrm{MA}(\partial\mathcal{O})$ lies inside the defined reconstructed object and the external part of this medial axis lies outside the reconstructed object.

Definition 19 (Separation Condition) We say that the set of cutting planes verifies the Separation Condition if

$$\mathrm{MA}_i(\partial\mathcal{O}) \subset \mathcal{R} \quad \text{and} \quad \mathrm{MA}_e(\partial\mathcal{O}) \subset \mathbb{R}^3 \setminus \mathcal{R}\,.$$

In other words, *$\partial\mathcal{R}$ separates the internal and the external parts of the medial axis of $\partial\mathcal{O}$.* (That is where the name comes from.)

We will show that in each cell $\mathcal{C}$, the Separation Condition implies that $\partial\mathcal{R}_\mathcal{C}$ separates the internal and the external parts of the medial axis of $\partial\mathcal{O}_\mathcal{C}$. In order to study the Separation Condition in a cell $\mathcal{C}$, we will need the following definition:

Definition 20 (Medial axes in a cell $\mathcal{C}$ of the arrangement) By $\mathrm{MA}_i(\partial\mathcal{O}_\mathcal{C})$ we denote the set of all points in $\mathcal{O}_\mathcal{C}$ with at least two closest points in $\partial\mathcal{O}_\mathcal{C}$, see Figure 1.7. Note that the two sets $\mathrm{MA}_i(\partial\mathcal{O}_\mathcal{C})$ and $\mathrm{MA}_i(\partial\mathcal{O}) \cap \mathcal{C}$ may be different. Symmetrically, $\mathrm{MA}_e(\partial\mathcal{O}_\mathcal{C})$ denotes the medial axis of the closure of $\mathcal{C} \setminus \mathcal{O}_\mathcal{C}$.

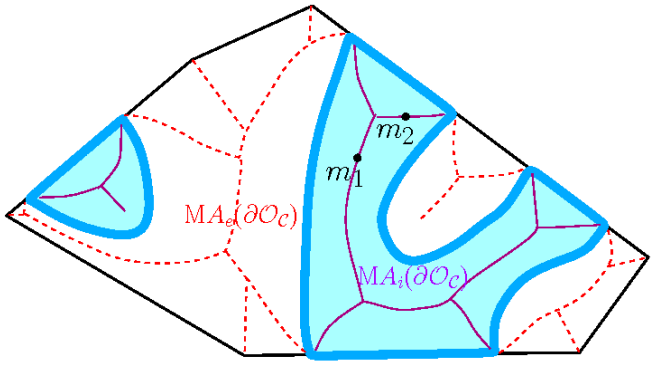

Figure 1.7: 2D example of medial axes in a cell $\mathcal{C}$ of the arrangement.

We also consider the *internal retract* $m_{i,\mathcal{C}} : \partial\mathcal{O}_\mathcal{C} \to \mathrm{MA}_i(\partial\mathcal{O}_\mathcal{C})$ defined as follows. For a point $x \in \partial\mathcal{O}_\mathcal{C}$, $m_{i,\mathcal{C}}(x)$ is the center of the maximum ball entirely included in $\mathcal{O}_\mathcal{C}$ which passes through x. Symmetrically, we can define *the external retract* $m_{e,\mathcal{C}} : \partial\mathcal{O}_\mathcal{C} \to \mathrm{MA}_e(\partial\mathcal{O}_\mathcal{C})$: for a point $x \in \partial\mathcal{O}_\mathcal{C}$, $m_{e,\mathcal{C}}(x)$ is the center of the maximum ball entirely included in $\mathcal{C} \setminus \mathcal{O}_\mathcal{C}$ which passes through x. It is easy to see that for any $x \in \partial\mathcal{O} \cap \mathcal{C}$, the segments $[x, m_{i,\mathcal{C}}(x)]$ and $[x, m_{e,\mathcal{C}}(x)]$ are subsegments of $[x, m_i(x)]$ and $[x, m_e(x)]$ respectively, and lie on the line defined by the normal to $\partial\mathcal{O}$ at x.

Lemma 2 (Separation Condition Restricted to $\mathcal{C}$) *If the Separation Condition is verified, then $MA_i(\partial\mathcal{O}_\mathcal{C}) \subset \mathcal{R}_\mathcal{C}$ and $MA_e(\partial\mathcal{O}_\mathcal{C}) \subset \mathcal{C} \setminus \mathcal{R}_\mathcal{C}$.*

Proof We prove the first part, i.e., $\mathrm{MA}_i(\partial\mathcal{O}_\mathcal{C}) \subset \mathcal{R}_\mathcal{C}$. A similar proof gives the second part. Let m be a point in $\mathrm{MA}_i(\partial\mathcal{O}_\mathcal{C})$. Let $B(m)$ be the open ball centered at m which passes through the closest points to m in $\partial\mathcal{O}_\mathcal{C}$. Two cases can happen:

• Either, the closest points to m in $\partial\mathcal{O}_\mathcal{C}$ are in $\partial\mathcal{O}$, see m_1 in Figure 1.7. In this case m is a point in $\mathrm{MA}_i(\partial\mathcal{O})$. The Separation Condition states that $\mathrm{MA}_i(\partial\mathcal{O}) \subset \mathcal{R}$, and so $m \in \mathcal{R}_\mathcal{C} = \mathcal{R} \cap \mathcal{C}$.

• Otherwise, one of the closest points to m in $\partial\mathcal{O}_\mathcal{C}$ is a point a in some section $A \in \mathcal{S}_\mathcal{C}$, see m_2 in Figure 1.7. If a is on the boundary of A, then since along the section-contours $\partial\mathcal{O}_\mathcal{C}$ is non-smooth, a lies in $\mathrm{MA}_i(\partial\mathcal{O}_\mathcal{C})$ and coincides with m, and $m = a$ is trivially in $\mathcal{R}_\mathcal{C}$. Hence, we may assume that a lies in the interior of A. Therefore, the ball $B(m)$ is tangent to A at a, and the line segment $[a, m]$ is orthogonal to A. Since $B(m) \cap \partial\mathcal{C} = \emptyset$, m and a are in the same Voronoi cell of the Voronoi diagram of $\mathcal{C}$. Thus, $a \in \mathcal{S}_\mathcal{C}$ is the nearest point in $\partial\mathcal{C}$ to m. By the definition of $\mathcal{R}_\mathcal{C}$, we deduce that $m \in \mathcal{R}_\mathcal{C}$. □

Assume that the Separation Condition is verified. The first idea which comes to mind is to retract points of $\partial\mathcal{O}$ to $\partial\mathcal{R}$ by following the normal-directions. A point $x \in \partial\mathcal{O}$ which lies outside $\mathcal{R}$ can move towards $m_i(x) \in \mathcal{R}$ and stop when $\partial\mathcal{R}$ is reached. A point $x \in \partial\mathcal{O}$ which lies inside $\mathcal{R}$, can move toward $m_e(x)$ and stop when $\partial\mathcal{R}$ is reached. According to a theorem by Wolter [Wol92], since $\partial\mathcal{O}$ is assumed to be of class C^2, this deformation will be a continuous retraction if each normal intersects $\partial\mathcal{R}$ at a single point. In such a case, $\partial\mathcal{O}$ can be deformed to $\partial\mathcal{R}$ homeomorphically. But a major problem is that $\mathcal{R}$ may have a complex shape (with cavities), so that a normal to $\partial\mathcal{O}$ intersects $\partial\mathcal{R}$ in several points. In such a case, such a retraction is not continuous and does not provide a deformation retract of $\mathcal{O}$ onto $\mathcal{R}$. However, we will be essentially following this intuitive idea by looking for a similar deformation retract of $\mathcal{O}$ onto a subshape of $\mathcal{R}$ (the so-called medial shape). See Section 4.

In the next section we will obtain a set of consequences of the Separation Condition.

2.2 Guarantees on the Connections Between the Sections

We now show that if the sample of cutting planes verifies the Separation Condition, then in each cell $\mathcal{C}$ of the arrangement, the connection between the sections is the same in $\mathcal{O}_\mathcal{C}$ and $\mathcal{R}_\mathcal{C}$.

Theorem 3 If the sample of cutting planes verifies the Separation Condition, $\mathcal{R}_\mathcal{C}$ and $\mathcal{O}_\mathcal{C}$ induce the same connectivity components on the sections of $\mathcal{C}$.

Proof The proof is given in two parts :

(I) **If two sections are connected in $\mathcal{R}_\mathcal{C}$, then they are connected in $\mathcal{O}_\mathcal{C}$.** Let A and A' be two sections connected in $\mathcal{R}_\mathcal{C}$. Let γ be a path in $\mathcal{R}_\mathcal{C}$ that connects a point $a \in A$ to a point $a' \in A'$. For the sake of a contradiction, suppose that a and a' are not in the same connected component of $\mathcal{O}_\mathcal{C}$. In this case, as γ joins two points in two different connected components of $\mathcal{O}_\mathcal{C}$, it intersects $\mathrm{MA}_e(\partial\mathcal{O}_\mathcal{C})$. This is a contradiction with the fact that $\gamma \subset \mathcal{R}_\mathcal{C}$, since according to Lemma 2 we have $\mathrm{MA}_e(\partial\mathcal{O}_\mathcal{C}) \cap \mathcal{R}_\mathcal{C} = \emptyset$.

(II) **If two sections are connected in $\mathcal{O}_\mathcal{C}$, then they are connected in $\mathcal{R}_\mathcal{C}$.** Let A and A' be two sections in a same connected component K of $\mathcal{O}_\mathcal{C}$. According to the non-smoothness of $\partial\mathcal{O}_\mathcal{C}$ at the boundary of the sections, ∂A and $\partial A'$ are contained in $\mathrm{MA}_i(\partial\mathcal{O}_\mathcal{C})$. Thus, since $\mathrm{MA}_i(\partial\mathcal{O}_\mathcal{C})$ is connected [Lie04], there is a path γ in $\mathrm{MA}_i(\partial\mathcal{O}_\mathcal{C}) \cap K$ that connects a point $a \in \partial A$ to a point $a' \in \partial A'$. According to Lemma 2, $\mathrm{MA}_i(\partial\mathcal{O}_\mathcal{C}) \subset \mathcal{R}_\mathcal{C}$. Thus, γ is a path in $\mathcal{R}_\mathcal{C}$ that connects A to A'.

□

Let us state the following proposition that will be used later in this section and in Section 4.

Proposition 2 Under the Separation Condition, any connected component of $\partial\mathcal{O}$ is cut by at least one cutting plane.

Proof Suppose that K is a connected component of $\partial\mathcal{O}$ which is not cut by any cutting plane. There exists a cell $\mathcal{C}$ of the arrangement of hyperplanes such that one of the following two (symmetric) cases can happen: Either, there exists a connected component H of O which lies in the interior of $\mathcal{C}$ such that $K \subset \partial H$, Or, there exists a connected component H of the closure of $\mathbb{R}^3 \setminus \mathcal{O}$ which lies in the interior of $\mathcal{C}$ such that $K \subset \partial H$. Without loss of generality, let us suppose the first case, and the other case follows similarly. In this case, ∂H bounds a connected component H of $\mathcal{O}$ in $\mathcal{C}$, H is entirely contained in the interior of $\mathcal{C}$, and $K \subset \partial H$, see Figure 1.8. Take a point m in the medial axis of H, i.e., $m \in H \cap \mathrm{MA}_i(\partial\mathcal{O})$. According to the Separation Condition, m belongs to $\mathcal{R}$. Thus, by the definition of $\mathcal{R}$, one of the nearest points of m in $\partial\mathcal{C}$, say $\mathrm{np}(m)$, belongs to $\mathcal{S}$. Since H is not cut by any cutting plane, $H \cap \partial\mathcal{C}$ is empty and $\mathrm{np}(m) \notin H$. Therefore, m and $\mathrm{np}(m)$ are in two different connected components of $\mathcal{O}$, and the segment $[m, \mathrm{np}(m)]$ should intersect $\mathrm{MA}_e(\partial\mathcal{O})$ at a point x. On the other hand, by the definition of $\mathcal{R}$, the segment $[m, \mathrm{np}(m)] \subset \mathcal{R}$. This contradicts the assumption of Separation Condition that $\mathcal{R} \cap \mathrm{MA}_e(\partial\mathcal{O}) = \emptyset$. □

2.3 How to Ensure the Separation Condition?

In this section we provide a sufficient condition for ensuring the Separation Condition. For this, we need first some definitions.

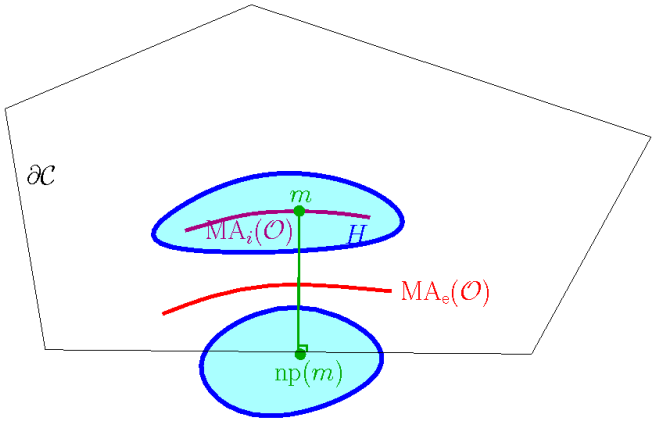

Figure 1.8: For the proof of Proposition 2.

Definition 21 (Reach) Let $\mathcal{O}$ be a connected compact 3-manifold with smooth boundary $\partial\mathcal{O}$ in $\mathbb{R}^3$. For $a \in \partial\mathcal{O}$, we define $\mathrm{reach}(a) = \min\big(d(a, m_i(a)), d(a, m_e(a))\big)$. The quantity $\mathrm{reach}(\mathcal{O})$ is defined as the minimum distance of $\partial\mathcal{O}$ from the medial axis of $\partial\mathcal{O}$:

$$\mathrm{reach}(\mathcal{O}) := \min_{m \in \mathrm{MA}(\partial\mathcal{O})} d(m, \partial\mathcal{O}) = \min_{a \in \partial\mathcal{O}} \mathrm{reach}(a).$$

Note that as $\mathcal{O}$ is compact and $\partial\mathcal{O}$ is of class C^2, $\mathrm{reach}(\mathcal{O})$ is strictly positive (see [Fed59b] for a proof).

Definition 22 (Reach restricted to a cell of the arrangement) Given a cell $\mathcal{C}$ of the arrangement, we define $\mathrm{reach}_{\mathcal{C}}(\mathcal{O}) = \min d(a, m(a))$, where either $a \in \partial\mathcal{O} \cap \mathcal{C}$ or $m(a) \in \mathrm{MA}(\partial\mathcal{O}) \cap \mathcal{C}$. By definition, we have $\mathrm{reach}(\mathcal{O}) = \min_{\mathcal{C}} (\mathrm{reach}_{\mathcal{C}}(\mathcal{O}))$.

Definition 23 (Height of a Cell) Let $\mathcal{C}$ be a cell of the arrangement of the cutting planes. The *height* of $\mathcal{C}$, denoted by $h_{\mathcal{C}}$, is defined as the maximum distance of a point $x \in \mathcal{C}$ to the boundary of $\mathcal{C}$. In other words, $h_{\mathcal{C}} := \max_{x \in \mathcal{C}} d(x, \mathrm{np}(x))$.

We remark that the height of any cell $\mathcal{C}$ is at most half of the diameter of $\mathcal{C}$. However, as the example of Figure 1.9 (right figure) shows, it may be much smaller than half of the diameter. Moreover, in the case of parallel planes, while the cell between two consecutive planes is unbounded, the height of the cell is the half of the distance between the two planes. We now show that by bounding from above the height of the cells by a factor related to the reach of the object, we can ensure the Separation Condition.

Lemma 3 (Sufficient Condition) If for any cell $\mathcal{C}$ of the arrangement, $h_{\mathcal{C}} < \mathrm{reach}_{\mathcal{C}}(\mathcal{O})$ then the Separation Condition is verified.

Proof

Let m_i be any point in $\mathrm{MA}_i(\partial\mathcal{O})$ in a cell $\mathcal{C}$ of the arrangement. We have

$$d(m_i, \mathrm{np}(m_i)) \leq h_{\mathcal{C}} < \mathrm{reach}_{\mathcal{C}}(\mathcal{O}) \leq d(m_i, \partial\mathcal{O}).$$

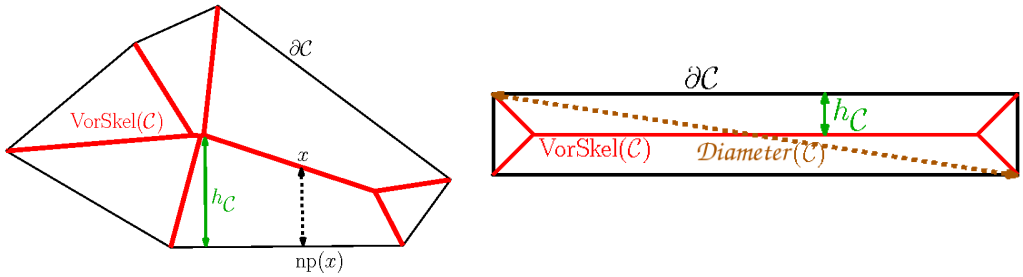

Figure 1.9: Left) Definition of the height of a cell $\mathcal{C}$. Right) Height of a cell $\mathcal{C}$ is bounded from above by half of the diameter of $\mathcal{C}$, but may be much smaller for many configurations of cutting planes.

Therefore, $\text{np}(m_i)$ is in $\mathcal{O}$ (and so in $\mathcal{S}$), and according to the definition of $\mathcal{R}$, m_i is in $\mathcal{R}$. This proves that $\text{MA}_i(\partial\mathcal{O}) \subset \mathcal{R}$. For any point $m_e \in \text{MA}_e(\partial\mathcal{O})$, we can similarly show that $\text{np}(m_e)$ is not in $\mathcal{O}$, and so $\text{MA}_e(\partial\mathcal{O}) \subset \mathbb{R}^3 \setminus \mathcal{R}$. Therefore, the Separation Condition is verified. □

Remark 1 : Higher Dimensional Reconstruction Problem In the d-dimensional framework of the problem, that consists of reconstructing a d-dimensional shape from its $(d-1)$-dimensional intersections with hyperplanes, the same strategy to perform connectivity between the sections can be considered. The guarantees on the connectivity we provided in this section remain valid for any dimension d.

Remark 2 : Case of Parallel Cross-Sections Let us consider the particular case of parallel cross-sections, where the orientation of the cutting planes is fixed and they are all parallel to each other. In this case, the maximum height of the cells of the arrangement is the maximum distance between two consecutive cutting planes. According to Lemma 3, if this maximum distance is less than the reach of $\mathcal{O}$, then the Separation Condition is verified. As a consequence, using Proposition 3 we deduce :

Corollary 2 *If the maximum distance between two consecutive cutting planes is less than the reach of $\mathcal{O}$, then the connection between the sections is the same in $\mathcal{R}_{\mathcal{C}}$ and $\mathcal{O}_{\mathcal{C}}$.*

We now present some other consequences of the Separation Condition for some particular cases of the problem.

3 Separation Condition & Topological Guarantees for Particular Cases

In the previous section, we showed that by bounding from above the height of the cells by a factor related to the reach of the object, we can ensure the Separation Condition. We

also proved that under the Separation condition, the connectivity between the sections of $\mathcal{C}$ induced by the reconstructed object $\mathcal{R}_\mathcal{C}$ is coherent with the original shape $\mathcal{O}_\mathcal{C}$. This will imply the homotopy equivalence between $\mathcal{R}_\mathcal{C}$ and $\mathcal{O}_\mathcal{C}$ for some particular cases of data.

3.1 Guarantees for 2D Shape Reconstruction from Line Cross-Sections

We proved that under the Separation condition, the connectivity between the sections of $\mathcal{C}$ induced by the reconstructed object $\mathcal{R}_\mathcal{C}$ is coherent with the original shape $\mathcal{O}_\mathcal{C}$. We presented the proofs for the 3D case of the problem, but the proofs easily show that result is valid in any dimension. We show in this section that this is strong enough to imply the homotopy equivalence between $\mathcal{R}_\mathcal{C}$ and $\mathcal{O}_\mathcal{C}$ for the 2-dimensional variant of the reconstruction problem.

Consider the 2-dimensional variant of the reconstruction problem, that consists of reconstructing a 2D-shape from its intersections with arbitrarily oriented *cutting lines*. In this case the sections are line-segments.

We can focus on a cell $\mathcal{C}$ of the arrangement of the plane by the cutting lines. Similar definitions for the Voronoi diagram and the Voronoi skeleton of $\mathcal{C}$, the lift function and the reconstructed object $\mathcal{R}_\mathcal{C}$ can be considered. Using the sufficient condition presented in the last section, if for any cell $\mathcal{C}$ of the arrangement, $h_\mathcal{C} < \text{reach}_\mathcal{C}(\mathcal{O})$, then the Separation Condition is ensured. We deduce the following theorem.

Theorem 4 (Provably Good 2D Reconstruction) *If for any cell $\mathcal{C}$ of the arrangement of the cutting lines, $h_\mathcal{C} < reach_\mathcal{C}(\mathcal{O})$, then $\mathcal{R}$ is homeomorphic to $\mathcal{O}$.*

Proof By the definition of the reconstructed object, it is easy to see that any connected component of $\mathcal{R}_\mathcal{C}$ is a topological disk. On the other hand, according to Proposition 2, under the Separation Condition, any connected component of $\partial\mathcal{O}$ is cut by at least one cutting line. We easily deduce that any connected component of $\mathcal{O}_\mathcal{C}$ is a topological disk. Therefore, all the connected components of $\mathcal{O}_\mathcal{C}$ or $\mathcal{R}_\mathcal{C}$ are 2-dimensional disks. On the other hand, according to Theorem 3, under the separation condition, there is a bijection between the connected components of $\mathcal{R}_\mathcal{C}$ and $\mathcal{O}_\mathcal{C}$. Therefore, there is a homotopy equivalence between each pair of corresponding connected components of $\mathcal{O}_\mathcal{C}$ or $\mathcal{R}_\mathcal{C}$. This provides a homotopy equivalence between $\mathcal{R}_\mathcal{C}$ and $\mathcal{O}_\mathcal{C}$. As we will explain in detail in Section 4.4, the homotopy equivalences in the different cells of the arrangement can be extended to a homotopy equivalence between $\mathcal{R}$ and $\mathcal{O}$. Finally, since $\mathcal{R}$ and $\mathcal{O}$ are two homotopy equivalent 2-dimensional submanifolds of $\mathbb{R}^2$, we deduce that there is a homeomorphism between $\mathcal{R}$ and $\mathcal{O}$. □

Comparison with our results presented in [MB08] We note that in [MB08], we presented a Delaunay-based 2-dimensional reconstruction algorithm from line cross-sections, and provided a sampling condition under which the same topological guarantees are ensured. Rather than using the Voronoi diagram of the cells, in [MB08] the nearest point definition is based on the Voronoi diagram of all the sections. However, the particularity of

this algorithm is that the reconstruction is performed in a single step, which contrasts with the divide-and-conquer reconstruction method that is done in each cell of the arrangement of the cutting lines independently. According to the experimental results of [MB08], this algorithm performs well for the case of reconstructing tree-like objects from sparse sectional data. In addition, a sampling condition is provided in [MB08] for this algorithm, which can be ensured by bounding from above the equivalent *height function* of the sections by a factor related to the reach of the object. Note that since in this case the Voronoi cells are not restricted to the cells of the arrangement, the equivalent *height function* of the sections may be too big and the sampling condition may be more difficult to ensure, i.e., more restrictive. Therefore, the sampling condition provided in this thesis seems more appropriate.

3.2 Reconstruction of a Collection of Convex Bodies

Another interesting particular data is the case of a union of 3D convex bodies. In this case $\mathcal{O}_\mathcal{C}$, which is the intersection of a set of convex bodies with a convex polyhedron $\mathcal{C}$, is composed of convex components as well.

We claim that the presented reconstruction method can be adapted to the case of union of convex bodies so that the resulting reconstructed object is homeomorphic to $\mathcal{O}_\mathcal{C}$ under the Separation Condition:

Reconstruction Algorithm Adapted to a Union of Convex Bodies: Consider the connectivity between the sections induced by the defined reconstructed object $\mathcal{R}_\mathcal{C}$. Consider the connectivity classes of the sections in $\mathcal{R}_\mathcal{C}$, i.e., groups of sections that are in the same connected component of $\mathcal{R}_\mathcal{C}$. We define the new reconstructed object $\text{Conv}_\mathcal{C}$ as the union of the convex hulls of the connectivity classes of sections in $\mathcal{R}_\mathcal{C}$. In other words, for each group of sections K that are in the same connected component of $\mathcal{R}_\mathcal{C}$, we consider the convex hull of all the sections of K, denoted by $\text{conv}(K)$. The new reconstructed object is then defined as $\text{Conv} := \bigcup_\mathcal{C} \text{Conv}_\mathcal{C}$.

Lemma 4 Under the Separation Condition, the reconstructed object Conv conforms with the given sections $\mathcal{S}$, and is homeomorphic to $\mathcal{O}$.

Proof Consider any group K of sections in $\mathcal{S}_\mathcal{C}$ that are in the same connected component of $\mathcal{R}_\mathcal{C}$. We first show that K has at most one section at each face of $\mathcal{C}$. We use the fact that, under the Separation Condition, there is a bijection between the connected components of $\mathcal{R}_\mathcal{C}$ and $\mathcal{O}_\mathcal{C}$. According to this bijection, the sections of K are in the same connected component of $\mathcal{O}_\mathcal{C}$ (and so $\mathcal{O}$). Therefore, all the sections of K belong to a convex body in $\mathcal{O}$. We deduce that each face of $\mathcal{C}$ intersects K in at most one connected component (section). On the other hand, since $\mathcal{C}$ is convex, the convex hull of K lies inside $\mathcal{C}$ and we have $\text{conv}(K) \cap \partial\mathcal{C} = K$ for any K. Thus, for any cell $\mathcal{C}$, $\text{Conv}_\mathcal{C}$ conforms with $\mathcal{S}_\mathcal{C}$.

On the other hand, all the connected components of $\mathcal{O}_\mathcal{C}$ and $\text{Conv}_\mathcal{C}$ are convex and form 3-dimensional topological disks. Thus, the bijection between the connected components of

$\mathcal{O}_\mathcal{C}$ and $\mathcal{R}_\mathcal{C}$ (and so $\text{Conv}_\mathcal{C}$) provides a homotopy equivalence between the components that are all 3D topological disks. In Section 4.4, we will see how the homotopy equivalences in the different cells of the arrangement can be extended to a homotopy equivalence (and a homeomorphism) between $\mathcal{O}$ and Conv. □

Using the sufficient condition that implies the Separation Condition, we deduce the following theorem:

Theorem 5 (Reconstruction of a Collection of Convex Bodies) Let $\mathcal{O}$ be a union of convex bodies. We define the new reconstructed object as $\text{Conv} := \bigcup_\mathcal{C} \text{Conv}_\mathcal{C}$, where $\text{Conv}_\mathcal{C}$ is the union of the convex hulls of the connectivity classes of sections in $\mathcal{R}_\mathcal{C}$. If for any cell $\mathcal{C}$ of the arrangement of the cutting lines, $h_\mathcal{C} < \text{reach}_\mathcal{C}(\mathcal{O})$ then Conv conforms with the given sections $\mathcal{S}$, and is homeomorphic to $\mathcal{O}$.

Conclusion

In the previous sections, we presented the first sampling condition on the sample of cutting planes, called the Separation Condition, which is ensured if the height of the cells of the arrangement of the cutting planes is sufficiently small (with respect to the reach of the object). We showed that the Separation Condition implies that the connectivity between the sections is correctly reconstructed. However, it only implies the homotopy equivalence between the reconstructed object and the original shape for the 2D variant of the problem or some simple 3D cases as the case of union of convex bodies. In the next section, we will impose a second sampling condition on the sample of the cutting planes in order to ensure the homotopy equivalence in the general case.

4 General Topological Guarantees

This section is devoted to prove that under two appropriate sampling conditions, $\mathcal{R}$ and $\mathcal{O}$ are homotopy equivalent, and are in addition homeomorphic. To clarify the connection between the upcoming sections, let us shortly outline the general strategy employed in proving the homotopy equivalence between $\mathcal{R}$ and $\mathcal{O}$.

4.1 Proof Outline of the Homotopy Equivalence Between $\mathcal{R}$ and $\mathcal{O}$

We will provide a homotopy equivalence between $\mathcal{R}_\mathcal{C}$ and $\mathcal{O}_\mathcal{C}$ in each cell of the arrangement. (And then glue these homotopy equivalences together to form a global homotopy equivalence between $\mathcal{R}$ and $\mathcal{O}$.) In Section 2 we showed that under the first sampling condition called *Separation Condition* the connection between the sections in the reconstructed object $\mathcal{R}_\mathcal{C}$ is the same as in $\mathcal{O}_\mathcal{C}$, in the sense that there is a bijection between the connected components of $\mathcal{R}_\mathcal{C}$ and the connected components of $\mathcal{O}_\mathcal{C}$. This implies that for proving the homotopy equivalence between $\mathcal{R}_\mathcal{C}$ and $\mathcal{O}_\mathcal{C}$, it will be enough to show that the corresponding connected components have the same homotopy type. In order to extend these homotopy equivalences to a homotopy equivalence between $\mathcal{R}$ and $\mathcal{O}$, we will have to glue together the homotopy equivalences we obtain in the cells of the arrangement. This needs some care since the restriction to a section S of the two homotopy equivalences defined in the two adjacent cells of S may be different. To overcome this problem, we need to define an intermediate shape $\mathcal{M}_\mathcal{C}$ in each cell $\mathcal{C}$, called the *medial shape*. The medial shape has the following three properties :

(i) The medial shape contains the sections of $\mathcal{C}$, i.e., $\mathcal{S}_\mathcal{C} \subseteq \mathcal{M}_\mathcal{C}$.

(ii) There is a (strong) deformation retract r from $\mathcal{O}_\mathcal{C}$ to $\mathcal{M}_\mathcal{C}$. In particular, this map is a homotopy equivalence between $\mathcal{O}_\mathcal{C}$ and $\mathcal{M}_\mathcal{C}$. And its restriction to $\mathcal{S}_\mathcal{C}$ is the identity map.

(iii) Under the first sampling condition (Separation Condition), $\mathcal{M}_\mathcal{C} \subseteq \mathcal{R}_\mathcal{C}$.

The first two properties will be crucial to guarantee that the homotopy equivalences conform on each section under the Separation Condition. Indeed, the map $\mathcal{O}_\mathcal{C} \to \mathcal{M}_\mathcal{C} \hookrightarrow \mathcal{R}_\mathcal{C}$, obtained by composing the deformation retract and the inclusion, restricts to the identity map on each section of $\mathcal{S}_\mathcal{C}$. Thus, we can glue all these maps to obtain a global map from $\mathcal{O}$ to $\mathcal{R}$.

Using a generalized version of the nerve theorem (see Section 4.4) and property (ii) above, we can then reduce the problem to prove that the inclusion $i : \mathcal{M}_\mathcal{C} \hookrightarrow \mathcal{R}_\mathcal{C}$ forms a homotopy equivalence in each cell. Using Whitehead's theorem, it will be enough to show that the inclusion i induces isomorphisms between the corresponding homotopy groups. Under the Separation Condition, we prove that i induces an injective map on the first homotopy groups, and that all higher homotopy groups of $\mathcal{M}_\mathcal{C}$ and $\mathcal{R}_\mathcal{C}$ are trivial. Unfortunately, the Separation Condition does not ensure in general the surjectivity of i on the first homotopy groups. To overcome this problem, we need to impose a second condition

called *Intersection Condition*. Under the Intersection Condition, the map i will be surjective on the first homotopy groups, leading to a homotopy equivalence between $\mathcal{O}$ and $\mathcal{R}$.

According to the guarantees on the connectivity between the sections (Theorem 3), to prove the homotopy equivalence between $\mathcal{R}_\mathcal{C}$ and $\mathcal{O}_\mathcal{C}$ under the Separation Condition, we may restrict our attention to each of the corresponding connected components.

In the sequel, to simplify the notations and the presentation, we suppose that $\mathcal{O}_\mathcal{C}$ and thus $\mathcal{R}_\mathcal{C}$ are connected, and we show that $\mathcal{O}_\mathcal{C}$ and $\mathcal{R}_\mathcal{C}$ have the same homotopy type. It is clear that the same proofs can be applied to each corresponding connected components of $\mathcal{O}_\mathcal{C}$ and $\mathcal{R}_\mathcal{C}$ to imply the homotopy equivalence in the general case of multiple connected components.

4.2 Medial Shape

In this section, we define an intermediate shape in each cell $\mathcal{C}$ of the arrangement called the *medial shape*. The medial shape enjoys a certain number of important properties, discussed in this section, which makes it playing an important role in obtaining the homotopy equivalence of the next sections.

Definition 24 (Medial Shape $\mathcal{M}_\mathcal{C}$) Let x be a point in $\mathcal{S}_\mathcal{C} \subset \partial\mathcal{O}_\mathcal{C}$. Let $w(x) = [x, m_{i,\mathcal{C}}(x)]$ be the segment in the direction of the normal to $\partial\mathcal{O}_\mathcal{C}$ at x which connects x to the point $m_{i,\mathcal{C}}(x) \in \mathrm{MA}_i(\partial\mathcal{O}_\mathcal{C})$. We add to $\mathrm{MA}_i(\partial\mathcal{O}_\mathcal{C})$ all the segments $w(x)$ for all the points $x \in \mathcal{S}_\mathcal{C}$. We call the resulting shape $\mathcal{M}_\mathcal{C}$, see Figure 1.10-left. More precisely, $\mathcal{M}_\mathcal{C} := \mathrm{MA}_i(\partial\mathcal{O}_\mathcal{C}) \cup (\bigcup_{x\in\mathcal{S}_\mathcal{C}} w(x))$.

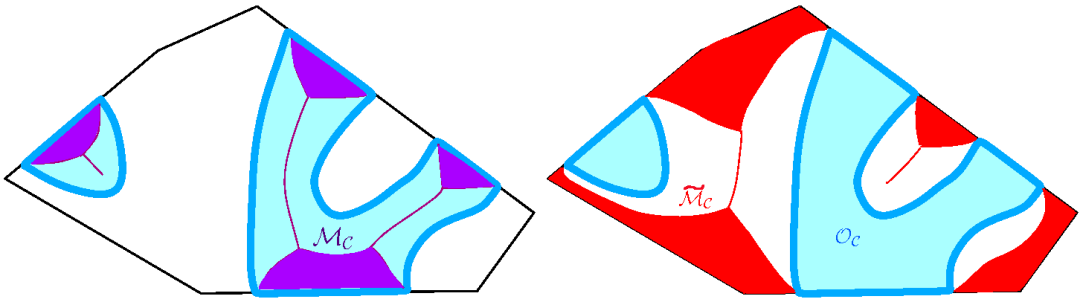

Figure 1.10: A 2D illustration of the medial shape $\mathcal{M}_\mathcal{C}$ in purple (left) and $\widetilde{\mathcal{M}}_\mathcal{C}$ in red (right).

Proposition 3 The medial shape verifies the following set of properties :

(i) The medial shape contains the sections of $\mathcal{C}$, i.e., $\mathcal{S}_\mathcal{C} \subseteq \mathcal{M}_\mathcal{C}$.

(*ii*) There is a (strong) deformation retract r from $\mathcal{O}_\mathcal{C}$ to $\mathcal{M}_\mathcal{C}$. In particular, this map is a homotopy equivalence between $\mathcal{O}_\mathcal{C}$ and $\mathcal{M}_\mathcal{C}$. And its restriction to $\mathcal{S}_\mathcal{C}$ is the identity map.

(*iii*) Under the Separation Condition, $\mathcal{M}_\mathcal{C} \subseteq \mathcal{R}_\mathcal{C}$.

Proof

(*i*) This property is true by the definition of the medial shape.

(*ii*) This is obtained by deforming $\mathcal{O}_\mathcal{C}$ to $\mathcal{M}_\mathcal{C}$ in the direction of the normals to the boundary $\partial\mathcal{O}_\mathcal{C}$. Note that the boundary $\partial\mathcal{O}_\mathcal{C}$ is smooth except on the boundaries of sections in $\mathcal{S}_\mathcal{C}$, and the boundaries of the sections in $\mathcal{S}_\mathcal{C}$ are already in $\mathcal{M}_\mathcal{C}$, thus, the deformation retract is well defined. Moreover, since $\partial\mathcal{O}$ (and so $\partial\mathcal{O}_\mathcal{C}$) is supposed to be of class C^2, according to a theorem by Wolter ([Wol92]), this deformation is continuous and is hence a continuous deformation retract from $\mathcal{O}_\mathcal{C}$ to $\mathcal{M}_\mathcal{C}$.

(*iii*) Since $\mathcal{M}_\mathcal{C} = \mathrm{MA}_i(\partial\mathcal{O}_\mathcal{C}) \cup \left(\bigcup_{x\in\mathcal{S}_\mathcal{C}} w(x)\right)$ and $\mathrm{MA}_i(\partial\mathcal{O}_\mathcal{C}) \subset \mathcal{R}_\mathcal{C}$, it will be sufficient to show that for any x in a section $A \in \mathcal{S}_\mathcal{C}$, $w(x) \subset \mathcal{R}_\mathcal{C}$. (Recall that $w(x)$ is the orthogonal segment to $\partial\mathcal{O}_\mathcal{C}$ at x that joins x to the corresponding medial point $m_{i,\mathcal{C}}(x)$ in $\mathrm{MA}_i(\partial\mathcal{O}_\mathcal{C})$.) We will show that $w(x)$ is contained in the segment $[x, \mathrm{lift}(x)]$. The point x is the closest point in $\partial\mathcal{O}_\mathcal{C}$ to $m_{i,\mathcal{C}}(x)$. Thus, the ball centered at $m_{i,\mathcal{C}}(a)$ and passing through x is entirely contained in $\mathcal{O}$ and its interior is empty of points of $\partial\mathcal{C}$. Thus, in the Voronoi diagram of $\mathcal{C}$, $m_{i,\mathcal{C}}(a)$ is in the same Voronoi cell as x. On the other hand, x is the closest point in $\mathcal{S}_\mathcal{C} \subset \partial\mathcal{O}_\mathcal{C}$ to $\mathrm{lift}(x)$. It easily follows that $d(x, \mathrm{lift}(x)) \geq d(x, m_{i,\mathcal{C}}(x))$. It follows that the segment $[x, m_{i,\mathcal{C}}(x)] = w(x)$ is a subsegment of $[x, \mathrm{lift}(x)]$. Therefore, by the definition of $\mathcal{R}_\mathcal{C}$, $w(x) \subset \mathcal{R}_\mathcal{C}$.

□

We end this section with the following important remark and proposition which will be used in the next section. By replacing the shape $\mathcal{O}_\mathcal{C}$ with its complementary set we may define an *exterior medial shape* $\widetilde{\mathcal{M}}_\mathcal{C}$. This is more precisely defined as follows. Let $\widetilde{\mathcal{O}}$ be the closure of the complementary of $\mathcal{O}$ in $\mathbb{R}^3$. And let $\widetilde{\mathcal{O}}_\mathcal{C}$ be the intersection of $\widetilde{\mathcal{O}}$ with the cell $\mathcal{C}$. The medial shape of $\widetilde{\mathcal{O}}_\mathcal{C}$, denoted by $\widetilde{\mathcal{M}}_\mathcal{C}$, is the union of the medial shapes of the connected components of $\widetilde{\mathcal{O}}_\mathcal{C}$, see Figure 1.10-right. Similarly, under the Separation Condition, the following proposition holds.

Proposition 4 Let $\widetilde{\mathcal{O}}_\mathcal{C}$ be the closure of the complementary of $\mathcal{O}_\mathcal{C}$ in $\mathcal{C}$ and $\widetilde{\mathcal{M}}_\mathcal{C}$ be the medial shape of $\widetilde{\mathcal{O}}_\mathcal{C}$. Under the Separation Condition : (*i*) There is a strong deformation retract from $\mathcal{C} \setminus \widetilde{\mathcal{M}}_\mathcal{C}$ to $\mathcal{O}_\mathcal{C}$, and (*ii*) We have $\mathcal{R}_\mathcal{C} \subset \mathcal{C} \setminus \widetilde{\mathcal{M}}_\mathcal{C}$.

Proof The proof of Property (*i*) is similar to the proof of Proposition 3 by deforming along the normal vectors to the boundary of $\widetilde{\mathcal{O}}_\mathcal{C}$. The second property (*ii*) is equivalent to $\widetilde{\mathcal{M}}_\mathcal{C} \subset \mathcal{C} \setminus \mathcal{R}_\mathcal{C}$. □

4.3 Topological Guarantees Implied by the Separation Condition

Throughout this section, we suppose that the Separation Condition holds. By the discussion at the end of Section 4.1, and without loss of generality, we may assume that $\mathcal{O}_\mathcal{C}$ and hence $\mathcal{R}_\mathcal{C}$ are connected. Thus, $\mathcal{O}_\mathcal{C}$ and $\mathcal{R}_\mathcal{C}$ are connected compact topological 3-manifolds embedded in $\mathbb{R}^3$.

We showed that the medial shape $\mathcal{M}_\mathcal{C}$ is homotopy equivalent to $\mathcal{O}_\mathcal{C}$, and under the Separation Condition, $\mathcal{M}_\mathcal{C} \subset \mathcal{R}_\mathcal{C}$. Using these properties, we will show that $\mathcal{L} : \mathcal{M}_\mathcal{C} \to \text{lift}(\mathcal{S}_\mathcal{C})$ (the restriction of the lift function to $\mathcal{M}_\mathcal{C}$) is a homotopy equivalence. On the other hand, according to Proposition 1, $\mathcal{L} : \mathcal{R}_\mathcal{C} \to \text{lift}(\mathcal{S}_\mathcal{C})$ is a homotopy equivalence as well. Hence, using the following comutative diagram, we can infer that $i : \mathcal{M}_\mathcal{C} \hookrightarrow \mathcal{R}_\mathcal{C}$ is a homotopy equivalence.

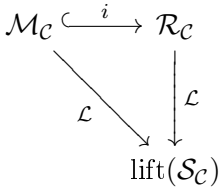

Moreover, since the objects we are manipulating are all CW-complexes, according to Whitehead's theorem homotopy equivalence is equivalent to weak homotopy equivalence. Hence, it will be enough to show that $\mathcal{L} : \mathcal{M}_\mathcal{C} \to \text{lift}(\mathcal{S}_\mathcal{C})$ induces isomorphism between the corresponding homotopy groups.

Injectivity on the Level of Homotopy Groups

We first show that under the Separation Condition, $\mathcal{L} : \mathcal{M}_\mathcal{C} \to \text{lift}(\mathcal{S}_\mathcal{C})$ induces injections on the level of homotopy groups.

Theorem 6 (Injectivity) *Under the Separation Condition, the homomorphisms between the homotopy groups of* $\mathcal{M}_\mathcal{C}$ *and* lift($\mathcal{S}_\mathcal{C}$)*, induced by the lift function* $\mathcal{L}$*, are injective.*

Proof Under the Separation Condition, we have $\mathcal{M}_\mathcal{C} \subset \mathcal{R}_\mathcal{C}$. Let $\widetilde{\mathcal{M}_\mathcal{C}}$ be the medial shape of the closure of the complementary set of $\mathcal{O}_\mathcal{C}$ in $\mathcal{C}$. We refer to the discussion at the end of the previous section for more details. Recall that by Proposition 4, we have $\mathcal{R}_\mathcal{C} \subset \mathcal{C} \setminus \widetilde{\mathcal{M}_\mathcal{C}}$, and there exists a deformation retract from $\mathcal{C} \setminus \widetilde{\mathcal{M}_\mathcal{C}}$ to $\mathcal{O}_\mathcal{C}$ (in particular $\mathcal{O}_\mathcal{C}$ and $\mathcal{C} \setminus \widetilde{\mathcal{M}_\mathcal{C}}$ are homotopy equivalent). We have now the following commutative diagram in which every map (except the lift function $\mathcal{L}$) is an injection (or an isomorphism) on the

level of homotopy groups.

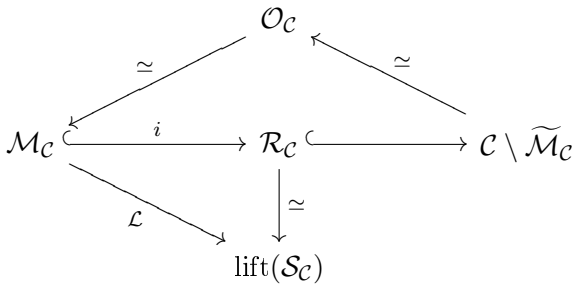

Using this diagram, the injectivity on the level of homotopy groups is clear: For any integer $j \geq 1$, consider the induced homomorphism $\mathcal{L}_* : \pi_j(\mathcal{M}_\mathcal{C}) \to \pi_j(\text{lift}(\mathcal{S}_\mathcal{C}))$. Let $x \in \pi_j(\mathcal{M}_\mathcal{C})$ be so that $\mathcal{L}_*(x)$ is the identity element of $\pi_j(\text{lift}(\mathcal{S}_\mathcal{C}))$. It is sufficient to show that x is the identity element of $\pi_j(\mathcal{M}_\mathcal{C})$. Following the maps of the diagram, and using the homotopy equivalence between lift($\mathcal{S}_\mathcal{C}$) and $\mathcal{R}_\mathcal{C}$, we have that $i_*(x)$ is mapped to the identity element of $\pi_j(\mathcal{R}_\mathcal{C})$. Then, by the inclusion $\mathcal{R}_\mathcal{C} \hookrightarrow \mathcal{C} \setminus \widetilde{\mathcal{M}}_\mathcal{C}$, it goes to the identity element of $\mathcal{C} \setminus \widetilde{\mathcal{M}}_\mathcal{C}$, and by the two retractions, it will be mapped to the identity element of $\pi_j(\mathcal{M}_\mathcal{C})$. As this diagram is commutative, we infer that x is the identity element of $\pi_j(\mathcal{M}_\mathcal{C})$. Thus, $\mathcal{L}_* : \pi_j(\mathcal{M}_\mathcal{C}) \to \pi_j(\text{lift}(\mathcal{S}_\mathcal{C}))$ is injective for all $j \geq 1$. The injectivity for $j = 0$ is already proved in Theorem 3. □

We have shown that under the Separation Condition, the lift function $\mathcal{L} : \mathcal{M}_\mathcal{C} \to$ lift($\mathcal{S}_\mathcal{C}$) induces injective morphisms between the homotopy groups of $\mathcal{M}_\mathcal{C}$ and lift($\mathcal{S}_\mathcal{C}$). If these induced morphisms were surjective, then $\mathcal{L}$ would be a homotopy equivalence (by Whitehead's theorem). We will show below that the Separation Condition implies the surjectivity for all the homotopy groups except for dimension one (fundamental groups). Indeed, we will show that under the Separation Condition, all the i-dimensional homotopy groups of $\mathcal{M}_\mathcal{C}$ and lift($\mathcal{S}_\mathcal{C}$) for $i \geq 2$ are trivial. Once this is proved, it will be sufficient to study the surjectivity of $\mathcal{L}_* : \pi_1(\mathcal{M}_\mathcal{C}) \to \pi_1(\text{lift}(\mathcal{S}_\mathcal{C}))$.

Remark : Note that the injectivity in the general form above remains valid for the corresponding reconstruction problems in dimensions greater than three. However, the vanishing results on higher homotopy groups of $\mathcal{O}_\mathcal{C}$ and $\mathcal{R}_\mathcal{C}$ are only valid in dimensions two and three.

The topological structures of $\mathcal{R}_\mathcal{C}$ and $\mathcal{O}_\mathcal{C}$ are determined by their fundamental groups.

In this section, we show that if the Separation Condition is verified, then the topological structure of the portion of $\mathcal{O}$ in a cell $\mathcal{C}$ (i.e., $\mathcal{O}_\mathcal{C}$) is simple enough, in the sense that for all $i \geq 2$, the i-dimensional homotopy group of $\mathcal{O}_\mathcal{C}$ is trivial. We can easily show that $\mathcal{R}_\mathcal{C}$ has the same property.[2] As a consequence, the topological structures of $\mathcal{O}_\mathcal{C}$ and $\mathcal{R}_\mathcal{C}$ are

[2]Recall that for simplifying the presentation, we assume that $\mathcal{O}_\mathcal{C}$ and so $\mathcal{R}_\mathcal{C}$ are connected. The same proof shows that in the general case, the same property holds for each connected component of $\mathcal{O}_\mathcal{C}$ or $\mathcal{R}_\mathcal{C}$.

determined by their fundamental group, $\pi_1(\mathcal{O}_\mathcal{C})$ and $\pi_1(\mathcal{R}_\mathcal{C})$.

We first state the following general theorem for an arbitrary embedded 3-manifold with connected boundary.

Theorem 7 Let K be a connected 3-manifold in $\mathbb{R}^3$ with a (non-empty) connected boundary. Then for all $i \geq 2$, $\pi_i(K) = \{0\}$.

We will provide a proof of this theorem in the following. This theorem can be also obtained from Corollary 3.9 of [Hat02][3]. From this theorem, we infer the two following theorems.

Theorem 8 Under the Separation Condition, $\pi_i(\mathcal{O}_\mathcal{C}) = \{0\}$, for all $i \geq 2$.

Proof We only make use of the fact that under the Separation Condition, any connected component of $\partial\mathcal{O}$ is cut by at least one cutting plane. In this case, every connected component of $\mathcal{O}_\mathcal{C}$ is a 3-manifold with connected boundary. The theorem follows as a corollary of Theorem 7. □

Theorem 9 $\pi_i(\mathcal{R}_\mathcal{C}) = \{0\}$, for all $i \geq 2$.

Proof Using Theorem 7, it will be sufficient to show that the boundary of any connected component K of $\mathcal{R}_\mathcal{C}$ is connected. Let x and y be two points on the boundary of K, and let S and S' be two sections so that $x \in [a, \text{lift}(a)]$ for some $a \in S$ and $y \in [b, \text{lift}(b)]$ for some $b \in S'$. By the definition of $\mathcal{R}_\mathcal{C}$, x is connected to S in $\partial\mathcal{R}_\mathcal{C}$, and y is connected to S' in $\partial\mathcal{R}_\mathcal{C}$. On the other hand, since S and S' are two sections in the connected component K of $\mathcal{R}_\mathcal{C}$, they lie on ∂K and are connected to each other in ∂K (and so in $\partial\mathcal{R}_\mathcal{C}$). Thus, x is connected to y in $\partial\mathcal{R}_\mathcal{C}$. □

Proof of Theorem 7

We will prove that for any connected 3-manifold K in $\mathbb{R}^3$ with a (non-empty) connected boundary, we have $\pi_i(K) = \{0\}$, for all $i \geq 2$. We use the continuity of the boundary of K to show that the two dimensional homotopy group of K is trivial. To this end, we need the following theorem called the Sphere Theorem (for 3-manifolds), see [Bat71] for a proof.

Theorem 10 (Sphere Theorem) Let K be an orientable 3-manifold such that $\pi_2(K)$ is not the trivial group. Then there exists an **embedding** $e : S^2 \to K$ which represents a non-zero element of $\pi_2(K)$.

Using the Sphere theorem, we prove Theorem 7 in two parts.

- We claim that if K is a connected 3-manifold in $\mathbb{R}^3$ with (non-empty) connected boundary, then $\pi_2(K) = \{0\}$.

[3] Thanks to Frederic Chazal for providing this reference.

For the sake of a contradiction, suppose that $\pi_2(K)$ is non-trivial. According to the Sphere theorem, there exists an embedding $e : S^2 \to K$ which represents a non-zero element of $\pi_2(K)$. The closed surface $e(S^2)$ separates $\mathbb{R}^3$ into two connected components, one bounded (the interior of $e(S^2)$) and the other unbounded (the exterior of $e(S^2)$). Since the boundary of K is connected, the complementary of K, denoted by K^c, is connected. K^c being connected and disjoint from $e(S^2)$, lies in the exterior of $e(S^2)$. Hence, the interior of $e(S^2)$ is contained in K; and e can be extended to the interior of $e(S^2)$ (which is a 2-disk). This contradicts the fact that e represents a non-zero element of $\pi_2(K)$.

- We now prove that the i-dimensional homotopy groups of K, for $i \geq 3$, are all trivial. Using the dimension of the manifold K, we will be able to prove that the corresponding homology groups are trivial. Then, in order to relate the homology and homotopy groups, one may think of applying Hurewicz Theorem. However, Hurewicz Theorem holds only for simply-connected spaces. Thus, we consider the universal cover of K, and apply Hurewicz Theorem to it. Afterwards, we make use of the relation between K and its universal cover to prove the purposed statement for K.

  Let $\widetilde{K}$ be the universal cover of K. By Corollary 1, it will be enough to show that $\pi_i(\widetilde{K}) = \{0\}$ for all i (since $\widetilde{K}$ is simply connected, so we have $\pi_1(\widetilde{K}) = \{0\}$). We already now that $\pi_2(\widetilde{K}) = \pi_2(K) = \{0\}$.

  The three dimensional homology group of any connected non-compact 3-manifold is trivial. As $\widetilde{K}\backslash\partial\widetilde{K}$ (the interior of $\widetilde{K}$) is a non-compact 3-manifold, its three-dimensional homology group is trivial. On the other hand, the homology groups of $\widetilde{K}$ and its interior are the same. Thus, we have $H_3(\widetilde{K}) = H_3(\widetilde{K}\backslash\partial\widetilde{K}) = \{0\}$. By Hurewicz Theorem, we infer that $\pi_3(\widetilde{K}) = \{0\}$ as well. Also, $\widetilde{K}$ being a 3-manifold, all the higher homology groups $H_i(\widetilde{K})$ are trivial, for all $i \geq 4$. Reasoning by induction, again by Hurewicz Theorem, we obtain $\pi_i(\widetilde{K}) = \{0\}$, for all $i \geq 4$. And the theorem follows.

4.4 Second Condition: Intersection Condition

In the previous section, we saw that under the Separation Condition, the topological structures of $\mathcal{O}_\mathcal{C}$ and $\mathcal{R}_\mathcal{C}$ are determined by their fundamental group $\pi_1(\mathcal{O}_\mathcal{C})$ and $\pi_1(\mathcal{R}_\mathcal{C})$, respectively. The goal of this section is to find a way to ensure an isomorphism between the fundamental groups of $\mathcal{R}_\mathcal{C}$ and $\mathcal{O}_\mathcal{C}$. We recall that as $\mathcal{O}_\mathcal{C}$ and $\mathcal{M}_\mathcal{C}$ are homotopy equivalent, $\pi_1(\mathcal{O}_\mathcal{C})$ is isomorphic to $\pi_1(\mathcal{M}_\mathcal{C})$. On the other hand, $\mathcal{R}_\mathcal{C}$ and $\text{lift}(\mathcal{S}_\mathcal{C})$ are homotopy equivalent, and $\pi_1(\mathcal{R}_\mathcal{C})$ is isomorphic to $\pi_1(\text{lift}(\mathcal{S}_\mathcal{C}))$ (c.f. last diagram). Thus, it will be sufficient to compare $\pi_1(\mathcal{M}_\mathcal{C})$ and $\pi_1(\text{lift}(\mathcal{S}_\mathcal{C}))$.

We consider $\mathcal{L}_* : \pi_1(\mathcal{M}_\mathcal{C}) \to \pi_1(\text{lift}(\mathcal{S}_\mathcal{C}))$, the map induced by the lift function from $\mathcal{M}_\mathcal{C}$ to $\text{lift}(\mathcal{S}_\mathcal{C})$ on fundamental groups . We showed that $\mathcal{L}_*$ is injective. A natural condition to ensure that $\mathcal{L}_*$ is an isomorphism is to impose that $\text{lift}(\mathcal{S}_\mathcal{C})$ *is contractible* (or more generally, each connected component of $\text{lift}(\mathcal{S}_\mathcal{C})$ is contractible). This is very common in

practice, where the sections are contractible and sufficiently close to each other. In this case, all the homotopy groups $\pi_j(\text{lift}(\mathcal{S}_\mathcal{C}))$ are trivial and by injectivity of $\mathcal{L}_*$ proved in the previous section, $\mathcal{L}_*$ becomes an isomorphism in each dimension. Hence, the homotopy equivalence between $\mathcal{R}_\mathcal{C}$ and $\mathcal{O}_\mathcal{C}$ can be deduced.

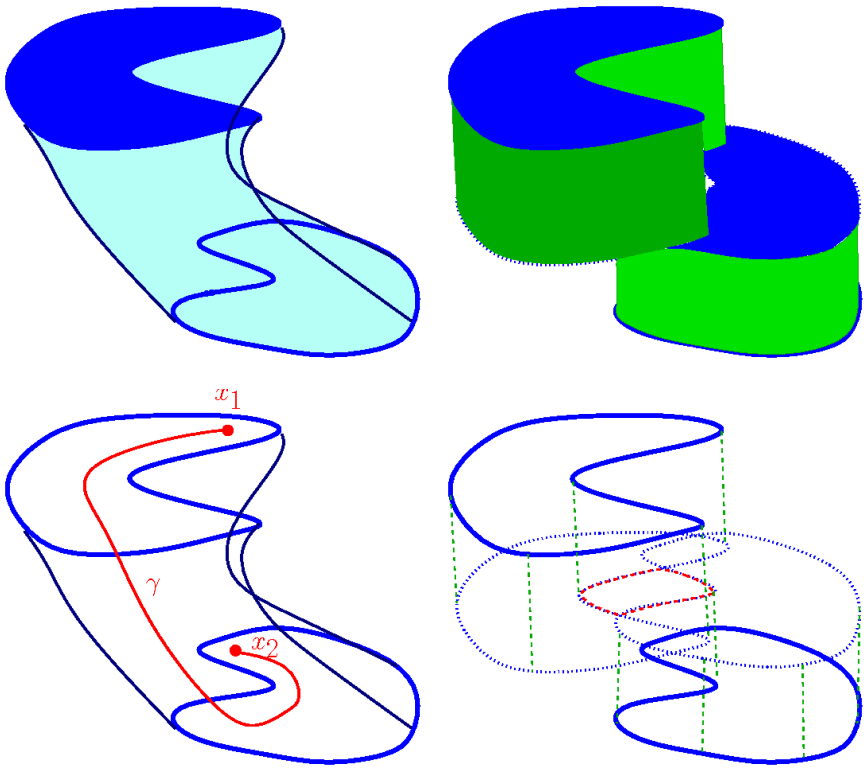

Figure 1.11: Left) Original shape. Right) Reconstructed shape. 3D example of the case where the lift function from $\mathcal{M}_\mathcal{C}$ to $\text{lift}(\mathcal{S}_\mathcal{C})$ fails to be surjective: x_1 and x_2 are two points with the same lift in $\text{lift}(\mathcal{S}_\mathcal{C})$. The lift of any curve γ connecting x_1 and x_2 in $\mathcal{M}_\mathcal{C}$ provides a non-zero element of $\pi_1(\text{lift}(\mathcal{S}_\mathcal{C}), x)$. The reconstructed shape is a torus and is not homotopy equivalent to the original shape which is a twisted cylinder.

However, the map $\mathcal{L}_* : \pi_1(\mathcal{M}_\mathcal{C}) \to \pi_1(\text{lift}(\mathcal{S}_\mathcal{C}))$ fails to be surjective in general (where the connected components of $\text{lift}(\mathcal{S}_\mathcal{C})$ are not necessarily contractible). Figure 1.11 shows two shapes with different topologies, a torus and a (*twisted*) cylinder, that have the same (inter)sections with a set of (two) cutting planes. Hence, whatever is the reconstructed object from these sections, it would not be topologically consistent for at least one of these objects. In particular, the proposed reconstructed object ($\mathcal{R}$) is a torus which is not homotopy equivalent to the (*twisted*) cylinder ($\mathcal{O}$). In addition, we note that the Separation Condition may be verified for such a situation. Indeed, such a situation is exactly the case when the injective morphism between the fundamental groups of $\mathcal{O}$ and $\mathcal{R}$ is not surjective. This situation can be explained as follows: let x_1 and x_2 be two points in the sections S_1 and S_2 with the same lift x in $\text{lift}(\mathcal{S}_\mathcal{C})$. The lift of any curve γ connecting x_1 and x_2 in

$\mathcal{M}_\mathcal{C}$ provides a non-identity element of $\pi_1(\text{lift}(\mathcal{S}_\mathcal{C}), x)$ which is not in the image of $\mathcal{L}_*$. We may avoid this situation with the following condition.

Definition 25 (Intersection Condition) We say that the set of cutting planes verifies the Intersection Condition if for any pair of sections S_i and S_j in $\mathcal{S}_\mathcal{C}$, and for any connected component X of $\text{lift}(S_i) \cap \text{lift}(S_j)$ (see Figure 1.12), the following holds: there is a path $\gamma \subset \mathcal{M}_\mathcal{C}$ from a point $a \in S_i$ to a point $b \in S_j$ with $\text{lift}(a) = \text{lift}(b) = x \in X$ so that $\mathcal{L}_*(\gamma)$ is the identity element of $\pi_1(\text{lift}(\mathcal{S}_\mathcal{C}), x)$, i.e., is contractible in $\text{lift}(\mathcal{S}_\mathcal{C})$ with a homotopy respecting the base point x.

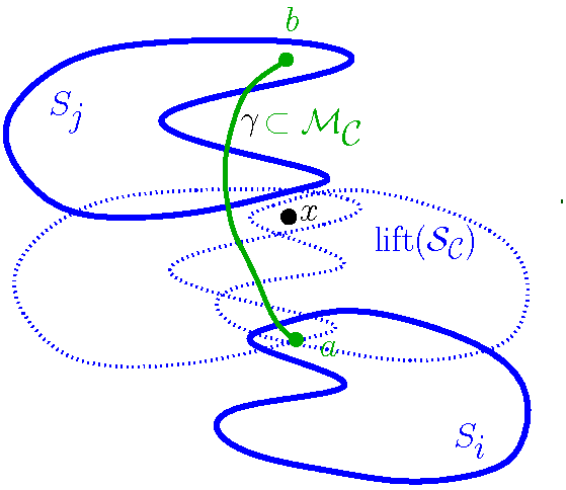

Figure 1.12: Intersection Condition.

In Section 4.5, we will show how to verify the Intersection Condition. Let us first prove the surjectivity of the map $\mathcal{L}_*$ which is deduced directly from the Intersection Condition.

Theorem 11 (Surjectivity) *Under the Intersection Condition, the induced map* $\mathcal{L}_* : \pi_1(\mathcal{M}_\mathcal{C}) \to \pi_1(\text{lift}(\mathcal{S}_\mathcal{C}))$ *is surjective.*

Proof Let y_0 be a fixed point of $\mathcal{M}_\mathcal{C}$ and $x_0 = \mathcal{L}(y_0)$. We show that $\mathcal{L}_* : \pi_1\big(\mathcal{M}_\mathcal{C}, y_0\big) \to \pi_1\big(\text{lift}(\mathcal{S}_\mathcal{C}), x_0\big)$ is surjective. Let α be a closed curve in $\text{lift}(\mathcal{S}_\mathcal{C})$ which represents an element of $\pi_1\big(\text{lift}(\mathcal{S}_\mathcal{C}), x_0\big)$. We show the existence of an element $\beta \in \pi_1\big(\mathcal{M}_\mathcal{C}, y_0\big)$ such that $\mathcal{L}_*(\beta) = [\alpha]$, where $[\alpha]$ denotes the homotopy class of α in $\pi_1\big(\text{lift}(\mathcal{S}_\mathcal{C}), x_0\big)$. We can divide α into subcurves $\alpha_1, \ldots, \alpha_m$ such that α_j joins two points x_{j-1} and x_j, and is entirely in the lift of one of the sections S_j, for $j = 1, \ldots, m$. We may assume $y_0 \in S_1 = S_m$. For each $j = 1, \ldots, m$, let β_j be the curve in S_j joining two points z_j to w_j which is mapped to α_j under $\mathcal{L}$. Note that w_j and z_{j+1} (possibly) live in two different sections, but have the same image (x_j) under the lift map $\mathcal{L}$. Let X_j be the connected component of $\text{lift}(S_j) \cap \text{lift}(S_{j+1})$ which contains x_j, see Figure 1.13. According to the Intersection Condition, there is a path $\gamma_j \subset \mathcal{M}_\mathcal{C}$ connecting a point $a_j \in S_j$ to a point $b_{j+1} \in S_{j+1}$ such that $\text{lift}(a_j) = \text{lift}(b_{j+1}) = x'_j \in X_j$ and the image of γ_j under $\mathcal{L}$ is the identity element of $\pi_1(\text{lift}(\mathcal{S}_\mathcal{C}), x'_j)$

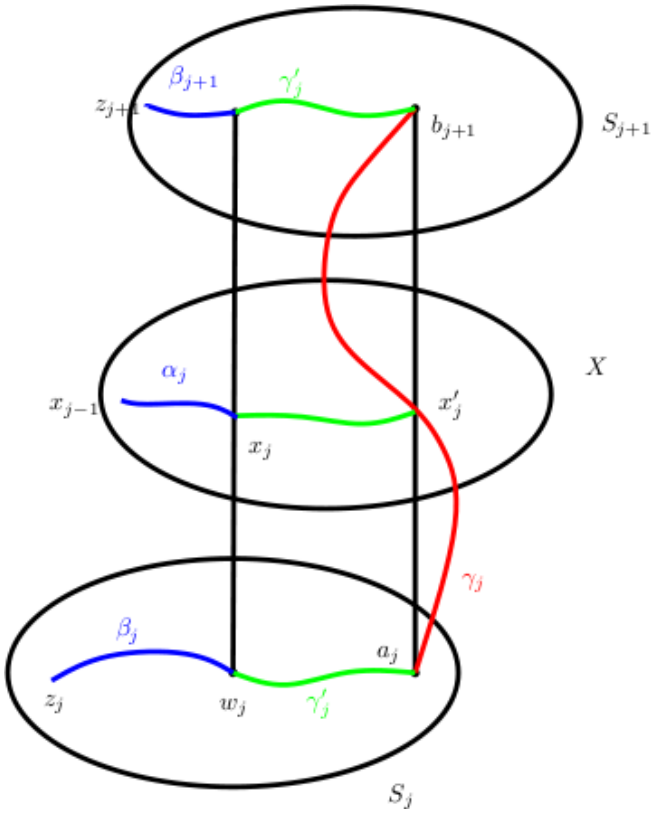

Figure 1.13: For the proof of Theorem 11.

(i.e., is contractible with a homotopy respecting the base point x'_j). Since X_j is connected, there is a path from x_j to x'_j in X_j, so lifting back this path to two paths from w_j to a_j in S_j and from b_{j+1} to z_{j+1} and taking the union of these two paths with γ_j, we infer the existence of a path $\gamma'_j \subset \mathcal{M}_{\mathcal{C}}$ connecting w_j to z_{j+1}, such that the image of γ'_j under $\mathcal{L}$ is contractible in lift($\mathcal{S}_{\mathcal{C}}$) with a homotopy respecting the base point x_j.

Let β be the path from x_0 to x_0 obtained by concatenating β_j and γ'_j alternatively, i.e., $\beta = \beta_1\gamma'_1\beta_2\gamma'_2 \dots \beta_{m-1}\gamma'_m\beta_m\gamma'_m$. We claim that $\mathcal{L}_*([\beta]) = [\alpha]$. This is now easy to show: we have $\mathcal{L}_*(\beta) = \alpha_1\mathcal{L}_*(\gamma'_1)\alpha_2 \dots \mathcal{L}_*(\gamma'_m)\alpha_m$, and all the paths $\mathcal{L}_*(\gamma'_j)$ are contractible to the constant path $[x_j]$ by a homotopy fixing x_j all the time. We deduce that under a homotopy fixing x_0, $\alpha_1\mathcal{L}_*(\gamma'_1) \dots \mathcal{L}_*(\gamma'_m)\alpha_m$ is homotopic to $\alpha_1\alpha_2 \dots \alpha_m = \alpha$, and this is exactly saying that $\mathcal{L}_*([\beta]) = [\alpha]$. The surjectivity follows. □

Putting together all the materials we have obtained, we infer the main theorem of this section.

Theorem 12 (Main Theorem-Part I) Under the Separation and the Intersection Conditions, $\mathcal{R}_{\mathcal{C}}$ is homotopy equivalent to $\mathcal{O}_{\mathcal{C}}$.

Generalized Nerve Theorem and Homotopy Equivalence of $\mathcal{R}$ and $\mathcal{O}$

In this section, we extend the homotopy equivalence between $\mathcal{R}_\mathcal{C}$ and $\mathcal{O}_\mathcal{C}$, in each cell $\mathcal{C}$, to a global homotopy equivalence between $\mathcal{R}$ and $\mathcal{O}$. To this end, we make use of a generalization of the nerve theorem. This is a folklore theorem and has been observed and used by different authors. For a modern proof of a still more general result, we refer to Segal's paper [Seg68]. (See also [May03], for a survey of similar results.)

Theorem 13 (Generalized Nerve Theorem) Let $H : X \to Y$ be a continuous map. Suppose that Y has an open cover $\mathcal{K}$ with the following two properties :

- Finite intersections of sets in $\mathcal{K}$ are in $\mathcal{K}$.
- For each $U \in \mathcal{K}$, the restriction $H : H^{-1}(U) \to U$ is a weak homotopy equivalence.

Then H is a weak homotopy equivalence.

Let $H_\mathcal{C} : \mathcal{O}_\mathcal{C} \to \mathcal{R}_\mathcal{C}$ be the homotopy equivalence obtained in the previous sections between $\mathcal{O}_\mathcal{C}$ and $\mathcal{R}_\mathcal{C}$. (So $H_\mathcal{C}$ is the composition of the retraction $\mathcal{O}_\mathcal{C} \to \mathcal{M}_\mathcal{C}$ and the inclusion $\mathcal{M}_\mathcal{C} \hookrightarrow \mathcal{R}_\mathcal{C}$.) Let $H : \mathcal{O} \to \mathcal{R}$ be the map defined by $H(x) = H_\mathcal{C}(x)$ if $x \in \mathcal{O}_\mathcal{C}$ for a cell $\mathcal{C}$ of the arrangement of the cutting planes. Note that H is well-defined since $H_\mathcal{C}|_{\mathcal{S}_\mathcal{C}} = id_{\mathcal{S}_\mathcal{C}}$, for all $\mathcal{C}$. In addition, since for any cell $\mathcal{C}$, $H_\mathcal{C}$ is continuous, H is continuous as well.

We can now apply the generalized nerve theorem by the following simple trick. Let ϵ be an infinitesimal positive value. For any cell $\mathcal{C}$ of the arrangement of the cutting planes, we define $\mathcal{O}^\epsilon_\mathcal{C} = \{x \in \mathbb{R}^3,\ d(x, \mathcal{O}_\mathcal{C}) < \epsilon\ \}$. Let us now consider the open covering $\mathcal{K}$ of $\mathcal{O}$ by these open sets and all their finite intersections. It is straightforward to check that for ϵ small enough, the restriction of H to each element of $\mathcal{K}$ is a weak homotopy equivalence. Therefore, according to the generalized nerve theorem, H is a weak homotopy equivalence between $\mathcal{R}$ and $\mathcal{O}$. And by Whitehead's theorem, H is a homotopy equivalence between $\mathcal{R}$ and $\mathcal{O}$. Thus, we have proved :

Theorem 14 (Main Theorem-Part II) Under the Separation and the Intersection Conditions, the reconstructed object $\mathcal{R}$ is homotopy equivalent to the unknown original shape $\mathcal{O}$.

4.5 How to Ensure the Intersection Condition?

In Section 2, we showed that the Separation Condition can be ensured with a sufficiently dense sample of cutting planes. In this section we provide a sufficient condition that implies the Intersection Condition.

We showed that by bounding from above the height of the cells by the reach of the object, we can ensure the Separation Condition. In order to ensure the Intersection Condition, we need a stronger condition on the height of the cells. As we will see, this condition is

a *transversality* condition on the cutting planes that can be measured by the angle between the cutting planes and the normal to $\partial\mathcal{O}$ at contour-points.

Definition 26 (Angle α_a) Let a be a point on the boundary of a section $A \in \mathcal{S}_\mathcal{C}$ on the plane P_A. We consider $m_i(a)$, that may be outside the cell $\mathcal{C}$. We define α_a as the angle between P_A and the normal to $\partial\mathcal{O}$ at a, i.e. $\alpha_a := \text{angle}(P_A, [a, m_i(a)])$, see Figure 1.14-left. We define $\alpha_\mathcal{C} = \max_{a\in\partial\mathcal{S}_\mathcal{C}} \alpha_a$.

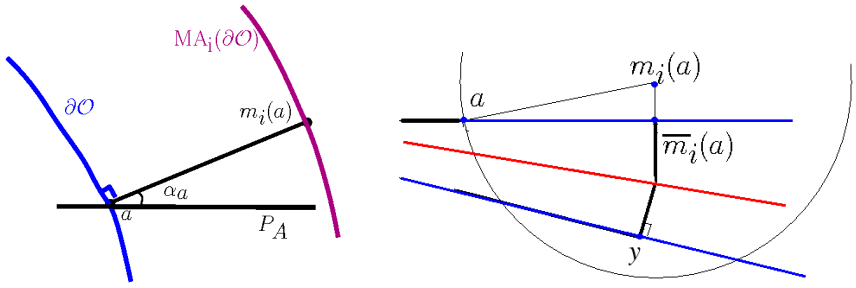

(a) Definition of α_a (b) For the proof of Lemma 5

Figure 1.14: Definitions

Sufficient Conditions We now define the sampling conditions on the cutting planes. (See Section 2.3 for the definitions of $h_\mathcal{C}$ and $\text{reach}_\mathcal{C}(\mathcal{O})$.)

(C1) Density Condition For any cell $\mathcal{C}$ of the arrangement, $h_\mathcal{C} < \text{reach}_\mathcal{C}(\mathcal{O})$.

(C2) Transversality Condition For any cell $\mathcal{C}$,

$$h_\mathcal{C} < \frac{1}{2}\left(1 - \sin(\alpha_\mathcal{C})\right) \text{reach}_\mathcal{C}(\mathcal{O}).$$

The Density Condition is based on the density of the sections. The Transversality Condition is defined in a way that the transversality of the cutting planes to $\partial\mathcal{O}$ and the *distance between the sections* are controlled simultaneously. (Indeed, $\sin(\alpha_a)$ is to control the transversality, and bounding from above $h_\mathcal{C}$ allows us to control the distance between the sections.)

Remark on the Transversality : The transversality of the cutting planes to $\partial\mathcal{O}$ seems to be a reasonable condition in practice, specially for applications in 3D ultrasound. Indeed, according to [Rou03] Section 1.2.1, from a technical point of view if a *cut* is not *sufficiently* transversal to the organ, the quality of the resulting 2D ultrasonic image is not acceptable for diagnosis. Therefore, assuming an upper bound α for the angle between the cutting planes and the normals to the surface of the organ along the cuts seems reasonable. In this case, $\forall\mathcal{C},\ h_\mathcal{C} < \frac{1}{2}\left(1 - \sin(\alpha)\right) \text{reach}_\mathcal{C}(\mathcal{O})$ implies the Transversality Condition.

According to Lemma 3 in Section 2, the Density Condition implies the Separation Condition. We will show that under the Transversality Condition, the Intersection Condition is verified. Therefore, by increasing the density of the sections of $\mathcal{O}$, with preferably transversal cutting planes, we can ensure the required sampling conditions, and as a consequence, provide a topologically consistent reconstruction of $\mathcal{O}$. This is one of the main results of this chapter :

Theorem 15 (Main Theorem-Part III) If the cutting planes verify the Density and the Transversality Conditions, then the Separation and the Intersection Conditions are verified. Therefore, the proposed reconstructed object $\mathcal{R}$ is homotopy equivalent to the unknown original shape $\mathcal{O}$.

To prove this theorem, we need the following notations.

Notation $\big(K_i(\mathcal{S}_\mathcal{C})$ and $K_e(\mathcal{S}_\mathcal{C})\big)$: Recall that VorSkel($\mathcal{C}$) is the locus of the points with more than one nearest point in $\partial\mathcal{C}$. We write $K_i(\mathcal{S}_\mathcal{C})$ (resp. $K_e(\mathcal{S}_\mathcal{C})$) for the set of points $x \in$ VorSkel($\mathcal{C}$) such that all the nearest points of x in $\partial\mathcal{C}$ lie inside (resp. outside) the sections.

Notation $\big(\bar{m}_i(a)$ and $\bar{m}_e(a)\big)$: Let a be a point on the boundary of a section $A \in \mathcal{S}_\mathcal{C}$ on the plane P_A. We write $\bar{m}_i(a)$ (resp. $\bar{m}_e(a)$) for the orthogonal projection of $m_i(a)$ (resp. $m_e(a)$) onto P_A. See Figure 1.14-right. We have $d(m_i(a), \bar{m}_i(a)) = \sin(\alpha_a)\ d(a, m_i(a))$ and $d(m_e(a), \bar{m}_e(a)) = \sin(\alpha_a)\ d(a, m_e(a))$.

Lemma 5 If the Transversality Condition is verified, for any $a \in \partial\mathcal{S}_\mathcal{C}$, we have lift$(\bar{m}_i(a)) \in K_i(\mathcal{S}_\mathcal{C})$ and lift$(\bar{m}_e(a)) \in K_e(\mathcal{S}_\mathcal{C})$. In addition, the two segments that join lift$(\bar{m}_i(a))$ to its nearest points in $\partial\mathcal{C}$ both lie entirely in $\mathcal{M}_\mathcal{C}$.

Proof We first show that lift$(\bar{m}_i(a)) \in K_i(\mathcal{S}_\mathcal{C})$. The symmetric property for lift$(\bar{m}_e(a))$ can be proved similarly. Let us simplify the notation by writing m_i for $m_i(a)$, and $\bar{m}_i$ for $\bar{m}_i(a)$. Let us also write $B(m_i)$ for the ball centered at m_i of radius $d(m_i, a)$. We have $d(m_i, \bar{m}_i) \leq d(m_i, a)$. Thus, $\bar{m}_i$ lies in $B(m_i)$. As this ball is contained in $\mathcal{O}$, $\bar{m}_i$ is in $\mathcal{O}$. Consider now lift$(\bar{m}_i)$ on VorSkel($\mathcal{C}$), and call y the point distinct from $\bar{m}_i$ such that lift$(\bar{m}_i) =$ lift(y), see Figure 1.14-right. To have lift$(m_i) \in K_i(\mathcal{S}_\mathcal{C})$, we need to show that y is in $\mathcal{O}$. We have

$$\begin{aligned} d(m_i, y) &\leq d(m_i, \bar{m}_i) + d(\bar{m}_i, \text{lift}(\bar{m}_i)) + d(\text{lift}(y), y) \\ &\leq \sin(\alpha_a) d(a, m_i) + 2\ h_\mathcal{C} \leq d(a, m_i). \end{aligned}$$

Thus, y belongs to $B(m_i)$, and we can deduce that $y \in \mathcal{O}$ and lift$(\bar{m}_i) \in K_i(\mathcal{S}_\mathcal{C})$. In addition, the ball B centered at lift$(\bar{m}_i)$ which passes through $\bar{m}_i$ and y is entirely contained in $B(m_i) \subset \mathcal{O}$. Thus, the interior of B is empty of points of $\partial\mathcal{O}_\mathcal{C}$ and B is a medial ball of $\mathcal{O}_\mathcal{C}$, and its center lift$(\bar{m}_i)$ belongs to MA$_i(\partial\mathcal{O}_\mathcal{C})$. Since $\bar{m}_i$ and y are in $\mathcal{S}_\mathcal{C}$, according to the definition of $\mathcal{M}_\mathcal{C}$, the line-segments [lift$(\bar{m}_i), \bar{m}_i$] and [lift$(\bar{m}_i), y$] lie entirely in $\mathcal{M}_\mathcal{C}$. □

Lemma 6 Under the Transversality Condition, the Intersection Condition is verified.

Proof Let S_a and S_b be two sections in $\mathcal{S}_\mathcal{C}$ such that $\text{lift}(S_a) \cap \text{lift}(S_b)$ is non-empty. We recall that $\mathcal{L}_*$ denotes the homomorphism $\mathcal{L}_* : \pi_j(\mathcal{M}_\mathcal{C}) \to \pi_j(\text{lift}(\mathcal{S}_\mathcal{C}))$ induced by the lift function $\mathcal{L} : \mathcal{M}_\mathcal{C} \to \text{lift}(\mathcal{S}_\mathcal{C})$. We will show that for any two points $a \in \partial S_a, b \in \partial S_b$ such that $\text{lift}(a) = \text{lift}(b)$, there exists a path $\gamma \subset \mathcal{M}_\mathcal{C}$ between a and b so that $\mathcal{L}_*(\gamma)$ is contractible in $\mathcal{L}_*(\pi_1(\mathcal{M}_\mathcal{C}))$. Let P_a and P_b be the cutting-planes of S_a and S_b respectively. One of the two following cases happen :

• If the segment $[a, \bar{m}_i(a)]$ (i.e., the projection of the segment $[a, m_i(a)]$ onto P_a) is not cut by any other cutting plane, then we claim that $\text{lift}(a)$ is connected to $\text{lift}(\bar{m}_i(a))$ in $K_i(\mathcal{S}_\mathcal{C})$.

Consider the 2 dimensional ball B in the plane P_a centered at $\bar{m}_i(a)$ and passing through a. This ball is contained in the 3D ball centered at $m_i(a)$ and passing through a, which lies entirely inside $\mathcal{O}$. Considering the intersection of this 3D ball with P_a, we infer that B lies in the section S_a. Therefore, $\text{lift}(B)$ is entirely contained in $\text{lift}(S_a)$. In Figure 1.15 $\text{lift}(B)$ is colored in green.

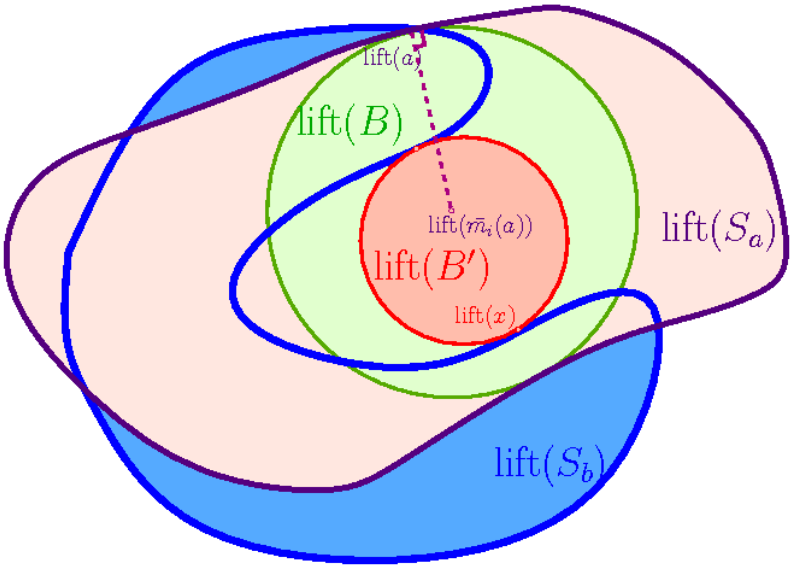

Figure 1.15: For the proof of Lemma 6: the lift of two sections S_a and S_b on VorSkel($\mathcal{C}$) is illustrated. We prove that the lift of the segment $[a, \bar{m}_i(a)]$ lies in $\text{lift}(S_a) \cap \text{lift}(S_b)$.

Since $\text{lift}(a) = \text{lift}(b)$, we have $\text{lift}(a) \in \text{lift}(S_a) \cap \text{lift}(S_b)$. On the other hand, according to Lemma 5, $\text{lift}(\bar{m}_i(a))$ lies in $\text{lift}(S_a) \cap \text{lift}(S_b)$. For the sake of contradiction, suppose that $\text{lift}(a)$ is not connected to $\text{lift}(\bar{m}_i(a))$ in $K_i(\mathcal{S}_\mathcal{C})$. In this case, $\text{lift}(B)$ intersects (at least) two different connected components of $\text{lift}(S_a) \cap \text{lift}(S_b)$, see Figure 1.15. Since $\text{lift}(B) \subset \text{lift}(S_a)$, we deduce that $\text{lift}(B)$ intersects $\text{lift}(S_b)$ in (at least) two different connected components. Then, consider the maximal open ball contained in $\text{lift}(B)$ which is empty of points of $\text{lift}(S_b)$. Such a ball consists of the lift of a 2D ball B' in the

plane P_b which is tangent to ∂S_b at two points x and x'. B' is the intersection of the 3D medial ball of the complementary set of $\mathcal{O}$ passing through x and x'. Thus $\bar{m}_e(x)$, which is the projection of the center of this 3D ball ($m_e(x)$) onto P_b, lies in B'. We have $\text{lift}(\bar{m}_e(x)) \in \text{lift}(B') \subseteq \text{lift}(B) \subset \text{lift}(S_a)$. Thus, one of the nearest points of $\text{lift}(\bar{m}_e(x))$ in $\partial\mathcal{C}$ lies in $S_a \subset \mathcal{S}_\mathcal{C}$. This contradicts $\text{lift}(\bar{m}_e(a)) \in K_e(\mathcal{S}_\mathcal{C})$ (Lemma 5).

Therefore, $\text{lift}(a)$ is connected to $\text{lift}(\bar{m}_i(a))$ in $K_i(\mathcal{S}_\mathcal{C})$. Let us call a' and b' the nearest points of $\text{lift}(\bar{m}_i(a))$ in S_a and S_b respectively, see Figure 1.16-left. According to Lemma 5, the line-segments $[a', \text{lift}(\bar{m}_i(a))]$ and $[b', \text{lift}(\bar{m}_i(a))]$ lie inside $\mathcal{M}_\mathcal{C}$. We now define a path γ, colored in red in Figure 1.16-left, as the concatenation of four line-segments : $[a, a'] \subset S_a$, $[a', \text{lift}(\bar{m}_i(a))]$, $[b', \text{lift}(\bar{m}_i(a))]$ and $[b', b] \subset S_b$. We know that $[a', \text{lift}(\bar{m}_i(a))]$ and $[b', \text{lift}(\bar{m}_i(a))]$ are mapped to a single point $\text{lift}(\bar{m}_i(a))$ by the lift function. Thus, the image of γ under the lift function is the line-segment $[\text{lift}(a), \text{lift}(\bar{m}_i(a))]$, which is trivially contractible in $\text{lift}(\mathcal{S}_\mathcal{C})$.

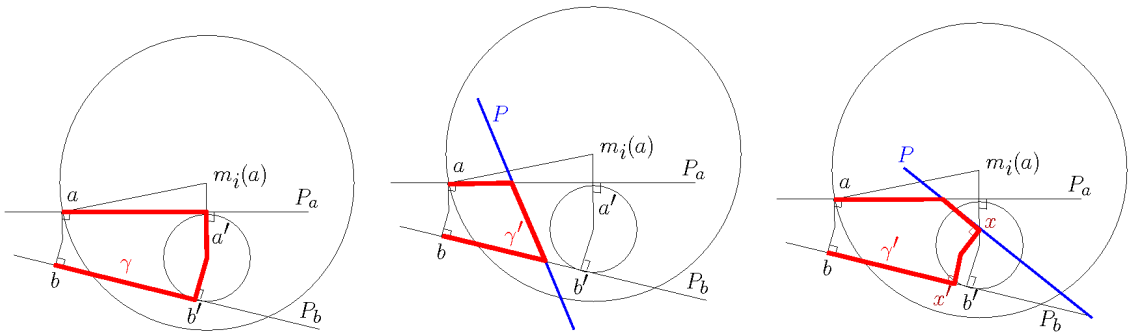

Figure 1.16: A 2D illustration of the cases considered in the proof of Lemma 6 : in red a path between a and b in $\mathcal{M}_\mathcal{C}$.

• We now consider the case where the segment $[a, \bar{m}_i(a)]$ is cut by a cutting plane P (colored in blue in Figure 1.16- middle and -right). If $\mathcal{C}$ is the cell which contains a and b, the path $\gamma = [aa'b'b]$ (defined above) does not entirely lie in $\mathcal{C}$. Let us consider the intersection of $\partial\mathcal{C}$ with the plane of γ denoted by P_0 (the plane of Figure 1.16). Two cases may happen:

- If $\partial\mathcal{C}$ does not intersect $[a', \text{lift}(\bar{m}_i(a))]$ and $[b', \text{lift}(\bar{m}_i(a))]$, we define $\gamma' := \partial\mathcal{C} \cap P_0$ which is a path that connects a to b. See Figure 1.16-middle. Note that γ' is a path in $\mathcal{M}_\mathcal{C}$, since it lies in $\partial\mathcal{C} \cap \mathcal{O} = \mathcal{S}_\mathcal{C}$.

- Otherwise, let x be an intersection point (the closest to a) between $\partial\mathcal{C}$ and $[a', \text{lift}(\bar{m}_i(a))] \cup [b', \text{lift}(\bar{m}_i(a))]$, see Figure 1.16-right. Let x' be so that $\text{lift}(x) = \text{lift}(x')$. We now define a path $\gamma' \subset \mathcal{M}_\mathcal{C}$ which connects a to b along $\partial\mathcal{C} \cap P_0$, while taking a shortcut from x to x' (by $[x, \text{lift}(x)]$ and $[\text{lift}(x), x']$). This path is colored in red in Figure 1.16-right. Note that in the case $\partial\mathcal{C} \cap P_0$ is formed of more planes, γ' can be defined in a similar way by following $\partial\mathcal{C} \cap P_0$ and making a shortcut at each intersection with γ, i.e. x in our example.

We now claim that (for both cases considered above) the lift of γ' is contractible in lift($\mathcal{S}_\mathcal{C}$). Indeed, the lift of the first and the last line-segments of γ', that lie respectively on P_a and P_b, is a line segment. Therefore, it is sufficient to check the contractibility of the lift of the part of γ' which is between P_a and P_b. The line-segments of γ' that connect P_a to P_b, lie on sections that are all entirely contained in the medial ball centered at $m_i(a)$. Therefore, the lift of these segments is contained in a disk and is contractible in lift($\mathcal{S}_\mathcal{C}$).

□

4.6 Deforming the Homotopy Equivalence to a Homeomorphism

Using the homotopy equivalence between $\mathcal{R}$ and $\mathcal{O}$, we can show that they are indeed homeomorphic.

Theorem 16 (Main Theorem-Part IV) Under the Separation and the Intersection Conditions, the two topological manifolds $\mathcal{R}$ and $\mathcal{O}$ are homeomorphic (in addition, they are isotopic).

Although this result is stronger than the homotopy equivalence, the way our proof works makes essentially use of the topological study of the previous sections. And so is based on the homotopy equivalence of the previous sections.

Proof Again, we first argue in each cell of the arrangement and show the existence of a homeomorphism between $\mathcal{O}_\mathcal{C}$ and $\mathcal{R}_\mathcal{C}$ whose restriction to $\mathcal{S}_\mathcal{C}$ is the identity map. Gluing these homeomorphisms together, one obtains a global homeomorphism between $\mathcal{R}$ and $\mathcal{O}$. Let $\mathcal{C}$ be a cell of the arrangement of the cutting planes. A similar method used to prove the homotopy equivalence between $\mathcal{R}_\mathcal{C}$ and $\mathcal{O}_\mathcal{C}$ shows that $\partial\mathcal{R} \cap \mathcal{C}$ and $\partial\mathcal{O} \cap \mathcal{C}$ are homotopy equivalent 2-manifolds and are therefore homeomorphic, and in addition there exists a homeomorphism $\beta_\mathcal{C} : \partial\mathcal{O} \cap \mathcal{C} \to \partial\mathcal{R} \cap \mathcal{C}$ which induces identity on the boundary of sections in $\mathcal{S}_\mathcal{C}$. We showed that the topology of $\mathcal{R}_\mathcal{C}$ and $\mathcal{O}_\mathcal{C}$ is completely determined by their fundamental groups, i.e., all the higher homotopy groups of $\mathcal{R}_\mathcal{C}$ and $\mathcal{O}_\mathcal{C}$ are trivial. Moreover, there is an isomorphism between $\pi_1(\mathcal{O}_\mathcal{C})$ and $\pi_1(\mathcal{R}_\mathcal{C})$, and the induced map $(\beta_\mathcal{C})_* : \pi_1(\partial\mathcal{O} \cap \mathcal{C}) \to \pi_1(\partial\mathcal{R} \cap \mathcal{C})$ on first homotopy groups is consistent with this isomorphism (in the sense that there exists a commutative diagram of first homotopy groups). This shows that there is no obstruction in extending $\beta_\mathcal{C}$ to a map $\alpha_\mathcal{C} : \mathcal{O}_\mathcal{C} \to \mathcal{R}_\mathcal{C}$, inducing the corresponding isomorphism between $\pi_1(\mathcal{O}_\mathcal{C})$ and $\pi_1(\mathcal{R}_\mathcal{C})$, and such that the restriction of $\alpha_\mathcal{C}$ to $\mathcal{S}_\mathcal{C}$ remains identity. Since all the higher homotopy groups of $\mathcal{O}_\mathcal{C}$ and $\mathcal{R}_\mathcal{C}$ are trivial, it follows that $\alpha_\mathcal{C}$ is a homotopy equivalence. We are now in order to apply the following theorem due to Waldhausen, which shows that α can be deformed to homeomorphism between $\mathcal{O}_\mathcal{C}$ and $\mathcal{R}_\mathcal{C}$, by a deformation which does not change the homeomorphism $\alpha_\mathcal{C}$ between the boundaries. A compact 3-manifold M is called *irreducible* if $\pi_2(M)$ is trivial. Remark that $\mathcal{O}_\mathcal{C}$ and $\mathcal{R}_\mathcal{C}$ are irreducible.

Theorem 17 (Waldhausen) Let $f : M \to M'$ be a homotopy equivalence between orientable irreducible 3-manifolds with boundaries such that f takes the boundary of M

onto the boundary of M' homeomorphically. Then f can be deformed to a homeomorphism $M \to M'$ by a homotopy which is fixed all the time on the boundary of M. (See [Mat03], page 220, for a proof.)

Applying Waldhausen's theorem, one obtains a homeomorphism $\tilde{\alpha}_{\mathcal{C}}$ from $\mathcal{O}_{\mathcal{C}}$ to $\mathcal{R}_{\mathcal{C}}$ which is identity on the sections in $\mathcal{S}_{\mathcal{C}}$. Gluing $\tilde{\alpha}_C$, one obtain a global homeomorphism form $\mathcal{O}$ to $\mathcal{R}$. Moreover, according to Chazal and Cohen-Steiner's work [CCS05] (Corollary 3.1), since $\mathcal{R}$ and $\mathcal{O}$ are homeomorphic and $\mathcal{R}$ contains the medial axis of $\mathcal{O}$, $\mathcal{R}$ is isotopic to $\mathcal{O}$. □

Conclusion

In this chapter, we presented one of the first topological studies in shape reconstruction from cross-sectional data. We showed that the generalization of the classical overlapping criterion to solve the *correspondence problem* between unorganized cross-sections, proposed by Liu et al. in [LBD+08], preserves the homotopy type of the shape under some appropriate sampling conditions. In addition, we proved that in this case, the homotopy equivalence between the reconstructed object and the original shape can be deformed to a homeomorphism. Even, more strongly, the two objects are isotopic.

Chapter 2

Second Method Based on the Voronoi Diagram of the Sections

In this chapter we present a reconstruction method based on the Voronoi diagram of the sections. Relating the connectivity of the sections to their Voronoi diagram allows us to perform topological studies and to compare this method with the first one presented in the previous chapter. Another advantage of considering the Voronoi diagram of the sections, instead of the Voronoi diagram of the cell, is that a Delaunay-based dual structure can be defined. Indeed, the analysis we carry out in this chapter, using the Voronoi-Delaunay duality, is to connect the methodology presented in the first chapter and the Delaunay-based methodology of Chapter 3.

1 Motivation

In the previous chapter of this thesis, we studied the reconstruction method introduced by Liu et al. in [LBD+08]. This method is *symmetric* with respect to $\mathcal{S}_\mathcal{C}$ and $\partial\mathcal{C}\backslash\mathcal{S}_\mathcal{C}$, in the sense that the points of $\partial\mathcal{C}$ that are *in* or *not in* $\mathcal{S}_\mathcal{C}$ play a symmetric role in the reconstruction procedure. As a result, $\mathbb{R}^3 \setminus \mathcal{O}$ can be reconstructed from the complementary of the sections on each face of $\partial\mathcal{C}$, and the resulting reconstructed object is the complementary in $\mathcal{C}$ of the reconstructed object from the original sections. This *symmetry property* makes the resulting reconstruction highly dependent on the position of the cutting planes. As the example of Figure 2.1 shows, for a same set of sections the method may produce different reconstructions if the configuration of the cutting planes changes close to these sections.

Therefore, this method does not perform well to reconstruct a thin object which fits within a narrow tube. In order to handle the case of tree-like structures which consist of thin branching structures distributed over a large volume, we may be interested to perform more connections between the sections. To this end, we propose to make use of the Voronoi diagram of the sections rather than the Voronoi diagram of the cell. We define the distance function from the boundary of $\mathcal{C}$, and the reconstructed object $\mathcal{R}'_\mathcal{C}$ as follows (we refer to the next section of this chapter for a formal definition):

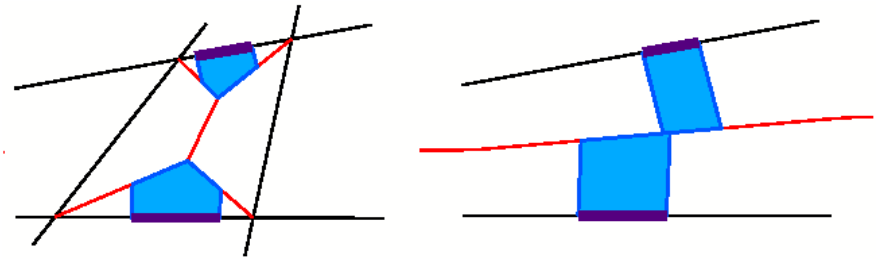

Figure 2.1: A 2D example : On the right side, we have two sections and their cutting lines and, on the left side, we have two additional cutting lines that miss the object. The associated reconstructed objects are different using the method of [LBD+08].

Let x be a point in $\mathcal{C}$ and in the Voronoi cell of a section $A \in \mathcal{S}_\mathcal{C}$. The *nearest point* to x in $\partial\mathcal{C}$ is the projection of x onto $\partial\mathcal{C}$ in the direction orthogonal to A (see Figure 2.4 of the next section). If this projection lies inside A then x is in the reconstructed object $\mathcal{R}'_\mathcal{C}$.

In order to compare the new reconstructed object $\mathcal{R}'$ with the previous one $\mathcal{R}$, let us define *the influence zone of a section* $A \in \mathcal{S}_\mathcal{C}$ in each method, as the set of points $x \in \mathcal{C}$ such that the nearest point to x in $\partial\mathcal{C}$ lies in A. As Figure 2.2 shows, using the Voronoi diagram of the sections rather than the Voronoi diagram of the cell, makes the influence zones of the sections bigger. In the sense that, the new reconstructed object $\mathcal{R}'$ contains $\mathcal{R}$ the reconstructed object of the previous chapter (see Theorem 18).

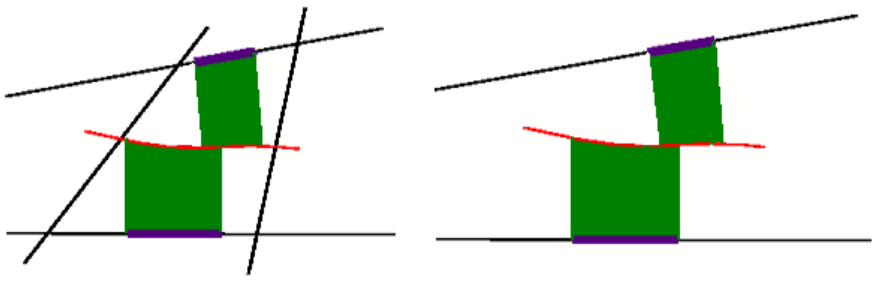

Figure 2.2: A 2D example : On the right side, we have two sections and their cutting lines and, on the left side, we have two additional cutting lines that miss the object. The associated reconstructed objects are the same using the new method.

Therefore the second method performs more connections between the sections and is motivated by reconstructing tree-like structures from sparse cross-sections. As Figure 2.2 shows, this method performs well to reconstruct a thin object which fits within a narrow tube. Another motivation for presenting this Voronoi-based method is its dual *Delaunay-based* approach that will be presented at the end of this chapter.

2 Reconstructed Object Definition

The reconstruction method, that will be presented in this section, is based on the Voronoi diagram of the *sections* of $\mathcal{C}$, defined as follows.

Voronoi diagram of the sections of a given cell. Let $\mathcal{C}$ be a cell of the arrangement of the cutting planes and A be a section in $\mathcal{S}_\mathcal{C}$. The *Voronoi cell* of A, denoted by $\mathrm{V}_\mathcal{C}(A)$, is defined as the set of all points in $\mathcal{C}$ that have A as the nearest section in $\mathcal{S}_\mathcal{C}$, i.e.,

$$\mathrm{V}_\mathcal{C}(A) = \{\ x \in \mathcal{C} \mid d(x, A) \leq d(x, A'),\ \forall A' \in \mathcal{S}_\mathcal{C}\ \}.$$

Recall that $d(.,.)$ is the Euclidean distance. The collection of $\mathrm{V}_\mathcal{C}(A)$ for all sections $A \in \mathcal{S}_\mathcal{C}$, called the Voronoi diagram of the sections of $\mathcal{C}$, forms a tiling of $\mathcal{C}$.

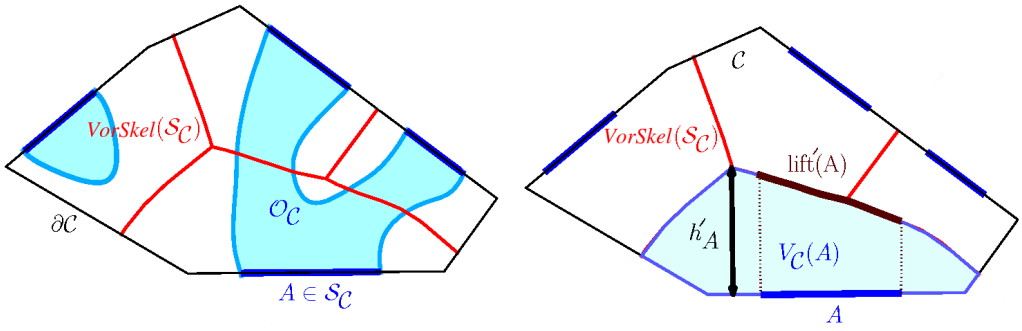

Figure 2.3: A 2D example: **Left.** The original shape $\mathcal{O}_\mathcal{C}$ and its sections are colored in blue. The Voronoi skeleton of the sections is colored in red. **Right.** For a section A, the Voronoi cell $\mathrm{V}_\mathcal{C}(A)$ (and its height h'_A), and $\mathrm{lift}'(A)$ are illustrated.

We write $\partial\mathrm{V}_\mathcal{C}(A)$ for the boundary of $\mathrm{V}_\mathcal{C}(A)$. The union of $\partial\mathrm{V}_\mathcal{C}(A)$ for all $A \in \mathcal{S}_\mathcal{C}$ is called the *Voronoi Skeleton of* $\mathcal{S}_\mathcal{C}$, and is denoted by $\mathrm{VorSkel}(\mathcal{S}_\mathcal{C})$. To simplify the notation, when the cell $\mathcal{C}$ is understood from the context, we simply remove the index $\mathcal{C}$ and write $\mathrm{V}(A)$, $\partial\mathrm{V}(A)$, etc.

Each point in $\mathrm{VorSkel}(\mathcal{S}_\mathcal{C})$ is either on the boundary of $\mathcal{C}$, or has at least two nearest sections in $\mathcal{S}_\mathcal{C}$ (see Figure 2.3). When the sections are in general position, which is the condition we will assume, a point $x \in \mathcal{C}$ has at most four nearest sections.

The key idea here is that the Voronoi diagram can be used to define the distance of $\partial\mathcal{C}$ from a point $x \in \mathcal{C}$, taking into account the sections in $\mathcal{S}_\mathcal{C}$. Indeed, the *nearest point* in $\partial\mathcal{C}$ to a point $x \in \mathcal{C}$ will depend on the Voronoi cell that contains x. This is the main difference of the new method we will present with the first method presented in the previous chapter.

Definition 27 (Nearest Point) Let x be a point in $\mathcal{C}$. If $\mathcal{S}_\mathcal{C} \neq \emptyset$, we consider the partition of $\mathcal{C}$ by the Voronoi cells of the sections in $\mathcal{S}_\mathcal{C}$. Let A be a section in $\mathcal{S}_\mathcal{C}$ whose

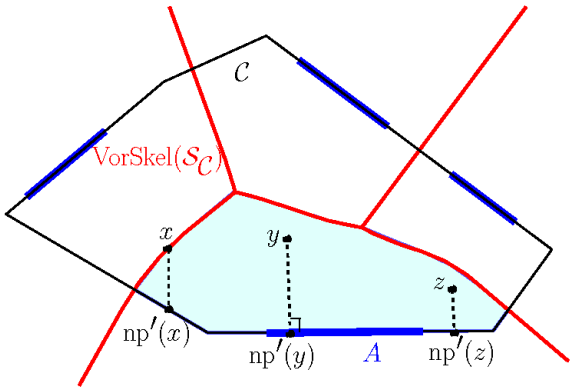

Figure 2.4: Nearest point definition, based on the Voronoi diagram of the sections.

Voronoi cell contains x, i.e., $x \in \mathrm{V}_\mathcal{C}(A)$. The projection of x onto $\partial\mathcal{C}$ in the direction orthogonal to A is called a *nearest point* to x in $\partial\mathcal{C}$ and is denoted by $\mathrm{np}'_A(x)$, see Figure 2.4.

The set of all the nearest points to x in $\mathcal{C}$ is denoted by $\mathrm{Np}'_\mathcal{C}(x)$. Note that for almost every point x, $\mathrm{Np}'_\mathcal{C}(x)$ is reduced to a single point. Based on this, and to simplify the presentation, sometimes we drop the index A and by $\mathrm{np}'(x)$ we denote a point of $\mathrm{Np}'_\mathcal{C}(x)$.

We can now define the reconstructed object in a given cell $\mathcal{C}$. We first give the formal definition, and then present a more detailed geometric characterization of the reconstructed object using the lifting procedure described below. This definition is based on the same methodology as in the first chapter. The only difference, due to the different definition of nearest point in $\partial\mathcal{C}$, is that the lifting procedure is defined on the Voronoi skeleton of the sections rather than the Voronoi skeleton of the cell.

Definition 28 (Reconstructed Object $\mathcal{R}'_\mathcal{C}$ in a cell $\mathcal{C}$) The *reconstructed object* $\mathcal{R}'_\mathcal{C}$ is the set of all points x in $\mathcal{C}$ that have a nearest point $\mathrm{np}'(x)$ in $\mathcal{S}_\mathcal{C}$, i.e., $\mathrm{Np}'_\mathcal{C}(x) \cap \mathcal{S}_\mathcal{C} \neq \emptyset$. In other words, for a section $A \in \mathcal{S}_\mathcal{C}$, a point $x \in \mathrm{V}_\mathcal{C}(A)$ is in $\mathcal{R}'_\mathcal{C}$ if $\mathrm{np}'(x) \in A$. If $\mathcal{S}_\mathcal{C}$ is empty, $\mathcal{R}'_\mathcal{C}$ is defined to be the empty set as well.

Definition 29 (Lift Function) Let A be a section in $\mathcal{S}_\mathcal{C}$ and $x \in \mathcal{C}$ be a point in the Voronoi cell $\mathrm{V}_\mathcal{C}(A)$ of A. The *lift of x in $\mathcal{C}$*, denoted by $\mathrm{lift}'_\mathcal{C}(x)$ (or simply $\mathrm{lift}'(x)$ if $\mathcal{C}$ is trivially implied), is defined to be the unique point of $\partial\mathrm{V}_\mathcal{C}(A)$ such that the line defined by the segment $[x, \mathrm{lift}'(x)]$ is orthogonal to the plane of A.

The *lift of a set of points* $X \subseteq \mathcal{C}$, denoted by $\mathrm{lift}'(X)$, is the set of all the points $\mathrm{lift}'(x)$ for $x \in X$, i.e., $\mathrm{lift}'(X) := \{\, \mathrm{lift}'(x) \mid x \in X \,\}$.

The function $\mathcal{L}' : \mathcal{C} \to \mathrm{VorSkel}(\mathcal{S}_\mathcal{C})$ that maps each point $x \in \mathcal{C}$ to its lift in $\mathrm{VorSkel}(\mathcal{S}_\mathcal{C})$ will be called the *lift function* in the sequel. For any $Y \subset \mathrm{VorSkel}(\mathcal{S}_\mathcal{C})$, $\mathcal{L}'^{-1}(Y)$ denotes the set of points $x \in \mathcal{C}$ such that $\mathrm{lift}'(x) = y$ for some $y \in Y$.

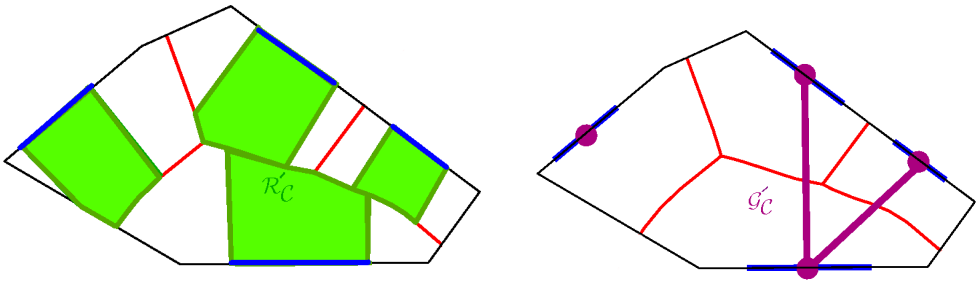

Figure 2.5: Left) Given Sections in blue, Reconstructed object $\mathcal{R}'_{\mathcal{C}}$ in green. Right) Connectivity of the sections: Two sections are connected in $\mathcal{R}'_{\mathcal{C}}$ if their lifts intersect.

Characterization of the Reconstructed Object $\mathcal{R}'_{\mathcal{C}}$. If $\mathcal{S}_{\mathcal{C}} = \emptyset$ then by definition $\mathcal{R}'_{\mathcal{C}}$ is empty. Otherwise, let $A \in \mathcal{S}_{\mathcal{C}}$ be a section lying on a face of $\mathcal{C}$. For each point $a \in A$, the locus of all the points $x \in \mathcal{C}$ that have a as their nearest point in $\partial\mathcal{C}$ is the line segment $[a, \text{lift}'(a)]$ joining a to its lift. Therefore, the reconstructed object $\mathcal{R}'_{\mathcal{C}}$ is the union of all the line-segments $[a, \text{lift}'(a)]$ for a point a in a section $A \in \mathcal{S}_{\mathcal{C}}$, i.e.,

$$\mathcal{R}'_{\mathcal{C}} := \bigcup_{A \in \mathcal{S}_{\mathcal{C}}} \bigcup_{a \in A} [a, \text{lift}'(a)].$$

According to this characterization, if the lifts of the sections intersect in $\text{VorSkel}(\mathcal{S}_{\mathcal{C}})$, then these two sections are connected in $\mathcal{R}'_{\mathcal{C}}$.

Note that the particularity of this reconstruction method is that the connectivity between the sections is based on their Voronoi diagram. However, to be conformal with the given sections, the Voronoi cells are restricted to each cell of the arrangement. In other words, the sections play the key role to guide the connections in the reconstruction, and the role of $\partial\mathcal{C} \setminus \mathcal{S}_{\mathcal{C}}$ is restricted to verify the conformity with the sections. As a result, the situation illustrated in Figure 2.6 may occur, in which a point $x \in \partial\mathcal{C} \setminus \mathcal{S}_{\mathcal{C}}$ lies on the boundary of the reconstructed object $\mathcal{R}'_{\mathcal{C}}$. This happens if the defined nearest point of $x \in \partial\mathcal{C} \setminus \mathcal{S}_{\mathcal{C}}$ is a point of a section. We caution and emphasize that the reconstructed object $\mathcal{R}'_{\mathcal{C}}$ can be seen as an *elementary* reconstructed object which is suitable for topological studies. See Section 3. In Section 4.4, we will present a homotopy equivalent object in which the non-conformal situation of Figure 2.6 can never arise.

Reconstructed Object $\mathcal{R}'$. According to the above discussion, in order to study the overall connectivity between the sections induced by the defined reconstructed object, it is necessary to impose that the reconstructed pieces in two neighboring cells of the arrangement intersect exclusively along the sections. In other words, during the final step, when gluing the reconstructed pieces of different cells of the arrangement, we should avoid the creation of new connections by gluing these pieces. To this end, an *infinitesimal thickening* of the cutting planes (with sufficiently small thickness compared to the size of

the Voronoi cells) will be considered, see Figure 2.6. The union of all the pieces $\mathcal{R}'_{\mathcal{C}}$ over all cells $\mathcal{C}$ with thickened cutting planes will be the overall reconstructed object $\mathcal{R}'$.

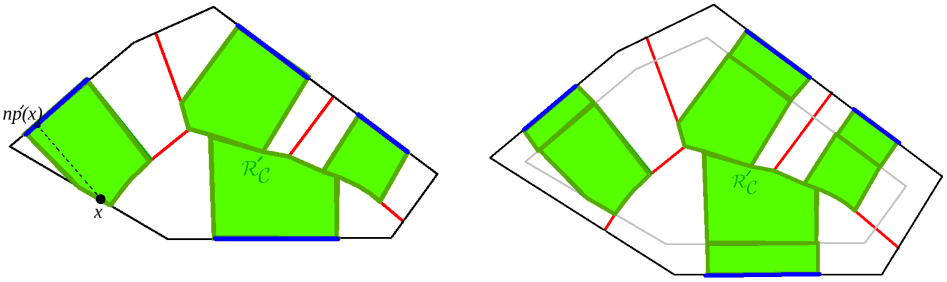

Figure 2.6: We consider a thickening of the cutting planes to make the reconstructed object $\mathcal{R}'_{\mathcal{C}}$ (in green) conformal with the given sections (in blue).

Theorem 18 (Comparison between the two methods) The reconstructed object $\mathcal{R}$ (presented in the previous chapter) is contained in $\mathcal{R}'$.

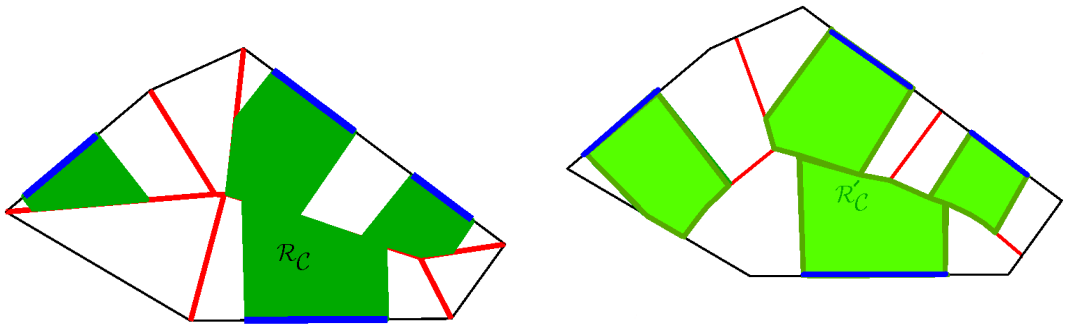

Figure 2.7: The reconstructed object $\mathcal{R}_{\mathcal{C}}$ (presented in the previous chapter) is contained in $\mathcal{R}'_{\mathcal{C}}$.

Proof We will show that for any cell $\mathcal{C}$ of the arrangement, $\mathcal{R}_{\mathcal{C}} \subseteq \mathcal{R}'_{\mathcal{C}}$, see Figure 2.7 for an illustration. It will be sufficeint to show that for any point a in some section $A \in \mathcal{S}_{\mathcal{C}}$, $[a, \text{lift}(a)] \subseteq [a, \text{lift}'(a)]$. Let x be a point in $[a, \text{lift}(a)]$. a is the nearest point in $\partial\mathcal{C}$ to x, i.e., $a \in \text{Np}_{\mathcal{C}}(x)$. Thus, the interior of the ball centered at x passing through a, is empty of the points of $\partial\mathcal{C}$. In particular, the interior of this ball is empty of the points of $\mathcal{S}_{\mathcal{C}}$. Therefore, x is a point in the Voronoi cell of the sections A. Moreover, since $x \in [a, \text{lift}(a)]$, the orthogonal projection of x onto A is a. Therefore, x lies on $[a, \text{lift}'(a)]$ and belongs to $\mathcal{R}'_{\mathcal{C}}$. □

According to the above theorem, the new reconstruction method may perform more connection between the given sections compared to the first method. As we will see in the following sections, this property makes this method better adapted to the case of sparse sectional data.

2.1 Connectivity Induced by the Reconstruction

Let us first study the sections connectivity induced by the proposed reconstruction.

Definition 30 (Connectivity Graph) The *connectivity graph* between the sections of $\mathcal{S}_\mathcal{C}$, denoted by $\mathcal{G}'_\mathcal{C}$, is defined as follows:

Each vertex in $\mathcal{G}'_\mathcal{C}$ corresponds to a section in $\mathcal{S}_\mathcal{C}$, and there is an edge between the corresponding vertices of two sections A and A' if $\text{lift}'(A)$ and $\text{lift}'(A')$ intersect on $\text{VorSkel}(\mathcal{S}_\mathcal{C})$, see Figure 2.5-right. According to the definition of $\mathcal{R}'_\mathcal{C}$, it is easy to see that A and A' are connected in $\mathcal{G}'_\mathcal{C}$ if and only if A and A' are connected in $\mathcal{R}'_\mathcal{C}$.

According to Theorem 18, we have the following proposition which compares the connectivity induced by the reconstruction presented in the first chapter to the new reconstruction.

Proposition 5 Let $\mathcal{G}_\mathcal{C}$ and $\mathcal{G}'_\mathcal{C}$ be the connectivity graphs between the sections of $\mathcal{S}_\mathcal{C}$ induced by $\mathcal{R}_\mathcal{C}$ (presented in Chapter 1) and $\mathcal{R}'_\mathcal{C}$ respectively. Then $\mathcal{G}_\mathcal{C}$ is a subgraph of $\mathcal{G}'_\mathcal{C}$.

Remark : In the d-dimensional version of the problem, that consists of reconstructing a d-dimensional shape from its $(d-1)$-dimensional intersections with hyperplanes, the same strategy to perform connectivity between the sections can be considered. The guarantees on the connectivity, we provide in Section 3, hold for any dimension.

3 Sampling Conditions and Topological Guarantees

In this section, we will prove that $\mathcal{R}'$ preserves the topology type of the original shape under appropriate sampling conditions. One can think of extending the topological guarantees enjoyed by the first method, presented in Sections 2 and 4 of the previous chapter, to this method. In this section, we will show that we can ensure the same topological guarantees as the ones we obtained for the first method, under sampling conditions that are better adapted to tree-like structures.

Instead of the Voronoi diagram of $\mathcal{C}$, the Voronoi diagram of the sections of $\mathcal{S}_\mathcal{C}$ should be considered. Also, the new lift function (denoted by lift') should be considered with respect to the Voronoi diagram of the sections. We define :

Definition 31 (Height of a Cell) Let $\mathcal{C}$ be a cell of the arrangement of the cutting planes and A be a section $\mathcal{S}_\mathcal{C}$. The *height* of A in $\mathcal{C}$, denoted by h'_A, is defined as $h'_A := \max_{x \in \text{V}_\mathcal{C}(A)} \; d(x, \text{np}'_A(x))$. We then define the height of $\mathcal{C}$ as $h'_\mathcal{C} := \; \max_{A \in \mathcal{S}_\mathcal{C}} h'_A$.

Let us also recall the definition of the reach : Let $\mathcal{O}$ be a compact 3-manifold with smooth boundary $\partial\mathcal{O}$ in $\mathbb{R}^3$. The reach of $\mathcal{O}$ is defined as:

$$\text{reach}(\mathcal{O}) := \min_{m \in \text{MA}(\partial\mathcal{O})} d(m, \partial\mathcal{O}).$$

In Chapter 1, to ensure that the sections-connectivity induced by $\mathcal{R}_\mathcal{C}$ is correct, we presented the Separation Condition which is satisfied if the height of the cell is less than the *reach* of the shape (the Density Condition). However, such a condition seems too restrictive for applications that we considered for the second method:
Because, as said before, the second method is motivated by reconstructing tree-like structures for which the reach may be small. In the following, we will propose new sampling conditions that are better adapted to be satisfied for tree-like structures.

To this end, we define two new quantities that correspond to the distance of the boundary of the object from the internal and external parts of the medial axis:

$$\text{reach}_i(\mathcal{O}) := \min_{m \in \text{MA}_i(\partial\mathcal{O})} d(m, \partial\mathcal{O}) \quad \text{and} \quad \text{reach}_e(\mathcal{O}) := \min_{m \in \text{MA}_e(\partial\mathcal{O})} d(m, \partial\mathcal{O}).$$

Given a cell $\mathcal{C}$ of the arrangement, we define $\text{reach}_i(\mathcal{O}_\mathcal{C}) = \min d(a, m_i(a))$, where either $a \in \partial\mathcal{O} \cap \mathcal{C}$ or $m_i(a) \in \text{MA}_i(\partial\mathcal{O}) \cap \mathcal{C}$. Symmetrically, $\text{reach}_e(\mathcal{O}_\mathcal{C}) = \min d(a, m_e(a))$, where either $a \in \partial\mathcal{O} \cap \mathcal{C}$ or $m_e(a) \in \text{MA}_e(\partial\mathcal{O}) \cap \mathcal{C}$.

The key idea is that usually in thin branching structures $\text{reach}_i(\mathcal{O})$ is much smaller than $\text{reach}_e(\mathcal{O})$. The Density Condition of the first method depends on both $\text{reach}_i(\mathcal{O})$ and $\text{reach}_e(\mathcal{O})$, and may be too restrictive for thin branching structures. Instead, we suggest a *Weak Density Condition* which bounds from above the height of the cells only by $\text{reach}_e(\mathcal{O})$. Nevertheless, to ensure good connectivities between the sections, we would need an additional condition, called *Weak Transversality Condition* defined as follows:

($C'1$) **Weak Density Condition :** For any cell $\mathcal{C}$ of the arrangement $h'_\mathcal{C} < \epsilon$, for some $\epsilon \leq \text{reach}_e(\mathcal{O}_\mathcal{C})$.

($C'2$) **Weak Transversality Condition :** For any cell $\mathcal{C}$ of the arrangement and any point $x \in \partial\mathcal{O}_\mathcal{C}$, we have $d(\text{np}'(x), \partial A) \leq \text{reach}_i(\mathcal{O}_\mathcal{C})$, where $A \in \mathcal{S}_\mathcal{C}$ is such that $x \in \text{V}(A)$. See Figure 2.8. More intuitively, the orthogonal projection of the boundary of the object restricted to the Voronoi cell of A, onto the plane of A, moves by at most $\text{reach}_i(\mathcal{O}_\mathcal{C})$. This is based on how the cutting planes are transversal to $\partial\mathcal{O}$.

We now show that these two sampling conditions lead to guarantees on the connection between the sections induced by the new reconstructed method. The proof, being different from the one presented in the previous chapter, will be detailed in the following.

Lemma 7 Under the Weak Transversality Condition, we have $\text{MA}_i(\partial\mathcal{O}_\mathcal{C}) \subset \mathcal{R}'_\mathcal{C}$.

Proof Let x be a point in $\text{MA}_i(\partial\mathcal{O}_\mathcal{C})$ and A be the section whose Voronoi cell contains x. Consider the intersection between the plane parallel to the plane of A which passes through x and the medial ball centered at x; this intersection is an open disk that we denote by D.

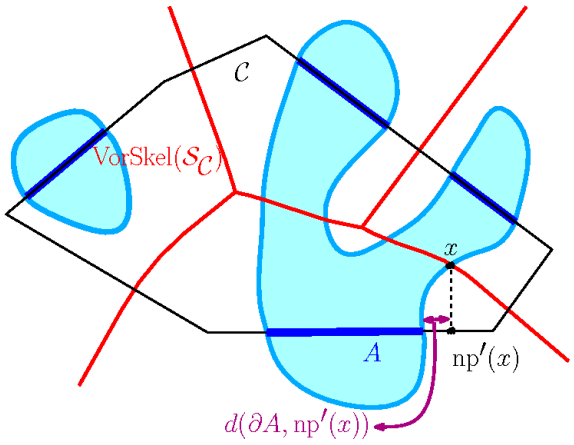

Figure 2.8: For the definition of the Weak Transversality Condition.

According to the Weak Transversality Condition, the orthogonal projection of the boundary of the object restricted to the Voronoi cell of A, onto the plane of A, moves by at most $\mathrm{reach}_i(\mathcal{O}_\mathcal{C})$. Since the radius of D is at least $\mathrm{reach}_i(\mathcal{O}_\mathcal{C})$, and D is empty of points of $\partial\mathcal{O}_\mathcal{C}$, the projection of its center x to A should belong to A. By the definition of $\mathcal{R}'_\mathcal{C}$, we deduce that x belongs to $\mathcal{R}'_\mathcal{C}$. □

Theorem 19 (Guarantees on the Connection Between the Sections) If the sample of cutting planes verifies the two above sampling conditions, then $\mathcal{R}'_\mathcal{C}$ and $\mathcal{O}_\mathcal{C}$ induce the same connectivity between the sections of $\mathcal{C}$. As a consequence, there is a bijection between the connected components of $\mathcal{R}'_\mathcal{C}$ and the connected components of $\mathcal{O}_\mathcal{C}$.

Proof The proof is given in two parts:

- From $\mathrm{MA}_i(\partial\mathcal{O}_\mathcal{C}) \subset \mathcal{R}'_\mathcal{C}$ we trivially conclude that if the Weak Transversality Condition is verified then two sections are connected in $\mathcal{R}'_\mathcal{C}$ if they are connected in $\mathcal{O}_\mathcal{C}$.

- We now show that the Weak Density Condition gives the converse implication : If the Weak Density Condition is verified, then two sections are connected in $\mathcal{O}_\mathcal{C}$ if they are connected in $\mathcal{R}'_\mathcal{C}$.

  Let A and A' be two sections connected in $\mathcal{R}'_\mathcal{C}$. According to the construction of $\mathcal{R}'$, and since the connectivity between sections is obtained locally, we may suppose that $\mathrm{lift}'(A) \cap \mathrm{lift}'(A')$ is non-empty. Let $x \in \mathrm{VorSkel}(\mathcal{S}_\mathcal{C})$ be a point in $\mathrm{lift}'(A) \cap \mathrm{lift}'(A')$. Let B be the ball centered at x and passing through the nearest points $\mathrm{np}'_A(x)$ and $\mathrm{np}'_{A'}(x)$. Remark that since $x \in \mathrm{lift}'(A) \cap \mathrm{lift}'(A')$, the two points $\mathrm{np}'_A(x)$ and $\mathrm{np}'_{A'}(x)$ have the same distance to x, which is at most the height of the cell. Therefore, according to the Weak Density Condition, this distance, which is indeed the radius of the ball B, is less than $\mathrm{reach}_e(\mathcal{O}_\mathcal{C})$.

  We claim that $\mathrm{np}'_A(x)$ and $\mathrm{np}'_{A'}(x)$ are connected in $\mathcal{O} \cap B$. For the sake of contradiction, suppose that $\mathrm{np}'_A(m)$ and $\mathrm{np}'_{A'}(m)$ belong to two different connected

components of $\mathcal{O} \cap B$, denoted by K and K', respectively. Consider the pencil of balls centered at x. Let B_1 be the smallest ball centered at x which intersects both K and K', see Figure 2.9. B_1 is tangent to ∂K or $\partial K'$, say (without loss of generality) ∂K and at a point $p \in \partial K$. We now consider the pencil of balls tangent to ∂K at p. Let B_2 be the maximal ball in this pencil which does not contain a point of K' in its interior. B_2 is tangent to $\partial K'$ at a point p'. Thus B_2 is a ball tangent to $\partial \mathcal{O}$ in two points p and p', and therefore its center o lies on the external part of the medial axis of $\partial \mathcal{O}$. Therefore, the radius of B_2 is at least $\text{reach}_e(\mathcal{O}_\mathcal{C})$. This contradicts the fact that B_2 is contained in B, and the radius of B is less than $\text{reach}_e(\mathcal{O}_\mathcal{C})$.

According to this contradiction, $\text{np}'_A(m)$ and $\text{np}'_{A'}(m)$ belong to the same connected component K of $\mathcal{O} \cap B$. Since the interior of B is empty of points of $\mathcal{S}_\mathcal{C}$, K cannot be cut by any cutting plane. Thus, K lies inside $\mathcal{C}$ and we have $K \subset \mathcal{O} \cap \mathcal{C}$. Hence, A and A' are connected in $\mathcal{O}_\mathcal{C}$.

□

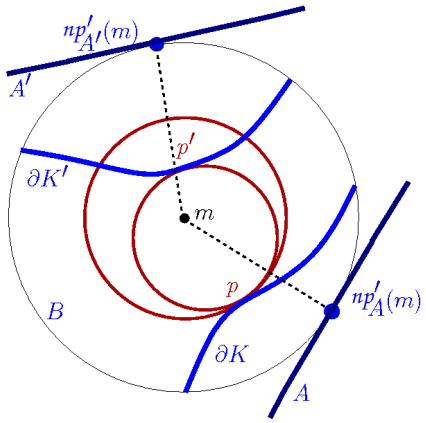

Figure 2.9: For the proof of Theorem 19.

3.1 Approximation Guarantees

We now show that the presented sampling conditions allow us to control the Hausdorff distance between $\mathcal{O}$ and its approximation $\mathcal{R}'$. Let us emphasize that this property is related to the Voronoi diagram of the sections and is not necessarily true for the first method based on the Voronoi diagram of the cell. The proof is based on the following lemma.

Lemma 8 Let y be a point in $\partial \mathcal{R}'_\mathcal{C}$, there exists a point $a \in \partial \mathcal{S}_\mathcal{C}$ such that $d(y, a) \leq h'_\mathcal{C}$.

Proof By the definition of $\mathcal{R}'_\mathcal{C}$, there are two cases for a point $y \in \partial \mathcal{R}'_\mathcal{C}$:

- Either y belongs to the segment $[a, \text{lift}'(a)]$ for some $a \in \partial\mathcal{S}_\mathcal{C}$: Then we have trivially $d(y,a) \leq d(a, \text{lift}'(a)) \leq h'_\mathcal{C}$.
- or y is the lift of a point a' in the interior of a section A': In this case, we have $y \in \text{VorSkel}(\mathcal{S}_\mathcal{C})$ and there exists a point a in another section A such that $d(y,a) = d(y,a')$. If a is in the interior of A, then y is in the interior of the lift of the two sections and cannot be in $\partial\mathcal{R}'_\mathcal{C}$. Therefore, a is a point in $\partial\mathcal{S}_\mathcal{C}$. Moreover, we have $d(y,a) = d(y,a') = d(\text{lift}'(a'), a') \leq h'_\mathcal{C}$.

□

Theorem 20 (Approximation Guarantees) If the set of cutting planes verifies the Weak Density and the Weak Transversality Conditions, then we have

$$d_H(\mathcal{O}, \mathcal{R}') \leq \max_\mathcal{C} h'_\mathcal{C} < \epsilon.$$

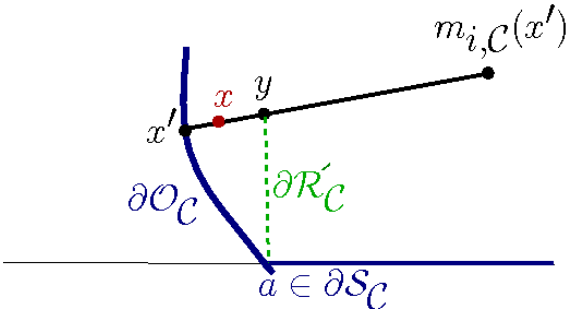

Figure 2.10: For (the second case considered in) the proof of Theorem 20.

Proof We claim that for any cell $\mathcal{C}$ of the arrangement $d_H(\mathcal{O}_\mathcal{C}, \mathcal{R}'_\mathcal{C}) \leq h'_\mathcal{C}$. The proof is given in two parts:

1. Let x be a point in $\mathcal{R}'_\mathcal{C}$. According to the characterization of $\mathcal{R}'_\mathcal{C}$, there exists a point $a \in \mathcal{S}_\mathcal{C}$ such that x belongs to the segment $[a, \text{lift}'(a)]$. Since $a \in \mathcal{S}_\mathcal{C} \subset \mathcal{O}_\mathcal{C}$, we have $d(x, \mathcal{O}_\mathcal{C}) \leq d(x,a) \leq d(a, \text{lift}'(a)) \leq h'_\mathcal{C}$.
2. Let x be a point in $\mathcal{O}_\mathcal{C}$. If $x \in \mathcal{R}'_\mathcal{C}$, $d(x, \mathcal{R}'_\mathcal{C}) = 0$ and there is nothing to prove. Thus, we can suppose that x is not in $\mathcal{R}'_\mathcal{C}$. Let x' be the closest point in $\partial\mathcal{O}_\mathcal{C}$ to x. Therefore, x belongs to the segment $[x', m_{i,\mathcal{C}}(x')]$, see Figure 2.10. According to Corollary 7 and the Weak Transversality Condition, we have $m_{i,\mathcal{C}}(x') \in \text{MA}_i(\partial\mathcal{O}_\mathcal{C}) \subseteq \mathcal{R}'_\mathcal{C}$. Moreover, we have $x \notin \mathcal{R}'_\mathcal{C}$. Thus the segment joining x to $m_{i,\mathcal{C}}(x')$ intersects $\partial\mathcal{R}'_\mathcal{C}$. Let y be a point in $[x, m_{i,\mathcal{C}}(x')] \cap \partial\mathcal{R}'_\mathcal{C}$. According to Lemma 8, there exists a point $a \in \partial\mathcal{S}_\mathcal{C}$ such that $d(y,a) \leq h'_\mathcal{C}$.

   We claim that $d(y,x') \leq d(y,a)$. If $d(y,x') > d(y,a)$ then $d(x', m_{i,\mathcal{C}}(x')) = d(y,x') + d(y, m_{i,\mathcal{C}}(x')) > d(y,a) + d(y, m_{i,\mathcal{C}}(x')) \geq d(a, m_{i,\mathcal{C}}(x'))$. But $d(x', m_{i,\mathcal{C}}(x')) >$

$d(a, m_{i,\mathcal{C}}(x'))$ contradicts the fact that x' is the nearest point of $\partial\mathcal{O}_\mathcal{C}$ to $m_{i,\mathcal{C}}(x')$. Thus, $d(y, x') \leq d(y, a)$. On the other hand, since $y \in [x, m_{i,\mathcal{C}}(x')] \subseteq [x', m_{i,\mathcal{C}}(x')]$, $d(x, y) \leq d(x', y)$ and we have:

$$d(x, \mathcal{R}'_\mathcal{C}) \leq d(x, y) \leq d(x', y) \leq d(y, a) \leq h'_\mathcal{C}.$$

Therefore, $d_H(\mathcal{O}_\mathcal{C}, \mathcal{R}'_\mathcal{C}) \leq h'_\mathcal{C} < \epsilon$ for any cell $\mathcal{C}$ of the arrangement. □

3.2 Proof Outline of the Homotopy Equivalence Between $\mathcal{R}'$ and $\mathcal{O}$

Following the strategy employed in Section 4 of the previous chapter, for each cell $\mathcal{C}$ of the arrangement, we will show that $\mathcal{O}_\mathcal{C}$ and $\mathcal{R}'_\mathcal{C}$ have the same homotopy type. We will just highlight the differences between the two cases and refer to the previous chapter for detailed proofs.

Similarly to Proposition 1 of Chapter 1, we can prove that by the definition of $\mathcal{R}'_\mathcal{C}$, the lift function $\mathcal{L}' : \mathcal{R}'_\mathcal{C} \to \text{lift}'(\mathcal{S}_\mathcal{C})$ is a homotopy equivalence. On the other hand, the medial shape $\mathcal{M}_\mathcal{C}$ is homotopy equivalent to $\mathcal{O}_\mathcal{C}$ (Proposition 3, Chapter 1). Thus, it will be sufficient to show that $\text{lift}'(\mathcal{S}_\mathcal{C})$ is homotopy equivalent to $\mathcal{M}_\mathcal{C}$.

From $\text{MA}_i(\partial\mathcal{O}_\mathcal{C}) \subset \mathcal{R}'_\mathcal{C}$ and the definition of the medial shape we conclude $\mathcal{M}_\mathcal{C} \subseteq \mathcal{R}'_\mathcal{C}$. Following the same strategy as Section 4 of the first chapter, we will show that the lift function $\mathcal{L}' : \mathcal{M}_\mathcal{C} \to \text{lift}'(\mathcal{S}_\mathcal{C})$ is a weak homotopy equivalence.

The only difference here is that $\mathcal{R}'_\mathcal{C}$ is not defined in a symmetric way for the sections of $\mathcal{S}_\mathcal{C}$ and their complementary set in $\partial\mathcal{C}$. As a consequence, $\mathcal{R}'_\mathcal{C}$ is not necessarily contained in $\mathcal{C} \setminus \widetilde{\mathcal{M}}_\mathcal{C}$. However, the new sampling conditions leads us to define another object (homotopy equivalent to $\mathcal{O}_\mathcal{C}$) that will replace $\mathcal{C} \setminus \widetilde{\mathcal{M}}_\mathcal{C}$ in the proofs:

We consider $\mathcal{O}^\epsilon_\mathcal{C} = \{x \in \mathbb{R}^3, d(x, \mathcal{O}_\mathcal{C}) \leq \epsilon\}$. Since $\epsilon \leq \text{reach}_e(\mathcal{O}_\mathcal{C})$, $\mathcal{O}^\epsilon_\mathcal{C}$ is homotopy equivalent to $\mathcal{O}_\mathcal{C}$.

Lemma 9 If the Weak Density Condition is verified then $\mathcal{R}'_\mathcal{C} \subseteq \mathcal{O}^\epsilon_\mathcal{C}$.

Proof By the definition of $\mathcal{R}'_\mathcal{C}$, for any point $x \in \mathcal{R}'_\mathcal{C}$ there is a point a in $\mathcal{S}_\mathcal{C}$ such that $x \in [a, \text{lift}'(a)]$. Thus, $d(x, a) \leq d(a, \text{lift}'(a)) \leq h'_\mathcal{C} \leq \epsilon$. We conclude that $\mathcal{R}'_\mathcal{C}$ is a subset of $\mathcal{S}^\epsilon_\mathcal{C} = \{x \in \mathbb{R}^3, d(x, \mathcal{S}_\mathcal{C}) \leq \epsilon\}$ which is itself a subset of $\mathcal{O}^\epsilon_\mathcal{C}$. □

We will use $\mathcal{O}^\epsilon_\mathcal{C}$ instead of $\mathcal{C} \setminus \widetilde{\mathcal{M}}_\mathcal{C}$ in the homotopy proof of the first method and we consider the following diagram:

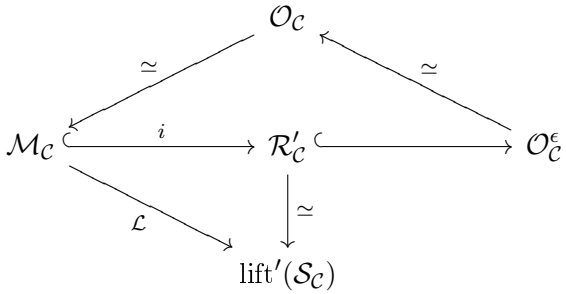

Using this diagram, the injectivity of $\mathcal{L}' : \mathcal{M}_\mathcal{C} \to \text{lift}'(\mathcal{S}_\mathcal{C})$ on the level of homotopy groups, under the Weak Density Condition and the Weak Transversality Condition, is deduced (see the Section 4 of Chapter 1 for more details). Therefore, to prove the homotopy equivalence between $\mathcal{M}_\mathcal{C}$ and $\text{lift}'(\mathcal{S}_\mathcal{C})$, it will be sufficient to prove the surjectivity of the induced maps $\mathcal{L}'^* : \pi_i(\mathcal{M}_\mathcal{C}) \to \pi_i(\text{lift}'(\mathcal{S}_\mathcal{C}))$ on the corresponding homotopy groups. Similarly to the first chapter, we will show that under the Weak Density Condition and the Weak Transversality Condition, the higher dimensional homotopy groups of $\mathcal{O}_\mathcal{C}$ and $\mathcal{R}'_\mathcal{C}$ are trivial.

Theorem 21 If the Weak Density Condition is verified then $\pi_i(\mathcal{O}_\mathcal{C}) = \{0\}$, for all $i \geq 2$..

Proof We only make use of the fact that under the Weak Density Condition, any connected component of $\partial\mathcal{O}$ is cut by at least one cutting plane. In this case, every connected component of $\mathcal{O}_\mathcal{C}$ is a 3-manifold with connected boundary. The theorem follows as a corollary of Theorem 7. □

Theorem 22 $\pi_i(\mathcal{R}'_\mathcal{C}) = \{0\}$, for all $i \geq 2$.

Proof Using Theorem 7, it will be sufficient to show that the boundary of any connected component of $\mathcal{R}'_\mathcal{C}$ is connected. Let x and y be two points on this boundary, and let S and S' be two sections so that $x \in \text{V}(S)$ and $y \in \text{V}(S')$. By the definition of $\mathcal{R}'_\mathcal{C}$, x is connected to S in $\partial\mathcal{R}'_\mathcal{C}$, and y is connected to S' in $\partial\mathcal{R}'_\mathcal{C}$. On the other hand, S and S' are connected in $\partial\mathcal{R}'_\mathcal{C}$. Thus, x is connected to y in $\partial\mathcal{R}'_\mathcal{C}$. □

Consequently, under the Weak Density Condition, the topological structures of $\mathcal{O}_\mathcal{C}$ and $\mathcal{R}'_\mathcal{C}$ are determined by their fundamental group $\pi_1(\mathcal{O}_\mathcal{C})$ and $\pi_1(\mathcal{R}'_\mathcal{C})$, respectively. According to the homotopy equivalences between $\mathcal{O}_\mathcal{C}$ and $\mathcal{M}_\mathcal{C}$, and between $\mathcal{R}'_\mathcal{C}$ and $\text{lift}'(\mathcal{S}_\mathcal{C})$, it will be sufficient to show that $\pi_1(\mathcal{M}_\mathcal{C})$ and $\pi_1(\text{lift}'(\mathcal{S}_\mathcal{C}))$ are isomorphic. As the injectivity of the map $\mathcal{L}'^* : \pi_1(\mathcal{M}_\mathcal{C}) \to \pi_1(\text{lift}'(\mathcal{S}_\mathcal{C}))$ is already proved, we need to prove the surjectivity.

A natural condition to ensure that $\mathcal{L}'_*$ is surjective is to imply that *any connected component of* $\text{lift}'(\mathcal{S}_\mathcal{C})$ *is contractible*. This is very common in practice, where the sections are contractible and sufficiently close to each other. In this case, since $\pi_1(\text{lift}'(\mathcal{S}_\mathcal{C}))$ is trivial and $\mathcal{L}'_*$ is surjective. Therefore, the homotopy equivalence between $\mathcal{R}'_\mathcal{C}$ and $\mathcal{O}_\mathcal{C}$ can be deduced.

Also, we can consider the more general condition we proposed in Chapter 1 based again on the transversality of the sections. We recall the definition of α_a :

Definition 32 (Angle α_a) Let a be a point on the boundary of a section $A \in \mathcal{S}_\mathcal{C}$ on the plane P_A. We consider $m_i(a)$, that may be outside the cell $\mathcal{C}$. We define α_a as the angle between P_A and the normal to $\partial\mathcal{O}$ at a, see Figure 2.11 : $\alpha_a := \text{angle}(P_A, [a, m_i(a)])$.

($C'3$) **Transversality Condition** For any cell $\mathcal{C}$ of the arrangement,

$$h'_\mathcal{C} < \frac{1}{2}\left(1 - \sin(\alpha_a)\right) \text{reach}(a), \forall a \in \partial\mathcal{S}_\mathcal{C}.$$

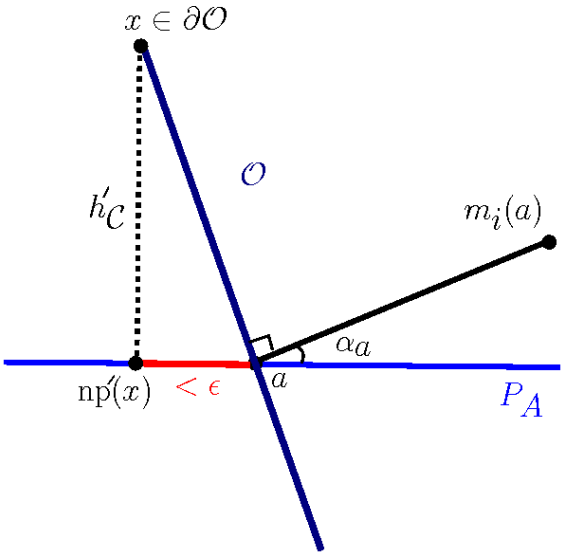

Figure 2.11: Weak Transversality Condition for piecewise linear shapes: the length of the red segment ($[\text{np}'(x), a]$) should be less than ϵ.

Remark on the Transversality Condition : Let us compare the Weak Transversality and the Transversality Conditions for piecewise linear shapes:

Let $\mathcal{O}$ be a piecewise linear shape. Consider a point a on the boundary of a section A of $\mathcal{O}$ on the plane P_A. As Figure 2.11 shows in this case, the angle between the boundary of $\mathcal{O}$ and P_A is equal to $\frac{\pi}{2} - \alpha_a$. Therefore, the Weak Transversality Condition implies the following inequality : $h'_\mathcal{C} < \cot(\alpha_a)\ \text{reach}(a)$. From $0 \leq \alpha_a \leq \frac{\pi}{2}$ we can easily deduce $\cot(\alpha_a) \geq \frac{1}{2}\left(1 - \sin(\alpha_a)\right)$. Therefore, the inequality required by the Transversality Condition is more restrictive.

A similar proof as the one presented in the previous chapter, shows that this condition implies the surjectivity of $\mathcal{L}'^* : \pi_1(\mathcal{M}_\mathcal{C}) \to \pi_1(\text{lift}'(\mathcal{S}_\mathcal{C}))$. Therefore, $\mathcal{M}_\mathcal{C}$ and $\text{lift}'(\mathcal{S}_\mathcal{C})$, and so $\mathcal{O}_\mathcal{C}$ and $\mathcal{R}'_\mathcal{C}$ are homotopy equivalent. Using the generalized nerve theorem we deduce the following theorem:

Theorem 23 (Topological Guarantees) If the cutting planes verify the Weak Density and the Transversality Conditions, then the proposed reconstructed object $\mathcal{R}'$ is homotopy equivalent to the unknown original shape $\mathcal{O}$.

Using the same strategy as the one employed in Section 4.6 of Chapter 1, we can deform the homotopy equivalence to a homeomorphism. Moreover, since $\mathrm{MA}_i(\partial\mathcal{O}) \subset \mathcal{R}'$, $\mathcal{R}'$ is isotopic to $\mathcal{O}$ (according to Corollary 3.1 of [CCS05]) and we have the following theorem :

Theorem 24 (Homeomorphism) If the cutting planes verify the Weak Density and the Transversality Conditions, the two topological manifolds $\mathcal{R}'$ and $\mathcal{O}$ are homeomorphic (in addition, they are isotopic).

Therefore, we obtain the same topological guarantees as the ones we obtained for the first method, under sampling conditions that are better adapted to be satisfied for tree-like structures. Let us note that if we consider the new sampling conditions for the first method, the same topological guarantees will be ensured. However, these new conditions may be more restrictive than the previous sampling conditions for shapes different from thin branching structures.

4 Dual Delaunay-Based Approach

In the previous section, we showed that the connectivity induced by $\mathcal{R}'$ is topologically correct if the sample of cutting planes is sufficiently dense. As discussed in Section 2.1, $\mathcal{R}'$ may exhibit a jagged and unnatural appearance, and can be seen as an intermediate shape that captures the good connectivity between the sections. This reconstructed object as it is cannot be directly used in applications where smooth surfaces are desired. The idea is to use the dual Delaunay-based structure to connect the corresponding sections in $\mathcal{G}'$ so that the resulting object is homotopy equivalent to $\mathcal{R}'$. The Delaunay structure, with its interesting geometrical properties, has been widely used in different reconstruction methods.

4.1 Delaunay Simplices

The dual structure of the Voronoi diagram of the section is composed of so-called Delaunay simplices defined as follows.

Definition 33 (Delaunay Simplices) To any point $m \in \mathrm{VorSkel}(\mathcal{S}_\mathcal{C})$, we associate the maximal ball centered at m such that its interior is empty of points of $\mathcal{S}_\mathcal{C}$. This ball is called a *medial ball* or a *Delaunay ball* and is denoted by $\sigma(m)$. As $\sigma(m)$ is the maximal ball such that its interior is empty of points of $\mathcal{S}_\mathcal{C}$, it passes through at least two points a and a' in $\mathcal{S}_\mathcal{C}$, called the *contact points* of $\sigma(m)$. In general, a medial ball has two contact points. The segment that joins these two contact points is called a *Delaunay fiber* or a *Delaunay 1-simplex*. It is easy to see that two Delaunay fibers do not intersect except possibly at one of their endpoints. See examples illustrated in Figure 2.12. More generally,

a medial ball with k contact points in $\mathcal{S}_\mathcal{C}$ circumscribes a *Delaunay* $(k-1)-$*simplex* which is defined as the convex hull of the contact points of the medial ball. Since any set of four points defines a sphere (ball), if the cutting planes are in general position (which is supposed in this thesis), any medial ball has at most four contact points, i.e., $k \in \{2, 3, 4\}$.

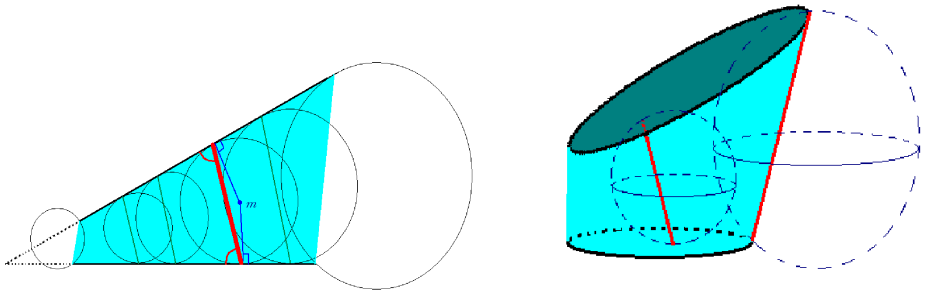

Figure 2.12: 2D and 3D examples: Delaunay Simplices between two sections (in blue) and a Delaunay fiber in red.

Voronoi-Delaunay Duality : For any $m \in \text{VorSkel}(\mathcal{S}_\mathcal{C})$, the dual of m (denoted by m^*) is the Delaunay simplex circumscribed by the ball $\sigma(m)$.

We now introduce the *tangent Delaunay simplices* that play a central role in our approach. This set of Delaunay simplices is indeed the dual of $\text{lift}'(\mathcal{S}_\mathcal{C})$ the lift of the sections:

Definition 34 (Tangent Delaunay Simplices) Let A be a section in $\mathcal{S}_\mathcal{C}$, and $m = \text{lift}'(a)$ for some point a in the interior of A. The corresponding Delaunay ball $\sigma(m)$ being empty of points of $\mathcal{S}_\mathcal{C}$, is tangent to the supporting cutting plane of A at a. Conversely, the center of any Delaunay ball tangent to the supporting cutting plane of A at a point a in the interior of A, is on the lift of A. The dual of such a point $m \in \text{lift}'(A)$ is called a *tangent Delaunay simplex*. In particular, let a' be one of the contact points of $\sigma(m)$ in $\mathcal{S}_\mathcal{C}$ distinct to a. The line segment $[a, a']$ is called a tangent Delaunay fiber of a.

Definition 35 (Labeling ϕ) We define a labeling ϕ that to each point a in a section in $\mathcal{S}_\mathcal{C}$ associates a set of points in $\mathcal{S}_\mathcal{C}$ such that: a' is said to be in $\phi(a)$ if $[a, a']$ is a tangent Delaunay fiber of a.

Generically, $\phi(a)$ consists of a single point. An important situation occurs when for some a, $\phi(a)$ contains more than one point. This defines the branching locus of the union of the tangent Delaunay fibers.

Definition 36 (Branching Diagram, and Branching Subsections of a Section) We define the *branching diagram* of a face f of $\mathcal{C}$ as the partition of f by the orthogonal projection of the 1-skeleton of $\text{VorSkel}(\mathcal{S}_\mathcal{C})$ onto f. See Figure 2.31-left. Given a section A

contained in a face f, the branching diagram of f subdivides A into so-called *branching subsections.*

4.2 Branching Diagram

We defined the branching diagram of a face f of $\mathcal{C}$ as the orthogonal projection of the 1-skeleton of VorSkel($\mathcal{S}_\mathcal{C}$) onto f. The skeleton of VorSkel($\mathcal{S}_\mathcal{C}$) is the locus of points in $\mathcal{C}$ that have at least three nearest points in the sections of $\mathcal{S}_\mathcal{C}$. A point a in a section of f has a unique tangent Delaunay ball in $\mathcal{C}$ that is centered on lift$'(a)$. If lift$'(a)$ is the skeleton of VorSkel($\mathcal{S}_\mathcal{C}$) then this Delaunay ball has at least three contact points in $\mathcal{S}_\mathcal{C}$, and bounds more than one Delaunay fiber. In this case, a is called a *branching point* and lies on the branching diagram defined previously.

Let A be a section in $\mathcal{S}_\mathcal{C}$. The branching diagram on the face of A forms a partition of A into so-called branching subsections of A. For a subsection E of A, lift$'(E)$ lies on a unique Voronoi 2-dimensional face. We define $\Phi(E)$ as the unique section A' such that lift$'(E)$ intersects $\partial \mathrm{V}_\mathcal{C}(A')$. We also define $\Phi(A)$ as the set of all $\Phi(E)$ for all branching subsections E of A. The subsection E is the locus of points a in A such that $\phi(a) \in \Phi(E)$ Indeed, $\phi(.)$ defines a continuous function everywhere in $\mathcal{S}_\mathcal{C}$ except on the branching diagram. As it can be seen in Figure 2.13, the branching diagram is on the branching Locus of the tangent Delaunay fibers. (That is where the name comes from.) In Section 5, we will provide an efficient algorithm to compute the branching diagram without computing the 3D Voronoi diagram of the sections. It plays a key role to determine the connectivity between sections induced by $\mathcal{R}'$.

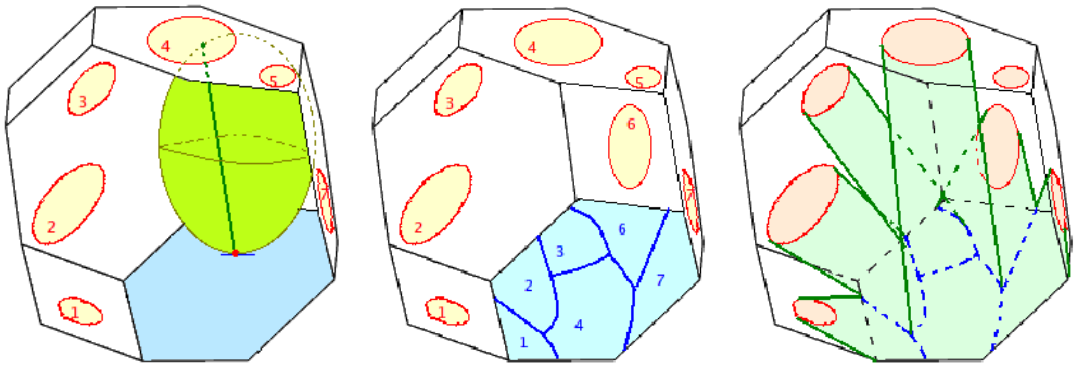

(a) A Delaunay fiber with an endpoint on a face f (in blue) of $\mathcal{C}$.

(b) The branching diagram of f.

(c) The set of Delaunay fibers (in green) with an endpoint on f.

Figure 2.13: Branching diagram of a face of $\mathcal{C}$.

As we will see in Section 5, in the case of parallel cutting planes, the branching diagram on a face is the orthogonal projection onto this face of the 2D-Voronoi diagram (external part of the medial axis) of the sections of the adjacent plane. See Figure 2.14-right. This justifies the improvement on the branching between dissimilar sections that was performed

by Boissonnat and Geiger in [BG93], by adding vertices (colored in green in Figure 2.14) on the projection of the medial axis of the adjacent contours, as had also been proposed in [Sha81].

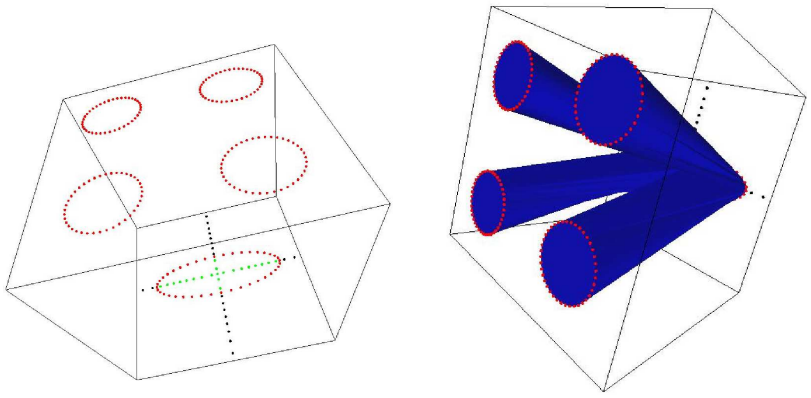

Figure 2.14: In the case of parallel cutting planes, the branching locus of the union of the Delaunay fibers lies on the orthogonal projection of (the external part of) the medial axis of the sections of the adjacent plane.

4.3 Singularities : Branching along the Boundary of Sections.

In the previous section, we saw that in the union of the tangent Delaunay fibers, branching may happen along the branching diagram. Moreover, as Figure 2.15-right shows, branching may also appear along the boundary of a section. Such a situation creates a *singularity* in the structure:

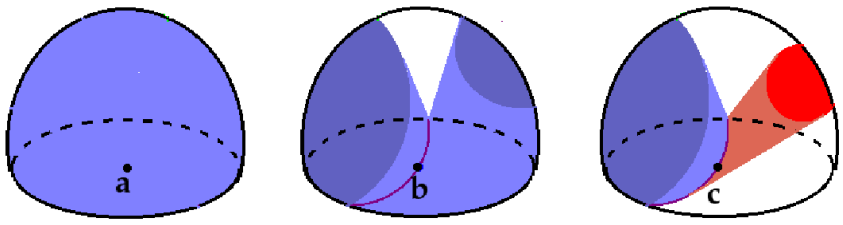

Figure 2.15: Branching along the boundary of a section creates a *singularity* (in red).

Definition 37 (Singularity) To any section-point $p \in \mathcal{S}_\mathcal{C}$, we associate the *normal cone* of $\mathcal{C}$ at p, i.e. the set of rays issued from p, lying outside $\mathcal{C}$ and directed along the normals to the supporting planes of $\mathcal{C}$ at p. The extended $\mathcal{S}_\mathcal{C}$ is the union of all such rays, denoted by $\widetilde{\mathcal{S}}_\mathcal{C}$. Let D be a set of Delaunay fibers between the sections in $\mathcal{S}_\mathcal{C}$. Points that do not have ball or half-ball neighborhoods in $D \cup \widetilde{\mathcal{S}}_\mathcal{C}$ are called singular. In this case, we say that D has a singularity at such a point, see Figure 2.16.

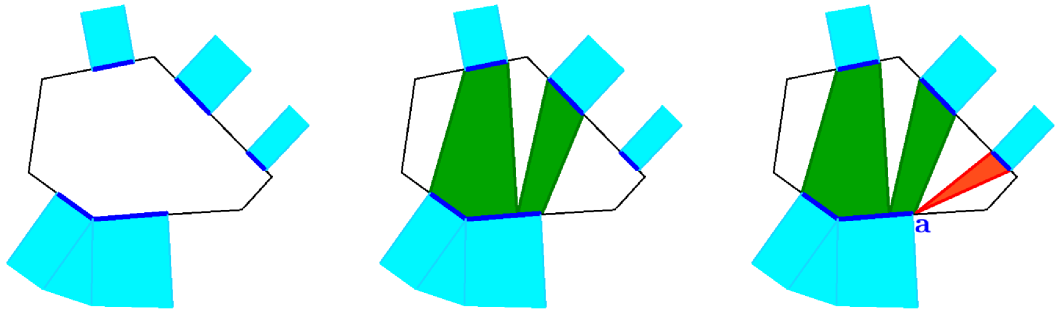

(a) (b) (c)

Figure 2.16: Singularities: (a) $\widetilde{\mathcal{S}_{\mathcal{C}}}$ (colored in blue) is the union of the normal cones. (b) For this reconstruction D (in green), $D \cup \widetilde{\mathcal{S}_{\mathcal{C}}}$ is a 3-manifold (with boundary). (c) The reconstruction of this example has a singularity at point a.

Two Types of Singularity

Two types of singularity can be observed in the union of the Delaunay fibers. The first one corresponds to the case where all Delaunay fibers between two subsections intersect one of them along its boundary. See Figure 2.17-left for an example. As we will see, this kind of singularity is easy to detect using the Moebius diagram and labeling Φ. The second type of singularities in the union of the Delaunay fibers corresponds to singularities that are created by some part of the Delaunay fibers between two sections, and intersect a section along a one dimensional feature, see Figure 2.17-right. Such singularities are more difficult to detect. In Chapter 3, we will provide a method to remove such singularities from a union of Delaunay simplices. Clearly, this type of singularity does not exist for the two dimensional version of the problem, where the sections are line-segments.

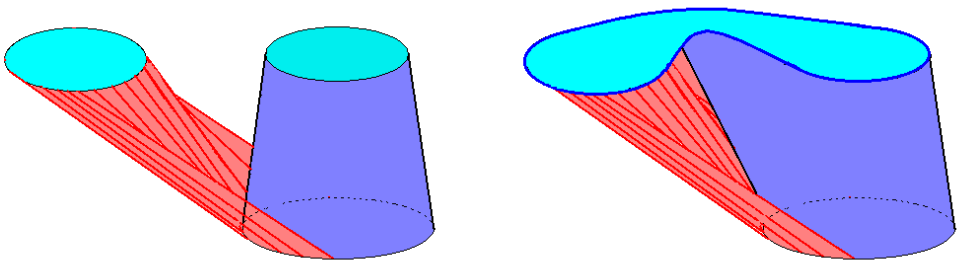

Figure 2.17: Two Types of Singularity.

We now show that the first type of singularity is easy to detect using the Moebius diagram and labeling Φ. Such a singularity corresponds to the case where all Delaunay

fibers between two subsections A and A' intersect one of them, say A, along its boundary. In this case, there is no point $a \in A$ such that $\phi(a) \in A'$. Consequently, $A' \notin \Phi(A)$. According to the following proposition, the converse is true as well.

Proposition 6 Let A and A' be two sections in $\mathcal{S}_\mathcal{C}$ such that $A \in \Phi(A')$ and $A' \notin \Phi(A)$. The tangent Delaunay fibers between A and A' create a singularity at A.

Proof Let $[a', a]$, $a \in A$ and $a' \in A'$, be a tangent Delaunay fiber at a'. We claim that a is on the boundary of A. Suppose that a is in the interior of A. By definition, the interior of the circumscribing ball B of $[a', a]$ is empty of points of $\mathcal{S}_\mathcal{C}$ (and in particular A). Therefore, B is tangent to A at a, and we have $A' \in \phi(a)$. We deduce that $A' \in \Phi(a)$ which is a contradiction. Therefore, any tangent Delaunay fibers between A and A' intersect A at a point on its boundary. We deduce that the union of the tangent Delaunay fibers between A and A' intersects A along a zero or one dimensional feature. □

The above proposition leads to the following definition:

Definition 38 (Symmetric Labeling) The labeling between A and A' is said to be *symmetric* if and only if $A \in \Phi(A')$ and $A' \in \Phi(A)$.

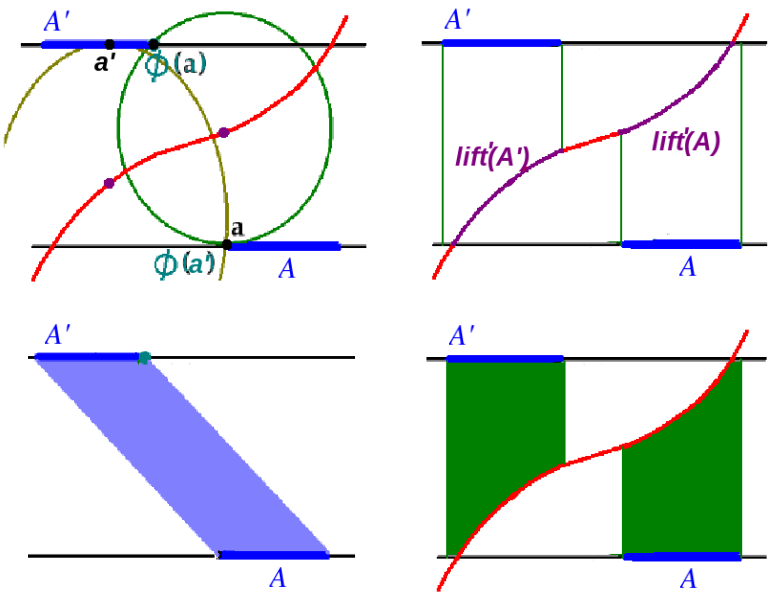

Figure 2.18: Symmetric labeling strategy, that consists of connecting two sections A and A' if $A \in \Phi(A')$ and $A' \in \Phi(A)$, allows us to perform connections between the sections by the Delaunay fibers as far as they do not create singularities in the structure. The reconstructed object we present in Chapter 3 (in blue) is based on pruning the singularities and performs more connections than the reconstructed object of the second method $\mathcal{R}'_\mathcal{C}$ (in green).

According to Proposition 6 and as can be seen in Figure 2.19(b)-right-down, the *non-symmetric* labellings corresponds to singularities in the union of the Delaunay fibers. We note that this proposition leads us to define a connectivity graph called $\mathcal{G}''_{\mathcal{C}}$ which will be used to efficiently compute the graph $\mathcal{G}'_{\mathcal{C}}$.

Definition 39 (Definition of the Graph $\mathcal{G}''_{\mathcal{C}}$) For each $\mathcal{S}_{\mathcal{C}}$, the graph $\mathcal{G}''_{\mathcal{C}}$ on the set of vertices $\mathcal{S}_{\mathcal{C}}$ is defined as follows: there is an edge between two sections A_1 and A_2 in $\mathcal{S}_{\mathcal{C}}$ if and only if the labeling between A and A' is symmetric.

Remark : This proposition justifies the symmetric labeling strategy which led to a method which induces $\mathcal{G}''_{\mathcal{C}}$ as the connectivity graph between the sections. The third reconstruction method we present in the next chapter has this property and performs connections between the sections by the Delaunay fibers as far as they do not create singularities in the structure.

By the definition of the connectivity graph $\mathcal{G}'_{\mathcal{C}}$, a given section $A \in \mathcal{S}_{\mathcal{C}}$ is connected to A' in $\mathcal{G}'_{\mathcal{C}}$ if $\text{lift}'(A)$ intersects $\text{lift}'(A')$. We have $\text{lift}'(A) \subset \text{V}_{\mathcal{C}}(A)$ and $\text{lift}'(A') \subset \text{V}_{\mathcal{C}}(A')$. Therefore, if $\text{lift}'(A)$ intersects $\text{lift}'(A')$ then both the intersections $\partial\text{V}_{\mathcal{C}}(A') \cap \text{lift}'(A)$ and $\partial\text{V}_{\mathcal{C}}(A) \cap \text{lift}'(A')$ are non-empty. On the other hand, by the definition of the labeling, if $\text{lift}'(A)$ intersects $\partial\text{V}_{\mathcal{C}}(A')$ then $A' \in \Phi(A)$. Therefore, if A is connected to A' in $\mathcal{G}'_{\mathcal{C}}$ then the labeling between A and A' is symmetric. We conclude that interestingly, the dual of $\mathcal{R}'_{\mathcal{C}}$ does not contain singularities of the first type. However, it may contain singularities of the second type that are more difficult to detect.

According to Proposition 6 and the above discussion, the union of the Delaunay fibers between the sections connected in the graph $\mathcal{G}'_{\mathcal{C}}$ does not contain any singularity of type 1. Thus, using the Delaunay fibers to connect the corresponding sections in $\mathcal{G}'_{\mathcal{C}}$ seems promising to improve the geometrical shape of $\mathcal{R}'_{\mathcal{C}}$.

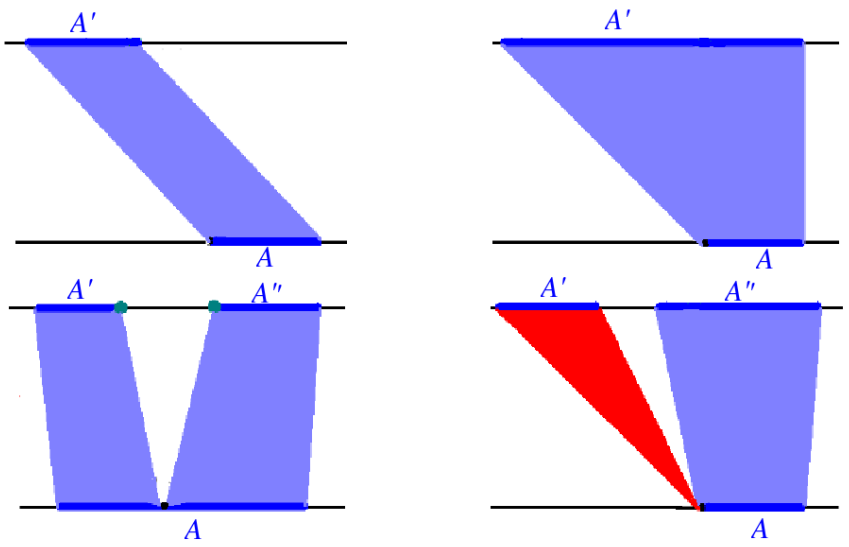

(a) Tangent Delaunay fibers between the sections.

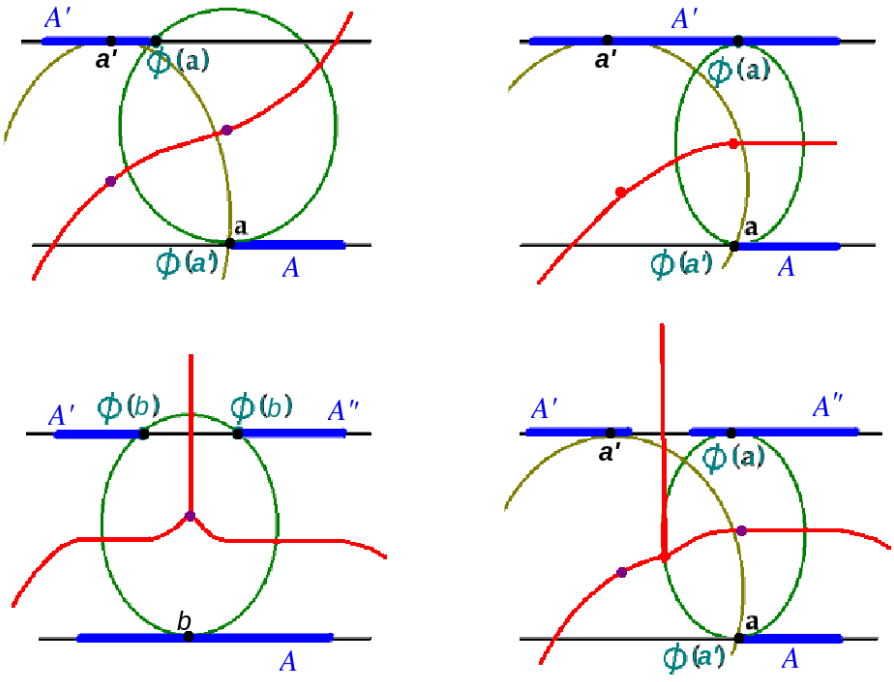

(b) Corresponding labeling between the sections: $A' \in \Phi(A)$ if there exists $a \in A$ such that $\phi(a)$ is a point in A'. The point b is an example of a branching point for which $\phi(b)$ is not unique.

Figure 2.19: In all cases, the labeling between A and A' is symmetric, except in the last case where $A \in \Phi(A')$ and $A' \notin \Phi(A)$. As the last figure shows, in this case the tangent Delaunay fibers between A and A' (in red) create a singularity at A. See Proposition 6.

4.4 Two Dual Objects : Kernel and Spine

In this section, we will use the Voronoi-Delaunay duality to present a set of Delaunay fibers, called the *spine* that has the same homotopy type as $\mathcal{R}'$. As a consequence, the topological guarantees for the reconstructed object $\mathcal{R}'_{\mathcal{C}}$ hold for the spine as well.

We have seen that the intersections of the lifts of the sections on VorSkel($\mathcal{S}_{\mathcal{C}}$) play a key role in the sections connectivity. This leads us to define a subset of VorSkel($\mathcal{S}_{\mathcal{C}}$) called the *All-Lift Part* that will be used later.

Definition 40 (All-Lift Part all $-$ lift($\mathcal{S}_{\mathcal{C}}$)**)** A point $m \in$ VorSkel($\mathcal{S}_{\mathcal{C}}$) is said to be in all $-$ lift($\mathcal{S}_{\mathcal{C}}$) if and only if m is on the lift of all its nearest points in $\mathcal{S}_{\mathcal{C}}$, i.e., all the orthogonal projections of m onto its nearest sections lie in $\mathcal{S}_{\mathcal{C}}$. See Figure 2.20-left. In particular, on a Voronoi 2-face of VorSkel($\mathcal{S}_{\mathcal{C}}$), the intersection of the lifts of the two corresponding sections is in all $-$ lift($\mathcal{S}_{\mathcal{C}}$).

Proposition 7 The all-lift part of VorSkel($\mathcal{S}_{\mathcal{C}}$) is *piecewise planar*, i.e., is composed of planar patches.

Proof Let S_1 and S_2 be two sections on the cutting planes P_1 and P_2, such that lift$'(S_1)$ and lift$'(S_2)$ intersect. This intersection is the locus of points in $\mathcal{C}$ that are at the same distance from P_1 and P_2. Thus, lift$'(S_1)$ and lift$'(S_2)$ lies on the bisector plane of P_1 and P_2. Therefore, the intersection of all $-$ lift($\mathcal{S}_{\mathcal{C}}$) with each Voronoi 2-face of VorSkel($\mathcal{S}_{\mathcal{C}}$) is planar. □

Using the all-lift part of VorSkel($\mathcal{S}_{\mathcal{C}}$), we first present a subset of $\mathcal{R}'_{\mathcal{C}}$, called the *Kernel*, that as we will see, has the same homotopy type as $\mathcal{R}'_{\mathcal{C}}$ and is easily computable.

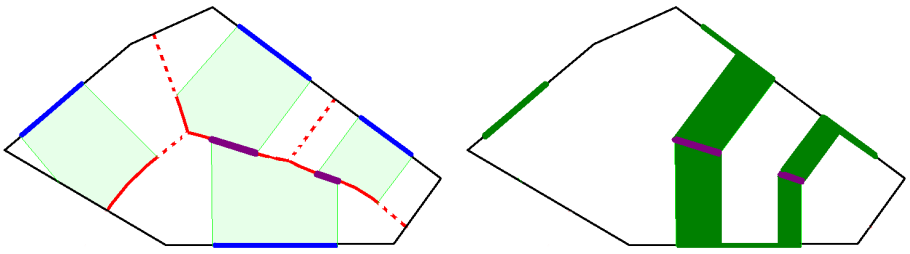

Figure 2.20: 2D example: Left) all $-$ lift($\mathcal{S}_{\mathcal{C}}$) in purple. Right) The kernel $\mathcal{K}_{\mathcal{C}} := \mathcal{S}_{\mathcal{C}} \cup \mathcal{L}'^{-1}$(all $-$ lift($\mathcal{S}_{\mathcal{C}}$)) in green, that captures the connectivity between the sections induced by $\mathcal{R}'_{\mathcal{C}}$.

Definition 41 (Kernel) The *kernel* of $\mathcal{C}$ is defined as $\mathcal{K}_{\mathcal{C}} := \mathcal{S}_{\mathcal{C}} \cup \mathcal{L}'^{-1}$(all $-$ lift($\mathcal{S}_{\mathcal{C}}$)) which is the union of the sections in $\mathcal{S}_{\mathcal{C}}$ and the segments that link each $m \in$ all $-$ lift($\mathcal{S}_{\mathcal{C}}$) to its orthogonal projections onto the nearest sections. The Kernel is then defined as $\mathcal{K} := \bigcup_{\mathcal{C}} \mathcal{K}_{\mathcal{C}}$, see Figure 2.20-right.

Conformity of the kernel with the given sections : Let us note that $\mathcal{K}$ conforms to the given sections. This is due to the fact that the all-lift part of VorSkel($\mathcal{S}_\mathcal{C}$) may intersect $\partial\mathcal{C}$ only along the sections. Therefore, $\mathcal{L}'^{-1}(\text{all}-\text{lift}(\mathcal{S}_\mathcal{C}))$ does not intersect $\partial\mathcal{C}\setminus\mathcal{S}_\mathcal{C}$. This is the principal geometrical advantage of the kernel with respect to the *intermediate* defined reconstructed object $\mathcal{R}'$. (No need to thicken the cutting planes.)

We now prove that the kernel captures the topology of the reconstructed object $\mathcal{R}'$.

Theorem 25 $\mathcal{K}$ is homotopy equivalent to the reconstructed object $\mathcal{R}'$.

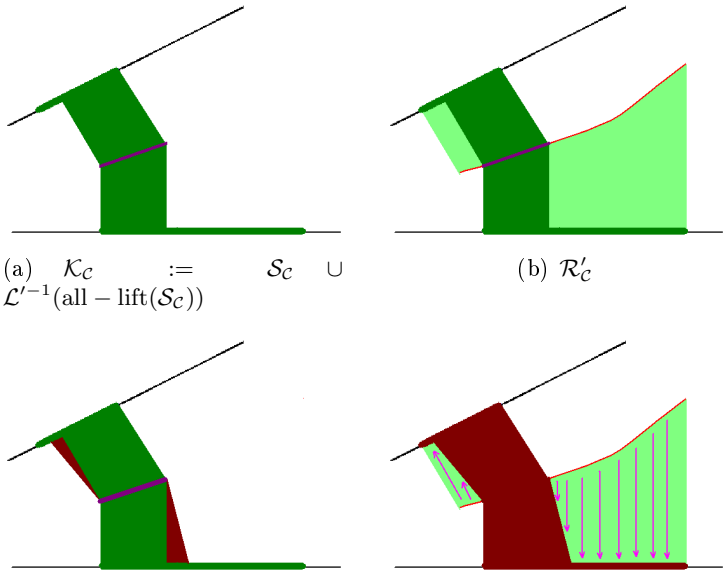

(a) $\mathcal{K}_\mathcal{C} := \mathcal{S}_\mathcal{C} \cup \mathcal{L}'^{-1}(\text{all}-\text{lift}(\mathcal{S}_\mathcal{C}))$ (b) $\mathcal{R}'_\mathcal{C}$

(c) An intermediate shape homotopy equivalent to $\mathcal{K}_\mathcal{C}$. (d) Deformation of $\mathcal{R}'_\mathcal{C}$ to the intermediate shape (in red).

Figure 2.21: Homotopy equivalence between $\mathcal{K}_\mathcal{C}$ and $\mathcal{R}'_\mathcal{C}$.

Proof For any cell $\mathcal{C}$ of the arrangement, we present a homotopy equivalence between $\mathcal{K}_\mathcal{C}$ and $\mathcal{R}'_\mathcal{C}$ whose restriction to $\mathcal{S}_\mathcal{C}$ is the identical map. According to the generalized nerve theorem, presented in the first chapter, these homotopy equivalences provide a homotopy equivalence between $\mathcal{K}$ and $\mathcal{R}'$.

Consider the union of the sections in $\mathcal{S}_\mathcal{C}$ and an infinitesimal thickening of $\mathcal{L}'^{-1}(\text{all}-\text{lift}(\mathcal{S}_\mathcal{C}))$ at each section, see Figure 2.21-c. This intermediate shape, denoted by $\widetilde{\mathcal{K}}_\mathcal{C}$, is homotopy equivalent to $\mathcal{K}_\mathcal{C}$. The key idea is that $\mathcal{R}'_\mathcal{C}$ can be retracted to this intermediate shape as follows (see Figure 2.21-d) : the deformation moves the points in $\mathcal{L}'^{-1}(\text{lift}'(\mathcal{S}_\mathcal{C})\setminus\text{all}-\text{lift}(\mathcal{S}_\mathcal{C}))$ in the direction orthogonal to the sections until a point in $\widetilde{\mathcal{K}}_\mathcal{C}$ is reached. This deformation gives a homotopy equivalence between $\mathcal{R}'_\mathcal{C}$ and $\widetilde{\mathcal{K}}_\mathcal{C}$, which is itself homotopy equivalent to $\mathcal{K}_\mathcal{C}$. □

In Section 2.1, we defined the all-lift part of VorSkel($\mathcal{S}_\mathcal{C}$) (denoted by $\text{all}-\text{lift}(\mathcal{S}_\mathcal{C})$) as the locus of points $m \in \text{VorSkel}(\mathcal{S}_\mathcal{C})$ such that m is on the lift of all its nearest points in

$\mathcal{S}_\mathcal{C}$. Using the Voronoi-Delaunay duality, we define a new object, called the *spine*, that is homotopy equivalent to the kernel with some geometrical advantages.

Definition 42 (Spine) Consider the dual of the all-lift part, denoted by $\text{all}-\text{lift}^*(\mathcal{S}_\mathcal{C})$. It is the union of the Delaunay simplices circumscribed by a ball $\sigma(m)$ so that m is on the lift of all the contact points of $\sigma(m)$ in $\mathcal{S}_\mathcal{C}$. In other words, $\text{all}-\text{lift}^*(\mathcal{S}_\mathcal{C})$ is the union of the Delaunay simplices $[a_1,\ldots,a_k]$ with vertices $a_1,\ldots,a_k \in \mathcal{S}_\mathcal{C}$, for $k \in \{2,3,4\}$, so that its circumscribing Delaunay ball is tangent to the supporting cutting planes of a_i, for all $1 \leq i \leq k$. We now define the *spine* as the union of $\text{all}-\text{lift}^*(\mathcal{S}_\mathcal{C})$ and the sections of $\mathcal{S}_\mathcal{C}$, see Figures 2.22and 2.23.

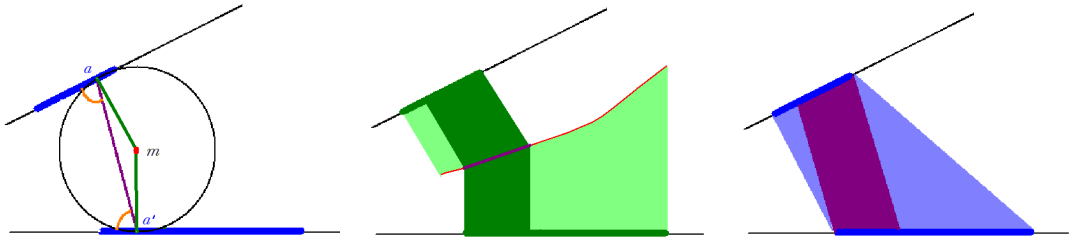

(a) A Delaunay fiber in the spine (in purple) dual to a point $m \in \text{all}-\text{lift}(\mathcal{S}_\mathcal{C})$.

(b) A part of $\text{VorSkel}(\mathcal{S}_\mathcal{C})$ colored in red, $\text{all}-\text{lift}(\mathcal{S}_\mathcal{C})$ is the bold part. $\mathcal{R}'_\mathcal{C}$ in green and the kernel in dark green.

(c) The Spine in purple. Other Delaunay fibers in blue.

Figure 2.22: 2D Example of Voronoi-Delaunay Duality.

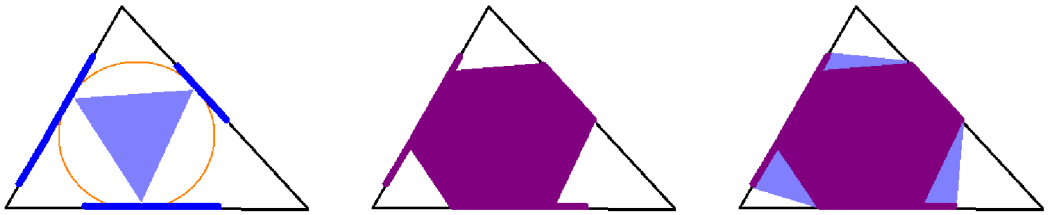

(a) A Delaunay simplex in the spine (in purple) dual to a point $m \in \text{all}-\text{lift}(\mathcal{S}_\mathcal{C})$.

(b) The spine in purple.

(c) Inflating the spine.

Figure 2.23: 2D Example of the spine.

Theorem 26 (Duality) The spine is homotopy equivalent to the kernel (and so to the reconstructed object).

Proof We recall that the spine is defined as $\mathcal{S}_\mathcal{C} \cup \text{all}-\text{lift}^*(\mathcal{S}_\mathcal{C})$ and the kernel is defined as $\mathcal{S}_\mathcal{C} \cup \mathcal{L}'^{-1}(\text{all}-\text{lift}(\mathcal{S}_\mathcal{C}))$. Thus, it will be sufficient to show that $\text{all}-\text{lift}^*(\mathcal{S}_\mathcal{C})$ and

$\mathcal{L}'^{-1}(\text{all} - \text{lift}(\mathcal{S}_\mathcal{C}))$ are homotopy equivalent. Consider $\mathcal{L}'^{-1}(\text{all} - \text{lift}(\mathcal{S}_\mathcal{C}))$ which is the union of the segments that link each $m \in \text{all} - \text{lift}(\mathcal{S}_\mathcal{C})$ to its orthogonal projections onto the nearest sections. As illustrated in Figure 2.24, the dual of such point $m^* = [a, a']$ can be deformed to the union of the two segments $[a, m]$ and $[m, a']$. Around the Delaunay simplices with three or four vertices of the spine, defining the deformation needs more care. Figure 2.25 shows the deformation in such a case in two steps. Consider a thickening (colored in green in Fig.2.25-a) of the three segments that connect the dual of the Delaunay triangle to its vertices. The triangle is easily deformable to this green object. On the other hand, Figure 2.25-b shows the deformation of each group of the Delaunay fibers (in blue) to the corresponding part of the kernel.

It is well-known that the Delaunay fibers do not intersect each other except on their endpoints. Moreover, the segments of $\mathcal{L}'^{-1}(\text{all} - \text{lift}(\mathcal{S}_\mathcal{C}))$ have trivially the same property. Therefore, the above deformation is well-defined and one-to-one continuous function and forms a homotopy equivalence (even a homeomorphism) between the spine and the kernel in each cell of the arrangement. □

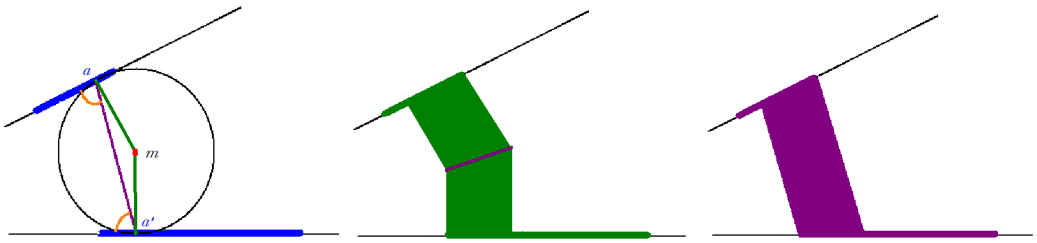

(a) The Delaunay fiber aa' can be deformed to the union of the two segments am and ma'.

(b) The kernel in dark green.

(c) The spine in purple.

Figure 2.24: The spine and the kernel are homotopy equivalent.

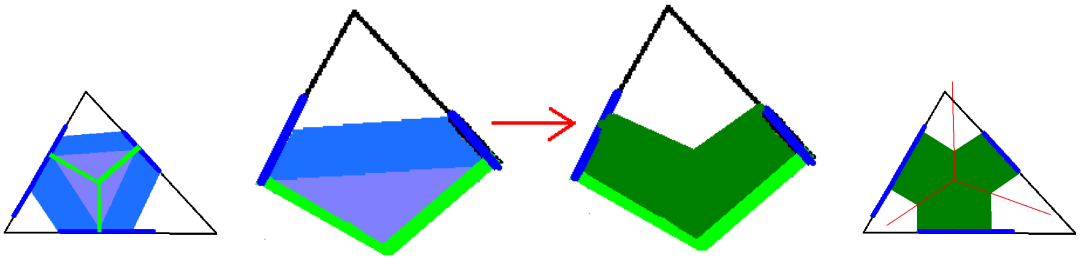

(a) The Delaunay triangle is deformed to the green part.

(b) Each group of the Delaunay fibers (in blue) is deformable to the corresponding part of the kernel.

(c) The kernel.

Figure 2.25: Deformation of the spine to the kernel around a Delaunay triangle.

4.5 Inflating the Spine

In the previous sections, we defined the spine Spine($\mathcal{S}_\mathcal{C}$) as the union of $\mathcal{S}_\mathcal{C}$ and the set of Delaunay simplices T such that the circumscribing Delaunay ball of T is tangent to the supporting cutting planes at all its contact points in $\mathcal{S}_\mathcal{C}$. According to Theorem 25 and Theorem 26 of the previous section, the spine has the same homotopy type as the reconstructed object $\mathcal{R}'_\mathcal{C}$. As a consequence, the topological guarantees for the reconstructed object $\mathcal{R}'_\mathcal{C}$ hold for Spine($\mathcal{S}_\mathcal{C}$) as well. As Figure 2.24 shows, using the spine as the connecting object between the sections provides a better appearance for the reconstructed object. Moeover, a natural idea is to *inflate* the spine by adding other Delaunay fibers, in order to obtain a well shaped object:

Definition 43 (Inflated Spine $\mathcal{D}$) We define $\mathcal{D}_\mathcal{C}$ as the union of $\mathcal{S}_\mathcal{C}$ and all tangent Delaunay fibers between the sections that are connected by some Delaunay fibers in Spine($\mathcal{S}_\mathcal{C}$). We define $\mathcal{D}$ as the union of $\mathcal{D}_\mathcal{C}$ for all $\mathcal{C}$. In particular, $\mathcal{D}$ contains the spine. See Figure 2.26.

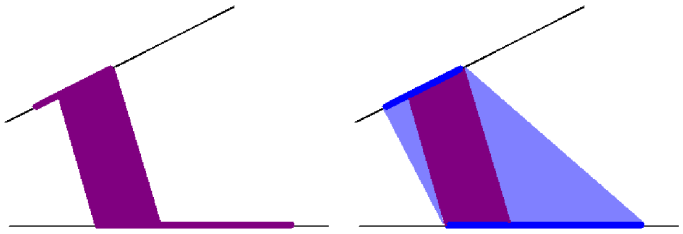

(a) The spine in purple.

(b) The Spine in purple. Other Delaunay fibers in blue.

Figure 2.26: Left) The spine of a cell. Right) Inflated Spine.

2D Case

Consider the 2-dimensional variant of the reconstruction problem, that consists of constructing a 2D-shape from its intersections with arbitrarily oriented cutting lines in general position. In this case, the sections (and the branching subsections) are line-segments. The Delaunay fibers between two subsections (subsegments) forms the convex hull of the two subsegments. We now show that $\mathcal{D}$ is homeomorphic to $\mathcal{R}'$. As a consequence, the topological guarantees for the reconstructed object $\mathcal{R}'$ hold for $\mathcal{D}$ as well.

Proposition 8 $\mathcal{D}$ is a topological manifold with boundary that conforms to the given sections.

Proof We will show that the inflated spine has no singularity. A singularity in the 2-dimensional variant of the reconstruction consists of connections between sections along zero dimensional features.

As Figure 2.26-right shows, the set of all tangent Delaunay fibers between two corresponding branching subsections in the spine coincides with their convex-hull. As any cell $\mathcal{C}$ of the arrangement of the cutting lines is convex, the Delaunay fibers between $\mathcal{S}_\mathcal{C}$ lie entirely inside $\mathcal{C}$ and conform to the given sections. Moreover, each group of tangent Delaunay fibers between two subsections intersects the cutting planes along these subsections that are one-dimensional. We can easily infer that for each cell $\mathcal{C}$ of the arrangement, $\mathcal{D}_\mathcal{C}$ has no singularity. When we glue the various $\mathcal{D}_\mathcal{C}$ together, a singularity may be created only in the following degenerate case:

Consider a face f of the arrangement and the two incident cells $\mathcal{C}$ and $\mathcal{C}'$. If the branching diagrams of $\mathcal{C}$ and $\mathcal{C}'$ intersect in f then intersection points are singular, see the singularity at point b in Figure 2.27. In 2D, as the cutting lines are supposed in general position such a case cannot happen, and $\mathcal{D}$ is a topological manifold with boundary. □

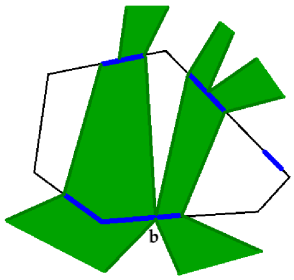

Figure 2.27: A degenerate case: A singularity at point b which is on the intersection of the two branching diagrams, corresponding to the two adjacent cells.

Proposition 9 (Provably Good 2D Reconstruction) $\mathcal{D}$ is homeomorphic to $\mathcal{R}'$.

Proof By the definition of the spine and $\mathcal{D}_\mathcal{C}$, there is a bijection between the connected components of $\mathcal{D}_\mathcal{C}$ and $\mathcal{R}'_\mathcal{C}$. On the other hand, all the connected components of $\mathcal{D}_\mathcal{C}$ or $\mathcal{R}'_\mathcal{C}$ are 2-dimensional disks. Therefore, there is a homotopy equivalence between each pair of corresponding connected components of $\mathcal{D}_\mathcal{C}$ or $\mathcal{R}'_\mathcal{C}$. This provides a homotopy equivalence between $\mathcal{D}_\mathcal{C}$ and $\mathcal{R}'_\mathcal{C}$. As we explained in detail in Section 4.4 of the first chapter, using the generalized nerve theorem, the homotopy equivalences in the different cells of the arrangement can be extended to a homotopy equivalence between $\mathcal{D}$ and $\mathcal{R}'$. Finally, since $\mathcal{D}$ and $\mathcal{R}'$ are two homotopy equivalent 2-dimensional topological manifolds, we conclude that they are indeed homeomorphic. □

3D Case

However, in the 3D case, the problem is that there may be some *singularities* in $\mathcal{D}_\mathcal{C}$. Figure 2.28 shows an example. These singularities should be detected and removed. Pruning

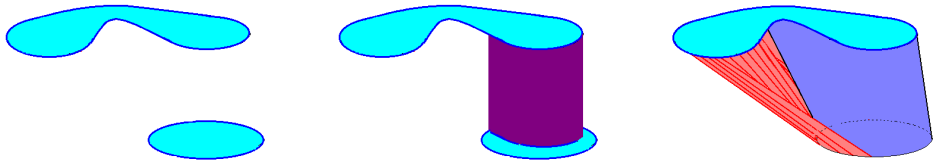

(a) Two parallel sections. (b) The spine. (c) All tangent Delaunay fibers between them ($\mathcal{D}_\mathcal{C}$).

Figure 2.28: The two (blue) sections are connected to each other in the spine (in purple). However, the set of all tangent Delaunay fibers between them ($\mathcal{D}_\mathcal{C}$) may have *singularities*, i.e., connections along zero or one dimensional features (in red).

$\mathcal{D}_\mathcal{C}$ until there are no singularities in the structure is the last step of the 3D reconstruction algorithm that will be presented in the following.

5 Discrete Algorithm

We consider the discrete case of the problem: We are given some polygonal contours in the cutting planes. We suppose that the contours are oriented in such a way that $\mathcal{O}$ is always on the left side of an oriented edge of a contour. For each cutting plane P, a connected component of $\mathcal{O} \cap P$ is called a *section*, and is bounded by some of the given contours (and may be nested). The vertices of these polygonal contours are called the *section-vertices*. The section-vertices and the equation of their planes form the input of our algorithm. (We will assume that at the intersection between the cutting planes, the corresponding sections conform with each other.) The Delaunay-based algorithm that we propose contains the following main steps:

1. Compute the sections of the cells of the arrangement.

   In each cell $\mathcal{C}$:

2. Compute the connectivity graph $\mathcal{G}'_{\mathcal{C}}$ between the sections induced by $\mathcal{R}'_{\mathcal{C}}$, in two steps:

   - First find a graph $\mathcal{G}''_{\mathcal{C}}$ such that $\mathcal{G}'_{\mathcal{C}}$ is a subgraph of $\mathcal{G}''_{\mathcal{C}}$ (see below for the definition).
   - Extract $\mathcal{G}'_{\mathcal{C}}$ from $\mathcal{G}''_{\mathcal{C}}$.

3. Compute $\mathcal{D}_{\mathcal{C}}$ the set of all Delaunay simplices between the sections connected in $\mathcal{G}'_{\mathcal{C}}$.

4. Prune $\mathcal{D}_{\mathcal{C}}$ to reach a subcomplex without singularities.

5. Glue the portions of the reconstructed object together.

In this section, we explain in detail the three first steps of this algorithm and present an efficient way to compute the connectivity between the sections. The last step which corresponds to the pruning procedure of $\mathcal{D}_{\mathcal{C}}$ is very similar to the pruning procedure we will present in Chapter 3. We refer to this chapter for more details on this procedure.

5.1 Step 1 : Computing the Sections in Each Cell of the Arrangement.

In this step, we apply a fast and easy method to cluster the sections into groups: each group consists of all the sections that appear on the boundary of a cell of the arrangement. The algorithm does not compute the arrangement of the cutting planes directly. (As we are not interested in the cells without sections, there is no need to compute them.) The method works as follows:

Let $\mathcal{P} = \{P_1, \ldots, P_k\}$ be the family of all the given cutting planes. Each P_i bounds two half spaces that we call $H_+(P_i)$ and $H_-(P_i)$. Each section-vertex a is either on the plane P_i or belongs to exactly one of the two half spaces $H_+(P_i)$ or $H_-(P_i)$. If a is on a cutting plane P_i, a is on the boundary of two cells of the arrangement, one contained in $H_+(P_i)$ and one contained in $H_-(P_i)$.

In order to find groups of section-vertices that are on the boundary of the same cell of the arrangement, to each section-vertex a we will associate two binary *signature*-vectors of size k which encodes the position of a with respect to the k cutting planes. The signature-vectors of a, denoted by $S_-(a) = \big(S_{-,1}(a), \ldots, S_{-,k}(a)\big)$ and $S_+(a) = \big(S_{+,1}(a), \ldots, S_{+,k}(a)\big)$, are defined as follows.

If $a \in H_+(P_i)$, we define $S_{-,i}(a) = S_{+,i}(a) = 1$. Symmetrically, if $a \in H_-(P_i)$, we define $S_{-,i}(a) = S_{+,i}(a) = 0$. If $a \in P_i$ then we define $S_{-,i}(a) = 0$ and $S_{+,i}(a) = 1$. Indeed, this definition can be seen as a duplication of the section-vertex $a \in P_i$ to two vertices, one on the boundary of the adjacent cell which is contained in $H_+(P_i)$ and one on the boundary of the cell which is contained in $H_-(P_i)$. This strategy allows us to distinguish between these two copies of a that correspond to the two different signatures of a. We note that, knowing the equation of P_i, $S_{\pm,i}(a)$ is easily computable by the sign of a determinant. All the section-vertices on the boundary of a cell of the arrangement have the same signature and vice versa. To identify them, it is sufficient to sort the set of signatures of the section-vertices. Any group of identical signatures corresponds to the group of all section-vertices on the boundary of a cell of the arrangement.

It may happen that the vertices of a section do not have the same signature: Figure 2.29-left shows an example of two sections that intersect along the intersection between their supporting cutting planes. Each of these sections should be divided into subsections that will appear on the boundary of different cells of the arrangement. This subdivision is determined by the signature of their vertices. A cluster of vertices with the same signature corresponds to a subsection. Using the signatures of these clusters, we characterize the cutting planes that intersect the section, and add some additional contour-points along the intersection between the cutting planes. After this first refinement obtained by subdividing the original sections into some new connected regions bounded by polygonal contours (called sections again), we can assume that each section is shared by two cells of the arrangement of the cutting planes.

5.2 Step 2 : Computing the Connectivity Graph between the Sections.

Let $\mathcal{S}_\mathcal{C}$ be the set of all the sections that appear on the boundary of a cell $\mathcal{C}$ of the arrangement. We note that $\mathcal{S}_\mathcal{C}$ is given by the clustering algorithm of the first step. We recall the definition of the *connectivity graph* between the sections of $\mathcal{S}_\mathcal{C}$, denoted by $\mathcal{G}'_\mathcal{C}$ (see Section 2.1):

Each vertex in $\mathcal{G}'_\mathcal{C}$ corresponds to a section in $\mathcal{S}_\mathcal{C}$, and there is an edge between the corresponding vertices of two sections A_1 and A_2 if $\text{lift}'(A_1)$ and $\text{lift}'(A_2)$ intersect on $\text{VorSkel}(\mathcal{S}_\mathcal{C})$.

We describe below how the connectivity graph $\mathcal{G}'_\mathcal{C}$ can be computed without computing the 3D Voronoi diagram of the sections.

By the definition of the connectivity graph, for a given section $A_1 \in \mathcal{S}_\mathcal{C}$, the goal will be to find all the sections A_2 in $\mathcal{S}_\mathcal{C}$ such that $\text{lift}'(A_1)$ intersects $\text{lift}'(A_2)$. We use the fact that by definition $\text{lift}'(A_1) \subset \text{V}_\mathcal{C}(A_1)$ and $\text{lift}'(A_2) \subset \text{V}_\mathcal{C}(A_2)$. Therefore, if $\text{lift}'(A_1)$ intersects $\text{lift}'(A_2)$ then both the intersections $\partial\text{V}_\mathcal{C}(A_2) \cap \text{lift}'(A_1)$ and $\partial\text{V}_\mathcal{C}(A_1) \cap \text{lift}'(A_2)$ are non-

empty. We will use this property to construct the connectivity graph $\mathcal{G}'_{\mathcal{C}}$. Note that as Figure 2.29-right shows the converse is not necessarily true.

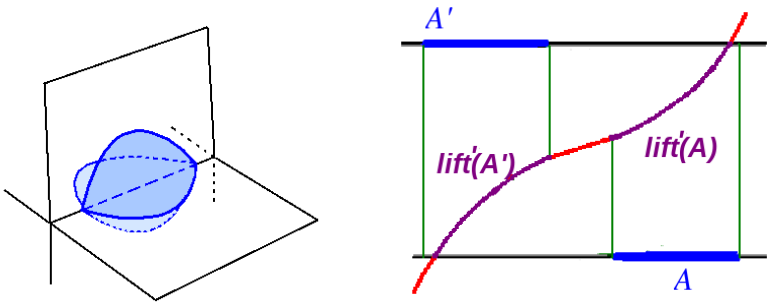

Figure 2.29: Left) An example of two sections that intersect along the intersection between their supporting cutting planes. Right) An example where both $\partial \mathrm{V}_{\mathcal{C}}(A') \cap \mathrm{lift}'(A)$ and $\partial \mathrm{V}_{\mathcal{C}}(A) \cap \mathrm{lift}'(A')$ are non-empty, but $\mathrm{lift}'(A) \cap \mathrm{lift}'(A')$ is empty.

Definition 44 (Definition of the Graph $\mathcal{G}''_{\mathcal{C}}$) For each $\mathcal{S}_{\mathcal{C}}$, the graph $\mathcal{G}''_{\mathcal{C}}$ on the set of vertices $\mathcal{S}_{\mathcal{C}}$ is defined as follows: there is an edge between two sections A_1 and A_2 in $\mathcal{S}_{\mathcal{C}}$ if and only if $\partial \mathrm{V}_{\mathcal{C}}(A_2) \cap \mathrm{lift}'(A_1) \neq \emptyset$ and $\partial \mathrm{V}_{\mathcal{C}}(A_1) \cap \mathrm{lift}'(A_2) \neq \emptyset$.

Proposition 10 $\mathcal{G}'_{\mathcal{C}}$ is a subgraph of $\mathcal{G}''_{\mathcal{C}}$.

Proof Two sections A_1 and A_2 are connected in $\mathcal{G}'_{\mathcal{C}}$ if and only if $\mathrm{lift}'(A_1) \cap \mathrm{lift}'(A_2) \neq \emptyset$. Since $\mathrm{lift}'(A_1) \subset \mathrm{V}_{\mathcal{C}}(A_1)$ and $\mathrm{lift}'(A_2) \subset \mathrm{V}_{\mathcal{C}}(A_2)$, both the intersections $\partial \mathrm{V}_{\mathcal{C}}(A_2) \cap \mathrm{lift}'(A_1)$ and $\partial \mathrm{V}_{\mathcal{C}}(A_1) \cap \mathrm{lift}'(A_2)$ are non-empty. Therefore, A_1 and A_2 are connected in $\mathcal{G}''_{\mathcal{C}}$. □

The advantage of defining the graph $\mathcal{G}''_{\mathcal{C}}$ is that it is easily computable, and using the edges of $\mathcal{G}''_{\mathcal{C}}$, we can find $\mathcal{G}'_{\mathcal{C}}$. We first explain how $\mathcal{G}'_{\mathcal{C}}$ can be extracted from $\mathcal{G}''_{\mathcal{C}}$. Then we provide an algorithm to compute $\mathcal{G}''_{\mathcal{C}}$

How to extract $\mathcal{G}'_{\mathcal{C}}$ from $\mathcal{G}''_{\mathcal{C}}$?

Let A_1 and A_2 be two different sections in $\mathcal{S}_{\mathcal{C}}$, on cutting planes P_1 and P_2, respectively, that are connected in $\mathcal{G}''_{\mathcal{C}}$. The intersection $\mathrm{lift}'(A_1) \cap \mathrm{lift}'(A_2)$ is the locus of points in $\mathcal{C}$ that are at the same distance from P_1 and P_2. Thus, if $\mathrm{lift}'(A_1) \cap \mathrm{lift}'(A_2) \neq \emptyset$, then this intersection should lie on the bisector plane of P_1 and P_2, denoted by P_{12}. This gives an easy way to extract $\mathcal{G}'_{\mathcal{C}}$ from $\mathcal{G}''_{\mathcal{C}}$:

For each pair of sections connected in $\mathcal{G}''_{\mathcal{C}}$, we compute the bisector plane of the supporting cutting plane. We consider the lift of each section on this bisector plane. The two sections are connected in $\mathcal{G}'_{\mathcal{C}}$ if and only if the two lifts intersect.

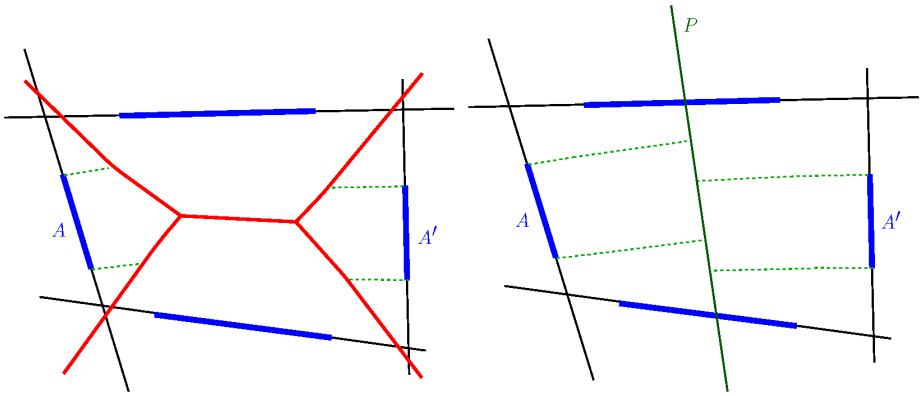

Figure 2.30: The role of $\mathcal{G}''_{\mathcal{C}}$ is crucial in this strategy: in this example, the lifts of two sections A and A' on the bisector plane P intersect, while the intersection of their lifts on VorSkel($\mathcal{S}_{\mathcal{C}}$) is empty. In this case, A and A' are not connected in $\mathcal{G}''_{\mathcal{C}}$.

Remark : One can think of applying this test on every pairs of sections, in order to compute $\mathcal{G}'_{\mathcal{C}}$ directly (without computing $\mathcal{G}''_{\mathcal{C}}$). Figure 2.30 shows an example where the lifts of two sections on the bisector plane intersect, but the intersection of their lifts on VorSkel($\mathcal{S}_{\mathcal{C}}$) is empty.

How to compute $\mathcal{G}''_{\mathcal{C}}$?

We now present an algorithm to construct $\mathcal{G}''_{\mathcal{C}}$ without computing the 3D Voronoi diagram of the sections. For a given section A, the goal is to find all the sections A' so that the lift of A on VorSkel($\mathcal{S}_{\mathcal{C}}$) intersects the Voronoi cell of A', i.e., $\partial \mathrm{V}_{\mathcal{C}}(A') \cap \mathrm{lift}'(A) \neq \emptyset$. Consider the skeleton of VorSkel($\mathcal{S}_{\mathcal{C}}$), which is the locus of points in $\mathcal{C}$ that have at least three nearest points in the sections of $\mathcal{S}_{\mathcal{C}}$. More intuitively, this is the part of VorSkel($\mathcal{S}_{\mathcal{C}}$) which separates the 2-dimensional Voronoi faces. We now orthogonally project the skeleton of VorSkel($\mathcal{S}_{\mathcal{C}}$) onto the cutting plane of A. This projection separates the projection of $\partial \mathrm{V}_{\mathcal{C}}(A')$ for $A' \in \mathcal{S}_{\mathcal{C}}$ distinct to A. The key idea is that in order to check the intersection $\partial \mathrm{V}_{\mathcal{C}}(A') \cap \mathrm{lift}'(A)$ on VorSkel($\mathcal{S}_{\mathcal{C}}$), we can verify the intersection of A with the projection of $\partial \mathrm{V}_{\mathcal{C}}(A')$. Using this idea, the graph $\mathcal{G}''_{\mathcal{C}}$ can be computed in tree steps:

- Compute the orthogonal projection of the skeleton of VorSkel($\mathcal{S}_{\mathcal{C}}$) onto each face of $\mathcal{C}$, called the *branching diagram*.
- Perform a *labeling* $\Phi(A)$ for each section A such that:

  A section A' is in $\Phi(A)$ if $\partial \mathrm{V}_{\mathcal{C}}(A') \cap \mathrm{lift}'(A)$ is non-empty.
- Extract pairs $[A, A']$ of sections such that $A' \in \Phi(A)$ and $A \in \Phi(A')$ (*symmetric labeling*).

The *branching diagram*, defined in Section 4.1, plays a key role here. Let us recall the definition.

Definition 45 (Branching Diagram, and Branching Subsections of a Section) The *branching diagram* of a face f of $\mathcal{C}$ is defined as the partition of f by the orthogonal projection of the 1-skeleton of VorSkel($\mathcal{S}_\mathcal{C}$) onto f. See Figure 2.31-left. Given a section A contained in a face f, the branching diagram of f subdivides A into so-called *branching subsections*.

Labeling Definition : Let A be a section in $\mathcal{S}_\mathcal{C}$ and let E be a branching subsection of A. lift$'(E)$ lies on a Voronoi 2-dimensional face. We define $\Phi(E)$ as the unique section A' such that lift$'(E)$ intersects $\partial \mathrm{V}_\mathcal{C}(A')$. We also define $\Phi(A)$ as the set of all $\Phi(E)$ for all branching subsections E of A. See Figure 2.31-right. By the definition, $A' \in \Phi(A)$ if lift$'(A)$ intersects $\partial \mathrm{V}_\mathcal{C}(A')$. Thus, A is connected to A' in $\mathcal{G}''_\mathcal{C}$ if and only if $A \in \Phi(A')$ and $A' \in \Phi(A)$. In this case, we say that the labeling between A and A' is *symmetric*.

Therefore, knowing the partition of the sections by the branching diagram, we can easily construct the graph $\mathcal{G}''_\mathcal{C}$. We will see that the branching diagram can be computed by a 2-dimensional geometric diagram, known as Moebius diagram, at each face of $\mathcal{C}$.

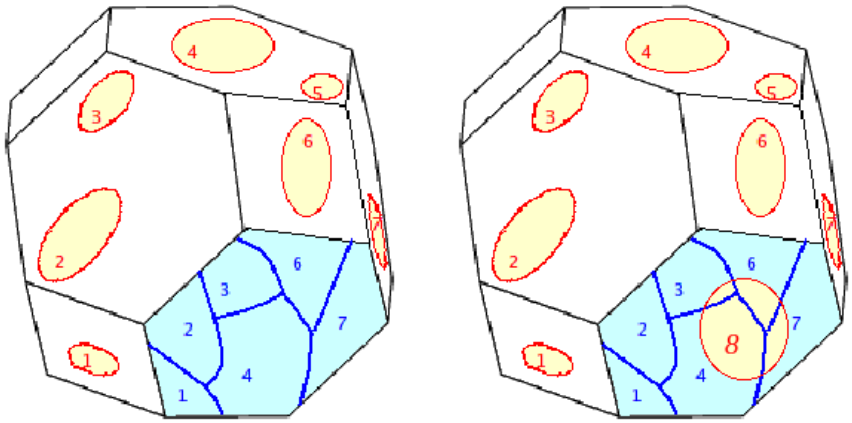

(a) The branching diagram of a face f of $\mathcal{C}$ (in blue).

(b) The partition of a section of f into branching subsections.

Figure 2.31: Labeling definition using the branching diagram: $\Phi(8) = \{3, 4, 6, 7\}$.

Branching Diagram Computation

In the case where all the cutting planes are parallel, any cell $\mathcal{C}$ of the arrangement is bounded by two parallel planes, say P and P'. It is easy to see that the branching diagram on the face P is the orthogonal projection onto P of the 2D-Voronoi diagram of the sections of P'. See Figure 2.32-left. In the general case, the computation of the branching diagram of a face of $\mathcal{C}$ can be done in the following way. Let P be the supporting plane of this face.

We show that the branching diagram on P can be computed by a 2D generalized Voronoi diagram called *Moebius diagram.*

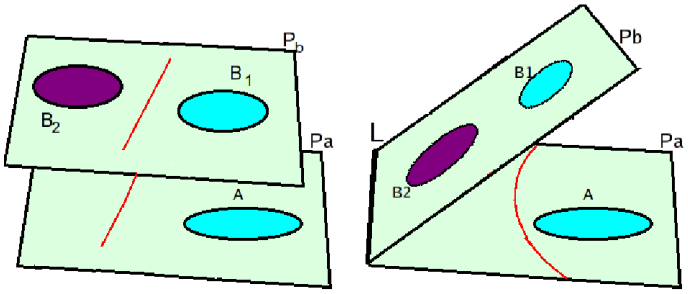

Figure 2.32: For a cell bounded by two parallel planes P and P', the branching diagram on a plane P is the orthogonal projection onto P of the 2D-Voronoi diagram of the sections of P'. In general case, the branching diagram is a 2D Moebius diagram with circular edges. The two sections colored in blue have symmetric labellings and are connected in $\mathcal{G}''_{\mathcal{C}}$.

Definition 46 (Moebius Diagram) *Let $\mathcal{U} = \{U_1, \ldots, U_k\}$ be a set of doubly weighted points of $\mathbb{R}^d$, where $U_i = (p_i, \lambda_i, \mu_i)$, p_i is a point of $\mathbb{R}^d$ and λ_i, μ_i are real numbers. For a point $x \in \mathbb{R}^d$, the distance from x to the doubly weighted point U_i is defined as*

$$d_M(x, U_i) = \lambda_i d(x, p_i)^2 - \mu_i.$$

We can then assign each point x to the doubly weighted point U_i that is closest to x with respect to the distance $d_M(.,.)$. The subdivision induced by this assignment is called the Moebius diagram *of $\mathcal{U}$. The Moebius diagram is a generalization of both the power diagram and the multiplicatively weighted Voronoi diagram, and has circular edges. See [BK03] for more details.*

To compute the branching diagram, we proceed as follows:

We know that a point on the branching diagram is the projection of a point x on the skeleton of VorSkel($\mathcal{S}_{\mathcal{C}}$). Such a point x has the same distance from P and two section-points b and b'. We denote by $\pi(b)$, $\pi(b')$ and $\pi(x)$, the projection of b, b' and x onto P, respectively. According to the definition, $\pi(x)$ is on the branching diagram of P. As Figure 2.33-left shows, we have:

$$d(x, P)^2 = d(x, b)^2 = d(\pi(x), \pi(b))^2 + (d(b, P) - d(x, P))^2$$

So

$$\frac{d(\pi(x), \pi(b))^2}{d(b, P)} + d(b, P) = 2d(x, P).$$

Since we have a similar equality for b', the branching diagram on P is the locus of the points $\pi(x)$ such that:

$$\frac{d(\pi(x), \pi(b))^2}{d(b, P)} + d(b, P) = \frac{d(\pi(x), \pi(b'))^2}{d(b', P)} + d(b', P)$$

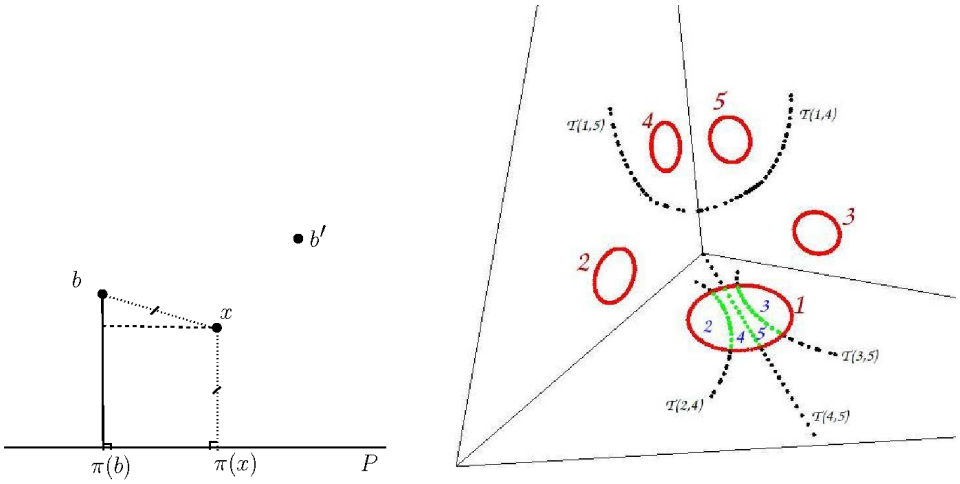

Figure 2.33: Right) To prove that the branching diagram is a 2D Moebius diagram. Left) An example of the partition of the sections with the branching diagram. Each branching subsection of Section 1 corresponds to a section in $\{2, 3, 4, 5\}$.

for some points b and b' in the sections of $\mathcal{S}_\mathcal{C}$. Thus, to compute the branching diagram of P, we project all the sections in $\mathcal{S}_\mathcal{C}$ (except the ones that lie on P) orthogonally to P. For each vertex b_i of a polygonal contour, $\pi(b_i)$ is weighted by $(\frac{1}{d(b_i,P)}, -d(b_i, P))$. The branching diagram of P is then included in the 2D Moebius diagram of the projected vertices of the sections. More precisely, it is on the intersection of the Moebius cells of the pairs of vertices that are not both in the same section.

Steps 3 and 4 : Delaunay Computation and Removal of Singularities.

According to discussions in Section 4, the branching locus of the union of the Delaunay fibers is on the branching diagram. In order to improve the branching between dissimilar sections, we propose to add a sample of the branching diagram (colored in green in Figure 2.34) to the given sample of contours. This strategy has been also employed by Boissonnat and Geiger in [BG93], by adding vertices on the projection of the medial axis of the adjacent contours for the case of parallel sections, as had been proposed in [Sha81]. The results provided in Figure 2.33-right and Figure 2.34 (generated using a CGAL-based([CGA]) prototype implementation of Moebius diagram by Christophe Delage [Del07]) show some examples of the branching diagram's computation.

We can now consider the Delaunay triangulation of the union of the contour points and the branching points. Using the branching diagram and the corresponding labeling Φ, we can find the set of all Delaunay simplices between the sections connected in $\mathcal{G}'_\mathcal{C}$, denoted by $\mathcal{D}_\mathcal{C}$. As said before, $\mathcal{D}_\mathcal{C}$ may contain singularities that should be detected and removed. We will present an algorithm to prune $\mathcal{D}_\mathcal{C}$ until there are no singularities in the structure. Nevertheless, one can think of pruning the whole Delaunay triangulation to reach a subcomplex without singularities. This is what will be presented in the next

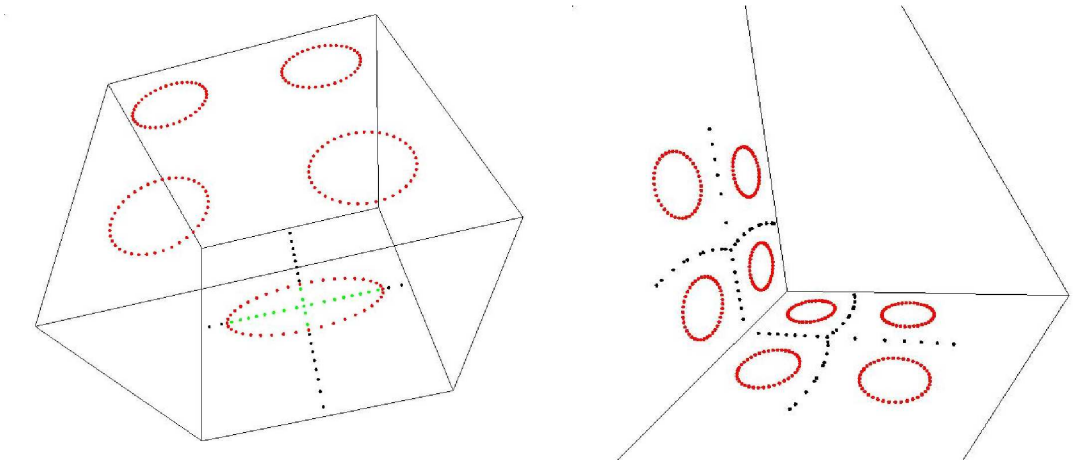

Figure 2.34: Some examples of the branching diagram's computation.

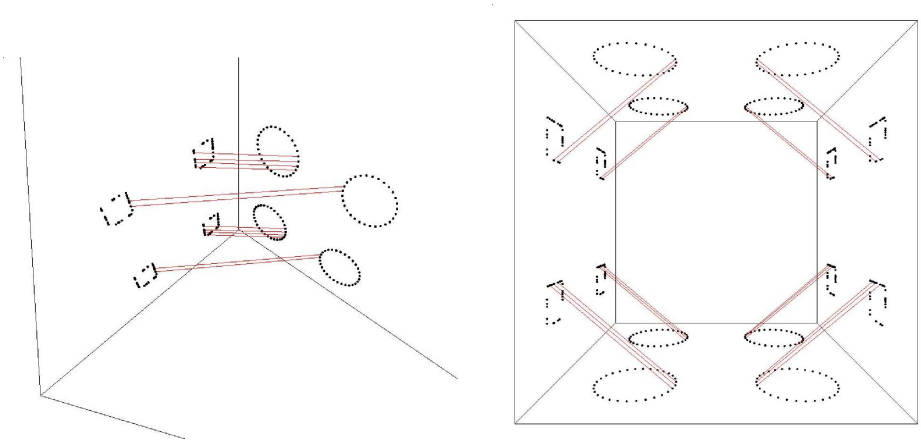

Figure 2.35: Some examples of the automatic computation of the connectivity graph: the input is a sample of the contours of the sections (points in red). In the input, a connectivity between two sections is illustrated by some thin red line segments.

chapter (which will be referred as Method 3). The pruning procedure of $\mathcal{D}_\mathcal{C}$ is identical to the pruning procedure that we will apply to the whole Delaunay complex, in the next chapter. Therefore, let us refer to Chapter 3 for the details of the pruning procedure. We end this chapter with presenting some preliminary experimental results of the algorithm, implemented in C++ using the CGAL library [CGA].

Complexity Analysis

We end this section by analyzing the complexity of the above algorithm. Suppose that we have k cutting planes and n points on the boundary of s sections. Let C_i be a cell

in the arrangement of the cutting planes. We write n_i for the number of points in C_i, and s_i for the number of sections in C_i. Assuming that the cutting planes are in general position, each point is on the boundary of $O(1)$ cells, and we have $\sum_i n_i = O(n)$. For the first step of the algorithm, we have $n.k$ orientation tests in order to define the signature of each point with respect to each cutting plane. There are $n.k$ signatures that are sorted in time $n.k\log(n.k)$. The subdivision of the sections is done in linear time. For the second step that concerns the computation of the connectivity graph, for each cell C_i, we need to compute the 2D Moebius diagram of at most n_i points in each face of C_i. As we know, we can compute 2D Moebius diagrams of n points in $Mob2(n) = O(n^2)$ time (see [BK03] and [Del03]). Finally, to find the connectivity between the sections, we have a test for each pair of the corresponding sections in $\mathcal{G}''_{\mathcal{C}}$ to check if their lifts intersect. This can be done in constant time for each pair of corresponding sections. Therefore, as each cell has at most k facets, the complexity of computing the connectivity between the sections (the two first steps of the algorithm) is at most:

$$n.k + n.k\log(n.k) + \sum_{C_i}(k.Mob2(n_i) + \frac{s_i(s_i-1)}{2})$$

$$\leq n.k + n.k\log(n.k) + \sum_{C_i}(k.O(n_i^2) + \frac{n_i(n_i-1)}{2}) \leq k.O(n^2).$$

As will be discussed in the next chapter, the two last steps of the algorithm can be done in $O(n^2)$ time.

Conclusion

In this chapter, motivated by reconstructing tree-like structures from sparse sectional data, we presented a Voronoi-based algorithm which performs more connections between the sections compared to the first method. We proved that the resulting reconstructed object $\mathcal{R}'$ is homeomorphic to the original shape $\mathcal{O}$ under appropriate sampling conditions. The particularity of the new sampling conditions, compared to the sampling conditions we proposed for the first method, is that they are easier to be satisfied for tree-like structures.

In order to improve the jagged and unnatural appearance of $\mathcal{R}'$, specially along the Voronoi diagram of the sections, we defined a Delaunay-based dual for the reconstructed object, called the spine. We proved that the spine is homotopy equivalent to $\mathcal{R}'$. Finally, we provided a discrete algorithm to reconstruct the spine.

From an algorithmic point of view, we showed that the computation of the whole arrangement of the cutting planes can be avoided, and the sections of each cell of the arrangement can be determined by some orientation tests with respect to the cutting planes. We also presented an efficient way to compute the connectivity between the sections, without computing the Voronoi diagram of the sections, using a 2-dimensional generalized Voronoi diagram on each face of the cell. According to the presented guarantees for the sections-connectivity induced by $\mathcal{R}'_{\mathcal{C}}$, this algorithm provides a provably good solution for the correspondence problem between the sections, and may be used independently of the

Delaunay structure. As we mentioned before, there are methods which consider the correspondence and the interpolation problems independently. So using this algorithm, one can obtain the provably good connectivity and then the interpolation between the corresponding sections can be performed by different methods, depending on the properties of interest for the reconstructed surface in each application.

Moreover, we characterized the branching locus of the union of the Delaunay simplices and presented an efficient algorithm to compute it. For the particular case of parallel sections, this result justifies the improvement on the branching between dissimilar sections that was performed by Boissonnat and Geiger in [BG93], by adding vertices on the projection of the medial axis of the adjacent contours. In the following chapter, we will present a generalization of their method to the case of arbitrarily oriented sections, and provide some experimental results.

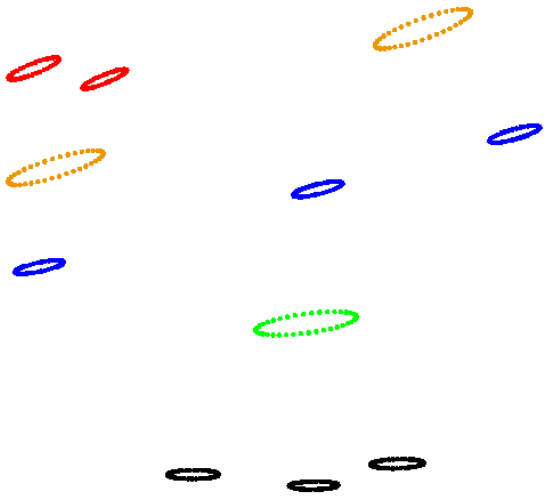

(a) The input is a sample of the contours of the sections (each slice in a different color).

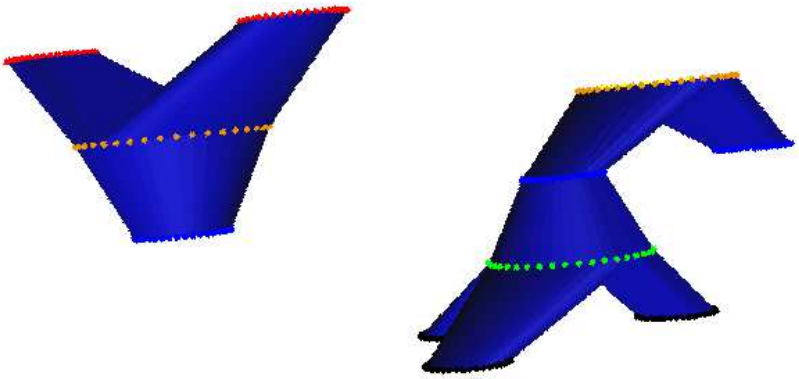

(b) Output.

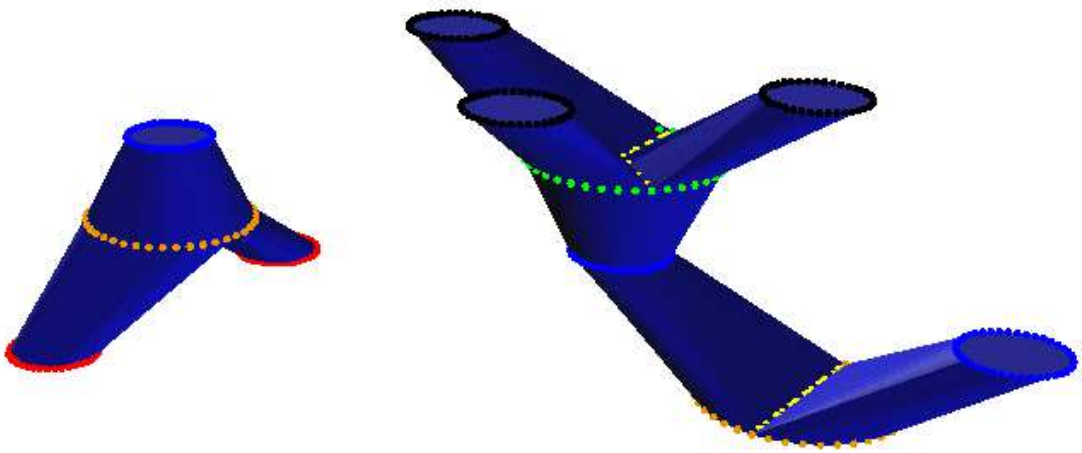

(c) Output (another view).

Figure 2.36: Reconstruction Example.

Chapter 3

Third Method: Generalization of Boissonnat and Geiger's Method

In the previous chapter, we presented a method based on the Voronoi diagram of the sections. Relating the sections connectivity to this Voronoi diagram, allowed us to obtain topological guarantees for the resulting reconstruction. Also, using the Voronoi-Delaunay duality, we obtained topological justifications for the dual Delaunay-based approach. The Delaunay-based algorithm we present in this chapter is somewhat different from the dual of the previous method, in the sense that it may perform more connections between the sections. Figure 3.1 shows a configuration of sections for which the resulting connectivity by the two methods is different.

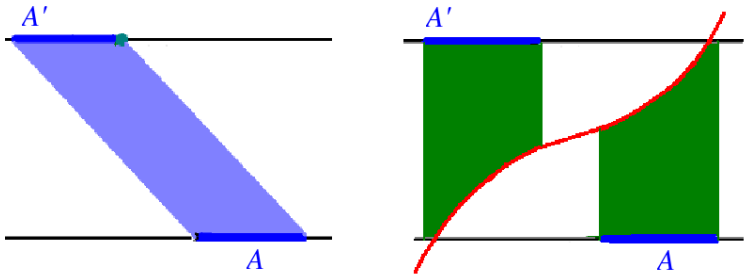

Figure 3.1: The reconstructed object $\mathcal{R}''_{\mathcal{C}}$ of the third method (left) performs more connections than the reconstructed object $\mathcal{R}'_{\mathcal{C}}$ of the second method (right).

Increasing the connectivity between the sections is motivated by reconstructing tree-like structures from sparse sectional data. Our preliminary experimental results presented at the end of this chapter, are quite promising, regarding the practicality of this approach to reconstruct complex cross-sectional branching situations such as the coronary arterial tree. This method can be seen as a generalization of Boissonnat and Geiger's method [BG93] that was restricted to the case of parallel (or serial) cutting planes.

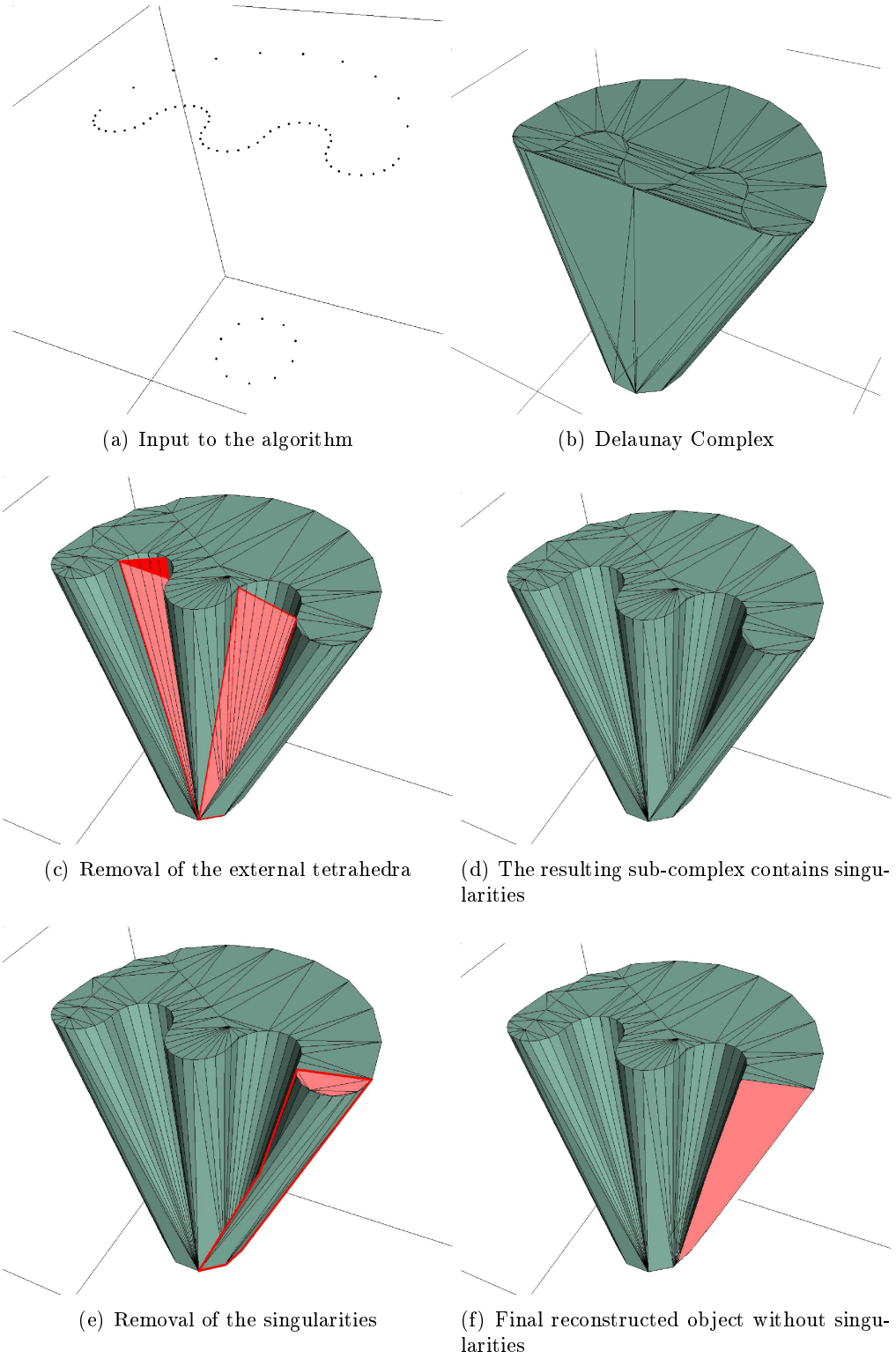

(a) Input to the algorithm

(b) Delaunay Complex

(c) Removal of the external tetrahedra

(d) The resulting sub-complex contains singularities

(e) Removal of the singularities

(f) Final reconstructed object without singularities

Figure 3.2: Different steps of the algorithm.

1 Discrete Delaunay Structure

In Section 5 of the previous chapter, we showed how the computation of the whole arrangement of the cutting planes can be avoided, and the sections of each cell of the arrangement can be determined by some orientation tests with respect to the cutting planes. Moreover, in Section 4 of the previous chapter, for each cell of the arrangement, we characterized the branching locus of the Delaunay structure which is on the branching diagram, and we presented an algorithm to compute it from a set of sample points on the contours of the sections. To consider the discrete Delaunay structure, instead of sampling the whole sections of the cell, we propose to consider a sample of the contours of the sections, called the *contour-vertices*, and a sample of the branching diagram, called the *branching points*. Let $\mathcal{B}_\mathcal{C}$ be a sample of the branching points of $\mathcal{C}$ and $\mathcal{V}_\mathcal{C}$ be the set of contour-vertices. We consider now $DT(\mathcal{V}_\mathcal{C} \cup \mathcal{B}_\mathcal{C})$, the 3D Delaunay triangulation of the union of the contour-vertices and these added points. This triangulation, called D_0 in the sequel, contains the reconstructed object $\mathcal{R}''_\mathcal{C}$ as a subcomplex. All the considered vertices are in the sections and called *section-vertices*.

We will assume the following condition to be satisfied, which can always be ensured by adding finitely many new vertices on the section contours and on the branching diagram. More details are provided in [ET93].

Delaunay Conformity Condition on $\mathcal{V}_\mathcal{C}$ and $\mathcal{B}_\mathcal{C}$: We assume that the edges of the section-contours are edges of D_0. Similarly, we assume that any two branching vertices that are consecutive along $\mathcal{B}_\mathcal{C}$ are joined by an edge in D_0.

Let us fix some notations for the simplices of D_0.

Grounded simplex is a simplex whose vertices all lie in a same cutting plane. We distinguish three types of grounded edges depending on the relative position of the edge with the corresponding section

1. **Contour-edge** A grounded edge which is an edge of the section-contour.
2. **Internal-edge** A grounded edge which lies inside the section (but not on its contour).
3. **External-edge** A grounded edge which lies outside the section.

We distinguish two types of grounded triangles :

1. **Internal-triangle** A grounded triangle which lies inside the section.
2. **External-triangle** A grounded triangle which lies outside the section.

Ground of an edge To each grounded edge e, we associate the two grounded triangles $t_r(e)$ and $t_l(e)$ that are incident to e. The ground of e is the intersection of $\{t_r(e),\ t_l(e)\}$ with the sections. For example, if e is a contour-edge then the ground of e contains a single triangle.

Ground of a section-vertex To each section-vertex v, we associate $G(v)$ the set of grounded triangles incident to v. The *ground* of v is the intersection of $G(v)$ with the section.

Types of tetrahedra The tetrahedra of D_0 are of four types, see Figure 3.3. A tetrahedron of the first type, T_{vf}, has a grounded face (triangle) on a cutting plane. The tetrahedra of type T_{ee} have two grounded edges on two different cutting planes. The tetrahedra of type T_{evv} have a single grounded edge and intersects two other cutting planes at a single vertex. The tetrahedra of type T_{vvvv} have a vertex on four different cutting planes.

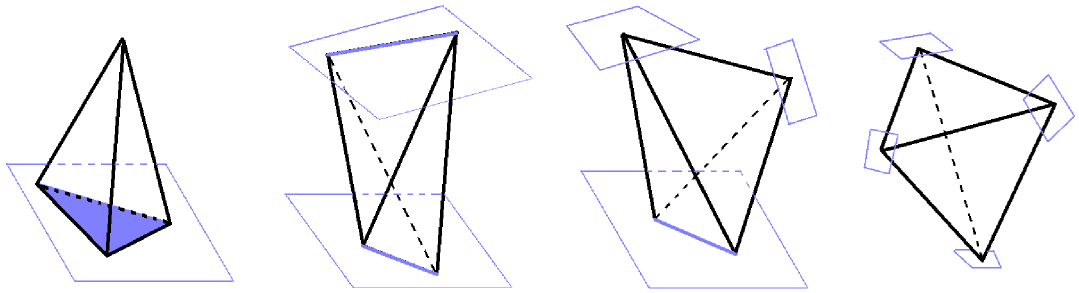

(a) T_{vf} (b) T_{ee} (c) T_{evv} (d) T_{vvvv}

Figure 3.3: Types of tetrahedra.

According to the Delaunay conformity condition, any grounded edge is either a contour-edge, an internal-edge, or an external-edge, and any grounded triangle is either internal or external.

Definition 47 (External Tetrahedron) A tetrahedron of D_0 with an external grounded edge or triangle will be called *external*, see Figure 3.2c.

2 Pruning of the Delaunay Complex

Figure 3.2b shows an example of the 3-dimensional Delaunay triangulation. We will prune the 3-dimensional Delaunay triangulation D_0, to obtain a complex which (i) conforms to the given sections and (ii) has no *singularities*, i.e., connections between sections along zero or one dimensional features. In the sequel, the latter condition is called the *solidity condition*. The pruning of D_0 is done in three steps. We call the resulting subcomplexes D_1, D_2 and D_3 respectively. D_1 is the maximal subset of D_0 that conforms to the given sections. D_1 may not satisfy the solidity condition and further tetrahedra have to be removed until the solidity condition is verified. This procedure is done in two steps : in Step 2, we compute the maximal set of tetrahedra of types T_{vf} and T_{ee} (each linking two cutting planes), which verifies the solidity condition, see Section 2. Then in Step 3, we add to D_2, as many tetrahedra of type T_{evv} and T_{vvvv} as possible while maintaining the solidity condition.

Step 1 : Removal of the external tetrahedra We remove from D_0 all the external tetrahedra. The resulting subcomplex of D_0 is noted D_1.

Step 2 : Solidity check around grounded edges Let us make precise the solidity condition in this context. For this, we need the following definitions.

Definition 48 (Shell of a grounded edge (section-vertex)) For $D' \subset D_0$, the shell of a grounded edge (section-vertex) e is defined as the tetrahedra of D' which contain e. In the sequel, we write $Sh_{D'}(e)$ for the shell of e in D'. When the context is unambiguous, we may occasionally drop D' and write $Sh(e)$.

Definition 49 (Face-to-face connectivity) Two tetrahedra T and T', are said to be face-to-face connected in D', if there exists a sequence of tetrahedra $T = T_0, \ldots, T_k = T'$ such that for all i, $T_i \in D'$, and T_{i-1} and T_i share a face.

Definition 50 (Solidity at a grounded edge (section-vertex)) D' is solid at a grounded edge or section-vertex e, if any tetrahedron in $Sh(e)$ is face-to-face connected (in D') to at least one tetrahedron containing a grounded triangle incident to e. Such a shell is called *solid*.

The goal of this step is to prune D_1 to obtain a solid complex, whose tetrahedra are all incident to a pair of cutting planes. To consider the connections between the pairs of planes, we remove the tetrahedra of type T_{evv} and T_{vvvv}. The goal is now to prune around the grounded edges. We prune the incident tetrahedra of a grounded edge until we obtain a solid shell. Figure 3.4*b* shows all the possible configurations of a solid shell, resulting from Step 2.

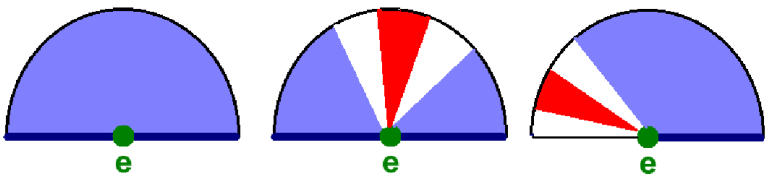

(a) Disconnected tetrahedra from the ground are colored in red. They form a singularity at e.

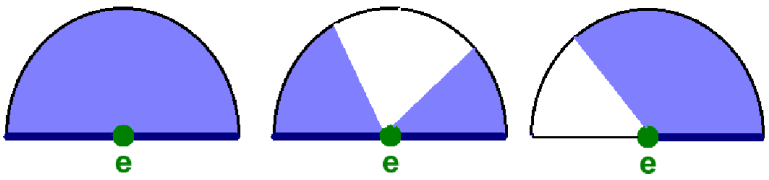

(b) Configurations of a solid shell.

Figure 3.4: A 2D view of the shell of a grounded edge e. e is perpendicular to the figure plane.

Shell Pruning Description Let T and T' be two tetrahedra incident to a grounded edge e. A *pivot* from T to T' around e is a sequence of face-to-face connected tetrahedra incident to e joining T to T', see Figure 3.5.

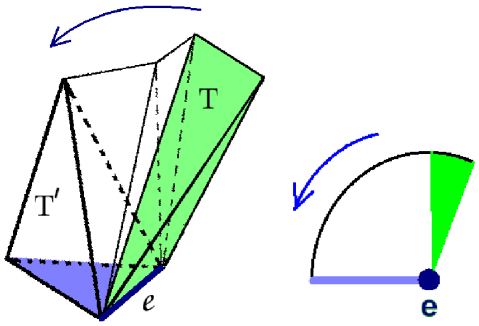

Figure 3.5: A pivot from T to T' around e, that contains four tetrahedra. A 2D view of these tetrahedra is shown on the right.

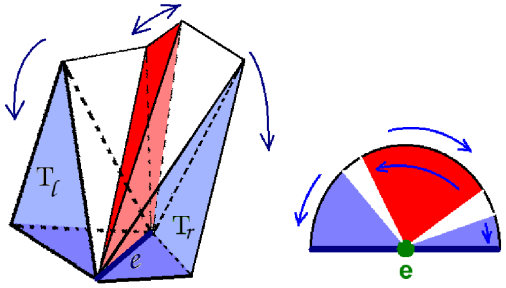

Figure 3.6: A disconnected tetrahedron from the ground of e is between two eliminated tetrahedra. A 2D view of $Sh(e)$ is shown on the right.

During the pruning process, a tetrahedron $t \in Sh(e)$ is disconnected from the ground of e if and only if it lies between two eliminated tetrahedra incident to e, see Figure 3.4*a*. We compute these tetrahedra as follows. For an eliminated tetrahedron $T \in Sh(e)$, we start pivoting at T around e until we find another eliminated tetrahedron or a T_{vf} tetrahedron incident to e, called T'. The pivot sequence consists of T_{ee} tetrahedra all sharing edge e. To any such T_{ee} tetrahedron, we can associate a direction corresponding to the direction of the pivot. In our algorithm, we store this orientation as an orientation on the other grounded edge of the tetrahedron (distinct from e).

We apply the same procedure to all the eliminated tetrahedra of $Sh(e)$. A T_{ee} tetrahedron incident to e is disconnected from the ground of e if it is visited twice with different directions, Figure 3.6. Note that if during a pivot we reach a tetrahedron already oriented with the same orientation as the pivot, we can stop the propagation.

We are now in a position to describe Step 2 of the algorithm :

1. We put all the eliminated tetrahedra in a list EL.
2. **While** $EL \neq \emptyset$ do
   (a) **For** a tetrahedron $T \in EL$ do
   (b) **For** any grounded edge e of T do
      - Start pivoting at T around e and orient the visited tetrahedra until an eliminated or T_{vf} tetrahedron is reached.
      - If a tetrahedron t receives two opposite orientations, mark t as eliminated and add it to EL.

   (c) Remove T from the list ($EL = EL \backslash T$).
3. Eliminate the face-to-face connected subsets of T_{vf} which share no face with the non-eliminated T_{ee} tetrahedra.
4. D_2 is the set of non-eliminated tetrahedra.

Complexity of Step 2 Let s be the total number of tetrahedra in D_0. We claim that Step 2 can be performed in $O(s)$ time. Indeed, a tetrahedron of type T_{ee} has at most two pivoting edges and can receive at most two (opposite) orientations for each edge before being eliminated.

Solidity of D_2 D_2 is a set of tetrahedra of type T_{vf} and T_{ee}, which satisfies the following properties.

Property 1 (Solidity at grounded edges) Let e be a grounded edge. Any tetrahedron $t \in Sh_{D_2}(e)$ is face-to-face connected (in D_2) to the ground of e.

Proof If t is a T_{vf} tetrahedron in D_2, it is not external and is itself in the ground of e. Let t be a T_{ee} tetrahedron disconnected from the ground of e. Hence, t is between two eliminated tetrahedra and has been visited with two opposite directions. Thus, t does not belong to D_2. □

Property 2 (Solidity at section-vertices) Let v be a section-vertex. Any tetrahedron $t \in Sh_{D_2}(v)$ is face-to-face connected (in D_2) to the ground of v.

Proof Let t be a T_{ee} tetrahedron in D_2 which passes through an incident grounded edge of v. Thus, t is face-to-face connected to the ground of e and in particular to the ground of v.

Let t be a T_{vf} tetrahedron in D_2, with v as the fourth vertex (not in the plane of the grounded triangle of t). According to the algorithm, t is in a connected set of T_{vf} tetrahedra (with v as the fourth vertex), which share a face with a T_{ee} tetrahedron in D_2. This T_{ee} tetrahedron is thus incident to a grounded edge e on the ground of v. Thus, t is face-to-face connected to the ground of e and in particular to the ground of v. □

Maximality of D_2 The following lemma shows that the order of elimination of the tetrahedra is not important.

Lemma 10 *Let D' be subset of D_0. If T is a tetrahedron that creates a singularity in D', then T creates a singularity in any subset of D' containing T.*

Proof If t is disconnected from the ground of one of its grounded edges e, in D', then it is also disconnected from this ground in any subset of D'. □

In Step 2, the algorithm eliminates all the tetrahedra which create a singularity. According to the previous lemma, the elimination of some tetrahedron does not make disappear any other singularity, and so the order of elimination is not important. However, this elimination may make appear some other singularities in the resulting subset. Then, the algorithm removes these new singularities and so on until obtaining some subset of D_1 without singularity. Note that the number of the tetrahedra is finite and this process finishes. As at each step the order of the elimination is not important the resulting subset is maximal.

Proposition 11 *D_2 is the maximal subset of T_{ee} and T_{vf} tetrahedra which has no singularity along the sections.*

Step 3 : Connecting more than two planes As said before, D_2 consists of Delaunay tetrahedra of type T_{ee} and T_{vf} exclusively. In this step, we add to D_2 as many tetrahedra of type T_{evv} and T_{vvvv} as possible provided that the only tetrahedra that can be added are those with exactly four, three or two faces in the current reconstruction. Clearly, as the intersection of such a tetrahedron with the current reconstruction is a topological disk or sphere, its insertion does not create singularities in the overall complex. Figure 3.7 provides some examples.

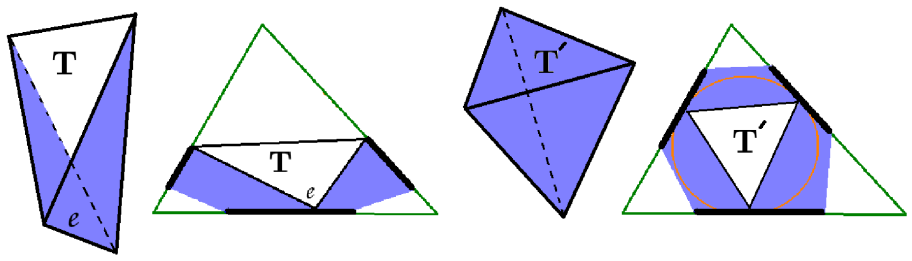

Figure 3.7: Step 3 examples : T and T' do not create singularity and can be added to the reconstruction. A 2D view is also given.

The algorithm maintains a list L of the tetrahedra of types T_{vvvv} and T_{evv} with such an intersection with the current reconstructed object. As long as this list is not empty, we add its first element to the current reconstructed object and update L. We call D_3 the

resulting complex which is , by construction, solid at any section-point and any grounded edge.

D_3 constitutes the reconstructed object (portion) $\mathcal{R}''_{\mathcal{C}}$, corresponding to the cell of the arrangement $\mathcal{C}$. The overall reconstructed object is the union of these portions for all the cells of the arrangement.

Complexity Analysis Let k be the number of cutting planes and n the total number of vertices, including the vertices of the section contours and the points on the branching diagram. In the previous chapter, we showed that the sections of the cells of the arrangement and the branching diagrams can be computed in $k.O(n^2)$ time.

Let C_i be a cell in the arrangement of the cutting planes. We write n_i for the number of points in C_i. Assuming that the cutting planes are in general position, each point is on the boundary of $O(1)$ cells, and we have $\sum_i n_i = O(n)$. We need to compute the 3D Delaunay tetrahedrization of the points in C_i. Although the complexity of computing the 3D Delaunay tetrahedrization of points in $\mathbb{R}^3$ may be quadratic in the worst case, Attali and Boissonnat showed in [AB04] that it is only linear when the points are distributed on the planar facets of a polyhedral cell in $\mathbb{R}^3$. According to this result, the Delaunay tetrahedrization of the points in C_i can be computed in $O(n_i^2)$ time. Once the Delaunay tetrahedrization is computed, we eliminate the external tetrahedra. In this step, we have to visit each tetrahedron to decide if it is inside or outside the section-contours. Since the size of the 3D Delaunay triangulation is quadratic in the number of points, Steps 2 and 3 can be done in $O(n_i^2)$ time for the cell C_i. Thus, the overall complexity of the algorithm in time is at most $k.O(n^2) + \sum_{C_i} O(n_i^2) \leq k.O(n^2)$, and for $k = O(1)$, the complexity is $O(n^2)$.

Properties of the Reconstruction

Generality There is no assumption on the position and orientation of the cutting planes neither on the geometry and topology of the sections. Complex section-contours with multiple branching and holes can be handled, see Section 3 for some experimental examples.

Solidity and Topological Correctness By the shell pruning step we removed all the singularities in the sections. Therefore, the reconstructed object $\mathcal{R}''_{\mathcal{C}}$ in each cell $\mathcal{C}$ of the arrangement has no singularity. As said before, the boundary of the $\mathcal{R}''_{\mathcal{C}}$ contains the section-contours, the branching diagram, and some flat regions. When we glue the various $\mathcal{R}''_{\mathcal{C}}$ together, some singularity may appear on the boundary.

Consider a face f of the arrangement and the two incident cells $\mathcal{C}$ and $\mathcal{C}'$. If the branching diagrams of $\mathcal{C}$ and $\mathcal{C}'$ intersect in f then the intersection points are singular, see the singularity at point b in Figure 3.8a. In general position, the intersection points of the branching diagrams are isolated. The overall object is therefore locally a manifold except at some isolated points. Note that this problem can be handled by displacing the branching points slightly *inside* the corresponding cells, or by thickening the cutting planes, Figure 3.8b.

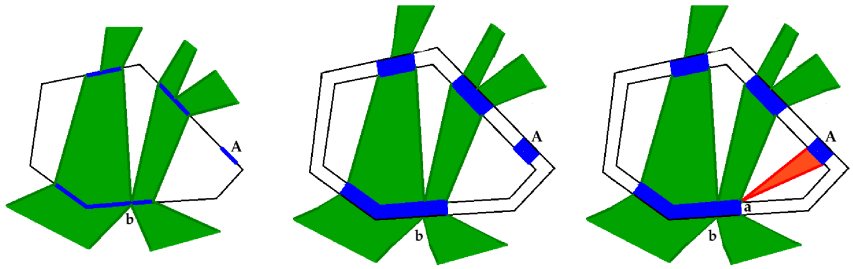

(a) (b) (c)

Figure 3.8: (a) A singularity at point b which is on the intersection of the two branching diagrams, corresponding to the two adjacent cells. (b) This singularity disappears after thickening the cutting planes.(c) The flat region A is also thickened by this procedure. However, this thickening procedure does not make disappear the singularity at a.

Conformity With the Given Sections By definition, the reconstructed object does not intersect the cutting planes outside the given sections. Conversely, it should be observed that $\mathcal{R}''_{\mathcal{C}}$ does not necessarily contain all the grounded triangles of the sections. This particular situation occurs when a region of a section is flat in the two adjacent reconstructed portions corresponding to the two cells. According to the presented topological guarantees, this only happens when the set of cutting planes is very sparse, Figure 3.10.

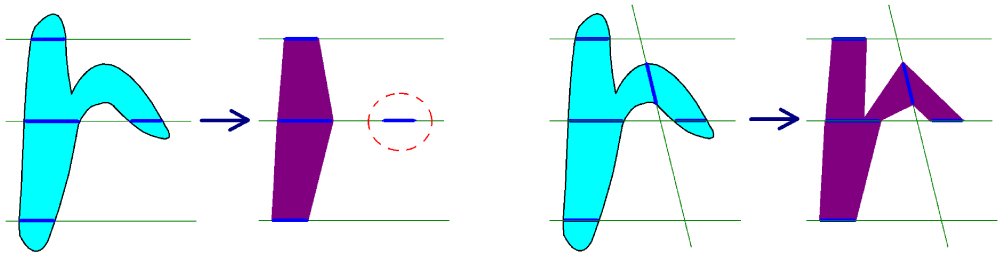

Figure 3.9: A sufficiently dense sampling (right) of the cutting planes can guarantee that there is no isolated portion (left) of sections in the overall reconstruction.

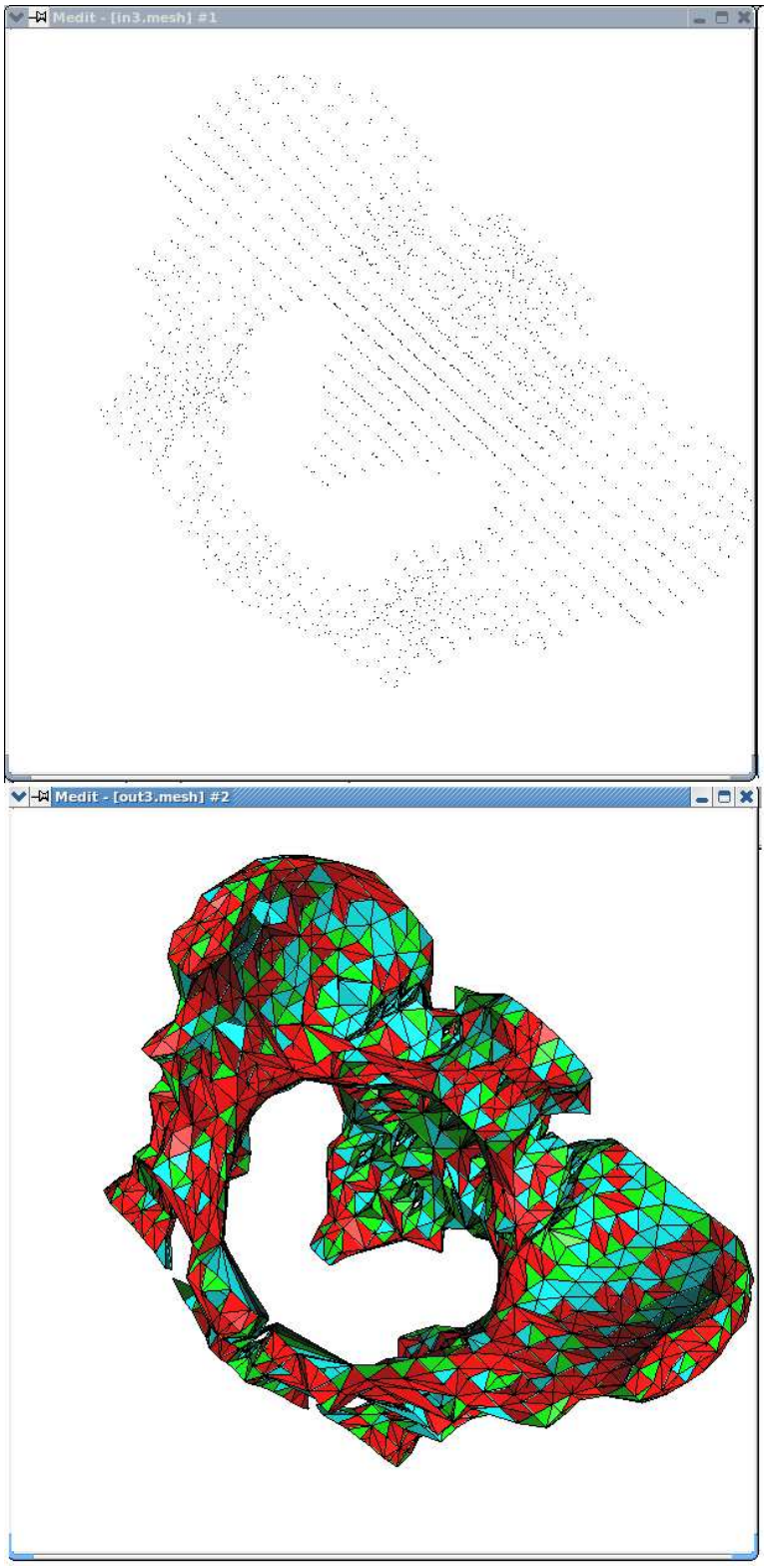

Figure 3.10: A reconstruction example: different colors correspond to different types of tetrahedra. We use Medit [Med] to visualize the input points and the output mesh.

3 Experimental Results

A preliminary version of the algorithm has been implemented in C++, using the CGAL library [CGA]. The *input* of the algorithm consists of a cell of the arrangement (a convex polyhedron), and a set of polygonal contours lying on the boundary of this polyhedron. The contours are assumed to be Delaunay-conform and non self-intersecting, some possibly lying inside others. The contours are oriented in such a way that the interior of the section they bound is on the righthand side.

We present the results of the algorithm applied to a variety of input models. To gain more intuition, in addition to the 3D results, some figures of 2D reconstructions are also given. Figure 3.11 illustrates the reconstruction of a sphere cut by the faces of a cube. In this case, the reconstructed object is the convex hull of the contours.

Figures 3.13 and 3.12 show how the method eliminates successfully the singularities of

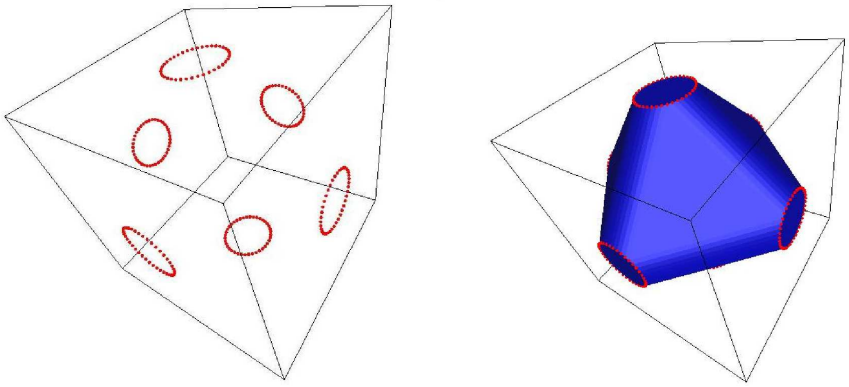

(a) Input points. (b) The reconstructed object.

Figure 3.11: The reconstructed object corresponding to a sphere, cut by the faces of a cube.

the Delaunay triangulation to guarantee the topological correctness of the reconstructed object.

Some examples of branching between the sections are presented in Figures 3.14 and 3.15. These examples illustrate perfectly the role of the points added on the branching diagram, to obtain an identified branching locus of the object. As we can see in Figure 3.14(a), the branching diagram corresponds to the projection of the external medial axis of the sections. In the non-parallel case of planes, the branching is handled as well as the parallel case, see Figure 3.15.

The algorithm handles the complex branching of non-convex sections possibly with holes. The last figures provide some examples of these complex cases.

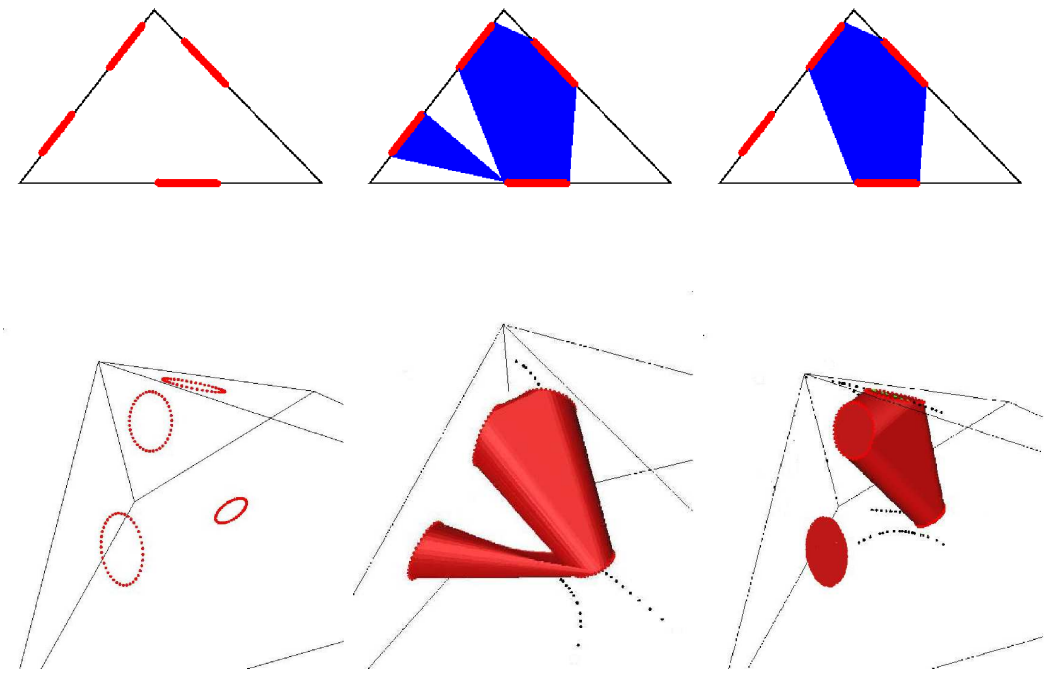

(d) Input points. (e) Delaunay simplices of input points. (f) Reconstructed object

Figure 3.12: Elimination of a singularity during the reconstruction. A single contour disappears in the reconstructed object.

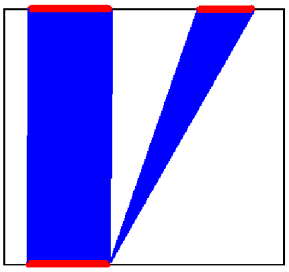

(a) 2D view of Delaunay simplices of sections.

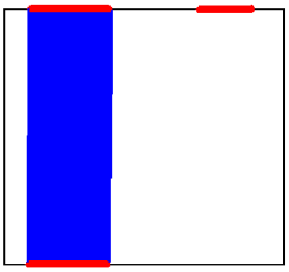

(b) 2D view of reconstructed object.

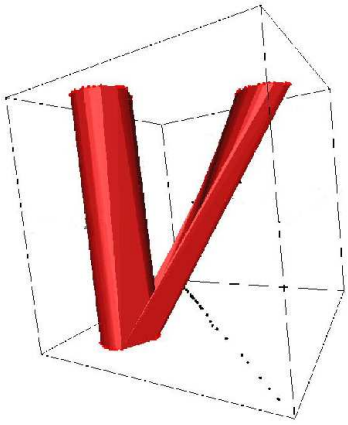

(c) Delaunay simplices of input points.

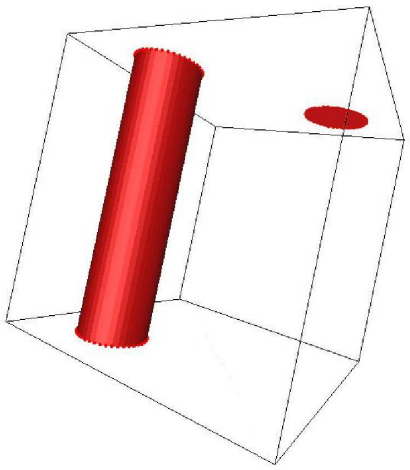

(d) Reconstructed object

Figure 3.13: Elimination of the singularities during the reconstruction.

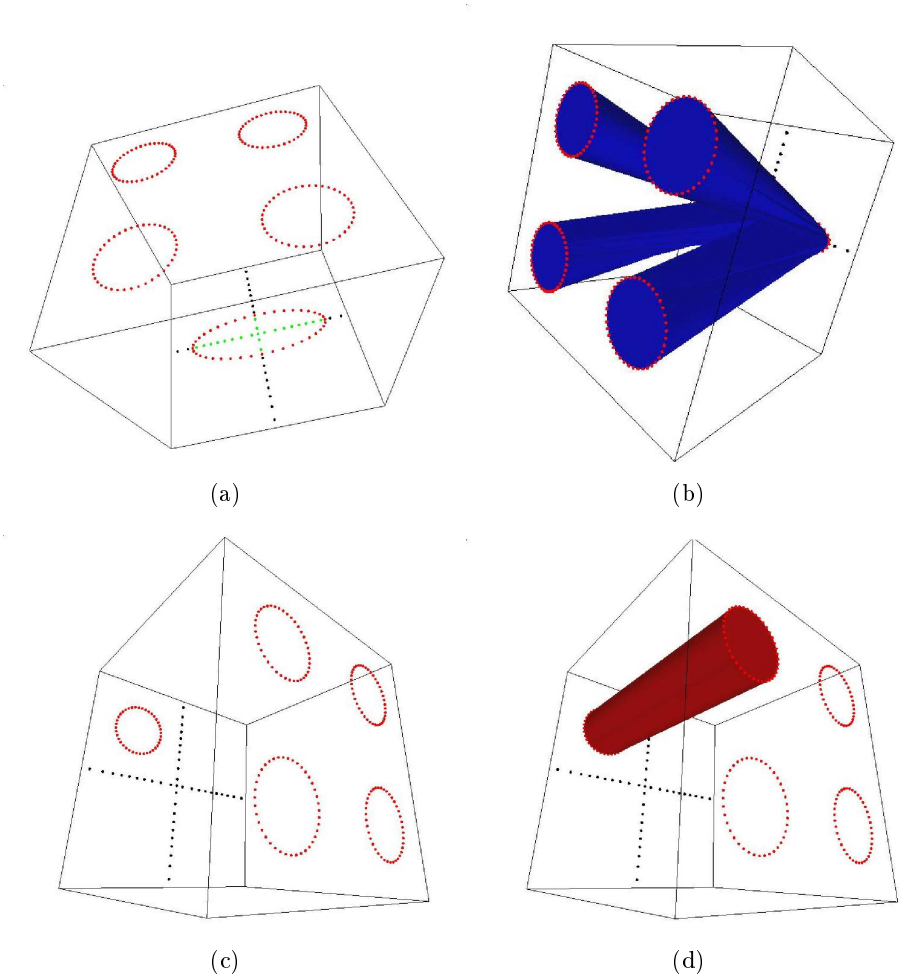

Figure 3.14: (a) The single circle is at the same distance from all the other circles (b) There is a multiple branching between these four circles without any singularity. (c) As the circle is shifted, there is no branching anymore in the reconstructed object (d).

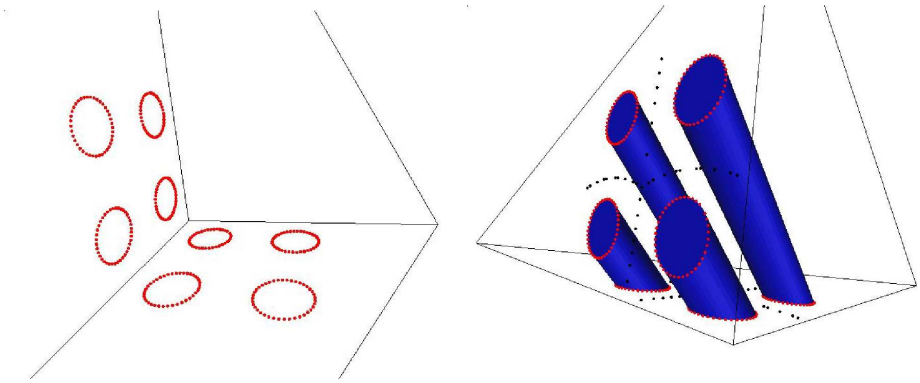

(a) Input points. (b) Reconstructed object

Figure 3.15: An example with two non-parallel cutting planes.

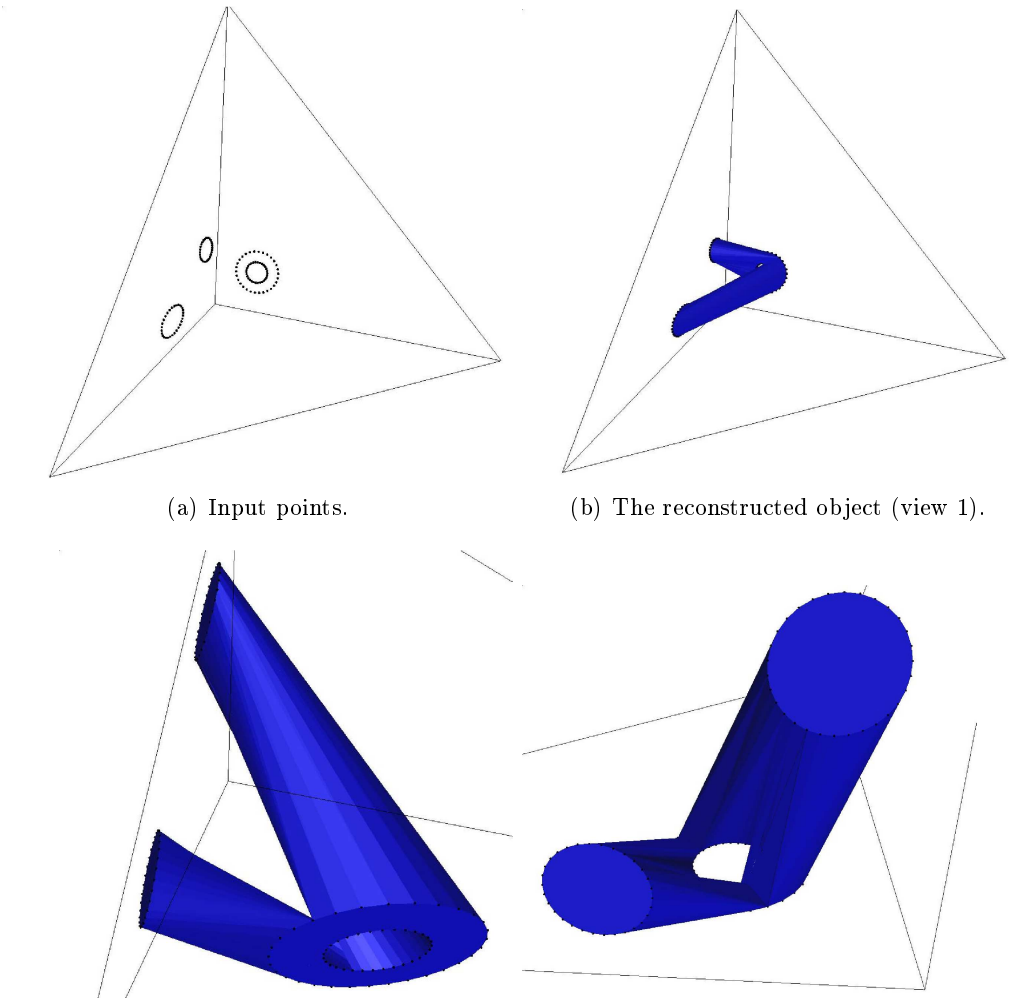

(a) Input points.

(b) The reconstructed object (view 1).

(c) The reconstructed object (view 2).

(d) The reconstructed object (view 3).

Figure 3.16: A complex branching of a section with a hole.

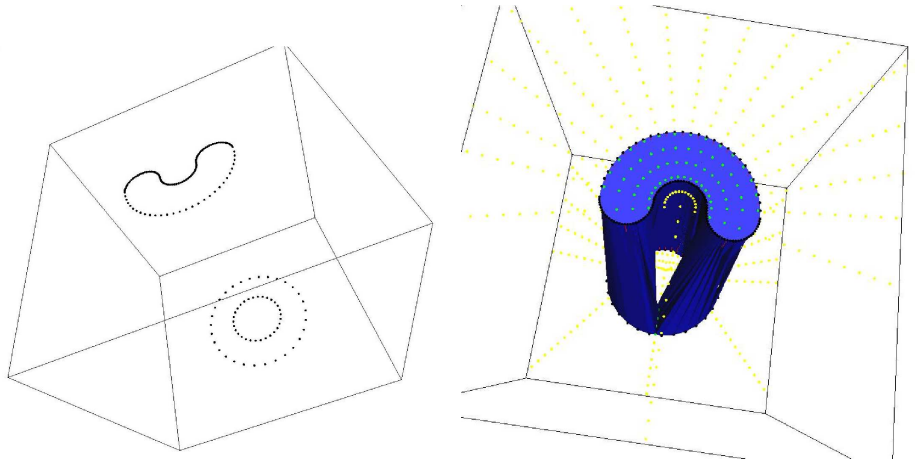

(a) Input points. (b) The reconstructed object.

Figure 3.17: A result for non-convex sections. There is no singularity in the reconstructed object.

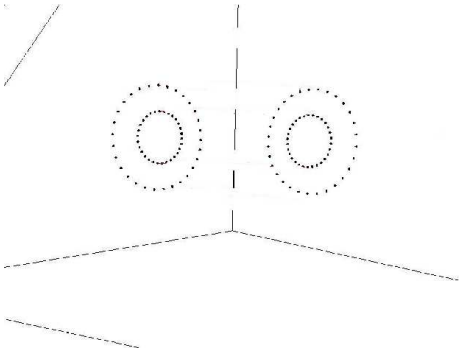

(a) Input points.

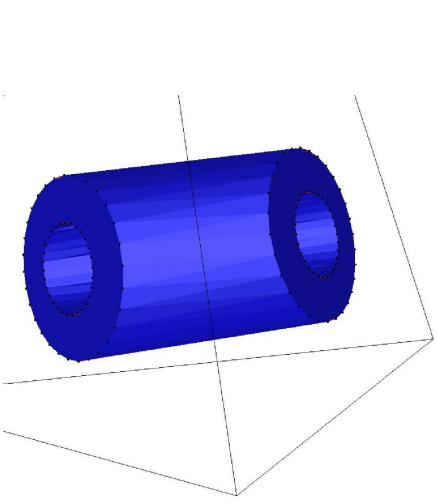

(b) Output (view 1).

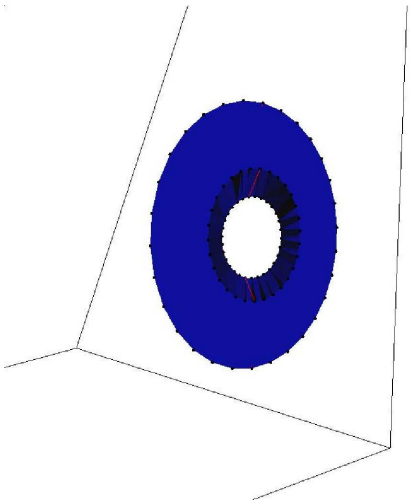

(c) Output (view 2).

Figure 3.18: An example with nested section-contours.

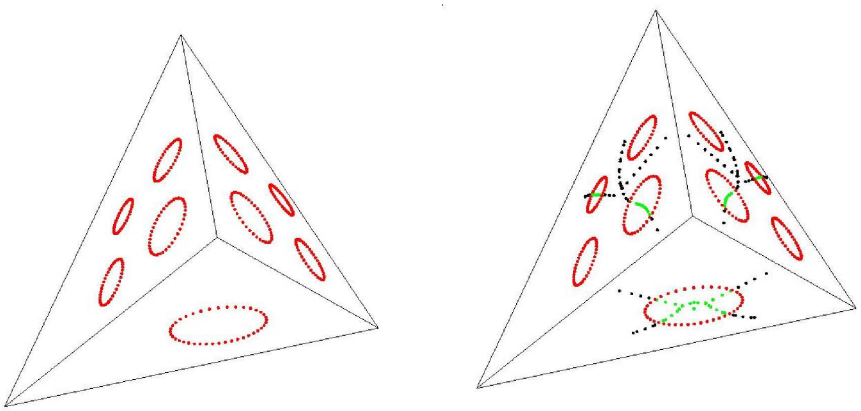

(a) (b)

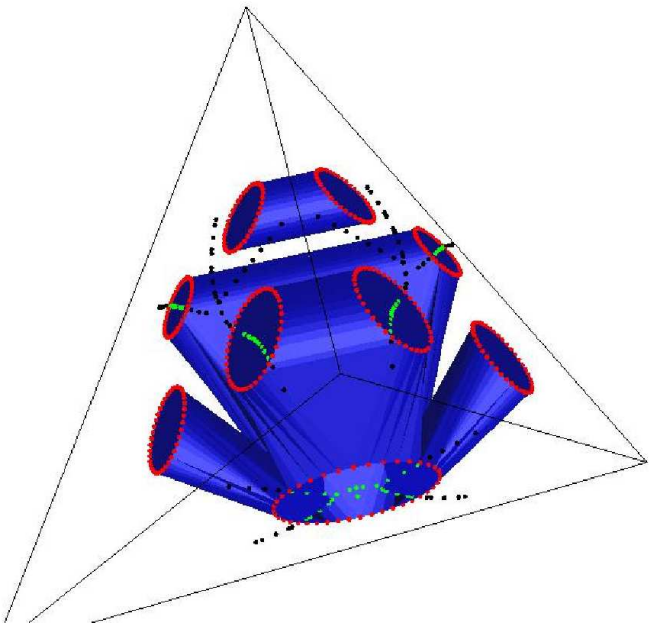

(c)

Figure 3.19: Multiple branching between the sections:(a) Input points. (b) Input points in red and the added branching points in green. (c) Reconstructed object

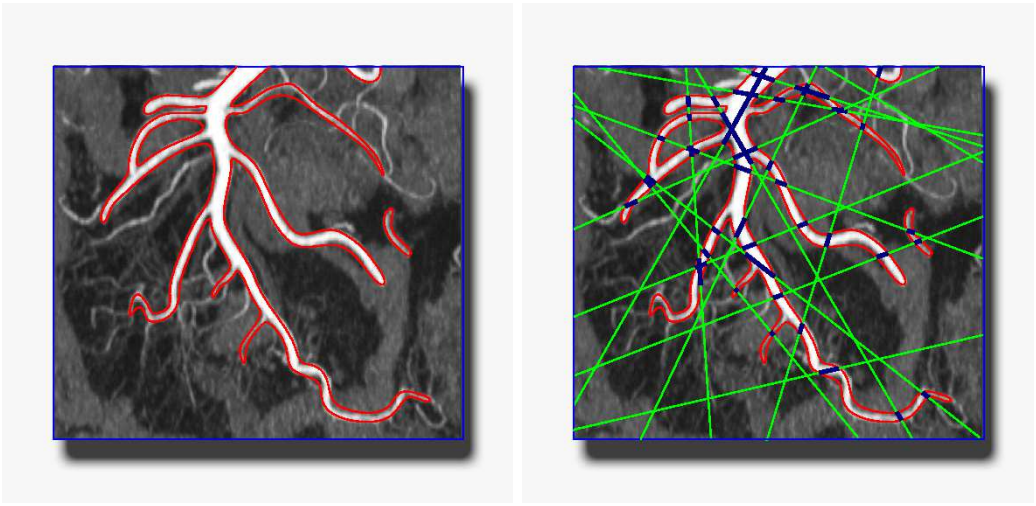

(a) Original Object

(b) Data Acquisition

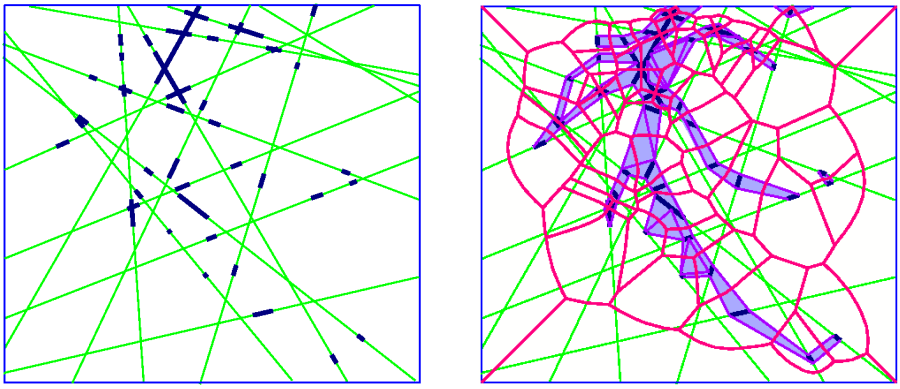

(c) Input of the Algorithm

(d) Algorithm based on the Voronoi Diagram of the Sections

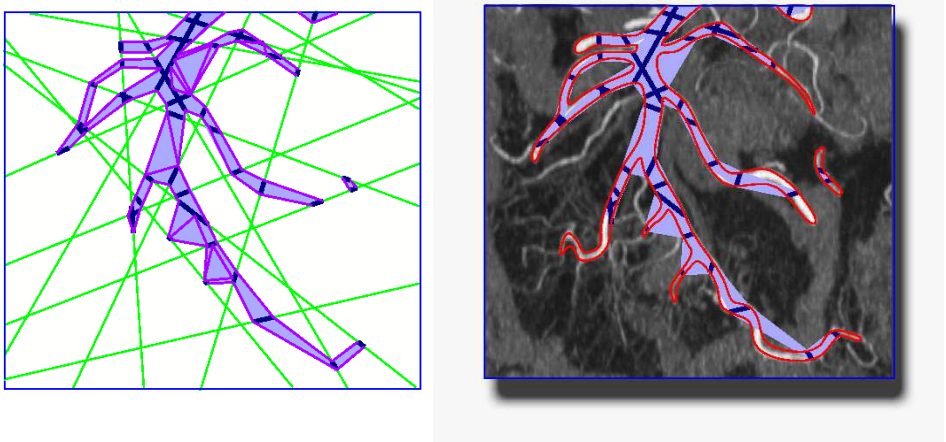

(e) Output of the Algorithm

(f) Superposition of the original object and its approximation

Figure 3.20: 2D Reconstruction Example

Conclusion and Future Work

In this thesis, we made the first geometric analysis of the reliability and validity of reconstruction methods from cross-sectional data. In the first chapter, we studied the most natural way to connect the sections, which is a generalization of the classical overlapping criterion between the orthogonal projections of the sections for the case of parallel cutting planes. We provided two sampling conditions for the set of cutting planes, called the Separation and the Intersection Conditions, under which the reconstructed object is isotopic to the original unknown object. In the second chapter, motivated by reconstructing tree-like structures from sectional data, we presented a reconstruction method, based on the Voronoi diagram of the sections, which is well suited for connecting sparse set of sections distributed over a large volume. According to the presented sampling conditions, as far as the cutting planes are sufficiently transversal to the boundary of the original shape, the method preserves the homotopy type of the original unknown shape. The Voronoi-Delaunay duality links this method to a Delaunay based method which is presented in the third chapter. According to our preliminary experimental results, the third method can handle complex cross-sectional branching situations such as the coronary arterial tree.

From Geometry to Medical Imaging : The reconstruction problem from cross-sections is particularly motivated by medical imaging technology where organs need to be simulated from a set of sectional data obtained by CT, MRI or other scanning devices. The hope is that this thesis will be a first step to provide solid foundations for medical diagnostic software and to help remedy this lack of research examining the quality of simulations with respect to the original shape (organ). Of course, further research and investment is needed to apply these theoretical guidelines in developments of medical imaging softwares in practice.

According to the theoretical analysis presented in this thesis, the *transversality* of the cutting planes to the boundary (surface) of the shape (organ) leads to a better resulting reconstruction. Interestingly, the transversality of the cutting planes is also crucial in practice for the data acquisition by ultrasound devices. Indeed, from a technical point of view if a *cut* is not *sufficiently* transversal to the organ, the quality of the resulting 2D ultrasonic image is not acceptable for diagnosis. Using such theoretical properties may allow us to define a pertinent guideline for radiologists in order to improve the quality of simulations. Perhaps, for instance, such an alternative interactive method may be a more appropriate method of examining the obtained theoretical criteria in practice.

Another extension that needs further investment is the case of multilabel sections, i.e., multiple materials. The two first methods presented in this thesis are easily extendable to this case. And the provided topological guarantees remain valid for the case of multiple materials. However, the Delaunay-based method dual to the second method needs more care to be generalized. The generalization should be consistent in the sense that the endpoints of each Delaunay simplex should be of the same label (material). A natural idea would be to compute the connectivity between the sections by the second method, and then interpolate the corresponding sections using the Delaunay triangulation of each material independently. Let us note that Barequet and Vaxman's work [BV09], that makes use of straight skeletons of polyhedra, is the most recent work that can handle the case of multilabel sections.

Noisy Data : We consider a noise-free model, where every point of the sample of the section-contours lies precisely on the boundary of the original shape, and the given sections conform along the intersection of the cutting planes. Due to data acquisition error, such a free-noise model is not pertinent in practice. Two different frameworks may be considered. 1) Given a set of noisy images, each noisy image should be segmented in order to extract the corresponding section-contours. Classical image segmentation methods, that make use of level-set methods introduced by Osher and Sethian in [OS88] or active contour models (Snakes) introduced in [KWT88] may be applied. One can also use wavelet based methods, such as [Shi05] which is specifically developed for extracting contours from an image. 2) The second framework corresponds to the case where we are given a noisy sample of sections-contours rather than the images. Reconstruction from a noisy set of sample points has been studied by different authors, such as in [CL05] and [DG06]. A nice extension of our work would be to adapt these ideas to the case of sectional data.

Higher Dimensions : We can consider higher dimensional variants of this reconstruction problem. Where the goal is to reconstruct an n-dimensional shape from its $(n-1)$-dimensional intersections with hyperplanes. The method [LBD$^+$08] studied in the first chapter, seems to be the most natural way to tackle this high dimensional reconstruction problem.

In the first chapter, we presented topological guarantees for the three-dimensional problem and proved the homotopy equivalence between the original shape $\mathcal{O}_\mathcal{C}$ and the reconstructed object $\mathcal{R}_\mathcal{C}$. Similar analysis can be carried out for the resulting n-dimensional reconstruction: The Separation Condition can be defined in any dimension. Under this condition, the guarantees on the connectivity between the sections remain valid. The proof is straightforward. In dimension 3, using the lift function, we proved that under the Separation Condition, there is a function between $\mathcal{O}_\mathcal{C}$ and $\mathcal{R}_\mathcal{C}$ that induces injective morphisms between the homotopy groups of $\mathcal{O}_\mathcal{C}$ and $\mathcal{R}_\mathcal{C}$. Moreover, we showed that under the Separation Condition, all the i-dimensional homotopy groups of $\mathcal{O}_\mathcal{C}$ and $\mathcal{R}_\mathcal{C}$ for $i \geq 2$ are trivial. Using that, it was sufficient to have the surjectivity of the function for the fundamental groups : $\pi_1(\mathcal{O}_\mathcal{C}) \to \pi_1(\mathcal{R}_\mathcal{C})$. This is verified under the second sampling condition, called Intersection Condition. This led to a homotopy equivalence between $\mathcal{O}_\mathcal{C}$ and $\mathcal{R}_\mathcal{C}$ under the Separation and the Intersection Conditions.

For the corresponding reconstruction problem in higher dimensions, the injectivity of the function on the level of homotopy groups remains valid. However, the vanishing results on higher homotopy groups of $\mathcal{O}_\mathcal{C}$ and $\mathcal{R}_\mathcal{C}$ are only valid in dimensions two and three. A new sampling condition is needed to impose these vanishing results or a different strategy should be performed to prove the surjectivity of the function for homotopy groups of any dimension. If this surjectivity is imposed under some sampling conditions on the cutting planes, there is a homotopy equivalence between $\mathcal{O}_\mathcal{C}$ and $\mathcal{R}_\mathcal{C}$.

Considering *time* as the fourth dimension, the four dimensional version of this problem corresponds to reconstructing a *moving shape* (for example the beating heart). In the sense that the movement of the object can be reconstructed knowing the position of the object at some constant values of time. This is one of the motivations to perform further research on higher dimensional variants of reconstruction from cross-sections.

3D Reconstruction from 1-Sections : Another possible variant of this reconstruction problem corresponds to reconstructing a 3D shape from its intersections with a set of lines, i.e., one dimensional sections. This problem is motivated by measurement of volume and surface area of an object from a one dimensional sampling (see [KJ01]). The hope is that a framework similar to the one presented in this thesis provides a good strategy for this variant of the problem, where the *influence zone* of each 1-dimensional section is its Voronoi cell with respect to the other sections.

Bibliography

[AB99] N. Amenta and M. Bern. Surface reconstruction by Voronoi filtering. *Discrete and Computational Geometry*, 22(4):481–504, 1999.

[AB04] D. Attali and J.D. Boissonnat. A linear bound on the complexity of the Delaunay triangulation of points on polyhedral surfaces. *Discrete and Computational Geometry*, 31(3):369–384, 2004.

[ABM09] O. Amini, J-D. Boissonnat, and P. Memari. Geometric Tomography with Topological Guarantees. *INRIA Report 7147*, 2009. To appear in the proceedings of the 26th Symposium on Computational Geometry 2010.

[AEIR03] L. Antiga, B. Ene-Iordache, and A. Remuzzi. Computational geometry for patient-specific reconstruction and meshing of blood vessels from MR and CT angiography. *IEEE transactions on medical imaging*, 22(5):674–684, 2003.

[Bat71] J.L. Batude. Singularité générique des applications différentiables de la 2-sphère dans une 3-variété différentiable. In *Annales de l'institut Fourier*, volume 21, pages 155–172, 1971.

[BCDT96] J.D. Boissonnat, A. Cerezo, O. Devillers, and M. Teillaud. Output sensitive construction of the Delaunay triangulation of points lying in two planes. *International Journal of Computational Geometry and Applications*, 6(1):1–14, 1996.

[BCL96] C.L. Bajaj, E.J. Coyle, and K.N. Lin. Arbitrary topology shape reconstruction from planar cross sections. *Graphical Models and Image Processing*, 58:524–543, 1996.

[BG93] J.D. Boissonnat and B. Geiger. Three dimensional reconstruction of complex shapes based on the delaunay triangulation. *Biomedical Image Processing and Visualization*, page 964, 1993.

[BGLSS04] G. Barequet, M.T. Goodrich, A. Levi-Steiner, and D. Steiner. Contour interpolation by straight skeletons. *Graphical Models*, 66:245–260, 2004.

[BK03] J.D. Boissonnat and M.I. Karavelas. On the combinatorial complexity of Euclidean Voronoi cells and convex hulls of d-dimensional spheres. In *Proceedings of the fourteenth annual ACM-SIAM symposium on Discrete algorithms*,

pages 305–312. Society for Industrial and Applied Mathematics Philadelphia, PA, USA, 2003.

[BM07] J.D. Boissonnat and P. Memari. Shape reconstruction from unorganized cross sections. *Symposium on Geometry Processing*, pages 89–98, 2007.

[BO05] J.D. Boissonnat and S. Oudot. Provably good sampling and meshing of surfaces. *Graphical Models*, 67(5):405–451, 2005.

[Boi88] J.D. Boissonnat. Shape reconstruction from planar cross sections. *Computer Vision, Graphics, and Image Processing*, 44(1):1–29, 1988.

[Bra05] I. Braude. *Smooth 3D Surface Reconstruction from Contours of Biological Data with MPU Implicits*. PhD thesis, Drexel University, 2005.

[BS96] G. Barequet and M. Sharir. Piecewise-linear interpolation between polygonal slices. *Computer Vision and Image Understanding*, 63:251–272, 1996.

[BV09] G. Barequet and A. Vaxman. Reconstruction of multi-label domains from partial planar cross-sections. *Symposium on Geometry Processing*, 2009.

[CCS05] F. Chazal and D. Cohen-Steiner. A condition for isotopic approximation. *Graphical Models*, 67(5):390–404, 2005.

[CD99] S.W. Cheng and T.K. Dey. Improved constructions of Delaunay based contour surfaces. In *Proceedings of the fifth ACM symposium on Solid modeling and applications*, pages 322–323. ACM New York, 1999.

[CGA] CGAL, Computational Geometry Algorithms Library. http://www.cgal.org.

[CGY04] F. Cazals, J. Giesen, and M. Yvinec. Delaunay triangulation based surface reconstruction: a short survey. 2004.

[CL05] F. Chazal and A. Lieutier. Weak feature size and persistent homology: computing homology of solids in R n from noisy data samples. In *Proceedings of the twenty-first annual symposium on Computational geometry*, page 262. ACM, 2005.

[CM03] Z. Chen and S. Molloi. Automatic 3D vascular tree construction in CT angiography. *Computerized Medical Imaging and Graphics*, 27(6):469–479, 2003.

[COL96] D. Cohen-Or and D. Levin. Guided Multi-Dimensional Reconstruction from Cross-Sections. *Series in approximations and decompositions*, 8:47–56, 1996.

[CP94] Y.K. Choi and K.H. Park. A heuristic triangulation algorithm for multiple planar contours using an extended double branching procedure. *The Visual Computer*, 10(7):372–387, 1994.

[CP01] G. Cong and B. Parvin. Robust and efficient surface reconstruction from contours. *The Visual Computer*, 17(4):199–208, 2001.

[CS78] HN Christiansen and TW Sederberg. Conversion of complex contour line definitions into polygonal element mosaics. In *Proceedings of the 5th annual conference on Computer graphics and interactive techniques*, pages 187–192. ACM New York, 1978.

[CS01] N. Coll and J.A. Sellares. Planar shape reconstruction from random sections. In *17th European Workshop on Computational Geometry*, pages 121–124, 2001.

[Da02] T. K. Frank Da. *L'interpolation de formes.* PhD thesis, INRIA Sophia-Antipolis, 2002.

[Del03] C. Delage. Diagrammes de Mobius en dimension 2. 2003. Master Thesis.

[Del07] C. Delage. CGAL-based first prototype implementation of moebius diagram in 2d, 2007.

[Dey07] T.K. Dey. *Curve and surface reconstruction: algorithms with mathematical analysis.* Cambridge Univ Pr, 2007.

[DG06] T.K. Dey and S. Goswami. Provable surface reconstruction from noisy samples. *Computational Geometry: Theory and Applications*, 35(1-2):124–141, 2006.

[DP97] C.R. Dance and R.W. Prager. Delaunay Reconstruction from Multiaxial Planar Cross-Sections. 1997.

[DVA+96] H.A. Drury, D.C. Van Essen, C.H. Anderson, C.W. Lee, T.A. Coogan, and J.W. Lewis. Computerized mappings of the cerebral cortex: a multiresolution flattening method and a surface-based coordinate system. *Journal of cognitive neuroscience*, 8(1):1–28, 1996.

[Ede87] H. Edelsbrunner. *Algorithms in combinatorial geometry.* Springer, 1987.

[EPO91] AB Ekoule, FC Peyrin, and CL Odet. A triangulation algorithm from arbitrary shaped multiple planar contours. *ACM Transactions on Graphics (TOG)*, 10(2):182–199, 1991.

[ES97] H. Edelsbrunner and N. Shah. Triangulating topological spaces. Intl. *Journal of Comput. Geom. and Appl*, 7:365–378, 1997.

[ET93] H. Edelsbrunner and T.S. Tan. An upper bound for conforming Delaunay triangulations. *Discrete and Computational Geometry*, 10(1):197–213, 1993.

[Fed59a] H. Federer. Curvature measures. *Transactions of the American Mathematical Society*, pages 418–491, 1959.

[Fed59b] H. Federer. Curvature measures. *Transactions of the American Mathematical Society*, pages 418–491, 1959.

[FKU77] H. Fuchs, ZM Kedem, and SP Uselton. Optimal surface reconstruction from planar contours. *Communications*, 1977.

[GD82] S. Ganapathy and TG Dennehy. A new general triangulation method for planar contours. *ACM Siggraph Computer Graphics*, 16(3):69–75, 1982.

[Gei93] B. Geiger. *Construction et utilisation des modèles d'organes en vue de l'assistance au diagnostic et aux interventions chirurgicales.* PhD thesis, INRIA, 1993.

[GGK06] NC Gabrielides, AI Ginnis, and PD Kaklis. Constructing smooth branching surfaces from cross sections. In *Proceedings of the ACM symposium on Solid and physical modeling*, pages 161–170. ACM New York, 2006.

[Hat02] A. Hatcher. *Algebraic topology.* Cambridge University Press, 2002.

[HDM+96] SW Hughes, TJ D'Arcy, DJ Maxwell, W. Chiu, A. Milner, JE Saunders, and RJ Sheppard. Volume estimation from multiplanar 2D ultrasound images using a remote electromagnetic position and orientation sensor. *Ultrasound in medicine & biology*, 22(5):561, 1996.

[HJT95] M.H. Herbert, C.B. Jones, and D.S. Tudhope. Three-dimensional reconstruction of geoscientific objects from serial sections. *The Visual Computer*, 11(7):343–359, 1995.

[HMR93] WE Higgins, C. Morice, and EL Ritman. Shape-based interpolation of tree-like structures in three-dimensional images. *IEEE transactions on medical imaging*, 12(3):439, 1993.

[HSD+04] J. Huisken, J. Swoger, F. Del Bene, J. Wittbrodt, and E.H.K. Stelzer. Optical sectioning deep inside live embryos by selective plane illumination microscopy. *Science*, 305(5686):1007, 2004.

[HSS03] K. Hormann, S. Spinello, and P. Schroder. C1-continuous terrain reconstruction from sparse contours. *Proc. Vision, Modeling, and Visualization, T. Ertl, B. Girod, G. Greiner, H. Niemann, H.-P. Seidel, E. Steinbach, and R. Westermann, eds*, pages 289–297, 2003.

[IM06] T. Ido and Y. Murai. A recursive interpolation algorithm for particle tracking velocimetry. *Flow Measurement and Instrumentation*, 17(5):267–275, 2006.

[JWC+05] T. Ju, J. Warren, J. Carson, G. Eichele, C. Thaller, W. Chiu, M. Bello, and I. Kakadiaris. Building 3D surface networks from 2D curve networks with application to anatomical modeling. *The Visual Computer*, 21(8):764–773, 2005.

[Kep75] E. Keppel. Approximating complex surfaces by triangulation of contour lines. *IBM Journal of Research and Development*, 19(1):2–11, 1975.

[KJ01] L. Kubinova and J. Janácek. Confocal microscopy and stereology: estimating volume, number, surface area and length by virtual test probes applied to three-dimensional images. *Microscopy Research and Technique*, 53(6):425–435, 2001.

[KMA+07] A. Kurjak, B. Miskovic, W. Andonotopo, M. Stanojevic, G. Azumendi, and H. Vrcic. How useful is 3D and 4D ultrasound in perinatal medicine? *Journal of perinatal medicine*, 35(1):10–27, 2007.

[KWT88] M. Kass, A. Witkin, and D. Terzopoulos. Snakes: Active contour models. *International journal of computer vision*, 1(4):321–331, 1988.

[LBD+08] L. Liu, C.L. Bajaj, J.O. Deasy, D.A. Low, and T. Ju. Surface reconstruction from non-parallel curve networks. *Computer Graphics Forum*, 27:155–163, 2008.

[LC87] W.E. Lorensen and H.E. Cline. Marching cubes: A high resolution 3D surface construction algorithm. In *Proceedings of the 14th annual conference on Computer graphics and interactive techniques*, page 169. ACM, 1987.

[Lie04] A. Lieutier. Any open bounded subset of R n has the same homotopy type as its medial axis. *Computer-Aided Design*, 36(11):1029–1046, 2004.

[Mat03] S.V. Matveev. *Algorithmic topology and classification of 3-manifolds*. Springer, 2003.

[May03] JP May. Finite spaces and simplicial complexes. *Notes for REU*, 2003.

[MB08] P. Memari and J.D. Boissonnat. Provably good 2d shape reconstruction from unorganized cross sections. *Computer Graphics Forum*, 27(5):1403–1410, 2008.

[MBMB06] J. Marker, I. Braude, K. Museth, and D. Breen. Contour-based surface reconstruction using implicit curve fitting, and distance field filtering and interpolation. In *Proc. International Workshop on Volume Graphics*, pages 95–102, 2006.

[Med] MEDIT, opengl-based scientific visualization software. http://www.ann.jussieu.fr/ frey/software.html.

[Mey94] D. Meyers. *Reconstruction of Surfaces From Planar Contours*. PhD thesis, University of Washington, 1994.

[MLB05] W. Marande, J. Lukes, and G. Burger. Unique mitochondrial genome structure in diplonemids, the sister group of kinetoplastids. *Eukaryotic Cell*, 4(6):1137, 2005.

[MLP88] M. Marko, A. Leith, and D. Parsons. Three-dimensional reconstruction of cells from serial sections and whole-cell mounts using multilevel contouring of stereo micrographs. *Journal of Electron Microscopy Technique*, 9(4):395–411, 1988.

[NH91] G.M. Nielson and B. Hamann. The asymptotic decider: resolving the ambiguity in marching cubes. In *Proceedings of the 2nd conference on Visualization'91*, page 91. IEEE Computer Society Press, 1991.

[Nul98] S. Nullans. *Reconstruction géométrique de formes - Application à la géologie.* PhD thesis, INRIA, 1998.

[OPC96] JM Oliva, M. Perrin, and S. Coquillart. 3D reconstruction of complex polyhedral shapes from contours using a simplified generalized Voronoi diagram. In *Computer Graphics Forum*, volume 15, pages 397–408. Blackwell Science Ltd, 1996.

[OS88] S. Osher and J.A. Sethian. Fronts propagating with curvature-dependent speed: algorithms based on Hamilton-Jacobi formulations. *Journal of computational physics*, 79(1):12–49, 1988.

[Par05] H. Park. A hybrid approach to smooth surface reconstruction from 2-D cross sections. *The International Journal of Advanced Manufacturing Technology*, 25(11):1130–1136, 2005.

[PK96] H. Park and K. Kim. Smooth surface approximation to serial cross-sections. *Computer-Aided Design*, 28(12):995–1005, 1996.

[Pra00] A.K. Prasad. Particle image velocimetry. *Current science*, 79(1):51–60, 2000.

[PT94] B.A. Payne and A.W. Toga. Surface reconstruction by multiaxial triangulation. *IEEE Computer Graphics and Applications*, 14(6):28–35, 1994.

[PT96] L. Piegl and W. Tiller. Algorithm for approximate NURBS skinning. *Computer Aided Design*, 28(9):699–706, 1996.

[RGPS05] P. Ruhnau, C. Guetter, T. Putze, and C. Schnorr. A variational approach for particle tracking velocimetry. *Measurement Science and Technology*, 16:1449–1458, 2005.

[Rou03] F. Rousseau. *Méthodes d'analyse d'images et de calibration pour l'échographie 3D en mode main-libre.* PhD thesis, 2003.

[RY09] Laurent Rineau and Mariette Yvinec. 3D surface mesh generation. In *CGAL User and Reference Manual.* CGAL Editorial Board, 3.5 edition, 2009.

[SBG06] A. Sidlesky, G. Barequet, and C. Gotsman. Polygon reconstruction from line cross-sections. *Canadian Conference on Computational Geometry*, 2006.

[Seg68] G. Segal. Classifying spaces and spectral sequences. *Publications Mathématiques de l'IHÉS*, 34(1):105–112, 1968.

[Sha81] M. Shantz. Surface definition for branching, contour-defined objects. *ACM Siggraph Computer Graphics*, 15(2):242–270, 1981.

[She68] D. Shepard. A two-dimensional interpolation function for irregularly spaced data. In *Proceedings of the 23rd ACM National Conference*, pages 517–524, 1968.

[Shi05] M.Y. Shih. *Wavelet-based Image Processing and Cross-section Model Reconstruction*. PhD thesis, 2005.

[SJ05] B.S. SHIN and H.O.E.S. JUNG. Contour-Based Terrain Model Reconstruction Using Distance Information. *Lecture notes in computer science*, 2005.

[SYIM99] X. Song, F. Yamamoto, M. Iguchi, and Y. Murai. A new tracking algorithm of PIV and removal of spurious vectors using Delaunay tessellation. *Experiments in Fluids*, 26(4):371–380, 1999.

[TCC94] G. Tracton, J. Chen, and E. Chaney. CTI: automatic construction of complex 3D surfaces from contours using the Delaunay triangulation. *Mathematical Methods in Medical Imaging III*, pages 86–97, 1994.

[WHMW06] D. Wang, O. Hassan, K. Morgan, and N. Weatherill. Efficient surface reconstruction from contours based on two-dimensional Delaunay triangulation. *Int. J. Numer. Meth. Engng*, 65:734–751, 2006.

[Wol92] F.E. Wolter. Cut locus and medial axis in global shape interrogation and representation. *Computer Aided Geometric Design*, pages 92–2, 1992.

[WW94] E. Welzl and B. Wolfers. Surface reconstruction between simple polygons via angle criteria. *Journal of Symbolic Computation*, 17(4):351, 1994.

[Zse05] G. Zsemlye. *Shape prediction from partial information*. PhD thesis, Swiss Federal Institute of Technology Zurich, 2005.

Abstract

The purpose of this doctoral thesis was to provide a method to reconstruct three dimensional shapes from cross-sections. The principal motivation is 3D reconstructions of organs that are widely considered to be an important diagnostic aid in the medical world. However, the actual simulation results, namely in 3D ultrasonic simulation, are not reliable to be used in diagnosis. This thesis is the first geometric analysis of the reliability and validity of reconstruction methods from cross-sectional data.

We consider the problem of reconstructing a compact 3-manifold (with boundary) embedded in $\mathbb{R}^3$ from its cross-sections $\mathcal{S}$ with a given set of cutting planes $\mathcal{P}$ having arbitrary orientations. Using the fact that a point $x \in \mathcal{P}$ belongs to the original object if and only if it belongs to $\mathcal{S}$, we follow a very natural reconstruction strategy: we say that a point $x \in \mathbb{R}^3$ belongs to the reconstructed object if (at least one of) its nearest point(s) in $\mathcal{P}$ belongs to $\mathcal{S}$. This coincides with the algorithm presented by Liu et al. in [LBD$^+$08]. The first Chapter of this manuscript is devoted to analyzing this method. We prove that under appropriate sampling conditions that are satisfied when the set of cutting planes is dense enough, this reconstruction method preserves the homotopy type of the original shape. Using the homotopy equivalence, we also show that the reconstructed object is homeomorphic (and isotopic) to the original object.

In the second chapter of this thesis, we present a second reconstruction method that makes use of the Voronoi diagram of the sections. This method performs more connections between the sections comparing to the method [LBD$^+$08]. Increasing the connectivity between the sections is motivated by reconstructing tree-like structures from sparse sectional data. The provided sampling conditions, leading to topological guarantees, are adapted to tree-like structures: Indeed, we show that if the cutting planes are sufficiently transversal to the surface we want to reconstruct, then the method can handle complex branching structures from sparse sectional data distributed over a large volume. These theoretical analysis also provide topological justifications for the dual Delaunay-based approach.

The Voronoi-Delaunay duality leads us to a third reconstruction method that can be seen as a generalization of Boissonnat and Geiger's method [BG93] to the case of unorganized sections. This method performs still more connections between the sections comparing to the two first methods. The preliminary experimental results are quite promising, regarding the practicality of the approach to reconstruct complex cross-sectional branching situations such as the coronary arterial tree.

The theoretical studies of this thesis have consistently shown that if the sample of cutting planes is sufficiently dense, an accurate approximation of the unknown object can be provided. These studies provide the way to guide the sampling process to achieve the purposed *density* of cutting planes, or more formally, to verify the provided sampling conditions on the sections. The hope is that this thesis will be a first step to provide solid foundations and theoretical guarantees for medical diagnostic software. Of course, further research and investment is needed to apply these theoretical guidelines in developments of medical imaging softwares. Perhaps, for instance, an alternative interactive method may be a more appropriate method of examining the obtained theoretical criteria in practice.